Predicting Attainable Goals and Depletion Timeframes for DNAPL Source Zones

by

Grant R. Carey

A Thesis
presented to
The University of Guelph

In partial fulfilment of requirements
for the degree of
Doctor of Philosophy
in
Engineering

Guelph, Ontario, Canada

ABSTRACT

PREDICTING ATTAINABLE GOALS AND DEPLETION TIMEFRAMES

FOR DNAPL SOURCE ZONES

Grant R. Carey
University of Guelph, 2015

Advisor:
Professor Edward A. McBean

The primary goal of this research was to develop and validate new statistical and process-based, screening-level modeling tools for estimating attainable goals and depletion timeframes for DNAPL source zones under a wide range of soil texture and other conditions. A process-based screening model (NAPL Depletion Model, or NDM) was developed to simulate the relative influence of surface discharge and through-discharge for one or more DNAPL sub-zones in an overall source zone. Empirical assessment of depletion rates at field sites are compared to model simulated results for pool-dominated source zones to provide insights on the influence of site complexity. Statistical analysis of empirical data for a similar site dataset defined the mean confidence interval for technology-specific, attainable mass discharge reduction. The lower end of this confidence interval is demonstrated to be applicable to complex sites.

Empirical regression equations are derived for estimating the tortuosity coefficient based on either hydraulic conductivity or effective porosity, and for estimating total porosity and effective porosity based on hydraulic conductivity. An

empirical regression equation is also developed for estimating transverse vertical dispersivity based on hydraulic conductivity, demonstrating that this relationship is inverse to what has been concluded in previous studies.

An alternative model for simulating the decline in through-discharge for layers of residual DNAPL is presented, and is demonstrated to be more applicable to a broad range of conditions relative to previously developed regression equations. NDM was used to simulate complex multicomponent DNAPL dissolution trends based on a previously published study (Emplaced Source experiment in Borden, Ontario). Model results demonstrate the influence of re-equilibration and transient effective solubility in a multicomponent DNAPL source zone, on the overall through-discharge decline rate that was observed during the physical experiment. An empirical regression equation is developed for estimating the through-discharge decline rate for residual DNAPL layers over a broad range of conditions. This regression equation allows estimation of the decline rate *a priori* i.e. without fitting to site-specific data.

“Learn from yesterday, live for today, and hope for tomorrow.

The important thing is not to stop questioning.”

- Albert Einstein

ACKNOWLEDGEMENTS

I dedicate this thesis to my lovely wife Gwendolin, my One and Only, who's constant encouragement and support kept me moving towards this day. And to our beautiful children, Gillian and Gabriel, who also encouraged me throughout.

My family makes me complete; for them I will always be grateful.

I would also like to acknowledge the never-ending support of my parents, without whom none of this would have been possible. We came to Canada in 1967 to complete a Ph.D., but work has intercepted that goal on a few occasions now. No matter, we've finally completed that circle!

I owe many, many thanks to Dr. Ed McBean, my supervisor, mentor, and colleague for several decades now. I will always remember how Ed took a chance on hiring me when I was but a poor undergraduate student with some good, and some not-so-good marks. That work term started me on computer modeling. We haven't looked back since. Thanks Ed, for your never-ending encouragement and direction!

I would also like to thank Stan Feenstra for his many hours of assistance and support on this endeavour. I've learned a great deal from Stan, including what to watch out for when fishing from a kayak. Not sure which of us holds the record for length of part-time Ph.D. study, probably close enough to be a draw.

And to Beth Parker who took me out of my comfort zone by having me look at back-diffusion. She really opened my eyes to an important element I had previously been missing, and has now changed the way that I approach DNAPL sites.

Table of Contents

List of Tables

List of Figures

List of Abbreviations

1,1,2-DCA	1,1,2-trichloroethane
1,2-DCA	1,2-dichloroethane
CLM	constant-length NAPL pool depletion model
COC	chemical of concern
DNAPL	dense non-aqueous phase liquid
EISB	enhanced in-situ bioremediation
ISCO	in-situ chemical oxidation
ITRC	Inter-State Technical & Regulatory Council
LE	local equilibrium
LE(K)	local equilibrium model for estimating transverse dispersivity based on hydraulic conducitivity
LNAPL	light non-aqueous phase liquid
Md	mass discharge
Mddiff	mass discharge resulting from diffusion into or out of a low-permeability zone
MdR	mass discharge reduction factor
Mdsurf	mass discharge from surface of a NAPL pool or residual layer
Mdthru	mass discharge resulting from groundwater flow through a NAPL layer
MNA	monitored natural attenuation
NAPL	non-aqueous phase liquid

NDM	NAPL Depletion Model
NE	non-equilibrium
NPV	net present value
P&T	pump-and-treat with rates sufficient for hydraulic containment of source zone and/or plume
PCE	tetrachloroethene
SP&T	strategic pump-and-and-treat
SVE	soil vapor extraction
TCE	trichloroethene
VOCs	volatile organic chemicals

Chapter 1

Introduction

Dense non-aqueous phase liquids (DNAPLs) in the subsurface create a long-term contamination problem. Chlorinated solvent DNAPLs are a common source of contamination at sites throughout the world. For example, 80% of Superfund sites in the United States have chlorinated solvents in groundwater, and the U.S. Department of Defense has more than 3,000 sites contaminated with chlorinated solvents with estimated lifecycle costs of at least several billion dollars (SERDP, 2014).

Mass discharge refers to the total mass of a contaminant crossing a transect plane in an aquifer over a unit of time, and typically is expressed in units of kg/y or g/d. The use of mass discharge as a metric at DNAPL sites has increased rapidly over the past decade (ITRC, 2010 and 2014a). One of the main advantages to measuring mass discharge for a DNAPL source zone is that the length of the downgradient groundwater plume and the magnitudes of risks to receptors are directly proportional

to the mass discharge from a source zone (i.e. *source strength*). If a target level of risk reduction is required to be protective of downgradient receptors, such as a drinking water supply well, then an interim goal for source strength reduction may be readily determined.

Although DNAPL source zones may undergo significant natural attenuation over time, the rate of attenuation may not be sufficiently protective, or in other cases there is still a regulatory requirement to attempt to clean-up, or *treat* the source zone to enhance the rate of DNAPL depletion. Common in-situ remediation technologies used in DNAPL source zones include enhanced in-situ bioremediation (EISB) and in-situ chemical oxidation (ISCO), all of which are intended to enhance the rate of dissolution and depletion of the DNAPL source. Thermal treatment is another technology which is being used at sites to enhance the volatilization of DNAPL in the subsurface. Another alternative which is not typically considered is the use of groundwater pump-and-treat to enhance DNAPL dissolution through the strategic placement of extraction wells and selection of pumping rates. This alternative is referred to in this study as *strategic pump-and-treat*, or SP&T. The main objectives of applying an in-situ remediation technology are to reduce source strength, groundwater concentrations, plume length, and risk to downgradient receptors.

It is recognized among practitioners and site owners, and is beginning to become more recognized by regulators, that it is not practicable to completely restore

groundwater to background conditions at many DNAPL sites in a reasonable timeframe. This challenge is due to a variety of factors, including:

- Some DNAPLs have low solubility which inhibits their rate of dissolution;
- DNAPL constituents may have very low cleanup criteria, which means that a long time is required for these DNAPLs to become completely depleted in order for groundwater to be restored to background conditions;
- DNAPL is difficult to locate in the subsurface, which creates a challenge when attempting to delineate the overall extent of a DNAPL source zone;
- DNAPL distribution has a high degree of heterogeneity within an overall source zone;
- Geologic heterogeneity results in preferential groundwater flow through more permeable lenses or layers, which in some cases makes it difficult to facilitate contact between injected remedial reagents and the DNAPL-water interface;
- Forward diffusion of constituents from a DNAPL into an adjacent fine-grained geologic layer (e.g. silt or clay) creates aqueous mass storage reservoirs. These reservoirs will begin to release mass to the more transmissive zones, creating sustained secondary sources for decades or longer (Chapman and Parker, 2005; Parker et al., 2008), once the pooled

DNAPL has been completely depleted (i.e. the reveral of the diffusion direction creates a condition referred to as back-diffusion).

In addition to back-diffusion from a depleted DNAPL source zone, back-diffusion may also occur in the downgradient plume area, creating an even larger secondary source as a result of back-diffusion.

Kavanaugh et al. (2012) state that there are approximately 126,000 contaminated sites in the United States, and at least 12,000 of these sites are not expected to be cleaned up in a reasonable timeframe due to a high degree of complexity in site geology, contaminant distribution, and other factors. Reasonable timeframe used to be typically defined as 30 years, although recently it appears that this definition has increased to 100 years or longer with some regulatory agencies or project managers. The degree of complexity in site conditions will influence the magnitude of the source strength (i.e. mass discharge) reduction which is attainable at a given site, and the corresponding timeframe to reach this goal. The Inter-State Technology and Regulatory Council (ITRC) is currently developing a guidance manual to help regulators and practitioners with management of complex sites such as these.

To facilitate an improved understanding of site complexity and how it may impact the extent of remedial efficiency and the attainability of site management goals, there has been increasing utilization of high resolution site characterization tools and

methods (e.g. Parker et al., 2003 and 2004; Guilbeault et al., 2005; ITRC, 2014b). Use of high resolution characterization tools may improve our understanding of heterogeneity in geology and the distribution of DNAPL architecture within a source zone, and may identify the core of the source zone which is predominantly contributing to the source strength, downgradient plume, and risk. This level of characterization may be used to focus remediation efforts, resulting in higher efficiency and reduced costs and timeframes (ITRC, 2014a,b).

One of the most challenging management decisions at a DNAPL site is to decide how much cost and time should be expended on aggressive DNAPL source zone treatment, with the knowledge that complete restoration is not likely to be attainable in a reasonable timeframe. Hence, decision-making analysis should include consideration of the benefits of partial DNAPL depletion, which may include reduction of risk and groundwater plume length, societal benefits, reduction in remediation timeframe, and reduction of lifecycle costs for site management.

The magnitude of these potential benefits should be balanced with the cost and time required for source treatment, to determine when site remediation may be transitioned from active to passive source treatment. For example, it would not make fiscal sense to spend ten million dollars to aggressively treat a DNAPL source in an attempt to reduce source strength at a site by a factor of 100 to 1,000, if the back-diffusion will limit the plume and risk reduction to a factor of 10 and remediation timeframe is still going to be on the order of centuries or longer (e.g. similar to the

limit in plume reduction observed at a site studied by Chapman and Parker, 2005). The effort to be spent on aggressive source treatment, if any, should be balanced by the benefits that will be gained from this effort.

Some of the problems facing the industry with this type of cost-benefit analysis is that it is difficult to predict: (1) how much reduction in DNAPL mass and groundwater concentration is realistically attainable for a specific site; and, (2) the timeframe required to attain a target goal of mass discharge reduction in a DNAPL source zone based on natural or enhanced attenuation alternatives.

A number of studies over the past decade have developed or evaluated screening-level models for simulating DNAPL depletion (Sale and McWhorter, 2001; Zhu and Sykes, 2004; Parker and Park, 2004; Jawitz et al., 2005; Fure et al., 2006; Christ et al., 2006 and 2010; Basu et al., 2008; Zhang et al., 2008; Saenton and Illangasekare, 2007; Farthing et al., 2012). While this research has helped to develop an improved understanding of general factors which influence DNAPL depletion rates, the screening (or *upscaled*) models developed to date are limited in their applicability to contaminated sites due to the use of input parameters which are not readily available or able to be determined at field-scale (Farthing et al., 2012).

Another disadvantage of many of these models is that they rely on a lumped mass transfer coefficient, which represents the overall DNAPL depletion rate. These lumped parameter models do not provide a simple means for evaluating the relative contribution of various processes which influence DNAPL depletion rates. When

evaluating naturally-occurring DNAPL dissolution in heterogeneous environments, numerical models are often used to provide a more sophisticated *process-based* representation, which allows for a more thorough analysis of how various processes influence the rate of DNAPL depletion (e.g. Brusseau et al., 2002; Marble et al., 2008; Mobile et al., 2012). This type of process-based modeling improves our understanding of the relative contribution that various characteristics will have on DNAPL depletion rates, and may be used to guide high resolution field investigations. For example, if it is known prior to an investigation that the depletion timeframe for a source zone is largely influenced by the thickness of DNAPL pools in a pool-dominated source zone, then more focus may be applied (and different methods used) during the investigation to characterize the range in thickness for pools that are encountered during the field investigation. An improved process-based understanding may also help to reduce uncertainty associated with predictions of DNAPL depletion timeframe. Other possible uses of a process-based model include forensic analyses to refine the characterization of DNAPL architecture, or to evaluate the influence of future enhancements to DNAPL dissolution such as enhanced dissolution rates (e.g. EISB, ISCO, SP&T).

The use of numerical models for this purpose is expensive, and the uncertainty associated with such an expensive analysis discourages the use of process-based models. However, there is merit in considering use of a screening-level, process-based model since they are easier to implement and can be used to provide valuable insights

that help to focus an investigation, reduce uncertainty, and ultimately to make more informed site management decisions.

At a mature contaminated site, where vertical fingers of residual DNAPL (ganglia) have been depleted, process-based models may facilitate estimation of transient mass discharge trends from one or more DNAPL layers (i.e. sub-zones) within an overall source zone. The total mass discharge (Md_{tot}) from an individual DNAPL layer is equal to the sum of contributions from: (1) surface discharge (Md_{surf}) at the top and/or bottom of the horizontal layer (Johnson and Pankow, 1992); (2) discharge from groundwater flow through the DNAPL layer (i.e. through-discharge, or Md_{thru}); and (3) diffusive discharge to underlying or overlying fine-grained zone ($Md_{f\text{-}diff}$). Mechanisms causing the naturally-occurring decline in mass discharge observed at aged DNAPL sites (Suarez et al., 2004; Newell et al., 2006) may include one or more of the following:

- declining lengths and thicknesses of DNAPL layers which causes a corresponding decline in surface discharge;
- complete depletion of distinct DNAPL layer sub-zones (e.g. layers); and
- formation of preferential groundwater flow channels within individual DNAPL layers (herein referred to as intra-source bypassing) which result in enhanced downgradient dilution of average concentrations and a corresponding reduction in through-discharge.

This latter mechanism, referring to a decline in mass discharge through a DNAPL layer (i.e. *through-discharge*) is the least understood and most difficult of the three mechanisms to quantify at the field-scale. The occurrence of through-discharge decline due to intra-source bypassing in residual DNAPL zones has been observed in a number of laboratory studies with residual DNAPL (e.g. Imhoff et al., 1996; Powers et al., 1998; Nambi and Powers, 2000; Brusseau et al. (2002); Marble et al., 2008; Russo et al., 2009; Farthing et al., 2012). At present, however, there is no broadly applicable methodology available for estimating the through-discharge decline rate for layers of residual DNAPL at the field-scale *a priori*, without fitting a model to high resolution monitoring data from a controlled dissolution experiment (e.g. Rivett and Feenstra, 2005; Farthing et al., 2012). Farthing et al. (2012) indicate that various upscaled (i.e. domain-averaged) models which were developed for this purpose have significant limitations in their range of applicability and/or data requirements.

When simulating mass discharge from a DNAPL pool, it is commonly assumed that through-flow is negligible and the only contribution is from surface dissolution which may be estimated using the analytical solution described in Johnson and Pankow (1992). Recent studies have demonstrated that through-discharge in pools may be significant in an upper transition zone, where the DNAPL saturation is sufficiently low that some groundwater through-flow does occur (Moreno-Barbaro and Illangasekare, 2006; Wilking et al., 2013). The influence of this through-discharge for DNAPL on remediation timeframe is poorly understood.

In addition, some of the input parameters used to estimate surface discharge (e.g. tortuosity coefficient and transverse vertical dispersivity) are not readily estimated for the range of soil textures in which DNAPL occurs at field-scale; these parameters have been quantified only for a narrow range of soil texture based on laboratory experiments. Thus, our ability to simulate mass discharge from DNAPL pools over a wide-range of field-scale soil textures is constrained by uncertainty in available input parameters.

1.1 Research Objectives

The goal of this research was to evaluate processes which influence the rate of DNAPL depletion under naturally-occurring and enhanced dissolution, with a focus on layers of residual and free phase DNAPL which are typically encountered at aged contaminated sites. This research will add to the existing state of knowledge regarding processes and model input parameters which govern the rate and timeframe of DNAPL depletion. In addition, this research will develop and validate tools which facilitate the use of screening-level, process-based DNAPL depletion models for a broad range of field-scale conditions, and which ultimately allow for more informed decision-making at contaminated sites.

The key objectives of this research were as follows:

- Conduct data mining of DNAPL sites to quantify technology-specific, attainable goals for enhanced mass discharge reduction with consideration of site complexity.
- Develop and validate a process-based screening model for simulating dissolution of individual or multiple DNAPL sub-zones, including combined contributions from surface and/or through-discharge for layers of residual and free phase (i.e. pooled) DNAPL.
- Derive a conceptual model which describes the relationship between tortuosity, and hydraulic conductivity or effective porosity; and derive a regression equation for estimation of the tortuosity coefficient over a wide range of soil textures.
- Derive a new regression model between transverse vertical dispersivity and hydraulic conductivity which contradicts previous literature studies, and derive a regression equation to facilitate estimation of dispersivity parameter over a wide range of soil textures.
- Validate the use of an alternative modeling approach and regression equation which provides a more reliable and simple means, relative to previously derived regression models, for estimating the rate of decline in through-discharge caused by intra-source bypassing, in layers of residual DNAPL.

- Evaluate factors which influence the rate of combined mass discharge reduction, and the fractional mass discharge versus mass remaining, for pool-dominated source zones, including the influence of through-discharge in transition zones within DNAPL pools.
- Assess relative timeframes for Monitored Natural Attenuation, EISB, containment P&T, and SP&T for a pool-dominated source zone.
- Identify types of conditions where the use of SP&T may result in significant cost savings at contaminated sites.

1.2 Organization

This thesis is organized in a *manuscript* format according to the University of Guelph 2013-2014 Graduate Calendar "Thesis Format" section. Following this format, chapters 2 through 6 are written as completely separate articles. The remaining chapters are outlined below.

Chapter 2 – DNAPL Source Depletion: Predicting Rates and Timeframes

NAPL Depletion Model (NDM), is a process-based screening model developed to simulate mass discharge trends for one or more DNAPL sub-zones. NDM

simulates the influence of declining DNAPL layer length on surface discharge, and has various functions which may be used to simulate transient through-discharge for layers of residual and pooled DNAPL. Pool dissolution dynamics are evaluated, including an assessment of the influence of through-discharge on depletion rates and timeframes. An empirical analysis is conducted based on 13 ISCO sites and 16 EISB sites, to estimate the technology-specific mean depletion rate and corresponding confidence interval. Comparison to pool-dominated source zones demonstrates that complex sites have a slower rate of DNAPL depletion than sites with less complexity (e.g. less heterogeneity), when an enhanced attenuation technology is implemented. This paper was published in the Remediation Journal in June 2014.

- Carey, G.R., E.A. McBean, and S. Feenstra, 2014. DNAPL Source Depletion: Predicting Rates and Timeframes. Remediation Journal, Summer 2014, p. 21-47.

Chapter 3 – DNAPL Source Depletion: Attainable Goals and Cost-Benefit Analyses

Provides an empirical analysis of the amount of source strength reduction achieved at a number of sites where ISCO, EISB, and thermal treatment were employed. The mean mass discharge reduction (MdR) and the corresponding confidence interval were estimated, so that a range of possible outcomes could be

estimated for a site based on its level of complexity (which in this case is represented by the degree of heterogeneity). An example feasibility analysis is presented for a case where the remediation timeframe due to back-diffusion in a downgradient plume, assuming complete removal of DNAPL from the source zone, is more than 1,000 years. The feasibility analysis demonstrates that Monitored Natural Attenuation (MNA) is the most cost-effective solution for treatment of the source zone. If regulatory conditions require some form of active treatment, then SP&T is shown to be the most cost-effective alternative when a containment pump-and-treat system already exists at a site. There is a small incremental cost for SP&T in this case, and the timeframe required to achieve a 90% reduction in source strength with SP&T is similar to that for EISB and ISCO. This outcome is shown to be insensitive to a range of DNAPL pool conditions. This paper was published in the Remediation Journal in September 2014.

- Carey, G.R., E.A. McBean, and S. Feenstra, 2014. DNAPL Source Depletion: Attainable Goals and Cost-Benefit Analyses. Remediation Journal, Fall 2014, p. 79-106.

Chapter 4 – Estimating Tortuosity Based on Hydraulic Conductivity

Presents a literature review which demonstrates that there is a correlation between the tortuosity coefficient, and hydraulic conductivity or effective porosity. Empirical regressions are derived for estimating total and effective porosity based on hydraulic conductivity, and for estimating the tortuosity coefficient based on effective porosity or hydraulic conductivity.

- Carey, G.R., E.A. McBean, and S. Feenstra, 2014. Estimating Tortuosity Based on Hydraulic Conductivity. Submitted to Ground Water (in review).

Chapter 5 – Estimating Properties Based on Hydraulic Conductivity: Transverse Vertical Dispersivity

Presents theory explaining why transverse vertical dispersivity should be inversely proportional to grain size and hydraulic conductivity, which is opposite to the trend suggested by recent studies. Derives an empirical regression for estimating the transverse vertical dispersivity based on hydraulic conductivity, based on a review – and in some cases, re-calculation – of transverse vertical dispersivity from previously published studies. Validates the use of a previously published methodology for estimating the reduction in transverse dispersivity when groundwater velocity exceeds a critical threshold. A new empirical model was derived fortuitously for estimating transverse dispersivity and is shown to be generally applicable for a

wide range of groundwater velocity conditions, to a lower limit of one-tenth of the critical velocity threshold. A sensitivity analysis demonstrates the influence the difference between local equilibrium, non-equilibrium, and the empirical model for estimating dispersivity for a wide range of soil textures and groundwater velocities.

- Carey, G.R., E.A. McBean, and S. Feenstra, 2014. Estimating Properties Based on Hydraulic Conductivity: Transverse Vertical Dispersivity. In preparation for submittal to Transport in Porous Media.

Chapter 6 – Empirical Regression of Through-Discharge Decline Rate for Residual DNAPL Layers

Presents a simple alternative, relative to previously published regression models, for estimating the transient decline in through-discharge for layers of residual DNAPL. Data from a previously published field-scale multicomponent DNAPL dissolution experiment are used to estimate overall decline rates, and a process-based screening model (NDM) is used to demonstrate that these overall decline rates are caused mainly by intra-source bypassing, and that transient mole fractions / effective solubility in the upgradient portion of the source zone have negligible influence on downgradient concentrations. The process of re-equilibration along the flowpath through the multicomponent source zone, where effective solubility varies spatially, is shown using NDM to be important for estimating mass discharge trends. A

correlation between the decline rate and three characteristics (effective solubility, groundwater velocity, and initial DNAPL mass) is hypothesized, and a regression equation based on data from previously published experiments is derived. This regression equation is shown to be more applicable to a broad range of conditions than the previously published regression models by Powers et al. (1994) and Imhoff et al. (1996).

- Carey, G.R., E.A. McBean, and S. Feenstra, 2014. Empirical Regression of Through-Discharge Decline Rate for Residual DNAPL Layers. In preparation for submittal to Water Resources Research.

Chapter 2

DNAPL Source Depletion: Predicting Rates and Timeframes

2.1 Abstract

Given the relatively rapid rate of DNAPL ganglia depletion, source zones are generally dominated by horizontal layers of DNAPL after a release to the saturated zone. Estimating the time required to attain specific source strength reduction targets resulting from partial DNAPL source depletion is challenging due to a lack of available screening models, and because little has been done to synthesize available empirical data. Analytical and semi-analytical models are used to study general DNAPL pool dissolution dynamics. The half-life for the decline in DNAPL source strength (i.e. aqueous mass discharge) is demonstrated as proportional to the square

root of the pool length, the thickness of the pool, and the solubility for single component DNAPLs. The through-pool discharge is shown to be potentially significant for thin pools or in upper regions of thicker pools. An empirical analysis is used to evaluate average concentration decline rates for 13 in-situ chemical oxidation (ISCO) and 16 enhanced in-situ bioremediation (EISB) sites. Mean apparent decline rates, based on the time required to achieve the observed source strength reduction, are calculated for the ISCO and EISB sites (half-lives of 0.39 years and 0.29 years, respectively). The empirical study sites are shown to have faster decline rates than for a large, complex study site where ISCO was implemented (half-life of 2.5 years), and for a conceptual pool-dominated TCE source zone where EISB was simulated (half-life of 2.5 years). Guidance is provided on using these findings in estimating timeframes for partial DNAPL depletion goals.

2.2 Introduction

Sites with dense non-aqueous phase liquid (DNAPL) contamination may require expensive long-term remediation due to persistence of the DNAPL source zone. While DNAPL ganglia (i.e. mainly vertical zones of residual DNAPL) may become depleted in a matter of years, thin horizontal lenses of residual and/or free phase DNAPL (i.e., pools) typically involve longer term problems (Parker et al.,

2003). Some studies have examined naturally-occurring source concentration decline rates (e.g., Newell et al., 2006; Suarez et al., 2004). While these studies did not specifically estimate source strength at each site, the use of well concentration trends within source zones is considered to be a reasonable approximation to source strength trends for the purpose of this study.

The concentration decline rates presented in Newell et al. (2006) and Suarez et al. (2004) are based on meta case study evaluations which did not involve detailed evaluation of site-specific geology or DNAPL source zone architecture, so little insight was available on how individual site characteristics influence naturally-occurring depletion rates. Other studies examined ranges in duration of enhanced in-situ DNAPL depletion (i.e., treatment) technologies (e.g., McGuire et al., 2006); however, these treatment duration data are difficult to apply at other sites because source strength (i.e. aqueous mass discharge) reduction goals may differ from the original studies. The source strength decline rate is more beneficial for estimating remediation timeframe.

The purpose of this study is to facilitate improved prediction of source strength decline rates at DNAPL sites. A new process-oriented DNAPL depletion screening model is used to demonstrate the sensitivity of source strength decline rates in pool-dominated source zones to various physical and chemical characteristics during natural and enhanced dissolution. Empirical average source strength decline rates were calculated for the application of in-situ chemical oxidation (ISCO) and enhanced in-

situ bioremediation (EISB) based on 14 and 18 sites, respectively. Natural and enhanced empirical source strength decline rates are compared to results from the DNAPL depletion screening model to provide qualitative insights on the relative ganglia-to-pool (GTP) ratio typical of the sites used for this empirical analysis. A companion paper (Carey et al., 2014a) presents guidance for defining attainable reduction goals for source strength and plume strength, as well as an example feasibility study of natural and enhanced DNAPL treatment alternatives. This study is focused on chlorinated solvent DNAPL that is present below the water table, although the concepts discussed here are applicable to other types of DNAPL.

2.3 Pool-Dominated DNAPL Depletion Rate

2.3.1 Background

After a release of DNAPL to the subsurface in unconsolidated porous media, two forms of DNAPL tend to accumulate: mainly vertical ganglia which are discontinuous, smaller volumes of DNAPL and horizontal layers of DNAPL. These horizontal layers may consist of free phase DNAPL (i.e. saturations larger than the residual saturation threshold), or they may occur at less-than-residual saturation due to drainage and dissolution. This study is focused on free phase DNAPL pool layers, although it should be recognized that DNAPL layers with lower saturation may be present and will exhibit faster source strength decline rates than free phase pools.

Carey et al. (2014b) provide a quantitative comparison of source strength decline rates for DNAPL layers with various saturation levels.

DNAPL below the water table will dissolve into adjacent groundwater and become depleted over time. DNAPL is defined to be *readily accessible* when groundwater flow in the direct vicinity of the DNAPL occurs at a reasonable rate. DNAPL is defined to be *poorly accessible* when it occurs in a portion of the porous medium that has relatively low groundwater flow rates (e.g. in lower permeability soil, dead end pores, etc.). The accessibility of DNAPL will influence its naturally-occurring depletion rate, as well as the performance of technologies which are intended to enhance DNAPL dissolution.

Interfacial area represents the DNAPL surface area at the interface where DNAPL is in direct contact with groundwater. A larger interfacial area typically corresponds with a higher rate of mass discharge from dissolution that occurs at this contact interface. When ganglia and pools of DNAPL are both readily accessible to groundwater flow at a site, the ganglia will become depleted more quickly than pools because they have a lower ratio of DNAPL volume to interfacial area. Relative to ganglia, pools have a large volume of DNAPL stored below the contact interface between the DNAPL and groundwater flowing over the surface of the DNAPL. The higher the ratio of total DNAPL volume to total interfacial area (i.e., average pool height), the higher the volume of DNAPL stored below the pool surface and, thus, less accessible to groundwater flow. Aged DNAPL source zones predominantly consist of

horizontal layers (i.e. lenses) of DNAPL (Parker et al., 2003), rather than vertical zones of ganglia because the horizontal layers have a relatively high volume to interfacial area ratio (compared to ganglia) and thus represent the most persistent elements of a DNAPL source zone.

There are few studies where the thickness of chlorinated solvent DNAPL pools has been characterized in the field. Parker et al. (2004) used a drainable core technique (Parker et al., 2003) to identify the presence of trichloroethene (TCE) DNAPL pools at 13 locations inside a source zone, with most pools having a thickness of 5 to 10 cm and typically less than 20 cm. Parker et al. (2003) documented thin layers of DNAPL present at three other sites (Connecticut B, Ontario, and Florida) using high resolution vertical sampling. Based on soil concentrations and calculated DNAPL saturations, to the extent that pools exist at these sites they appear to be at or less than 10 cm thick. Parker et al. (2003) demonstrated that thin (2 to 10 cm) DNAPL layers also occur as residual DNAPL zones which will have lower saturations than pools. Parker et al. (2003) identified an apparent 30 cm thick layer of tetrachloroethene (PCE) at a New Hampshire site, which was residual DNAPL based on the relative low saturations calculated. Meinardus et al. (2002) conducted high resolution vertical sampling (5 to 10 cm sampling intervals) in a DNAPL zone and found thin pools and chlorinated solvent DNAPL layers similar to those encountered by Parker et al. (2003). These high resolution studies indicate that chlorinated solvent

DNAPL pools in granular aquifers are typically thin although some sites may have thicker pools depending on release and subsurface conditions.

2.3.2 Surface Versus Through-Pool Discharge

In numerous simulation studies, DNAPL pools have been conceptualized as homogeneous blocks of high DNAPL saturation (*Sn*) through which there is negligible groundwater flux (Moreno-Barbero and Illangasekare, 2006). Moreno-Barbero and Illangasekare (2006) conceptualize a transition zone in the upper portion of DNAPL pools that ranges from residual to high DNAPL saturation through which groundwater does flow. Experimental studies demonstrating that flow occurs through the transition zone include Glover et al. (2007), Moreno-Barbero and Illangasekare (2006), and Wilking et al. (2013). Herein we will refer to mass discharge associated with dissolution at the surface of a DNAPL pool as *pool surface discharge*, and to mass discharge associated with dissolution into groundwater flowing through the pool layer as *through-pool discharge*.

The rate of groundwater flow which will occur through the DNAPL pool itself is dependent on the relative permeability of the porous medium to groundwater flow (*krw*), which in turn is dependent on the DNAPL saturation (S_n). van Genuchten (1980) defines the relative water permeability for a two-phase system as

$$krw = Se^{1/2}\left[1 - \left(1 - Se^{1/m}\right)^{m}\right]^{2} \qquad (2.1)$$

where *Se is* the effective saturation and *m* is an empirical parameter that represents the pore size distribution. The effective saturation is given by

$$Se = \frac{Sw - Swr}{1 - Swr} \tag{2.2}$$

where *Sw* is the water saturation defined as 1-*Sn* below the water table, and *Swr* is the irreducible water saturation.

However, the DNAPL saturation will vary with elevation within the pool. McWhorter and Kueper (1996) present an equation for estimating the elevation in a DNAPL pool that corresponds to a specific effective saturation, based on the condition that the capillary pressure at the top of the pool is zero. Re-arranging this equation to solve for DNAPL saturation as a function of elevation in the pool (*Sn(z)*) gives

$$Sn(z) = 1 - Swr - (Sm - Swr)\left[1 + \left(\frac{\alpha \Delta\rho (T - z)}{\rho_w}\right)^{\frac{1}{1-m}}\right]^{-m} \tag{2.3}$$

where *Sm* is the residual DNAPL saturation, α [L^{-1}] is an empirical parameter defined by van Genuchten (1980) to be a function of entry pressure, $\Delta\rho$ is the difference between DNAPL density (ρ_n) and water density (ρ_w), *T* is the pool thickness, and *z* is the elevation of a point in the pool. The bottom of the pool has a reference elevation of zero.

To illustrate the magnitude of through-pool discharge, four cases were simulated based on TCE DNAPL pools having a thickness of 5 cm, 10 cm, 20 cm, and 30 cm. Chlorinated solvent pools observed in aged source zones have been typically at

the lower end of this range (i.e., 10 cm or less) as discussed above; however, the larger pool thicknesses of 20 cm and 30 cm are included here to illustrate the sensitivity of through-pool discharge to thickness.

Figure 2.1a and 2.1b show calculated profiles of TCE DNAPL saturation (*Sn*) and relative permeability (k_{rw}) for a sand with α of 8.8 m^{-1}, *m* of 0.6, irreducible water saturation of 0.05, TCE density of 1,455 kg/m^3 and residual DNAPL saturation of 0.15. See Carey et al. (2014c) for the basis used to estimate capillary pressure-saturation characteristics based on a fine to medium sand with a hydraulic conductivity of 0.01 cm/s. Figure 2.1a and 2.1b show that pool thicknesses of 5 and 10 cm have maximum DNAPL saturations less than 0.2 (Figure 2.1a) and maximum relative permeabilities of 0.2 to 0.3 (Figure 2.1b). While these values for relative permeability may be considered significantly lower than ambient conditions (i.e. 0% NAPL saturation), they are still sufficiently high to allow some groundwater flow to occur through the pool itself.

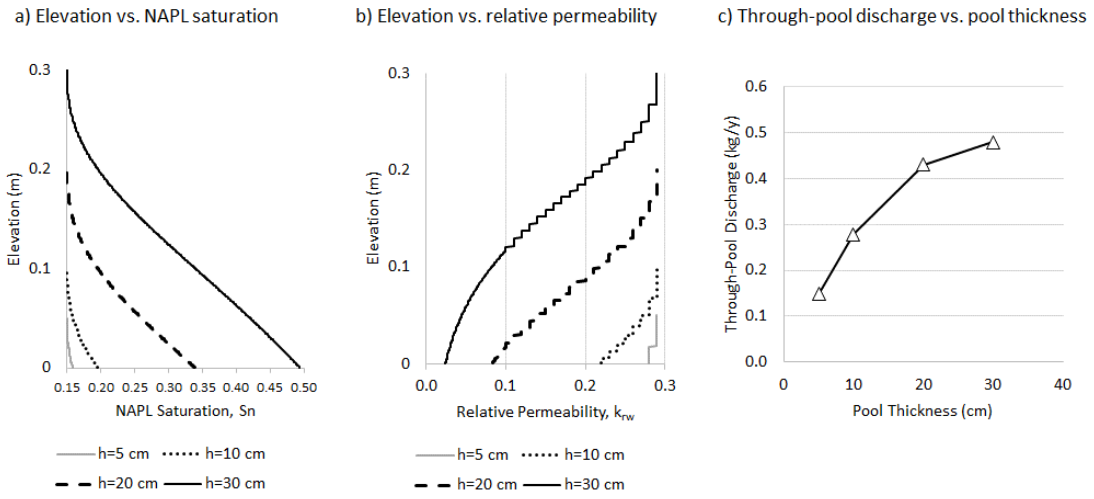

Figure 2.1 – Example profiles of TCE NAPL saturation and relative permeability, and through-pool discharge for varying TCE NAPL pool thicknesses.

The through-pool discharge (Md_{thru}) was estimated based on a hydraulic conductivity of 0.01 cm/s, a horizontal hydraulic gradient of 0.003 m/m, and a TCE effective solubility for a single component DNAPL of 1,100 mg/L and using

$$Md_{thru} = \left(\sum_{i=1}^{nlay} krw_i q_x C_{eff} w \Delta z\right) \quad (2.4)$$

where *nlay* is the number of vertical incremental layers defined for the pool with each pool having a thickness of Δz, krw_i is the relative permeability calculated for layer i, q_x is specific discharge, and C_{eff} is the effective solubility (which equals solubility for a single component DNAPL), and w is the width of the pool. Assuming an effective porosity of 0.25, the linear groundwater velocity above the pool for this example is 38

m/y. This is slightly lower than the velocity of 54 m/y cited by Seyedabbasi et al. (2012) as being the 60th percentile velocity from a comprehensive survey of more than 400 contaminated sites.

Through-pool discharge was calculated by summing the discharge calculated for individual layers (i) with a thickness of 0.0005 m for each of the four pool thickness cases and is shown on Figure 2.1c. For pool thicknesses of 5, 10, 20, and 30 cm the respective pool-through discharge was calculated to be 0.15 kg/y, 0.28 kg/y, 0.43 kg/y, and 0.48 kg/y, respectively. These data demonstrate that, for thicker pools, the pool-through discharge does not increase proportionally with pool thickness because the DNAPL saturation at the bottom of the pool increases and the relative permeability decreases as the thickness of a pool increases, as shown on Figure 2.1a and Figure 2.1b.

The analytical solution for pool surface discharge (Md_{surf}) for a pool of specified length is given by Hunt et al. (1988) and modified by Carey et al. (2014d) to

$$Md_{surf} = \left(2LwC_{eff}\sqrt{\frac{q_x}{\pi L}}\right)\sqrt{\alpha_{TV}q_x + \theta\tau D_o} \qquad (2.5)$$

where L is the length of the pool, w is the width of the pool, q_x is the specific discharge, α_{TV} is the transverse dispersivity, θ is the total porosity (as recommended by Carey et al., 2014d), τ is the tortuosity, and D_o is the free water diffusion coefficient (m^2/d). Carey et al. (2014b, 2014e) present empirically-derived relationships which may be used to estimate α_{TV} and τ based on hydraulic conductivity.

The pool surface discharge for the TCE pool was estimated based on the parameters described above and a free water diffusion coefficient of 9.1×10^{-10} m^2/s. The initial pool surface discharge was calculated for a pool with length and width of 1 m to be 0.34 kg/y. This surface discharge is not dependent on pool thickness and, thus, applies to all four pool thickness cases. For a pool of 5 cm thickness, the initial total discharge (which is the sum of the surface and through-pool discharges) is 0.49 kg/y, which is 44 percent higher than the surface discharge above. The total discharge for the 10 cm thick pool was 82 percent higher than the surface discharge. These examples demonstrate that through-pool flux may be significant and will increase the total mass discharge and cause more rapid DNAPL depletion.

The simulated total mass discharge for individual TCE pools with length and width of 1 m, and thicknesses of 5 and 10 cm, were 0.49 kg/y and 0.62 kg/y, respectively. For comparison, ITRC (2010) lists the estimated source strength (i.e., mass discharge estimated directly downgradient of a source zone) for 44 sites as ranging from 0.00029 kg/y to 680 kg/y. Figure 2.2 presents a histogram of the source strength estimates cited in ITRC (2010) which indicates that the typical range for source strength is from 1 to 100 kg/y which is considered to be generally representative for average chlorinated solvent sites where DNAPL is present. Based on the relatively low mass discharge associated with one pool in the examples cited above, it is reasonable to expect that a typical site with a source strength of more than

5 to 10 kg/y and an aged source zone may have multiple pools present and generally low to negligible contribution from ganglia.

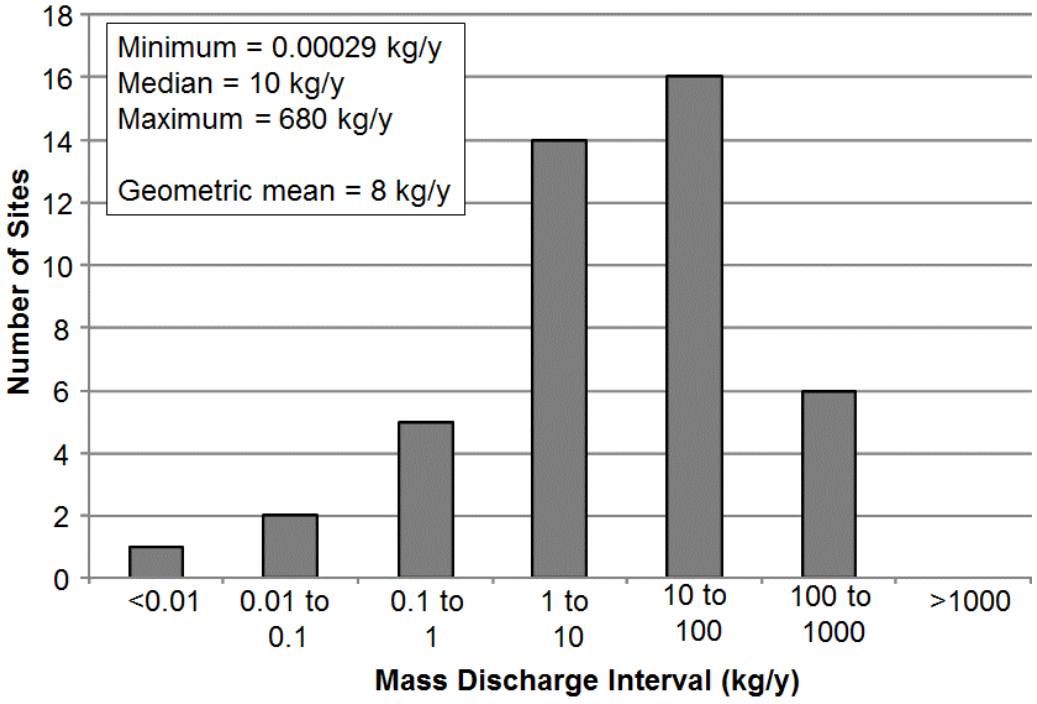

Figure 2.2 – Histogram of source strengths at typical chlorinated solvent sites. (data from ITRC, 2010.)

2.3.3 DNAPL Depletion Rates

Source strength is a single metric that represents the aqueous mass discharge from a DNAPL source zone. When evaluating historical or predicting future source depletion rates, it is convenient to discuss these depletion rates in terms of source

strength decline rates since quantification of DNAPL mass in the subsurface has high uncertainty and source strength is directly proportional to plume strength and risk. It is implicitly easier to predict a decline rate for source strength than for concentrations, given that concentration trends vary from well to well at any given site. Some wells may have a large reduction in concentration, some a small reduction, and other wells may actually exhibit an increase in concentration at the source during in-situ DNAPL treatment.

Predicting future changes to source strength has an additional advantage in that this will correlate to corresponding reductions in plume length and risk to downgradient receptors (ITRC, 2013). The use of mass discharge (e.g., source strength or plume strength) as a metric for designing and monitoring DNAPL treatment remedies and for predicting downgradient plume response has grown rapidly in the past decade (ITRC, 2010 and 2013).

The rate of naturally-occurring dissolution of DNAPL ganglia and/or pools will govern the depletion timeframe, which is defined as the time required for complete DNAPL dissolution. (Back-diffusion from lower hydraulic zones will create a secondary source even after DNAPL has become depleted in the primary source zone; the implications of this for remediation timeframes are discussed further below.) For example, Newell et al. (2006) calculated median source well concentration decline half-lives of 3.0 and 6.1 y for the naturally-occurring depletion of PCE and TCE at smaller DNAPL sites. Suarez et al. (2004) conducted a similar empirical analysis for

source concentration decline rates at dry cleaning sites and calculated median PCE and TCE half-lives of 2.2 and 1.6 years for naturally-occurring depletion.

Typical in-situ DNAPL depletion technologies are intended to enhance the dissolution (or in the case of some types of thermal treatment, volatilization) of DNAPL, in those circumstances when risks to groundwater are sufficiently high that monitored natural attenuation (MNA) alone is not effective as a remedial alternative. Examples of common, in-situ DNAPL depletion technologies include EISB, ISCO, and thermal treatment (McGuire et al., 2006; Stroo et al., 2012). As will be shown below, another technology which warrants consideration is termed strategic pump-and-treat (SP&T), which involves focused use of groundwater extraction wells within, or directly downgradient of, a DNAPL source zone to accelerate dissolution by increasing the velocity of groundwater flow (e.g., Carey and McBean, 2010; Reese Air Force Base case study cited in ITRC, 2013). This is in contrast to typical pump-and-treat (P&T), which involves pumping rates that are only sufficient for hydraulically containing a source zone (and, thus, involving little increase in groundwater velocity), or the pumping wells are too far downgradient of the DNAPL to enhance the rate of groundwater flow and dissolution. SP&T may also include re-injection of treated water upgradient to further accelerate source zone dissolution.

Brusseau et al. (2011) presented TCE source strength trends prior to implementation of soil vapor extraction (SVE) and ISCO at a large, complex site in Tucson, Arizona. DNAPL was present both above and below the water table at this

site as a result of seepage from unlined pits and ponds (Brusseau et al., 2011). Pre-treatment source strength trends are reproduced in Figure 2.3 for a 13-year period from approximately 1987 to 2000, and both linear and exponential decline regression trends are shown in this exhibit. The coefficient of determination (R^2) for both linear and exponential decline models are similar, indicating that either model may be used to estimate the source strength decline rate for this site. This is consistent with the finding by Newell et al. (2006) indicating some decline trends are better matched with an exponential decline model, some are better matched with a linear decline model, and some sites have similar R^2. Newell et al. (2006) note that many sites exhibit more of an exponential trend in later years when tailing is observed, which they indicate is a good reason to assume that exponential decline models are most suitable for evaluating DNAPL depletion rates.

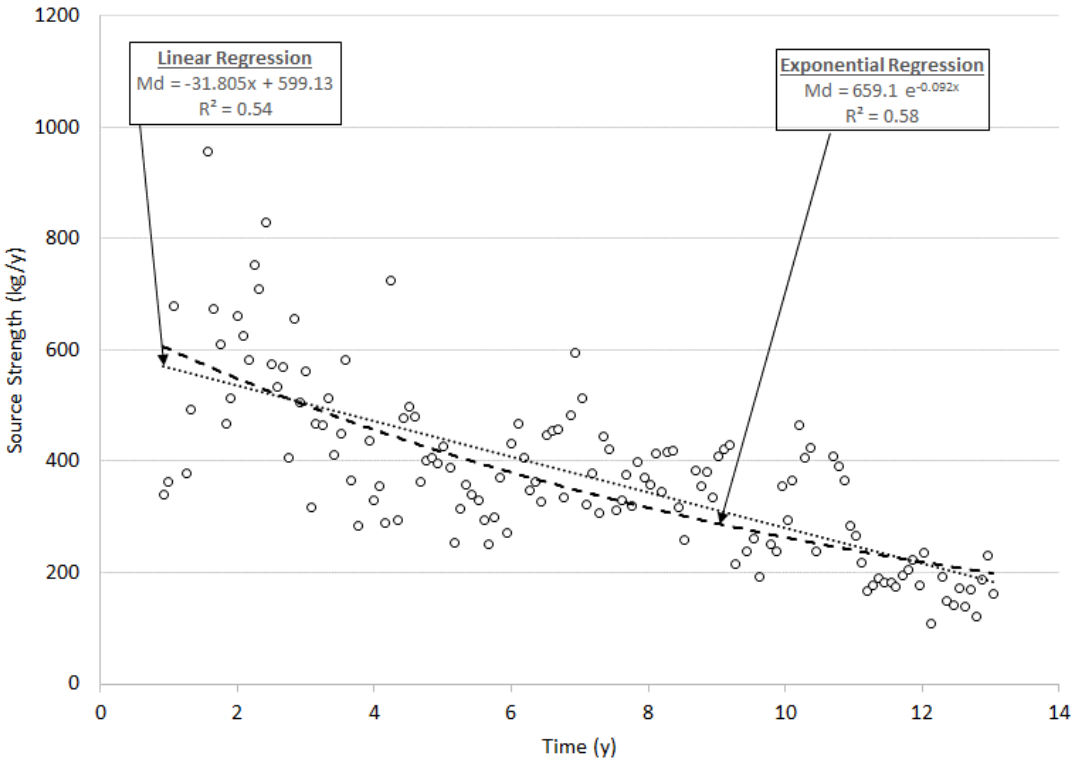

Figure 2.3 – Pre-treatment source strength versus time at Tuscon, Arizona site (modified from Brusseau et al., 2011).

Equation 2.5 indicates that the pool surface discharge is dependent on the length and width of the pool, effective solubility, specific discharge, transverse dispersivity, porosity, and the effective diffusion coefficient which is calculated as τD_o. Dissolution of DNAPL pools tends to occur primarily from the upgradient edge of the pool. Hence the length of the pool will decline over time which will lead to a

corresponding decline in surface discharge over time (see Figure 2.4 for a schematic depiction).

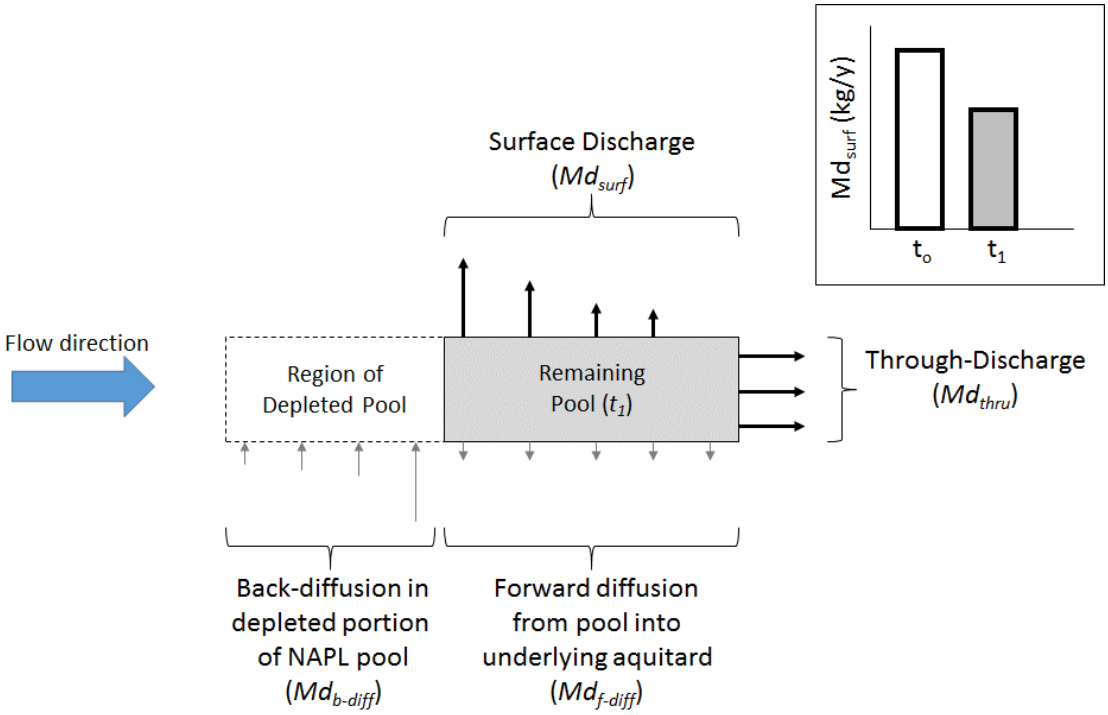

Figure 2.4 – Conceptual representation of mass discharge components for NAPL pool dissolution and back-diffusion once pool depletion occurs.

Johnson and Pankow (1992) and Seyedabbasi et al. (2012) present examples of constant-length pool surface discharge models (CLMs) which assume a constant pool length over time. These models are useful for predicting the initial surface discharge associated with a pool, but not the rate of decline in surface discharge because the pool length will decline over time. Carey (2014) and Carey et al. (2014d) present the

NAPL Depletion Model (NDM), which is a process-oriented semi-analytical model used as a screening tool for predicting depletion timeframes and source strength trends for naturally-occurring and enhanced dissolution of pool-dominated source zones. The main benefits of the NDM screening model is that it is easily applied and may be used to provide insights on how various physical and chemical characteristics influence remediation timeframes. NDM represents the declining pool length over time, and, thus, may be used to estimate individual pool or combined source zone depletion rates. NDM also has the option of simulating through-pool discharge in addition to surface discharge. Carey et al. (2014d) present more information on the functionality of the NDM. Figure 2.4 presents a schematic diagram of the various processes simulated using the NDM. Back-diffusion from a thick aquitard which may occur after depletion of a DNAPL pool was studied (e.g. Seyedabbasi et al., 2012) and is not considered herein.

To illustrate the general total mass discharge decline trend for a single DNAPL pool, an example was simulated using NDM based on a TCE pool with a length and width of 1 m. Four cases were used to represent different pool thicknesses: 1, 2, 5, and 10 cm. The elevation-specific DNAPL saturation in the four TCE pools with different thicknesses was estimated using NDM based on Equation 3 and the same input parameters presented above. The initial mass of TCE in the four pools was calculated to be 0.8, 1.5, 3.9, and 8.3 kilograms (kg), respectively. Through-pool discharge was not simulated for this example.

Figure 2.5 shows the simulated surface discharge for a single TCE pool with a thickness of 10 cm (see thick black line) for natural dissolution. As shown in this exhibit, the initial surface discharge declines very slowly in the first 10 years, then declines more rapidly until the pool becomes depleted at a time of approximately 31 years. Exponential and linear regression trends were fit to the source strength versus time curve using Microsoft Excel and are shown on Figure 2.5. The linear trend has a better correlation for the single pool with an R^2 of 0.86, whereas the exponential trend has an R^2 of 0.73. The largest difference between the linear and exponential trends occurs in the first five years of the pool dissolution, and both trends yield similar results after that time. The half-life calculated based on the exponential decline model was 21 years. While the decline curve does not explicitly exhibit an exponential decline trend, the exponential model appears to capture the general decline rate reasonably well over the middle of the pool depletion timeframe and, thus may be used to at least compare decline rates for different pool conditions. The exponential decline curve is also more likely to capture tailing expected to occur in later stages (Newell et al., 2006), such as may occur during back-diffusion and/or desorption.

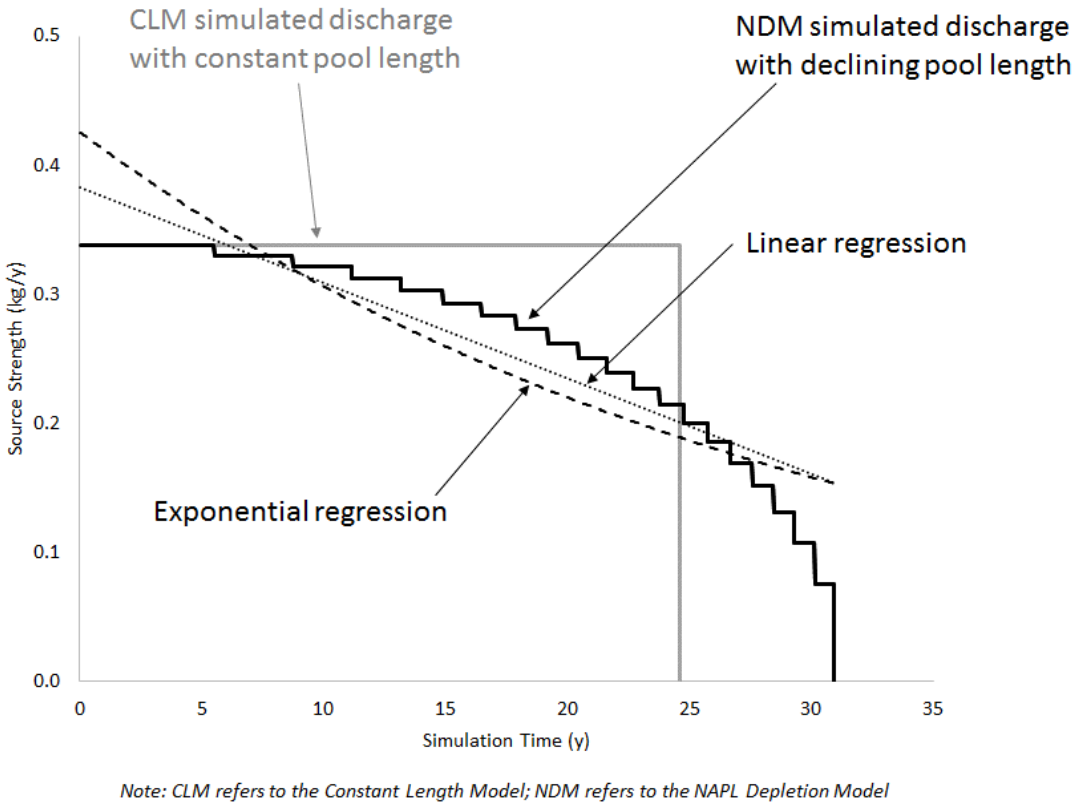

Figure 2.5 – Simulated mass discharge versus time for an individual DNAPL pool.

Figure 2.6 shows the simulated pool surface discharge versus time for the four thickness cases, as well as exponential model regression trendlines and corresponding half-lives and coefficients of determination (R^2). Figure 2.6 also shows that the exponential model facilitates an approximate quantitative comparison of the varying decline in source strength versus time for the different pool cases. Non-ideal processes likely to occur in the field, but are not represented in the model are expected to impart more tailing behavior in the latter portion of the source strength versus curve

relative to the NDM simulation. Based on these non-ideal processes, use of the exponential model is considered to be a reasonable approach for comparing decline rates for various pool scenarios.

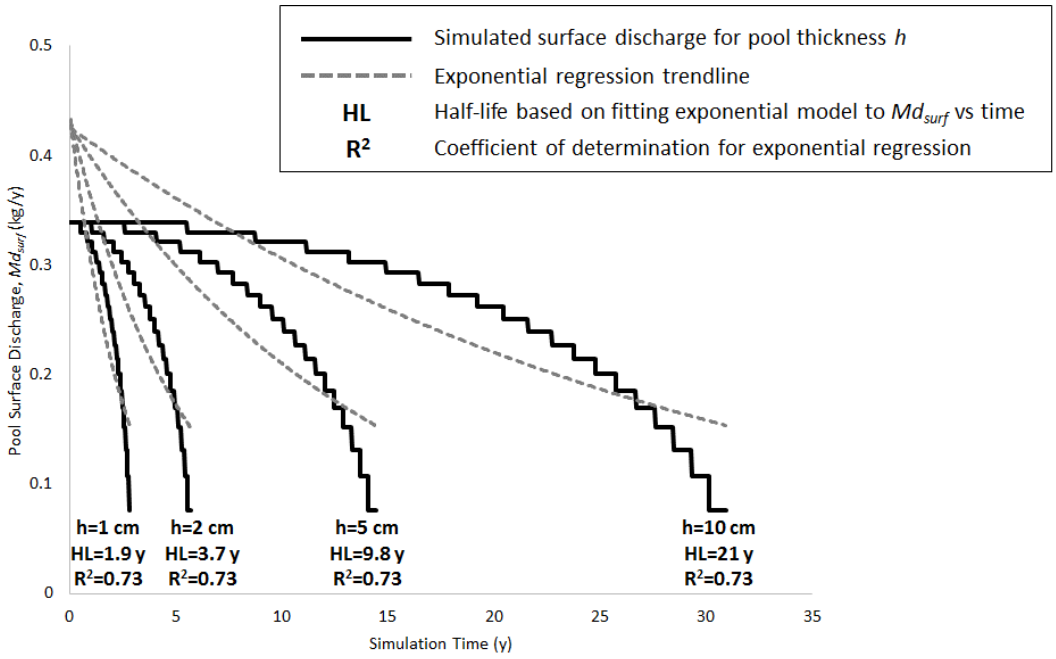

Figure 2.6 – Simulated mass discharge versus time and exponential regression for four TCE pools with varying thickness and naturally-occurring dissolution.

The simulated source strength decline half-lives for individual pools are not suitable for estimating remediation timeframe, however, given that these simulated half-lives do not incorporate representation of non-ideal behavior typically observed in the field. NDM may be used to estimate remediation timeframe based on the time

required for DNAPL source strength to reach an attainable goal (such as 90% reduction), or possibly based on empirical decline half-lives discussed below.

The surface discharge that would be simulated with a CLM is also shown on Figure 2.5 (gray line). The CLM simulates a constant surface discharge over time because of the implicit assumption that the length of the pool stays constant. As shown in Figure 2.5, the CLM is not appropriate for evaluating DNAPL pool depletion rates. Carey et al. (2014d) show, through a comprehensive sensitivity analysis, that the simulated depletion timeframe for the CLM is consistently about 80 percent of the simulated depletion time based on declining pool length.

Additional simulations were constructed to evaluate the sensitivity of DNAPL pool depletion timeframe to the various degrees of through-pool discharge. NDM incorporates a *pool flux factor* which is zero when through-pool discharge is not simulated, and 1.0 when the through-pool discharge is to be simulated at 100 percent of its calculated value. The simulated relative permeability is multiplied by the pool flux factor in the NDM model. Table 2.1 presents the simulation results for four simulations of a single TCE pool with a length of 1.0 m: two simulations using a pool flux factor of zero with pool thicknesses of 2 cm and 10 cm; and two simulations using a pool flux factor of 1.0 with the same pool thicknesses. For the thinner pool with thickness of 2 cm, the through-pool discharge had only a minor influence on the total initial discharge (33 percent higher than the case with zero through-pool discharge)

and a 16 percent reduction in the pool depletion timeframe (4.8 years versus 5.7 years). Simulating through-pool discharge had a more significant influence on the thicker pool (10 cm) simulations, with an increase of 82 percent in total mass discharge, and a reduction in depletion timeframe of 16 years versus 31 years without through-pool flux.

Table 2.1 - Comparison of pool source strength with and without through-pool discharge.

Pool Thickness (cm)	Initial Surface Discharge (kg/y)	Pool Flux Factor	Average Relative Permeability	Initial Through-Pool Discharge (kg/y)	Initial Total Mass Discharge (kg/y)	Pool Depletion Timeframe (y)
2	0.34	0	0	0	0.34	5.7
2	0.34	1.0	0.29	0.06	0.40	4.8
10	0.34	0	0	0	0.34	30.9
10	0.34	1.0	0.27	0.28	0.62	15.9

To compare the influence of DNAPL density and component solubility on pool surface mass discharge decline rates (also referred to as *depletion rates*), three single-component DNAPL pools were simulated: TCE, PCE, and 1,2-dichloroethane (1,2-DCA). The pool flux factor was defined to be zero for these and the other NDM simulations discussed below (i.e. through-pool discharge was zero). Each pool had the same dimensions: length and width of 1 m and thickness of 5 cm. The other input parameters used previously for TCE are described above. 1,2-DCA and PCE pools

were simulated using: α of 10.3 per m and 12.3 per m, respectively (this parameter is scaled based on the NAPL-water interfacial tension); DNAPL density of 1,250 kg/m^3 and 1,600 kg/m^3, respectively; solubility of 8,520 and 200 mg/L, respectively; and free-water diffusion coefficients of 9.9×10^{-10} m^2/s and 8.2×10^{-10} m^2/s, respectively.

While the pool dimensions are the same for each of the three cases, the initial mass of DNAPL in each simulation varies because of the different DNAPL density and interfacial tensions which govern the scaling of α. The initial mass of DNAPL for the 1,2-DCA, TCE, and PCE pools were calculated using NDM to be 3.3 kg, 3.9 kg, and 4.5 kg, respectively. The simulated pool depletion timeframes (i.e. times at which remaining DNAPL mass was zero) for 1,2-DCA, TCE, PCE and were 1.5 years, 14 years, and 95 years, respectively. Source strength (i.e. mass discharge) decline half-lives were estimated using regression to be 1.1 years, 9.8 years, and 63 years, respectively. These simulation results demonstrate that pools with predominantly high solubility components (e.g., 1,2-DCA) will become depleted more quickly than pools with lower solubility (e.g., PCE), and that the source strength decline half-life is generally proportional to solubility for single component DNAPLs.

Sensitivity analyses were conducted to evaluate the range of natural TCE source strength decline half-lives for pool thicknesses of 1 cm, 2 cm, 5 cm, and 10 cm, and for pool lengths of 0.1 m, 0.2 m, 0.5 m, 1 m, 2 m, 3 m, and 10 m. This range of pool thicknesses is different than the earlier example which was intended to demonstrate how through-pool discharge varies for thin versus relatively thick pools.

This sensitivity analyses use a thickness range of 1 to 10 cm because this is more representative of pool thicknesses expected in the field at chlorinated solvent sites as discussed above. Other NDM input parameters are consistent with those described above.

Figure 2.7 shows the simulated source strength decline half-lives as a function of pool length and thickness. The minimum source strength (i.e. mass discharge) decline half-life was simulated to be 0.6 year (pool length of 0.1 m and thickness of 1 cm) and the maximum half-life was 63 years (pool length of 10 m and thickness of 10 cm). For comparison, the average TCE source concentration or mass discharge decline half-lives for natural dissolution conditions that were determined based on three other field site studies are shown in Figure 2.7: Suarez et al. (2004) half-life of 1.6 years; Newell et al. (2006) half-life of 6.1 years; and the half-life of 7.5 years calculated in this study based on source strength data presented in Brusseau et al. (2011) for a large, complex site. Figure 2.7 shows the general relationship between the source strength decline half-life and the length and thickness of the pool. The source strength decline half-lives are proportional to the square root of the pool length and are linearly proportional to the thickness of the pool.

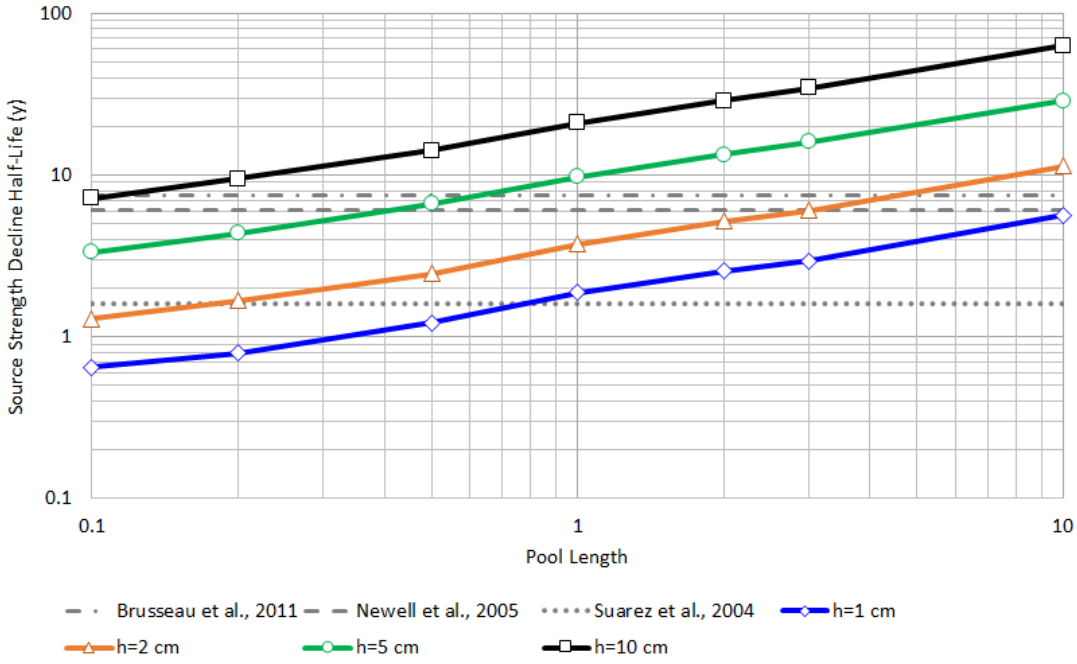

Figure 2.7 – Simulated TCE DNAPL pool depletion half-lives for naturally-occurring dissolution.

Comparison of the simulated half-lives using NDM with the average half-lives determined in the other studies indicates that on average the sites studied by Suarez et al. (2004) had lower source concentration or source strength (i.e. mass discharge) decline half-lives than were simulated using NDM; this indicates that either the empirical sites may not have DNAPL had free phase pools present in the source zone, or that there were pools present which were relatively thin and short in length. (The depletion half-life is insensitive to pool width.) The median TCE source concentration decline half-life of 6.1 years cited in Newell et al. (2006) is consistent with pools

having thicknesses of 1 to 2 cm, or pools having thickness up to 5 cm with short lengths. These comparisons are intended to provide general insights on what type of DNAPL architecture may be present on average at the sites included in these empirical studies; it is likely that some sites had larger pools than the ranges cited above.

Carey et al. (2014d) provide a detailed description of how NDM may be used to simulate enhanced dissolution based on two factors: a) enhanced dissolution represented with a multiplier for the total mass discharge relative to the natural dissolution case; or b) enhanced horizontal hydraulic gradient which increases the surface and/or through-pool discharge (refer to Equations 2.4 and 2.5, respectively). To simulate the influence of EISB, an enhancement factor of 3 was input to NDM based on the range of 2 to 4 for the EISB enhancement factor cited in Stroo et al. (2012). This means that the total mass discharge due to dissolution is three times higher for EISB in the NDM simulation than would be the case for natural dissolution. When simulating EISB, NDM simulates the parent compound mass discharge based on the conventional surface discharge equation presented in Equation 2.5; the enhanced dissolution and discharge from the pool is assumed to occur in the form of daughter products. This is consistent with the review of EISB studies in which most sites showed a general decline in parent compound concentrations after the start of EISB.

To provide a comparison of depletion timeframes for various treatment alternatives, NDM was used to simulate a hypothetical source zone with multiple

pools. The source zone was constructed using pool dimensions equal to those defined in the example presented in Seyedabbasi et al. (2012), namely 12 pools having lengths and widths ranging from 2 to 4 m and pool thicknesses ranging from 2 to 4 cm. This hypothetical example is similar to the New Hampshire field study presented in Guilbeault et al. (2005) which had 15 local hot spots on a source strength transect, and the width of these hot spots appear to be on the order of meters. Through-pool flux was assumed to be zero for this example. Superposition of aqueous plumes downgradient of each pool was also assumed to be negligible, so the total source strength was calculated based on the sum of individual pool mass discharge. TCE was simulated as the single component DNAPL. The same average linear groundwater velocity of 38 m/y was used to be consistent with the examples presented above.

The following alternatives were simulated using NDM: natural dissolution (MNA); pump-and-treat (P&T) which was assumed to increase the groundwater velocity in the source zone by an average factor of 1.5; SP&T which was assumed to increase the groundwater velocity in the source zone by an average factor of 3; and EISB which was assumed to enhance the dissolution rate by a factor of 3 based on the typical range of 2 to 4 cited in Stroo et al. (2012). Figure 2.8 presents the simulated source strength versus time for each of the four alternatives, where the source strength represents the sum of the individual pool surface discharges. The depletion timeframe and half-lives for each alternative are also shown in Figure 2.8. The significant changes in decline rate shown in Figure 2.8 for each alternative (e.g., at times of 8 and

15 years for MNA) represent when pools of a specific thickness become depleted (e.g., 2 cm and 3 cm).

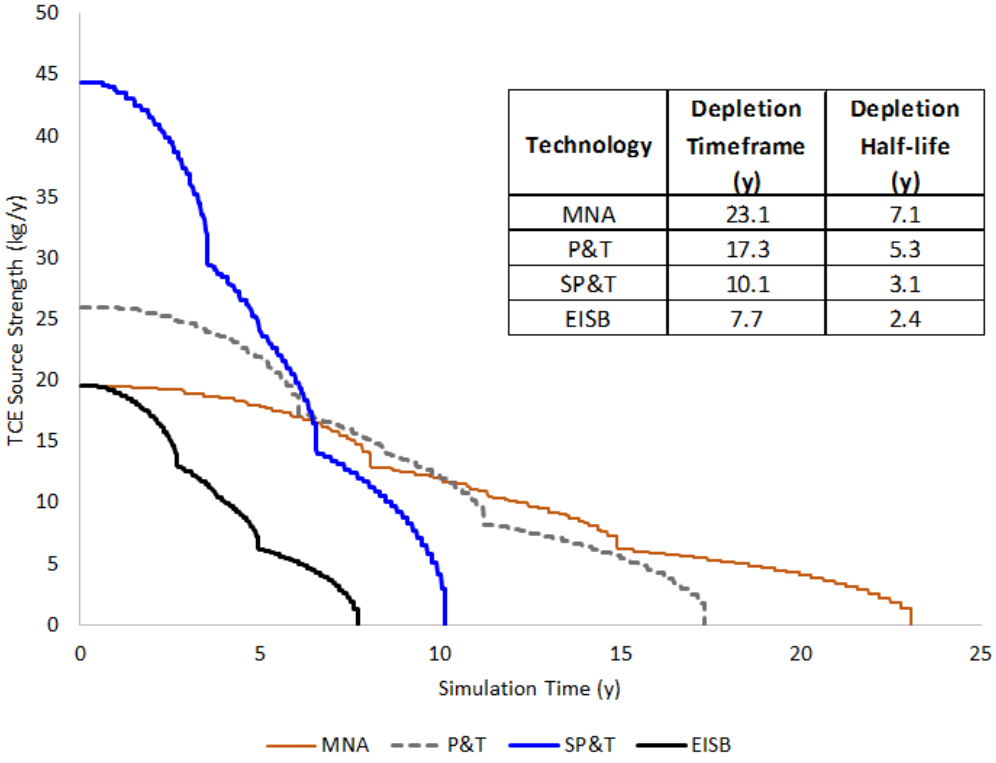

Technology	Depletion Timeframe (y)	Depletion Half-life (y)
MNA	23.1	7.1
P&T	17.3	5.3
SP&T	10.1	3.1
EISB	7.7	2.4

Figure 2.8 – Simulated source strength versus time for a pool-dominated source zone and various in-situ depletion technologies.

Estimating DNAPL Pool Dimensions

As discussed above, aged DNAPL source zones typically have a low ganglia-to-pool ratio. Use of the process-oriented NDM helps to inform predictions of timeframes for natural and enhanced dissolution. Although there are limited empirical

observations to characterize DNAPL pool dimensions required as inputs for the model, various methods may be used as multiple lines of evidence to estimate DNAPL pool thickness:

- Utilization of the core drainage technique described by Parker et al. (2003);
- Observation in a core of the zone where DNAPL is observed seeping out of the core, if the DNAPL is visible;
- Collection of high resolution soil samples at the centimeter scale where a pool is suspected (e.g., above a low-permeability layer where organic vapor meter readings are high) and partitioning relationships may be used to estimate the degree of DNAPL saturation (e.g., Parker et al., 2003; Meinardus et al., 2002; Kueper et al., 1993). This method has relatively high uncertainty due to potential volatilization and DNAPL losses when collecting and sampling soil cores (Meinardus et al., 2002);
- Similar to the above, use of high resolution membrane interface probe (MIP) at the centimeter scale to delineate thin lenses with elevated aqueous concentrations which may represent the maximum thickness of a pool where one is suspected to be present (e.g., above a low permeability layer). At best, this method may be used to represent the maximum thickness of a pool, as it is not possible to confirm DNAPL presence or DNAPL architecture (residual vs. free phase DNAPL) based solely on MIP readings;

- Calibration of various pool dimension scenarios using NDM and matching the overall source strength to a field-based estimate of source strength. This approach is expected to be highly non-unique, but in combination with the field techniques above, it may help to constrain the number of scenarios which potentially represent the site-specific conditions when the ganglia-to-pool ratio is low.

As discussed above, it is at a minimum challenging to characterize the thickness of any individual pool, and high resolution sampling is necessary to identify where pools exist or to estimate an approximate thickness. Probabilistic modeling of pool dimensions using Monte Carlo or Latin Hypercube with a screening tool like NDM is also an option, and constraining the realizations to those that match field-based estimates of source strength will help to reduce uncertainty in the simulated outcomes.

For the length of DNAPL pools, Seyedabbasi et al. (2012) cite studies which suggest that an average pool length of 3 m may be representative of field conditions based on the average continuity of low-permeability lenses. As discussed above, Guilbeault et al. (2005) present high resolution mass flux monitoring at a New Hampshire site where 15 maximae in PCE concentrations were observed in a transect directly downgradient of a DNAPL source zone. This suggests that at this site, which was an aged source zone, there may have been up to 15 pools or horizontal DNAPL layers present, and Figure 7 in Guilbeault et al. (2005) indicates that the width of these

hot spots on the transect appear to be on the order of meters. The combined source strength at this site was estimated to be 15 kg/y (Guilbeault et al., 2005). High resolution characterization using a screening tool like the membrane interface probe (MIP) may be used to estimate approximate dimensions of high concentration areas within a source zone. MIP does not provide direct evidence of DNAPL presence or DNAPL saturation so must be used in conjunction with high resolution soil coring to confirm the character of DNAPL pools. It is not anticipated that the length or width of any single pool can be fully delineated in the field given highly variable geologic and DNAPL architecture conditions observed at a micro scale at most sites.

In summary, NDM is a useful screening tool for understanding how various physical and chemical characteristics will influence DNAPL depletion rates and timeframes, and it may be used to evaluate how uncertainty in DNAPL architecture affects depletion rates and timeframes.

2.4 Empirical Analysis: DNAPL Depletion Rates

The main objective of the empirical analysis is to estimate the mean concentration decline rates observed at source zone monitoring wells during and following the implementation of ISCO and EISB at a number of sites where the presence of DNAPL was suspected or known. Given that these site monitoring wells were generally situated within, or in close proximity, to DNAPL source zones, it is

assumed that mean site concentration decline rates are representative of source strength decline rates. As discussed below, the statistical analysis of mean concentration decline rates was conducted in part using a methodology that is representative of overall source strength decline rates.

The ISCO and EISB site database used for this analysis is based on the original database prepared by McGuire et al. (2006) as part of a project funded by the Strategic Environmental Research and Development Program (SERDP). The original database includes concentrations measured at between one and four monitoring wells identified to be within or in close proximity to a source zone at a variety of sites. Details regarding the compilation of the original database are presented in McGuire et al. (2006).

As explained in a companion study (Carey et al., 2014a), a subset of the McGuire et al. (2006) database was used for this study. The main change to the database from that originally used by McGuire et al. was the exclusion of site monitoring well data which did not exhibit concentrations at or above 1 percent of solubility, which is considered to be a potential DNAPL indicator threshold by Kueper and Davies (2009). Based on these and other criteria, there were 13 ISCO sites and 16 EISB sites with available monitoring well data, and a total of 27 wells at ISCO sites and 31 wells at EISB sites with monitoring data. The majority of the ISCO and EISB sites were dry cleaning facilities (62 percent and 56 percent, respectively).

Only data for the main parent chemical of concern (COC) were available to the authors. The main COC for each site in the database was either PCE or TCE, with only one exception where a site had chlorobenzene as the main COC. Most of the ISCO and EISB sites (62 percent and 94 percent, respectively) were described by McGuire et al. (2006) as having predominantly fine-grained geology such as clays, silts, and/or silty/clayey sand in the treatment zone. McGuire et al. (2006) indicate that most of the wells are situated within 13 feet of a treatment point (e.g., injection well) which suggests that these wells are within or are in close proximity to a DNAPL source zone.

2.4.1 Decline Rate Regression Analysis

The objectives of the first step in the empirical analysis included:

- Estimation of the mean concentration decline rate for ISCO and EISB sites; and
- Determination of whether well concentration decline rates were best represented using an exponential or linear regression approach.

While an exponential decline model is typically assumed to be representative of source strength decline at DNAPL sites (e.g., Newell et al., 2006), little work has been done to validate this assumption particularly for pool-dominated source zones. As shown above, a linear regression is a slightly better match when fit to the surface

discharge decline for a single pool when compared to the exponential decline model regression. Newell et al. (2006) conducted an evaluation which showed that some sites were better fit using a linear regression model while others were better fit with an exponential regression model.

The first step of the decline rate regression analysis involved plotting concentration versus time data for each well included in the current study database. Wells which exhibited generally declining or increasing concentration trends based on visual inspection of the concentration versus time charts were then carried forward to the rate regression analysis. A minimum of three data points was required to support the regression analysis in this study. An example of a monitoring well trend which was deemed to not be suitable for regression analysis involved initial sharp declines in concentration, followed by a rapid increase, and then another sharp decline. While site-specific treatment details were not available to the authors, this type of trend is consistent with multiple treatment injection events which may have been implemented at these sites.

Ten ISCO site monitoring wells and 12 EISB site monitoring wells had temporal trends which were qualitatively determined to be suitable for a regression analysis (37 percent and 39 percent of the total number of available wells, respectively). Linear and exponential trend models were fit to the concentration versus time data for these 22 monitoring wells. There were no wells with general

increasing concentration trends after the start of treatment that could be used for a regression analysis.

Table 2.2 presents the list of ISCO and EISB site monitoring wells for which a regression analysis was conducted, as well as the exponential rates that were calculated to best fit the data and the corresponding half-lives. A statistical analysis using the Shapiro-Wilkes method (McBean and Rovers, 1998) confirmed that the exponential rate samples for both the ISCO and EISB sites followed a log-normal distribution. The mean exponential decline rates were estimated by transforming the samples using the natural logarithm and taking the arithmetic average of the transformed data.

Table 2.2 – Monitoring well decline rates determined from regression analysis.

Treatment Technology	Site ID	Chemical of Concern	Well Name	Exponential Concentration Decline Rate (1/y)	Concentration Decline Half-life (y)
ISCO	C-07	PCE	MW-2	5.64	0.12
ISCO	C-09	PCE	GO-MW2	0.83	0.84
ISCO	C-10	PCE	MW-1	15.71	0.04
ISCO	C-10	PCE	MW-6	10.33	0.07
ISCO	C-11	PCE	MW-4	0.91	0.76
ISCO	C-13	PCE	MW-4	0.58	1.20
ISCO	C-13	PCE	MW-5	0.66	1.05
ISCO	C-19	PCE	KBA-11-34	5.04	0.14
ISCO	C-21	TCE	76G	4.81	0.14
ISCO	C-23	TCE	BAT-5S	6.88	0.10
EISB	B-02	PCE	MW-9	1.19	0.58
EISB	B-05	TCE	HGRK-VEG4	3.11	0.22
EISB	B-10	PCE	MW-1	3.22	0.22
EISB	B-11	PCE	JEMW-4	5.46	0.13
EISB	B-11	PCE	MW-1	1.52	0.46
EISB	B-14	PCE	MW-1	13.41	0.05
EISB	B-19	TCE	MW023	3.93	0.18
EISB	B-20	PCE	EW-B	2.59	0.27
EISB	B-20	PCE	MW-A	5.65	0.12
EISB	B-20	PCE	MW-B	6.32	0.11
EISB	B-24	TCE	Inside	0.75	0.92
EISB	B-25	TCE	VE-1	1.02	0.68

The ISCO and EISB exponential decline rates estimated using regression on the subset of wells discussed above had similar statistics. The minimum, mean, and maximum half-lives for ISCO wells were 0.04, 0.24, and 1.20 years, respectively. The minimum, mean, and maximum half-lives for EISB wells were 0.05, 0.24, and 0.92 year, respectively. As shown above, the simulated source strength decline rate for EISB in a pool-dominated source zone (12 TCE pools with lengths and widths of

several meters and thicknesses ranging from 2 to 4 cm) was 2.5 years, which is significantly higher than even the maximum half-life (0.92 year) calculated above for regression of EISB well trends for the case study sites in Table 2.2. This suggests that the monitoring wells used to perform the regression analysis may not be representative of trends in pool-dominated source zones which are discussed further below. It should also be noted that these estimated regression rates represent only those monitoring wells which had general declining trends over time. Thus, these rates may overestimate average well trends because wells that had significant increases in concentration at some point after the start of treatment were not included in the regression analysis.

Figure 2.9a and 2.9b show scatter plots of linear versus exponential regression coefficients of determination (R^2) determined for ISCO and EISB monitoring wells, respectively. The gray dashed line in Figure 2.9a and 2.9b represent equal coefficients of determination for the linear and exponential regression. Points that fall below this line occur when the exponential regression R^2 is higher than the linear regression R^2, and points that fall above the dashed line have a higher linear regression R^2. As shown in these two exhibits, the exponential regression either has a similar R^2 to the linear regression, or is significantly higher than the linear regression. These data indicate that the exponential regression is consistently a representative fit for the subset of wells used for this analysis, which had general declining concentrations over time. This indicates that where enhanced treatment is being conducted and generally

declining concentration trends occur, an exponential decline model is a reasonable choice for calculating or predicting decline rates. These decline rates, which are based on historical data, may then be used to estimate a remediation timeframe for a given reduction in source strength, although separate evaluations of the limiting effects of back-diffusion and/or rate-limited desorption should be considered as demonstrated in Carey et al. (2014a).

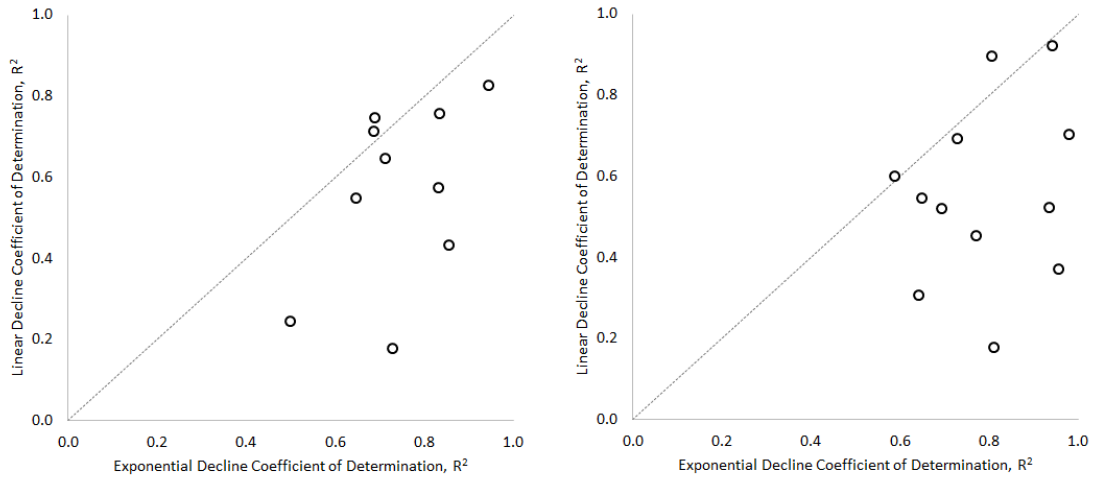

Figure 2.9 – Scatter plots of linear versus exponential decline coefficients of determination for: a) ISCO sites; and b) EISB sites.

Figure 2.10 presents a scatter plot of the exponential source concentration half-life versus the ratio of pre-treatment concentration (C_o) to COC solubility (S). One site has a C_o/S ratio less than 1 percent because the maximum concentration was

observed to be higher than 1 percent (i.e. the ratio indicating potential DNAPL presence) after treatment had started at the site. As shown on Figure 2.10, there is a general correlation between decline half-life and C_o/S ratio, in that the exponential half-life rate tends to decrease with higher C_o/S ratios. When a power model is fit to the data, the exponential rate is determined to be approximately proportional to the inverse square root of the C_o/S ratio with an R^2 of 0.49. This correlation may reflect that the higher pre-treatment concentrations may represent a higher degree of readily accessible DNAPL, which is consistent with a lower (i.e. more rapid) exponential decline half-life for EISB. That is, the more easily a reagent can contact DNAPL, the more rapid the decline in source strength (MdR) will be.

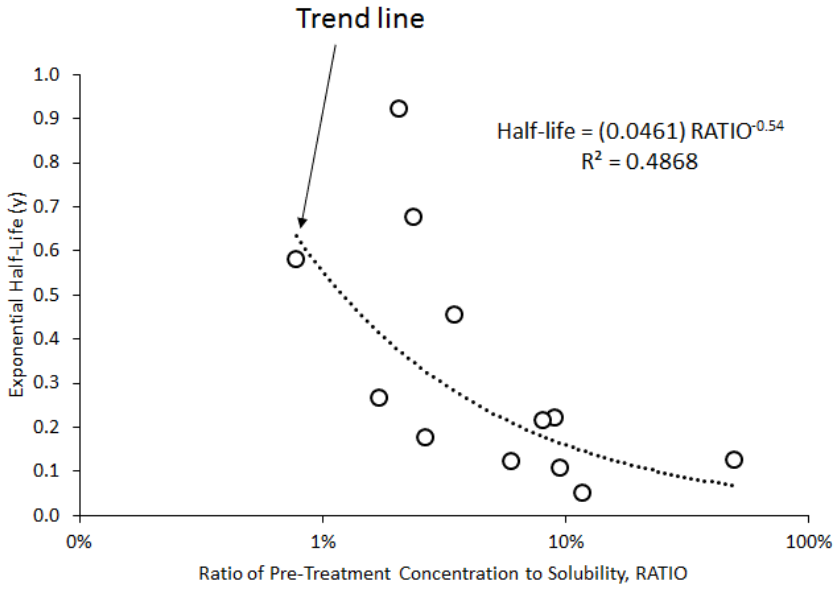

Figure 2.10 – Scatter plot of EISB exponential decline rate versus ratio of pre-treatment concentration to solubility.

2.4.2 Apparent Mean Decline Rates

As noted above, less than 40 percent of the available ISCO and EISB monitoring wells had general declining concentration trends that were suitable for regression of an exponential decline rate. Wells which had an initial decrease in concentration, followed by a sharp increase (and sometimes subsequent decline) were not used in the regression analysis. To compare ISCO and EISB decline rates, it was preferable to use a statistic which was based on all monitoring well data and not just a minority of wells as was used for the regression analysis. To accomplish this, apparent mean decline rates for ISCO and EISB sites were calculated based on the ratio of observed source concentration reduction (MdR) and the time in which this reduction was observed to occur, using

$$\lambda_a = \frac{\ln(MdR)}{t_f} \tag{2.6}$$

where λ_a is the mean apparent decline rate at each site, *MdR* is the mean ratio of the pre-treatment concentration to the concentration measured at or near the end of the available monitoring period based on all source wells at a site, and t_f is the arithmetic average of the final monitoring time for each site. Carey et al. (2014a) document the methodology used to estimate *MdR* and t_f for each ISCO and EISB site.

Table 2.3 presents the mean *MdR* and t_f determined for each ISCO and EISB site. As reported in Carey et al. (2014a), the mean *MdR* (i.e., concentration reduction)

for the 13 ISCO sites was a factor of 21, with a 95 percent confidence interval for the mean *MdR* of 4 to 110. Two of the 13 ISCO sites had a final concentration that was greater than the average pre-treatment concentration (i.e., *MdR* < 1). For the 16 EISB sites the mean *MdR* was a factor of 105 with a 95 percent confidence interval for the mean *MdR* of 20 to 556. None of the EISB sites had final concentrations that were higher than the average pre-treatment concentration. These results are discussed further in Carey et al. (2014a).

Table 2.3 – Site mean concentration reductions and final time of concentration monitoring after start of treatment.

Treatment Technology	Site ID	Chemical of Concern	Site Mean Reduction in Concentration, MdR	Final Time of Concentation Monitoring, t_f (y)
ISCO	C-04	PCE	112.7	2.83
ISCO	C-05	PCE	8.0	2.01
ISCO	C-07	PCE	170.6	2.98
ISCO	C-09	PCE	7.4	1.67
ISCO	C-10	PCE	677.2	0.40
ISCO	C-11	PCE	9.2	1.88
ISCO	C-13	PCE	8.6	3.31
ISCO	C-14	PCE	0.2	2.90
ISCO	C-15	Chlorobenzene	1.3	2.38
ISCO	C-17	PCE	183.1	0.58
ISCO	C-19	PCE	237.0	0.63
ISCO	C-21	TCE	0.4	0.30
ISCO	C-23	TCE	578.8	0.41
EISB	B-01	PCE	28.0	3.11
EISB	B-02	PCE	30.8	1.77
EISB	B-03	PCE	13.5	0.91
EISB	B-05	TCE	659.1	2.58
EISB	B-08	PCE	11463.3	2.45
EISB	B-10	PCE	44899.9	3.31
EISB	B-11	PCE	1386.9	3.79
EISB	B-13	TCE	3.1	0.72
EISB	B-14	PCE	133.5	0.42
EISB	B-15	PCE	104.7	3.37
EISB	B-16	PCE	3.1	2.86
EISB	B-19	TCE	78.4	0.42
EISB	B-20	PCE	11735.5	1.30
EISB	B-23	TCE	13.2	0.42
EISB	B-24	TCE	8.4	2.83
EISB	B-25	TCE	2.7	0.75

Based on the t_f values presented in Table 2.3, the mean t_f for ISCO and EISB sites is 1.7 and 1.9 years, respectively, with 95 percent confidence intervals on the mean t_f of 1.0 to 2.4 years and 1.3 to 2.6 years, respectively. Based on these data, the mean apparent decline rate (λ_a) for ISCO and EISB sites is 1.78 and 2.40 per years, respectively, with corresponding half-lives of 0.39 and 0.29 years, respectively. Similarly, the 95 percent confidence intervals for half-lives (based on rate calculations) for ISCO and EISB sites are 0.15 to 1.20 years and 0.14 to 0.60 years, respectively.

As discussed above, the EISB source strength decline rate for a pool-dominated source zone (12 TCE pools) has a corresponding half-life of 2.5 years based on the NDM simulation. The mean concentration decline rate determined for the EISB empirical study sites is approximately one order-of-magnitude faster than the NDM simulation for a site with 12 TCE pools. To further evaluate whether the mean decline half-life (0.29 year) determined for the EISB study sites could be representative of sites with a low ganglia-to-pool ratio, NDM was used to simulate surface discharge decline rates for TCE pools with: width of 1 m; lengths of 0.1, 0.2, 0.5, 1, 2, and 3 m; and thicknesses of 1, 2, 5, and 10 cm. Figure 2.11 presents the calculated half-life for each of these pool cases based on the surface discharge versus time simulated using NDM. As shown on this exhibit, the mean and mean confidence interval apparent decline rates determined for the EISB empirical study sites are

consistent with only a few of the TCE pool cases discussed above (i.e., pool thickness of 1 cm with length up to 1 m, or pool thickness of 2 cm with length up to 0.2 m).

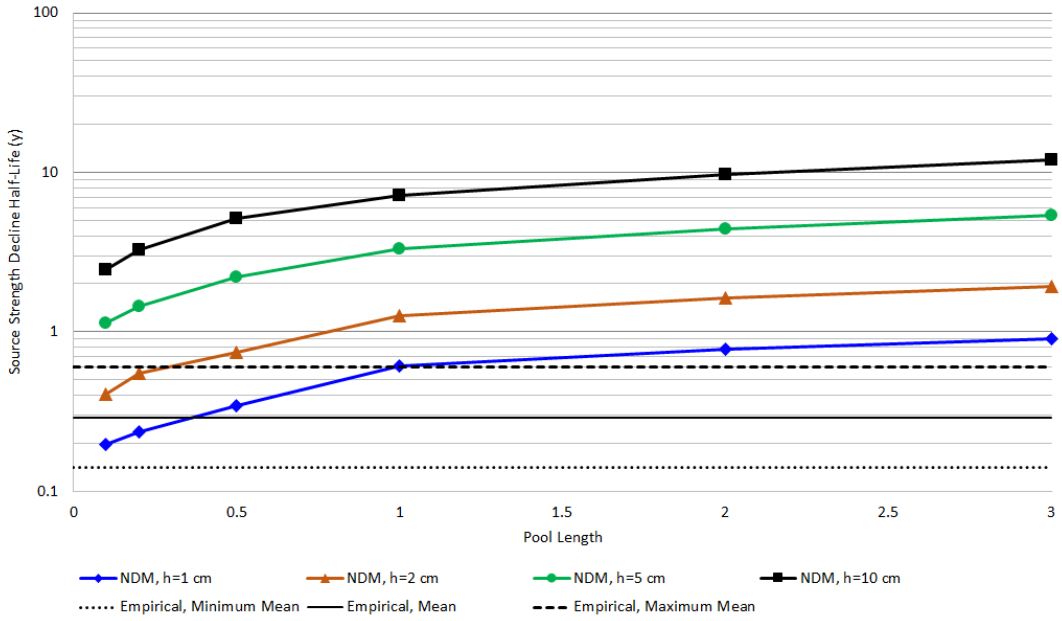

Figure 2.11 – Simulated single pool mass discharge decline half-life and empirical site concentration reduction half-lives for EISB. *h* refers to the pool thickness simulated using NDM.

One possible explanation for the difference between the fast decline rates determined for the empirical study sites and the slower decline rates for most of the NDM pool simulations is that the sites used for the empirical analysis were simply not representative of conditions assumed for the NDM simulations. This could be because ganglia dissolution is still a dominant process occurring at the empirical DNAPL study sites. This difference for EISB sites may also be due to the high number of EISB sites

(92 percent) characterized as consisting predominantly of fine-grained materials like silt and clay, which contrasts with the NDM simulations that were based on a fine to medium sand matrix. Given that many of the EISB sites have a slow groundwater velocity which is typically associated with a slow rate of source strength decline (see Equation 2.5), the observation of relatively rapid decline rates determined for thes sites indicate either little DNAPL remained at these sites, or preferential pathways result in non-ideal conditions for DNAPL depletion.

It is also possible that the implementation of EISB at the case study sites resulted in sustained treatment zones between the DNAPL source and the monitoring wells used to report concentration trends. The NDM model does not consider the effects of enhanced aqueous degradation downgradient of the DNAPL source which would effectively increase the *MdR* associated with EISB when measured at wells some distance downgradient of the DNAPL source. The occurrence of sustained biodegradation treatment zones after the initial injection events at EISB was discussed in McGuire et al. (2006). If the EISB decline rates were representative of DNAPL source zones in fine-grained materials, then the actual DNAPL depletion would likely be relatively small and the enhanced *MdR* would probably correspond primarily to enhanced aqueous degradation downgradient of the DNAPL.

To help clarify which of the above explanations may be most plausible, the ISCO depletion rate is compared to data presented by Brusseau et al. (2011) in a study of plume strength reduction after implementation of ISCO and SVE at a large,

complex TCE DNAPL site. Full-scale implementation of ISCO occurred at the site in Tuscon, Arizona between December 2002 and August 2006, and the observed plume strength based on Figure 4 in Brusseau et al. (2011) was reduced from 200 kg/y to 50 kg/y over a five-year period corresponding generally to the period of full-scale ISCO implementation. This observed *MdR* of 4 over a period of five years for the Tuscon site corresponds to a half-life of 2.5 years. While this aqueous mass discharge decline half-life is based on plume strength data some distance downgradient of the source zone, it is assumed for this example to correspond to the half-life for source strength decline resulting from ISCO implementation.

The decline half-life determined for the Tucson site is close to an order-of-magnitude higher than the mean decline half-life (0.39 year) determined for the ISCO case study sites presented in Table 2.2, and is even higher than the maximum half-life determined for mean confidence interval for the 13 ISCO case study sites (1.2 years). The discrepancy between the half-life determined for the Tucson site and the mean confidence interval for the sites used in the empirical analysis suggests that the empirical ISCO sites are not representative of decline rates expected at large, complex sites.

The ISCO and EISB empirical analysis sites (i.e., mainly dry cleaning sites and fine-grained source zones) are expected to have generally similar source zone conditions. Thus, it is assumed that the decline rates calculated based on the empirical EISB study sites are also not representative of large, complex sites or sites with pool-

dominated source zones as simulated above with NDM. The discrepancy between empirical study site decline rates, and the Tucson ISCO site or the NDM pool-dominated EISB simulation, is likely caused by differences in the ganglia-to-pool ratio between the empirical and latter sites, or because of complex geologic conditions at some sites which may reduce source strength decline rates during enhanced DNAPL treatment. It should be also noted that the empirical study sites are primarily dry cleaning sites and characterized as having predominantly fine-grained materials and, thus, will not be representative of other types of sites or geologic/hydrogeologic environments.

2.4.3 Estimating DNAPL Depletion Timeframe

The time (t_{goal}) required to attain an interim goal for the reduction in source strength (MdR) based on natural or enhanced dissolution may be determined using $t_{goal} = \ln(MdR)/\lambda_a$.

For smaller DNAPL sites that have a relatively high ganglia-to-pool ratio (e.g., fresh sources or relatively homogeneous geology) and/or predominantly fine-grained soils, the mean rates determined for ISCO and EISB sites may be applicable for predicting the time required to attain reduction goals. For large, complex sites or pool-dominated source zones, a higher half-life may be applicable when estimating

depletion timeframe (e.g., 2.5 years based on Brusseau et al. (2011) or the simulation of TCE pools with thicknesses of only 2 to 4 cm).

In some cases it may help to use a semi-analytical process-oriented model like NDM to simulate the sensitivity of the depletion timeframe to various physical and chemical processes. Simulations are typically conducted in a matter of seconds, and an improved understanding of critical site characteristics may help with planning field investigations in support of a feasibility evaluation.

2.5 Conclusions

To date there has been little work published providing insights on the rate of source strength (i.e., mass discharge) reduction that can be expected for enhanced dissolution technologies such as ISCO and EISB. Simulations of TCE DNAPL pool depletion using analytical solutions and the semi-analytical NDM were conducted to evaluate the sensitivity of source strength decline rates to various physical and chemical properties. Depletion of a DNAPL pool causes the length of the pool to decline over time, which has a corresponding reduction in the pool surface discharge over time. Naturally occurring pool depletion half-lives are proportional to the square root of the length of the pool and are linearly proportional to the thickness of the pool.

Constant-length pool discharge models (CLM) are not sufficient for evaluating DNAPL pool decline rates. Through-pool discharge was shown to be a potentially

significant process that reduces the DNAPL pool depletion timeframe, particularly for thin pools or from the upper regions of thicker pools. The pool decline half-life is shown to be generally proportional to solubility for single component DNAPLs.

The median naturally-occurring TCE DNAPL depletion half-life of 6.1 years reported in Newell et al. (2006) is shown to be consistent with pool-dominated source zones. A naturally-occurring source strength decline half-life of 7.5 years was estimated for a large, complex site in Tuscon, Arizona based on data reported in Brusseau et al. (2011). The median TCE decline half-life of 1.6 years determined by Suarez et al. (2004) appears to be too rapid to be representative of most pool-dominated source zones.

An empirical analysis was conducted to evaluate average concentration decline rates for ISCO and EISB sites, which are considered generally representive of source strength decline rates based on the statistical methodology employed in this study. The database used for this empirical analysis is based on the original database prepared by McGuire et al. (2006) for a project funded by SERDP. The main change to the database used for this study relative to the original McGuire et al. database is the exclusion of wells with concentrations that are not sufficiently high to indicate potential DNAPL presence. 13 ISCO sites and 16 EISB sites are available for the declining rate empirical analysis, with a total of 27 and 31 wells available, respectively.

Analysis of regression results for wells with generally declining trends indicates that the exponential decline model is a reasonable if not the best representation relative to a linear regression. Less than 40 percent of the ISCO and EISB wells exhibited general declining concentration trends that were deemed suitable for the regression analysis. The mean normalized decline rates calculated for ISCO and EISB sites show a concentration decline half-life for ISCO sites of 0.39 year, with a 95 percent confidence interval of 0.15 to 1.20 years. The mean concentration decline half-life for EISB sites is 0.29 years, with a confidence interval of 0.14 to 0.60 years.

The EISB empirical study sites have a decline rate that is significantly lower than expected for a pool-dominated source zone. EISB is simulated using NDM to have a corresponding decline half-life of 2.5 years for a pool-dominated source zone with 12 TCE pools with lengths and widths of several meters and thicknesses ranging from 2 to 4 cm. Data from a case study presented by Brusseau et al. (2011) are used to calculate an ISCO-enhanced decline half-life of 2.5 years for a large, complex site in Tucson, Arizona. Limitations in the general representativeness of the empirical study dataset are that most of the decline data are based on dry cleaning sites with source zone geology characterized as fine-grained (clay, silt, and/or silt/clayey sand).

2.6 References

Basu, N.B., Fure, A.D., & Jawitz, J.W. (2008). Predicting dense nonaqueous phase liquid dissolution using a simplified source depletion model parameterized with partitioning tracers. Water Resources Research, 44, W07414.

Brusseau, M. L., Hatton, J., & DiGuiseppi, W. (2011). Assessing the impact of source-zone remediation efforts at the contaminant-plume scale through analysis of contaminant mass discharge. Journal of Contaminant Hydrology, 126(3-4), 130-139.

Carey, G. R., (2014). NAPL depletion model user's guide (Version 1.0), Porewater Solutions, Ottawa, Ontario, http://www.porewater.com/NDM.htm.

Carey, G. R., & McBean, E. A. (2010). Back-diffusion and discount-rate implications for DNAPL remediation strategies, presented at the 2010 RPIC Federal Contaminated Sites Workshop, Montreal, Quebec, May 10-13, 2010.

Carey, G. R., McBean, E. A., & Feenstra, S. (2014a). DNAPL source depletion: 2. Attainable goals and cost-benefit analysis. Submitted to Remediation Journal, February 18, 2014.

Carey, G.R., McBean, E. A., & Feenstra, S. (2014b). Estimating tortuosity for diffusion based on hydraulic conductivity, in preparation.

Carey, G.R., McBean, E.A. & Feenstra, S. (2014c). Estimating DNAPL pool architecture and depletion rates based on hydraulic conductivity.

Carey, G. R., McBean, E. A., & Feenstra, S. (2014d). NAPL depletion model for evaluating performance of naturally-occurring and enhanced dissolution, in preparation.

Carey, G .R., McBean, E. A., & Feenstra, S. (2014e). Estimating vertical dispersivity based on hydraulic conductivity and groundwater velocity, in preparation.

Glover, K. C., & Munakata-Marr, J., & Illangasekare, T. H. (2007). Biologically enhanced mass transfer of tetrachloroethene from DNAPL in source zones: Experimental evaluation and influence of pool morphology. Environmental Science & Technology, 41(4), 1384-1389.

Guilbeault, M. A., Parker, B. L., & Cherry, J. A. (2005). Mass and flux distributions from DNAPL zones in sandy aquifers. Ground Water, 43(1), 70-86.

Hunt, J. R., & Sitar, N. (1988). Nonaqueous phase liquid rransport and cleanup: 1. Analysis of mechanisms. Water Resources Research, 24(8), 1247-1258.

Interstate Technology Regulatory Council (ITRC). (2010). Technology overview: Use and measurement of mass flux and mass discharge. Washington, D.C.: Author.

Interstate Technology Regulatory Council (ITRC). (2013). Use and Measurement of Mass Flux and Mass Discharge, Web Seminar.

Johnson, R. L., & Pankow, J. F. (1992). Dissolution of dense chlorinated solvents into groundwater: 2. Source functions for pools of solvent. Environmental Science & Technology, 26(5), 896-901.

Kueper, B. H., Redman, D., Starr, R. C., Reitsma, S. &Mah, M. (1993) A field experiment to study the behavior of tetrachloroethylene below the water table: Spatial distribution of residual and pooled DNAPL. Ground Water, 31, 756-766.

Kueper, B. H., & Davies, K. L. (2009). Assessment and delineation of DNAPL source zones at hazardous waste sites, EPA/600/R-09/119. Washington, D.C.: U. S. Environmental Protection Agency.

McBean, E. A., & Rovers, F.A. (1998). Statistical procedures for analysis of environmental monitoring data & risk assessment. Upper Saddle River, New Jersey: Prentice Hall.

McGuire, T. M., McDade, J. M., & Newell, C. J. (2006). Performance of DNAPL source depletion technologies at 59 chlorinated solvent-impacted sites. Ground Water Monitoring & Remediation, 26(1), 73-84.

McWhorter, D. B., & Kueper, B. H. (1996). Mechanics and mathematics of the movement of dense non-aqueous phase liquids (DNAPLs) in porous media, in Dense chlorinated solvents and other DNAPLs in groundwater: History, behavior and remediation, pp. 89-128, Portland, Oregon.

Meinardus, H. W., Dwarakanath, V., Ewing, J., Hirasaki, G. J., Jackson, R. E., Jin, M., Ginn, J. S., Londergan, J. T., Miller, C. A., & Pope, G. A. (2002). Performance assessment of NAPL remediation in heterogeneous alluvium. Journal of Contaminant Hydrology, 54, 173-193.

Moreno-Barbero, E., & Illangasekare, T.H. (2006). Influence of dense nonaqueous phase liquid pool morphology on the performance of partitioning tracer tests: Evaluation of the equilibrium assumption. Water Resources Research, 42(4), 1-11.

Newell, C.J., Cowie, I., McGuire, T.M., & McNab, W.W. (2006). Multiyear temporal changes in chlorinated solvent concentrations at 23 monitored natural attenuation sites. Journal of Environmental Engineering, 132(6), 653-663.

Parker, B. L., Cherry, J. A., Chapman, S.W., & Guilbeault, M.A. (2003). Review and analysis of chlorinated solvent dense nonaqueous phase liquid distribution at five sandy aquifers. Vadose Zone Journal, 2(2), 116-137.

Parker, B. L., Cherry, J. A., & Chapman, S. W. (2004). Field study of TCE diffusion profiles below DNAPL to assess aquitard integrity. Journal of Contaminant Hydrology, 74(1), 197-230.

Seyedabbasi, M. A., Newell, C. J., Adamson, D. T., & Sale, T. C. (2012). Relative contribution of DNAPL dissolution and matrix diffusion to the long-term persistence of chlorinated solvent source zones. Journal of Contaminant Hydrology, 134-135, 69-81.

Stroo, H. F., Leeson, A., Marqusee, J. A., Johnson, P. C., Ward, C. H., Kavanaugh, M. C., Sale, T. C., Newell, C. J., Pennell, K. D., Lebron, C. A., & Unger, M. (2012), Chlorinated Ethene source remediation: Lessons learned. Environmental Science & Technology, 46(12), 6438-6447.

Suarez, M. P., Rifai, H. S., Rittaler, T. J., & Hausman, S. (2004). Natural attenuation of chlorinated solvent plumes at Texas dry cleaners. Remediation, 2004, 14(3), 7-33.

van Genuchten, M.Th. (1980). A closed-form equation for predicting the hydraulic conductivity of unsaturated soils. Soil Science Society of America Journal, 44(5), 892-898.

Wilking, B. T., Rodriguez, D. R., & Illangasekare, T. H. (2013). Experimental study of the effects of DNAPL distribution on mass rebound. Ground Water, 51(2), 229-236.

Chapter 3

DNAPL Source Depletion: Attainable Goals and Cost-Benefit Analyses

3.1 Abstract

It is difficult to quantify the range in source strength reduction (*MdR*) which may be attainable from in-situ remediation of a DNAPL site given that available studies typically report only the median *MdR* without providing insights on site complexity which is often a governing factor. An empirical study of the performance of in-situ remediation at a wide range of DNAPL-contaminated sites determined source strength reduction factors (*MdR*) for in-situ bioremediation (EISB), in-situ chemical oxidation (ISCO), and thermal treatment remedies. Median *MdR*, geometric mean *MdR*, and lower/upper 95% confidence interval for the mean were: 49x, 105x,

20x/556x, respectively for EISB; 9x, 21x, and 4x/110x for ISCO; and, 19x, 31x, and 6x/150x for thermal treatment. Lower *MdR* values were determined for large, complex sites and for sites with DNAPL pool-dominated source zones.

A feasibility analysis of partial DNAPL depletion is described for a pool-dominated source zone. Back-diffusion from low-hydraulic conductivity units within a pool-dominated source zone is shown to potentially sustain a secondary source for more than 1,000 years, indicating that aggressive source treatment may not reduce the remediation timeframe. Estimated plume response demonstrates there may be no reduction in cost associated with aggressive treatment, and little difference in risk reduction associated with the various alternatives. Monitored natural attenuation (MNA) for the source zone is shown to be a reasonable alternative for the pool-dominated source zone considered in this example. It is demonstrated that pool-dominated source zones with a large range in initial DNAPL mass (250 to 1500 kg) may correspond to a narrow range in source strength (20 to 30 kg/y). This demonstrates that measured source strength is non-unique with respect to DNAPL mass in the subsurface, and thus source strength should not be used as the sole basis for predicting how much DNAPL mass remains or must be removed to achieve a target goal.

If aggressive source zone treatment is to be implemented due to regulatory requirements, strategic pump-and-treat is shown to be most cost effective. These remedial decisions are shown to be insensitive to a range of possible DNAPL pool

conditions. At sites with an existing pump-and-treat system, a significant increase in mass removal and source strength reduction may be achieved for a low incremental cost by strategic placement of extraction wells and pumping rate selection.

3.2 Introduction

There are thousands of complex contaminated sites which are unlikely to achieve complete groundwater restoration in a reasonable timeframe (Kavanaugh et al., 2013). In-situ treatment technologies are limited in their ability to achieve restoration at such sites, and these limitations should be more fully reflected in the decision-making process (Kavanaugh et al., 2013; Stroo et al., 2012).

Persistent dense non-aqueous phase liquid (DNAPL) presence is one of the main reasons that reductions in source strength and plume strength at complex sites are limited. While DNAPL ganglia may become depleted in a matter of years, DNAPL pools tend to create a longer term problem (Parker et al., 2003). DNAPL sites also create long-term management problems due to back-diffusion of aqueous mass arising from silts and clays which may sustain the existence of a plume for decades to centuries even after a DNAPL source zone has become depleted or isolated (Chapman and Parker, 2005; Parker et al., 2008; Sale et al., 2008; Seyedabbasi et al., 2012; Stroo et al., 2012; Kavanaugh et al., 2013).

Partial DNAPL source depletion may be all that can be expected from natural or enhanced in-situ treatment due to technological limitations and/or complex site conditions (Stroo et al., 2012; Kavanaugh et al., 2013). If it is determined that complete restoration at a site is unlikely to be achieved, or is not required to reach acceptable risk levels, then it becomes necessary to define what interim goal for source depletion may be attainable, and assess the expected remediation timeframe for partial DNAPL source treatment. In this case, the interim remedial goal may involve a target reduction in source strength (ITRC, 2010) which is defined herein as the mass discharge from a DNAPL source zone. Figure 3.1 presents a conceptual example of how site-specific interim goals for source strength reduction (*MdR*) may be used to decide when to transition from active source treatment to a more passive alternative for the remaining source. As a specific example, Lynch (2009) documents a site where an interim source strength reduction goal of 90 percent was negotiated with EPA, at which point the remedy will be transitioned from active source treatment to MNA.

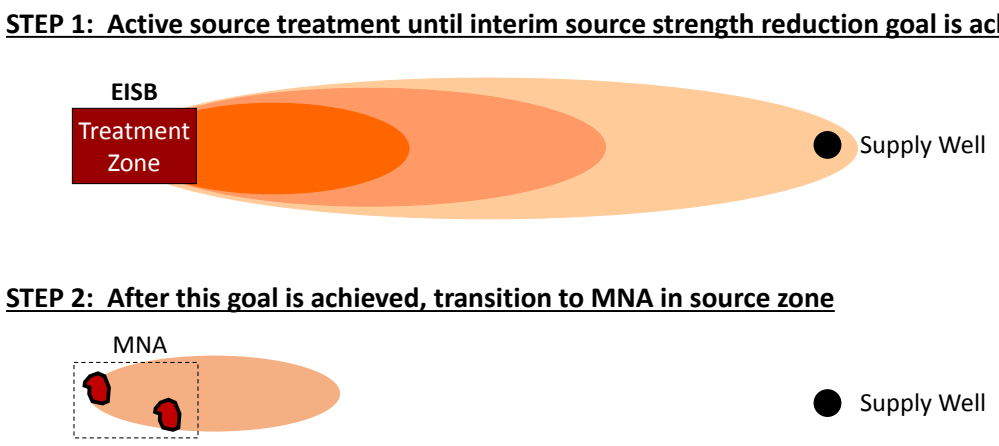

Figure 3.1 – Conceptual example using source strength reduction as an interim goal to determine when to transition from active source treatment to a more passive alternative like MNA.

There are various empirical meta-study databases that have been developed to summarize median changes to monitoring or extraction well concentrations after source treatment (e.g., McGuire et al., 2006; ESTCP, 2011; Krembs et al., 2010); however, these studies do not report the mean, or confidence interval for the mean, which may be more applicable for estimating the attainable source strength reduction factors (*MdR*) at a wide range of sites.

One of the objectives of this study is to facilitate improved estimation of attainable source strength reduction goals at DNAPL sites. An empirical analysis of source strength reduction observed at source wells indicative of DNAPL presence during in-situ chemical oxidation, enhanced in-situ bioremediation, and thermal

treatment is used to estimate the median, mean, and the 95 percent confidence interval for the mean of the source strength reduction. How the mean confidence interval may be used for estimating attainable *MdR* goals for large, complex sites is described.

Another objective of this study is to evaluate costs, benefits, and limitations associated with various methods for active or passive DNAPL source depletion. A feasibility screening analysis is presented for an example site with a pool-dominated source zone to provide a relative comparison of various treatment and containment alternatives. An analytical model is used to predict the role of back-diffusion in limiting attainable reductions in plume strength for active treatment alternatives. A companion paper (Carey et al., 2014a) reviews the range of DNAPL depletion rates expected for pool-dominated and other DNAPL source zones. This study is focused on chlorinated solvent DNAPL that is present below the water table, although the concepts discussed here are applicable to other types of non-aqueous phase liquids.

3.3 Attainable Source Strength Reduction Goals

McGuire et al. (2006) presented a study of source well concentration reductions for various DNAPL source depletion technologies including in-situ chemical oxidation (ISCO) and enhanced in situ bioremediation (EISB). Source zone monitoring well trends were evaluated as part of their study, including wells with concentrations well below 1 percent of component solubility. However, such wells

may not represent the trends downgradient of the DNAPL zone. McGuire et al. (2006) used the median concentration reduction for sites with multiple wells. However, the median may not be the most representative measure of overall source strength reductions.

The purpose of this study was to assess the mean source strength reduction (as an alternative to the median), as well as the 95 percent confidence interval of the mean to facilitate estimation of a range of reduction that may be expected during partial DNAPL depletion. In this study, a subset of the dataset used by McGuire et al. is used with only those wells exhibiting parent chemical of concern (COC) concentrations at, or greater than, 1 percent of solubility. Also, a weighted geometric mean approach based on initial well concentrations is used for sites with multiple source wells, because the mean *MdR* for a site will be influenced most by trends at wells with a high initial concentration and will influenced the least by wells with a low initial concentration. For example, the measured reduction in concentration at a well contributing 99% to the initial source strength will have a greater influence on the site mean *MdR* then a well that is contributing only 1% to the initial source strength. When there is a large range in initial concentration at source wells, this weighted mean approach provides a more accurate representation of the mean *MdR* at a site relative to an approach that provides equal weighting to all source wells.. A new empirical study of the geometric mean and corresponding confidence interval for source strength

reduction after thermal treatment is also presented, followed by a summary of results from various empirical studies reported previously.

The ISCO and EISB site dataset used for this analysis was prepared by McGuire et al. (2006) as part of a project funded by the Strategic Environmental Research and Development Program (SERDP). The dataset includes concentrations measured at between one and four monitoring wells at a variety of sites.

A subset of the McGuire et al. (2006) dataset was used for this study based on the following criteria: unconsolidated soil (fractured rock sites were excluded); the parent COC concentrations were greater than or equal to 1 percent of solubility (which is considered a potential NAPL indicator by Kueper and Davies, 2009) for at least one monitoring event in the last year of the pre-treatment period, or during or after treatment; and monitoring data were collected beyond at least the first three months after the start of treatment. Based on these criteria, there were 13 ISCO sites and 16 EISB sites with available data, and a total of 27 wells at the ISCO sites and 31 wells at the EISB sites with monitoring data. Parent COCs at these sites were mainly PCE and TCE, with only one site having chlorobenzene as the main COC. Most of the ISCO and EISB sites were described by McGuire et al. (2006) as having predominantly fine-grained geology, such as clays, silts, and/or silty/clayey sand, in the treatment zone. McGuire et al. (2006) indicate that most of the wells are situated within 13 feet of a treatment point (i.e., injection well) which suggests that these wells are within, or are in close proximity, to a DNAPL source zone.

Source strength is defined as the mass discharge that occurs at the downgradient boundary of a DNAPL source zone. To estimate the approximate source strength reduction based on concentration data for each source well, it was necessary to calculate the average pre-treatment concentration (C_o) and the final concentration (C_f), which represents the concentration at the end of the monitoring record. Monitoring well pre-treatment concentrations were calculated based on the geometric mean of all concentration results from the final year of monitoring prior to the start of treatment. A time of zero in the dataset corresponds to the time that ISCO or EISB was started at each site.

To estimate the final concentration for each monitoring well, a qualitative temporal trend analysis was conducted to identify if trends in the final year of the monitoring record were stable, increasing, or decreasing. C_f was taken as the last available concentration result for wells that were identified to have either an increasing or a decreasing trend; otherwise C_f was calculated based on the geometric mean concentration of all concentration results in the final year of the monitoring record. An increasing trend was identified if the last available concentration result was at least three times (i.e. half an order-of-magnitude) higher than the previous concentration result for the well. Similarly, a decreasing trend was identified if the last concentration result was at least three times lower than the previous concentration result. Wells that were not identified to have an increasing or decreasing trend were then identified as having a stable trend.

The *MdR* was calculated to be the ratio of the pre-treatment to the final concentration (i.e., C_o/C_f). Previous empirical studies typically refer to the percent change in concentrations or source strength; however, this does not illustrate the magnitude of large changes as well as the *MdR* factor.

For example, a source concentration reduction factor (MdR) of 10x translates to a 90 percent reduction. When multiple source wells were available at a site, a weighted geometric mean was used to estimate the site *MdR* as an alternative to the median. The disadvantage of taking a median is that it provides equal weight to all site wells regardless of their initial concentrations (i.e. contribution to initial source strength). The weighted geometric mean is used to better represent overall source strength reduction trends, where the weighting factor is based on the ratio of the individual well pre-treatment concentration to the sum of all well pre-treatment concentrations for the site. The weighted geometric mean site *MdR* and related input parameters for the calculation are shown in Table 3.1 for ISCO sites and Table 3.2 for EISB sites.

Table 3.1 – ISCO site data and calculation of Site *MdR*.

Site ID	Main Chemical of Concern	Well Name	Trend in Last Year	Pre-treatment Concentration, C_o (mg/L)	Final Concentration, C_f (mg/L)	Ratio of Pre-treatment to Final Concentration, *MdR*	*MdR*%	Weight for Geometric Mean, w_i	Weighted Geometric Mean Site MdR
C-04	PCE	MW-001	Stable	9.5	0.645	14.8	93.2%	0.49	112.7
C-04	PCE	MW-026	Stable	9.8	0.012	808.9	99.9%	0.51	
C-05	PCE	MW-110	Decreasing	0.3	0.033	8.0	87.5%	1.00	8.0
C-07	PCE	MW-2	Stable	23.2	0.126	183.8	99.5%	0.46	170.6
C-07	PCE	MW-1	Stable	26.1	2.967	183.8	99.5%	0.52	
C-07	PCE	OW-2	Stable	1.3	0.135	9.4	89.4%	0.03	
C-09	PCE	GO-MW2	Stable	19.0	2.560	7.4	86.5%	1.00	7.4
C-10	PCE	MW-1	Stable	4.1	0.005	820.3	99.9%	0.63	677.2
C-10	PCE	MW-6	Decreasing	2.5	0.005	491.9	99.8%	0.37	
C-11	PCE	MW-4	Stable	7.9	0.590	13.3	92.5%	0.92	9.2
C-11	PCE	MW-6	Stable	0.7	5.208	0.1	-651.7%	0.08	
C-13	PCE	MW-4	Decreasing	6.2	0.640	9.7	89.7%	0.68	8.6
C-13	PCE	MW-5	Stable	2.9	0.433	6.7	85.2%	0.32	
C-14	PCE	MW-1	Stable	0.7	3.186	0.2	-342.5%	1.00	0.2
C-15	Chlorobenzene	GW004	Increasing	34.0	42.500	0.8	-25.0%	0.31	1.3
C-15	Chlorobenzene	GW005	Increasing	16.0	29.500	0.5	-84.4%	0.15	
C-15	Chlorobenzene	GW008	Stable	16.0	12.000	1.3	25.0%	0.15	
C-15	Chlorobenzene	GW009	Increasing	42.5	15.000	2.8	64.7%	0.39	
C-17	PCE	MW-Y	Decreasing	119.0	0.650	183.1	99.5%	1.00	183.1
C-19	PCE	KBA-11-34	Stable	5.7	0.024	237.0	99.6%	1.00	237.0
C-21	TCE	76G	Increasing	110.2	629.506	0.2	-471.1%	0.32	0.4
C-21	TCE	86G	Increasing	224.1	315.867	0.7	-40.9%	0.65	
C-21	TCE	88G	Increasing	10.4	22.409	0.5	-116.5%	0.03	
C-23	TCE	BAT-2I	Stable	970.0	0.908	1068.2	99.9%	0.30	578.8
C-23	TCE	BAT-2S	Increasing	1110.0	0.019	58421.1	100.0%	0.34	
C-23	TCE	BAT-5I	Increasing	868.0	356.000	2.4	59.0%	0.27	
C-23	TCE	BAT-5S	Decreasing	298.0	13.300	22.4	95.5%	0.09	

Table 3.2 – EISB site data and calculation of Site *MdR*.

Site ID	Main Chemical of Concern	Well Name	Trend in Last Year	Pre-treatment Concentration, C_o (mg/L)	Final Concentration, C_f (mg/L)	Ratio of Pre-treatment to Final Concentration, *MdR*	*MdR*%	Weight for Geometric Mean, w_i	Weighted Geometric Mean Site MdR
B-01	PCE	MW-3	Decreasing	8.3	0.297	28.0	96.4%	1.00	28.0
B-02	PCE	MW-9	Stable	1.6	0.104	14.9	93.3%	0.57	30.8
B-02	PCE	MW-2	Decreasing	1.2	0.014	82.3	98.8%	0.43	
B-03	PCE	MW-3	Stable	21.3	1.577	13.5	92.6%	1.00	13.5
B-05	TCE	HGRK-VEG4	Decreasing	99.0	0.001	198000.0	100.0%	0.53	659.1
B-05	TCE	HGRK-VEG6	Stable	88.0	81.829	1.1	7.0%	0.47	
B-08	PCE	MW-019	Stable	14.5	0.001	11463.3	100.0%	1.00	11463.3
B-10	PCE	MW-1	Decreasing	16.0	0.000	133280.9	100.0%	0.81	44899.9
B-10	PCE	MW-2	Decreasing	2.1	0.073	28.9	96.5%	0.11	
B-10	PCE	MW-8	Decreasing	1.7	0.000	14208.4	100.0%	0.09	
B-11	PCE	JEMW-4	Stable	98.0	0.071	1385.9	99.9%	0.93	1386.9
B-11	PCE	MW-1	Decreasing	7.0	0.005	1400.0	99.9%	0.07	
B-13	TCE	MW-104D	Stable	55.8	18.014	3.1	67.7%	1.00	3.1
B-14	PCE	MW-1	Decreasing	23.4	0.005	4678.2	100.0%	0.55	133.5
B-14	PCE	MW-8	Stable	19.4	10.507	1.9	45.9%	0.45	
B-15	PCE	MW-2	Increasing	46.1	0.440	104.7	99.0%	1.00	104.7
B-16	PCE	MW-2	Stable	2.5	0.852	3.0	66.6%	0.64	3.1
B-16	PCE	MW-4	Stable	1.5	0.449	3.3	69.3%	0.36	
B-19	TCE	MW023	Stable	29.0	1.510	19.2	94.8%	0.21	78.4
B-19	TCE	MW024	Stable	8.2	5.583	1.5	31.9%	0.06	
B-19	TCE	Z4-17	Stable	98.9	0.600	164.7	99.4%	0.73	
B-20	PCE	EW-B	Stable	3.4	0.010	353.1	99.7%	0.09	11735.5
B-20	PCE	EW-A	Stable	2.1	0.028	74.4	98.7%	0.06	
B-20	PCE	MW-A	Decreasing	11.9	0.001	11949.9	100.0%	0.33	
B-20	PCE	MW-B	Decreasing	19.0	0.001	38000.0	100.0%	0.52	
B-23	TCE	PZ-10B	Decreasing	1700.0	74.000	23.0	95.6%	0.65	13.2
B-23	TCE	PZ-14B	Decreasing	380.0	300.000	1.3	21.1%	0.15	
B-23	TCE	PZ-16C	Decreasing	310.0	24.000	12.9	92.3%	0.12	
B-23	TCE	PZ-4B	Decreasing	210.0	20.000	10.5	90.5%	0.08	
B-24	TCE	Inside	Stable	22.7	2.698	8.4	88.1%	1.00	8.4
B-25	TCE	VE-1	Stable	26.0	9.585	2.7	63.1%	1.00	2.7

A statistical analysis based on the Shapiro-Wilks test (McBean and Rovers, 1998) confirms that the distribution of site *MdR* values follows a log-normal distribution for both the ISCO and EISB sites. For ISCO, the median *MdR of all sites* was determined to be 9x and the geometric mean *MdR* of all sites was calculated to be 21x. The geometric mean is considered to be more representative than the median for the purpose of this study because the mean considers the full range of site *MdR* results, whereas the median is simply based on the middle of the site *MdR* range. The 95

percent confidence interval of the mean *MdR* for ISCO sites is 4x to 110x based on a log-normal distribution.

Carey et al. (2014a) describe the MdR estimate of 4x for a large, complex ISCO site in Tuscon, Arizona based on data presented in Brusseau et al. (2011). The lower bound of the confidence interval (*MdR* = 4x) is the same as the MdR estimated for ISCO at the Tucson site. A lower *MdR* attained at a large, complex site is consistent with the expectation that simpler, smaller sites will have higher *MdR*. This suggests that the lower bound of the geometric mean confidence interval may be more appropriate to use for large, complex sites when predicting how much source strength reduction is attainable at other sites. It may also be reasonable to use the lower bound of the geometric mean confidence interval for sites with pool-dominated source zones given that some of the sites in this empirical analysis may not have significant pools present (see Carey et al., 2014a).

The median and geometric mean *MdR* for EISB sites were determined to be 49x and 105x, respectively. The mean confidence interval for EISB sites was determined to range from 20x to 556x. Note that the median values estimated for EISB and ISCO sites (49x and 9x, respectively) are generally similar to those estimated by McGuire et al. (2006) (i.e. 20x and 8x, respectively) using a larger dataset that included wells with concentrations well below 1 percent solubility.

Table 3.3 presents pre-treatment and final source strength estimates for 14 studies of thermal treatment remedies that were presented in Triplett Kingston (2008).

The source strength reduction factor (*MdR*) was calculated as part of the present study and is also included in Table 3.3. These data were confirmed to follow a log-normal distribution. The median *MdR* was determined to be 19x, and the mean source strength reduction for these 14 sites is 31x with a mean confidence interval of 6x to 150x. Figure 3.2 shows that there is generally a positive correlation between MdR and the pre-treatment source strength for thermal sites. That is, sites with large pre-treatment source strengths generally have a larger reduction in source strength after thermal treatment has been implemented.

Table 3.3 – Thermal treatment source strength data (Triplett Kingston, 2008) and calculation of Site *MdR*.

Triplett Kingston (2008) Site ID (Table 5.5)	Pre-Treatment Source Strength (kg/y)	Post-Treatment Source Strength (kg/y)	Ratio of Pre- to Post-Treatment Source Strength, MdR	MdR%	Geometric Mean Site MdR
Site 1	51.5	0.187	275.4	99.6%	275.4
Site 2	59.9	4.94 / 20.7	4.7	78.6%	4.7
Site 3	48	0.125	384.0	99.7%	384.0
Site 4	31.8	2.11	15.1	93.4%	15.1
Site 5	684	82.3	8.3	88.0%	8.3
Site 6	4.64	0.0734	63.2	98.4%	63.2
Site 7	9.42 4.93	0.0267 1.6	352.8 3.1	99.7% 67.5%	33.0
Site 8	1.71 2.43	0.595 0.969	2.9 2.5	65.2% 60.1%	2.7
Site 9	0.40	0.03	13.1	92.4%	13.1
Site 10	0.0192 2.86E-04	1.78E-07 1.07E-07	107,865.2 2,672.9	100.0% 100.0%	16,979.8
Site 11	0.0968	0.0607	1.6	37.3%	1.6
Site 12	1.24	0.0535	23.2	95.7%	23.2
Site 13	9.27 7.35	0.017 0.0163	545.3 450.9	99.8% 99.8%	495.9
Site 14	1.31	2.84	0.5	-116.8%	0.5

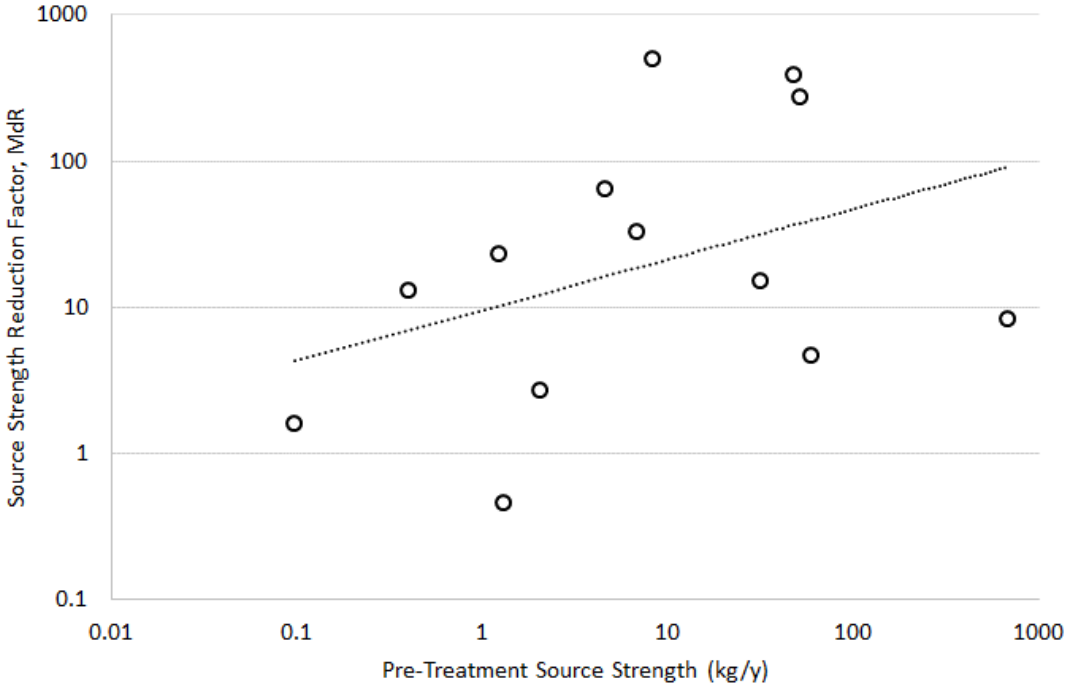

Figure 3.2 – General relationship between source strength reduction factor (*MdR*) and pre-treatment source strength (Md_o) for thermal remediation sites.

A summary of the median, mean, and mean confidence intervals for EISB, ISCO, and thermal determined in this study is presented in Table 3.4. The ratio of the upper and lower bounds on the mean confidence interval for all three technologies is approximately similar (25), indicating that there is a wide but similar distribution of depletion performance for all three technologies.

Table 3.4 – MdR statistics based on this study for ISCO, EISB, and thermal treatment at DNAPL sites.

	Site MdR Statistics				
Technology	Median	Mean	Mean 95% Confidence Interval	Minimum	Maximum
EISB	49	105	20 to 556	2.7	44,900
ISCO	9	21	4 to 110	0.2	677
Thermal	19	31	6 to150	0.5	16,980

Figure 3.3 presents a comparison of the median *MdR* determined for EISB, ISCO, and thermal sites in various empirical analyses including this study, McGuire et al. (2006), Krembs et al. (2010), and a search of the Chlorinated Solvent DNAPL Technology Evaluation Screening Tool (DNAPL TEST v1.0) which is described in ESTCP (2011). This figure shows that there is a general trend for high *MdR* factors when the parent compound concentration factors are used, and lower *MdR* factors when total volatile organic compound (TVOC) concentrations are used. This relationship should be considered when using published *MdR* values to estimate an attainable technology-specific *MdR* for a site. Also, while the median values represent the middle performance of the sites included in each empirical study, these median values may not be representative of a specific site of interest for which *MdR* needs to be estimated. Thus, the lower bound of the mean confidence interval determined in this study may be more useful, particularly when *MdR* is needed for a large, complex

site. Similar guidance is recommended for pool-dominated source zones which do not seem well represented in the EISB and ISCO site database used in the present study, based on a comparison of DNAPL depletion rates derived for these sites with simulations of pooled (i.e. layers of free phase DNAPL) using the NAPL Depletion Model (Carey et al., 2014a).

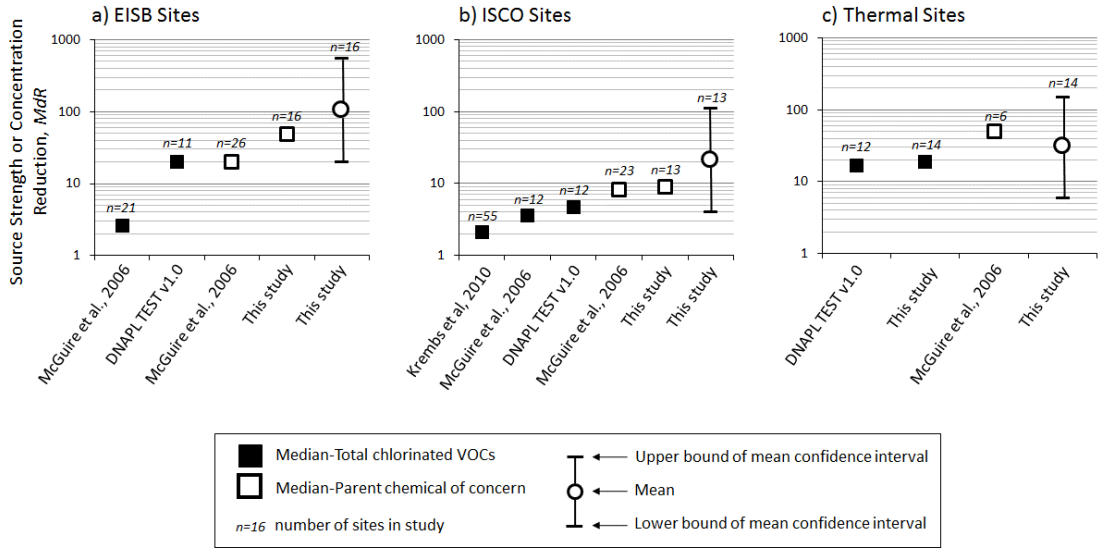

Figure 3.3 – Median concentration or source strength reduction (MdR) for EISB, ISCO, and thermal treatment sites based on various empirical studies.

3.4 Example Feasibility Analysis

As discussed above, there are natural and technological limitations which make it difficult, if not impracticable, to achieve complete groundwater restoration at DNAPL sites in a reasonable timeframe. At sites where it is recognized that complete

restoration is not attainable, there is often a question about the benefit which may be achieved by implementing an aggressive DNAPL depletion treatment strategy. An example feasibility screening analysis is presented to demonstrate how prediction of attainable interim source strength reduction goals and DNAPL depletion timeframe may be used to evaluate this question. The example analysis is based on a hypothetical site whose source zone is pool-dominated, similar to sites described in Parker et al. (2003 and 2004), Chapman and Parker (2005), and Guilbeault et al., (2005).

3.4.1 Site Setting

The site is conceptualized as having had TCE DNAPL releases over time, the last release occurring approximately 20 years ago. A river representing a regional discharge boundary is 300 meters (m) downgradient of the site source zone. The property between the site and the river is in the floodplain and is void of residential or commercial development. The river is the receptor of concern for groundwater contamination. There are no planned changes in land use or real estate transactions which would influence the target timeframe for achieving remedial goals for the site.

Since the last release, DNAPL ganglia have been depleted due to natural dissolution, and only the horizontal DNAPL pools remain. The site source zone is characterized as having 12 TCE DNAPL pools with horizontal dimensions as

specified in Seyedabbasi et al. (2012) and Anderson et al. (1992), with individual pool lengths and widths ranging from two to four meters.

The base case scenario for this analysis defines pool thicknesses that range from 2 to 20 cm. Typically, the distribution in pool thickness is not known explicitly at a site so a probabilistic analysis of the thickness of individual pools may be required. For this study, a sensitivity analysis is conducted (see below) to evaluate how different distributions of pool thickness and through-pool discharge (Carey et al. (2014a) influence DNAPL deletion timeframe and the final remedial decision.

The length and width of the DNAPL source zone are 20 m each, and the total depth of the source zone is 15 m, resulting in an approximate DNAPL source zone volume of 6,000 m^3. The source zone dimensions are similar in magnitude to the New Hampshire site PCE DNAPL source zone described by Guilbeault et al. (2005). For example, the New Hampshire DNAPL source zone has a length, width, and height of approximately 5, 17, and 14 m, respectively. A transect located 3 m downgradient of the New Hampshire site source zone indicate there were 15 local PCE hot spots (i.e., potential pools or layers of DNAPL), and a cross-section presented by Guilbeault et al. illustrates that individual hot spot widths perpendicular to groundwater flow are on the order of several meters in the source zone.

The saturated thickness of the mildly heterogeneous, unconfined sand aquifer in this example is approximately 15 m, and the aquifer overlies a thick, continuous clay aquitard. The average aquifer hydraulic conductivity is 0.01 centimeters per

second (cm/s), the horizontal hydraulic gradient is 0.003, effective porosity is 0.20, and the average linear groundwater velocity is approximately 47 meters per year (m/y). The retardation coefficient for TCE is 2.1.

The source strength (i.e., mass discharge measured directly downgradient of the source zone) is 25 kilograms per year (kg/y), and the plume strength is estimated to be 35 kg/y based on a transect of monitoring wells 270 m downgradient of the source zone. The increase in mass discharge with distance downgradient from the source zone is consistent with a declining source strength over time (i.e., the source strength earlier in time was more than 35 kg/y). TCE biodegradation in the aerobic aquifer is negligible. Data from the past five years of monitoring of the source zone indicate that the source strength is declining with a half-life of approximately 30 years, which is consistent with a pool-dominated source zone where the pools are relatively long and/or thick.

A two-dimensional (2-D) groundwater flow (MODFLOW) and chemical transport model (MT3DMS) was developed to simulate the extent of the aqueous plume downgradient from the source zone, and to evaluate the pumping rates required for containment of the source zone and/or plume, or for a strategic pump-and-treat alternative for source zone treatment (see Figure 3.7). The model utilized uniform horizontal grid spacing of 4 m outside the source zone and 1 m inside the source zone. The model simulated a TCE aqueous plume width of approximately 70 m at a distance of 270 m downgradient of the source zone. The plume is defined based on a

hypothetical risk-based cleanup criterion of 0.05 mg/L for TCE which is derived from a conservative mixing factor applied at the river receptor.

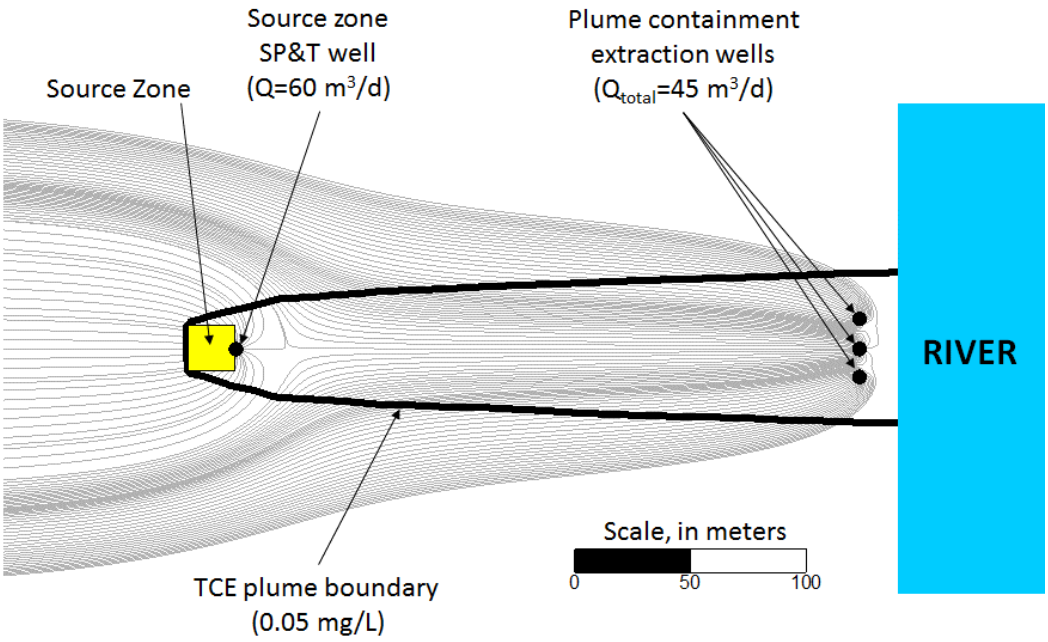

Figure 3.7 – Simulated pre-treatment plume boundary (TCE 0.05 mg/L) and extraction well capture zones for alternative with SP&T for source zone treatment and P&T for plume containment.

3.4.2 Influence of Back-Diffusion on Remediation Timeframe

It is important also to evaluate the role that back-diffusion may have on remediation timeframe. Both the DNAPL source zone and the downgradient groundwater plume occur at the site in a sand aquifer (i.e., *transmissive zone*) directly over a thick clay aquitard (i.e., *low-K zone*), which has been building up aqueous mass

in storage through the process of forward diffusion over multiple decades. The Matrix Diffusion ToolKit (Farhat et al., 2012), which was developed with funding from the Environmental Security Technology Certification Program (ESTCP), offers an analytical solution based on the Dandy-Sale Model (Sale et al., 2008) for evaluating how long it may take to reach cleanup levels after a DNAPL pool becomes completely depleted or contained.

The 2-D cross-section Dandy-Sale Model simulates the aqueous plume in the transmissive zone, and the build-up of mass due to forward diffusion into an underlying low-K zone (minimum thickness of 1 m) while the DNAPL layer is present. The Dandy-Sale Model also simulates the influence of back-diffusion from the aquitard as a secondary source that may sustain an aqueous plume in the overlying transmissive zone. The Matrix Diffusion ToolKit provided a useful interface for simulating this complex problem.

The Dandy-Sale Model was used in this example to simulate the concentration versus time that would be measured in monitoring wells having a 10-foot screen situated directly above the low-permeability zone at various distances downgradient of the source zone. The simulation assumed that at least one TCE DNAPL pool occurs at the site directly above the interface between the transmissive and low-permeability zones, and that this DNAPL was present from 1970 through 2014 at which time the DNAPL became contained, or depleted, through a future remedial action. Figure 3.4 presents a schematic diagram of back-diffusion that was simulated from the low-

permeability zone contributing to the aqueous plume observed in a monitoring well 270 m downgradient of the source zone.

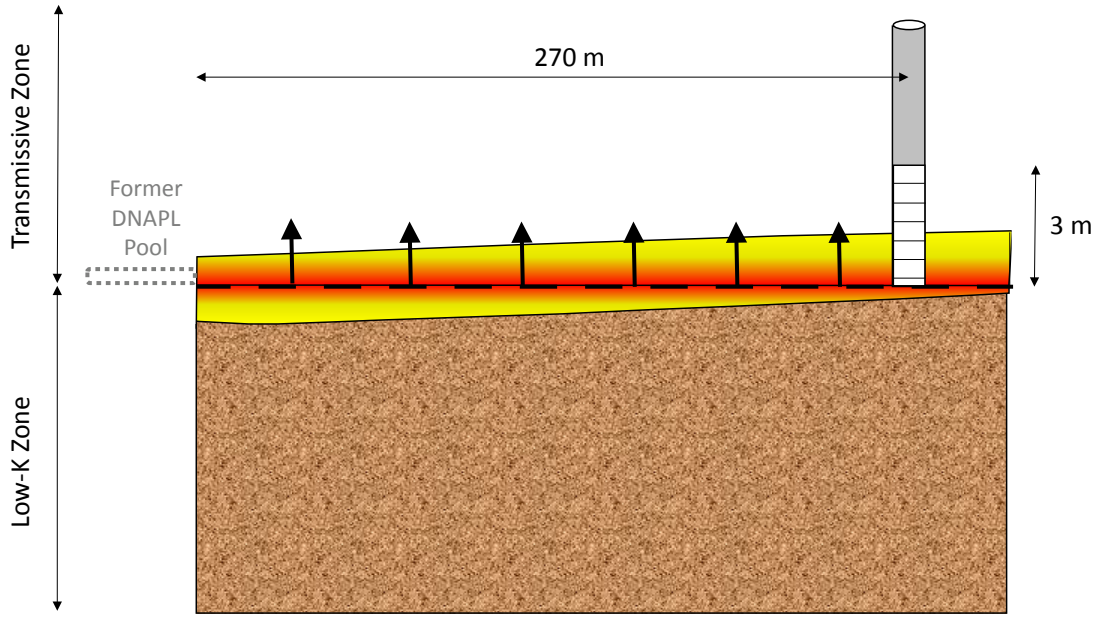

Figure 3.4 – Schematic diagram of simulated back-diffusion after a DNAPL pool becomes depleted or contained.

Figure 3.5 shows the simulated concentration versus distance that would be observed in transmissive zone monitoring wells at a time of zero and 40 years after containment or depletion of the DNAPL pool. This figure shows that some time after the source contribution to the plume has ceased, the TCE concentration in the transmissive zone increases with distance downgradient of the source, TCE concentrations close to the source declined in response to the source control remedy, but higher concentrations released previously from the source continue to migrate

downgradient. This is consistent with observations in laboratory experiments noted by Sale et al. (2008). The figure demonstrates that complete source depletion or containment results in a greater benefit (in terms of concentration reduction) for the portion of the transmissive zone closest to the source zone, and that the benefit from source treatment/containment declines with increasing distance from the source zone.

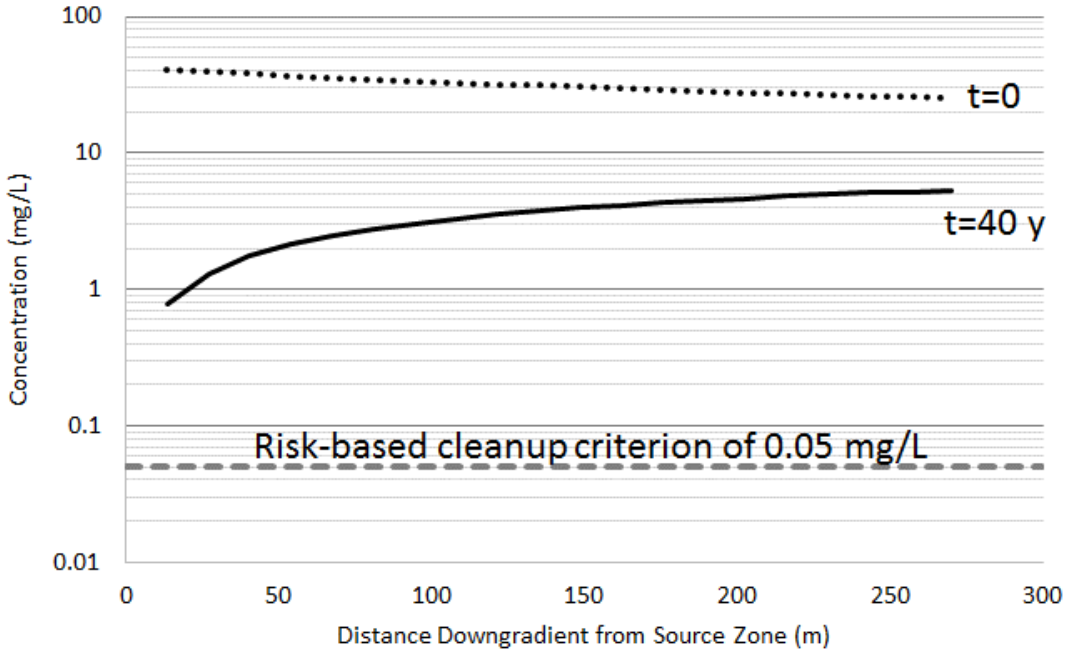

Figure 3.5 – Simulated TCE concentrations versus distance at times of zero and 40 years after the depletion or containment of a DNAPL pool.

Figure 3.5 also illustrates that 40 years after source depletion or containment, the TCE concentration at a monitoring well 270 m downgradient of the source zone and screened directly above the low-permeability zone would be 5 mg/L. The TCE

concentration was simulated to be 25 mg/L in this same well just prior to the source depletion (i.e., at a time of zero). This trend is similar to what was observed at a Connecticut site (Chapman and Parker, 2005) where back-diffusion was shown to have limited the decline in groundwater concentration after isolation of a large DNAPL pool with a sheetpile wall.

In our example there is a concentration reduction of only 5x in this well as a result of back-diffusion, even 40 years after the source has been completely depleted or contained. This indicates that aggressive source treatment alternatives that may cause a reduction in source strength of an order-of-magnitude or more in a short period of time, are not necessarily warranted for this site given that significant declines in source strength will take longer than 40 years to manifest themselves in downgradient plume strength at a distance of 270 m due to back-diffusion. It is also important to note that the model results were based on the assumption of a source strength declining to zero in 2014, so simulated concentrations are lower than what would be expected for a DNAPL remedy which achieved only partial cleanup of the DNAPL source.

Figure 3.6 shows the concentration versus time simulated to occur in a monitoring well directly above the low-permeability zone at a distance of 270 m downgradient from the source zone. This figure indicates that plume concentrations are relatively stable for at least 10 years after containment or complete depletion of the source because the travel time of the depleted front to this well is approximately 12

years from the source. After this time, concentrations at this well decline over time at a rate that is consistent with the power law decline model (i.e. the concentration versus time curve is linear on a log-log plot). Factors that contribute to the slope of this decline curve may include groundwater velocity in the transmissive zone, retardation coefficients in the transmissive and low-permeability zones, and the duration of the initial DNAPL presence (assuming zero biodegradation), although a sensitivity analysis would be needed to confirm the relative influence of these factors and is beyond the scope of this study.

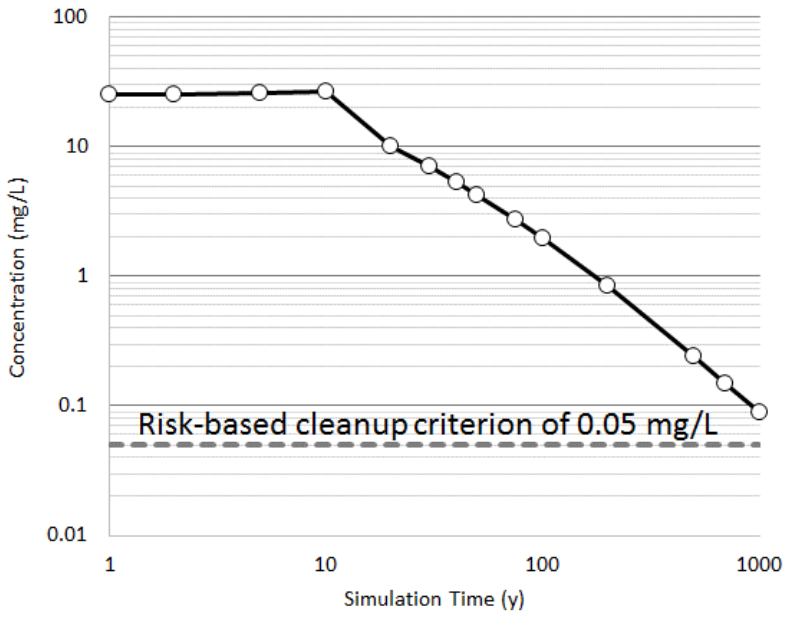

Figure 3.6 – Simulated monitoring well TCE concentrations versus time post-DNAPL depletion or containment at a monitoring well situated 270 m downgradient of the original source zone.

The important result shown in Figure 3.6 is that concentrations at a monitoring well 270 m downgradient of the source zone take more than 1,000 years to reach the risk-based cleanup level of 0.05 mg/L, after the source has been completely depleted or contained. This result is important because it shows that even if the DNAPL pool were completely removed at the top of the aquitard in this example, containment or treatment of the plume is likely still required at the site for more than 1,000 years into the future due to back-diffusion from the aquitard. This suggests that aggressive source zone remediation will not be beneficial for this site in terms of a reduction to the overall remediation timeframe. There may be other benefits, however, such as risk reduction or a reduction in lifecycle costs which will be evaluated below.

3.4.3 Treatment and Containment Alternatives

The site in this example has recently had a remedial investigation completed, and no remedial actions have been conducted to date. As discussed above, even if source zone treatment was completely successful in terms of removal of all DNAPL in the source zone, there are long-term plume mitigation actions needed to protect the river as a result of back-diffusion that occurs downgradient of the source zone. Thus, it is important to conduct an integrated assessment of both source zone and downgradient plume mitigation concurrently.

Both active and passive alternatives were considered for the source zone. Active alternatives included thermal treatment, ISCO, EISB, strategic pump and treat (SP&T; which provides containment and also treatment through enhanced dissolution), and pump and treat (P&T; which is more of a containment alternative but has a minor treatment benefit because of a slight increase in groundwater velocity in the source zone). Passive alternatives for the source zone considered in this analysis included MNA (i.e., naturally-occurring dissolution), and a permeable reactive barrier (PRB) to effectively contain the source zone (which results in DNAPL depletion through naturally-occurring dissolution). For plume management, two containment alternatives were considered: P&T or a PRB at a distance of 270 m downgradient of the source zone (i.e., 30 m upgradient of the river).

The 2-D areal groundwater flow model (MODFLOW) was used to confirm pumping rates for four alternatives:

a) Source zone P&T – minimum rates needed for containment of the source zone using one well (15 m^3/d);
b) Source zone SP&T – increased pumping rates (60 m^3/d) and enhanced groundwater velocity in the source zone which results in a corresponding enhancement of DNAPL dissolution;
c) Plume P&T - containment using three pumping wells at a distance of 270 m downgradient of the source zone (total rate of 60 m^3/d); and

d) Combined source zone SP&T and plume P&T (60 m^3/d for the source zone pumping well, and a total rate of 45 m^3/d for the plume pumping wells).

Figure 3.8 illustrates particle pathlines simulated using MODPATH and MODFLOW for the combined source zone SP&T and plume P&T alternative.

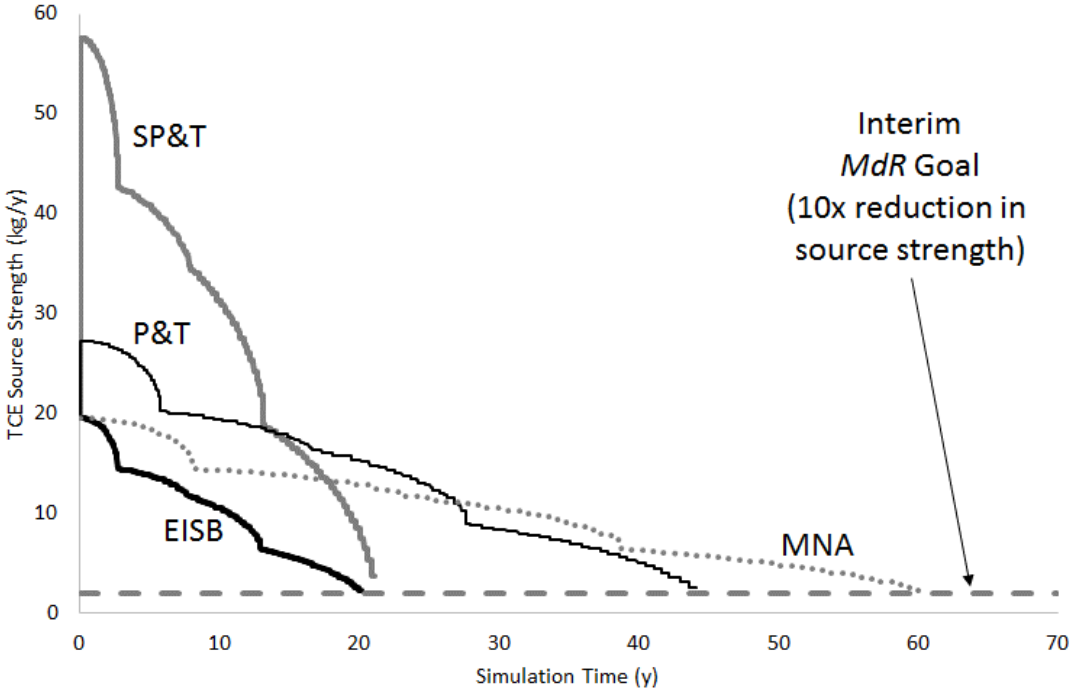

Figure 3.8 – Simulated source strength versus time for source zone treatment for base case.

3.4.4 Attainable Goals and Timeframes

Source Strength Reduction Goals

This feasibility study assumed that remediation at the site would be conducted in two phases:

- Phase I - treatment of the source zone to achieve an interim source strength reduction goal, which was defined to be the minimum attainable reduction for the various active treatment alternatives that were considered. Plume containment will also be maintained during Phase I; and
- Phase II - long-term plume containment.

Table 3.4 lists the mean, and the upper and lower confidence interval limits on the mean for the MdR (i.e., source strength reduction factor) determined for various empirical studies based on parent compound concentrations (ISCO and EISB sites) or total VOCs (thermal sites). As discussed above, various lines of evidence suggest that the typical ISCO and EISB sites included in this empirical study may not be representative of pool-dominated source zone behavior. The site example for this feasibility study has a pool-dominated source zone, however. If we use the minimum mean confidence interval limits for ISCO (*MdR* of 4x) and EISB (*MdR* of 20x) then it appears that ISCO is not as efficient in achieving mass reduction for this site as EISB. Given that ISCO sites in this empirical analysis typically had an implementation period that was half that for EISB (McGuire et al., 2006), it is possible that ISCO may

achieve closer to a 10x *MdR* if applied for a longer duration than the empirical studies used in the above analysis. For this feasibility study, it was assumed that both ISCO and EISB have similar attainable *MdR* goals of 10x. It was also assumed that a similar *MdR* of 10x was attainable for SP&T and P&T alternatives for the source zone. Note that the plume strength associated with SP&T and P&T will decline much faster than for EISB or ISCO because the former two alternatives result in containment of the source zone, whereas the latter two alternatives allow for continued downgradient migration; the benefits of this additional plume strength reduction are not quantified as part of this feasibility analysis.

As shown in Figure 3.2 and as discussed above, the *MdR* for thermal sites had a general correlation to the pre-treatment source strength. The mean *MdR* for thermal sites as shown in Table 4 is 31x. Of the 14 thermal sites listed in Table 3, 4 sites had pre-treatment source strengths between 10 and 100 kg/y which is the same range as the example site used for this feasibility study. Based on a log-normal distribution, the mean *MdR* for these four sites is 47x. This was the value that was used as the attainable interim source strength reduction goal for thermal sites.

Source Depletion Timeframes

For the thermal treatment alternative, it was assumed that this action was completed in the first year of the remedial action (which corresponds to Year 0 of the

Net Present Value analysis). The time required for EISB, SP&T, P&T, and MNA to achieve a 10x reduction in source strength (i.e., the interim remedial goal) was determined by simulations using the NAPL Depletion Model (NDM), which is a process-oriented semi-analytical screening model for predicting depletion timeframes and corresponding source strength versus time trends, for naturally-occurring and enhanced dissolution alternatives (Carey, 2014). In a companion study, Carey et al. (2014a) demonstrate the application of NDM for simulating pool-dominated source zone depletion timeframes. Carey et al. (2014b) and Carey (2014) present more details on the functionality and mathematical formulations incorporated into NDM.

To evaluate the dissolution enhancements that may occur with SP&T and P&T remedies, the 2-D MODFLOW model was used to evaluate the enhanced velocity with each of these two alternatives relative to natural flow conditions. Based on the MODFLOW simulation, the minimum pumping rate required to provide containment of the 20 m wide source zone is 15 m^3/d. This results in an average increase in source zone groundwater velocity of 50 percent relative to natural flow, and as shown in the companion study by Carey et al. (2014a), this increase in groundwater velocity results in a corresponding enhancement in DNAPL pool dissolution. The MODFLOW simulation indicates that a pumping rate of 60 m^3/d results in a corresponding increase in groundwater velocity of 300 percent relative to natural flow.

The NDM simulations of the time required to achieve a 10x reduction in source strength are consistent with the approach discussed in Carey et al. (2014a) and

the input parameters discussed above. Figure 3.8 shows the simulated TCE source strength for implementation of EISB, SP&T, P&T, and MNA, respectively, for the base case where pool thicknesses range from 2 to 10 cm and through-pool discharge was not simulated.

The times to reach the goal of 10x reduction in source strength for EISB, SP&T, P&T, and MNA were simulated to be 20, 27, 45, and 61 y, respectively. This indicates that SP&T and EISB have similar depletion timeframes which contradicts what is typically said about the use of any pump-and-treat alternative (e.g., Stroo et al., 2012). While the P&T remedy, which is based on the minimum pumping rates needed to hydraulically contain the source zone, had only a minor improvement in treatment depletion rates relative to MNA, the SP&T remedy had a substantial improvement because the pumping rate was four times higher than was used in the P&T remedy (i.e., containment only). This demonstrates that when pump-and-treat is strategically employed so that wells are in close proximity to DNAPL and pumping rates are higher than typically used for containment, there may be a substantial treatment benefit which is often not considered. The use of strategic pump-and-treat has been documented at sites, such as Reese Air Force Base (Lubbock, Texas), where source discharge was enhanced through the strategic placement of additional extraction wells (ITRC, 2013). As discussed above, both the SP&T and P&T alternatives result in containment of the source zone, and thus the plume strength declines much more rapidly with these two

alternatives than with EISB or ISCO. The benefit of this additional reduction in plume strength have not been quantified in this analysis.

Figure 3.8 indicates that there is a significant increase in source strength for SP&T due to enhanced dissolution. NDM has the option of simulating source strength from total VOCs for EISB including TCE daughter products which would result in a similar increase in source strength, but Figure 3.8 only shows the simulated TCE source strength trends. NDM was not used to simulate the timeframe for ISCO because a dissolution enhancement factor has not been widely studied for this technology. Validation of NDM for simulating ISCO depletion is currently being conducted based on various laboratory studies. The ISCO depletion timeframe was assumed to be equal to the EISB timeframe, and the source zone PRB timeframe was assumed to be equal to the MNA timeframe.

3.4.5 Feasibility Screening Analysis

A screening analysis was conducted to compare the relative costs, benefits, and limitations of various alternatives for treatment and/or containment of the source zone, as well as for containment of the aqueous plume at a distance of approximately 270 m downgradient from the source zone (i.e., 30 m upgradient of the river). Due to the long-term sustained secondary source conditions created by back-diffusion from the

thick aquitard at the site, plume treatment alternatives were not considered in this analysis.

Seven source zone alternatives were included for the scenario where P&T is used for plume containment: P&T, SP&T, EISB, ISCO, thermal, PRB (adjacent to the downgradient boundary of the source zone), and MNA. These same 7 source zone alternatives were also included for the scenario where a PRB was used for plume containment, resulting in a total of 14 scenarios for the base case cost analysis. Table 3.5 presents the capital costs, deployment operation and maintenance (O&M) costs, monitoring and reporting costs (which, in this example, were calculated separately from O&M costs), as well as periodic costs for the PRB wall media replacement which were assumed to recur every ten years. Various studies were used to inform these cost estimates, including EPA (2001, 2005), Battelle (2007), McDade et al. (2005), AFCEE (2009), and ESTCP (2008).

Table 3.5 – Unit costs used for cost estimate.

Alternative	Capital Cost	Deployment O&M[1]	Monitoring & Reporting[2]	Total O&M	Periodic Cost[3]	Comment
P&T - source zone (15 m^3/d)	$250,000	$60,000	$50,000	$110,000		
P&T - plume (60 m^3/d)	$350,000	$70,000	$50,000	$120,000		
P&T - source zone and plume (75 m^3/d)	$400,000	$80,000	$100,000	$180,000		
SP&T - source zone (60 m^3/d)	$350,000	$70,000	$50,000	$120,000		
SP&T - source zone; P&T - plume (105 m^3/d)	$500,000	$100,000	$100,000	$200,000		
EISB - source zone	$400,000	$75,000	$50,000	$125,000		
ISCO - source zone	$400,000	$100,000	$50,000	$150,000		
Thermal - source zone	$1,789,534	n/a	$25,000	$25,000		
PRB - source zone	$680,000	$0	$25,000	$25,000	$226,667	media replacement every 10 y
PRB - plume	$1,530,000	$0	$50,000	$50,000	$793,333	media replacement every 10 y
MNA - source zone	$0	$0	$25,000	$25,000		

Notes:

[1] Deployment O&M costs do not include cost of monitoring and reporting

[2] Annual monitoring and reporting costs are specified as follows: active source zone treatment, $50,000; passive source zone treatment, $25,000; plume containment, $50,000 (including periodic river monitoring)

[3] Periodic cost not shown in table is $125,000 for a five-year review, which is common to all site alternatives

The P&T and SP&T O&M costs were based on the assumption that the treatment system would be located off-site near the plume extraction wells, and at a sufficient distance from developed areas that off-gas treatment is not required. The incremental annual O&M costs of SP&T or P&T ($30,000 and $10,000, respectively) are relatively minor when P&T is also used as the alternative for plume containment because the pumping rates for combined source and plume systems are relatively low for this site. These incremental O&M costs are significantly lower than the estimated annual O&M costs for EISB and ISCO, which demonstrates how cost savings may be realized when combining source zone and plume management strategies.

The EISB system was conceptualized as having an initial biostimulation and bioaugmentation phase (similar to the Dover Air Force Base (Dover, Delaware) pilot study described in ESTCP, 2008), with automated biostimulation through multi-level injection wells over the longer term. Although a recirculation system would have the added benefit of providing source zone containment, recirculation was not specified for this alternative because of the biofouling and frequent well rehabilitation which may occur in the system similar to what was reported in ESTCP (2008). While EISB is not necessarily recommended for depletion of pool-dominated source zones (Stroo et al., 2012), it is included in this analysis for relative comparison to the other alternatives. ISCO O&M costs are slightly higher than the EISB costs on the basis of more labor being involved to facilitate two or three injections per year, and a longer-lived oxidant is assumed for application given the long-term dissolution enhancements

needed for a pool-dominated source zone. ISCO and EISB were each defined to have an implementation period of 20 years for this analysis.

A limiting performance factor for EISB and ISCO is that they may result in preferential pathway development for injected reagents due to bioclogging (ESTCP, 2008), precipitation reactions (Heiderscheidt et al., 2008), or methane gas generation (ESTCP, 2008) which may divert the necessary reagents away from the DNAPL pools. The development of preferential flowpaths may contribute to a limitation in source strength reduction for these two alternatives in a pool-dominated source zone, where multiple pools occur in a relatively small source zone volume and delivery to the DNAPL-groundwater interface of each pool is an important performance criterion.

Net present values (NPV) were calculated for each of the 14 combined source zone/plume alternatives based on the methodology presented in EPA (2000). A discount factor of 7 percent was used, consistent with EPA (1993). Capital construction was assumed to occur in the first year (i.e., Year 0). Implementation of thermal treatment was assumed to be completed in Year 0 given that applications typically have durations of less than one year (Triplett Kingston, 2008; McGuire et al., 2006).

3.4.5.1 Base Case

One of the potential benefits of aggressive DNAPL source zone treatment is the future reduction in lifecycle costs such as reduced groundwater treatment costs which may be facilitated by a reduction in source strength. To evaluate the influence that the various source zone alternatives may have on treatment system influent loading, the average influent TVOC concentration was estimated for each alternative using P&T for plume containment (see Figure 3.9). These concentrations were estimated based on simulated or estimated source strength and plume strength versus time. Plug flow conditions between the source zone and the downgradient plume were assumed when estimating plume strength versus time at the downgradient P&T wells.

Figure 3.9 illustrates that the SP&T and P&T source zone alternatives and, to a lesser extent, EISB have elevated influent concentrations that are as high as 2.5 to 3 mg/L, relative to the starting influent concentration of 1.5 mg/L for the other source zone alternatives. Given that off-gas treatment is not required for this example site, these concentrations are not anticipated to result in different costs. Thus, the magnitude of source zone treatment is not expected to have a benefit in terms of reduced plume P&T costs over time.

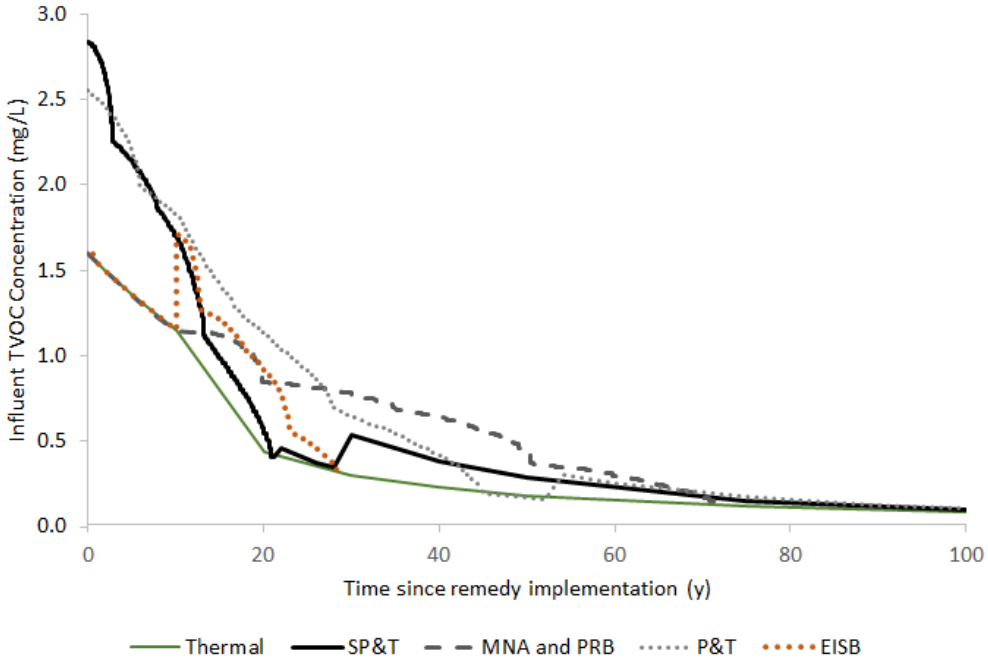

Figure 3.9 – Simulated influent TVOC concentration versus time for groundwater treatment system for various source zone treatment alternatives combined with the plume P&T alternative.

Figure 3.10 shows estimates of TVOC plume strength versus time measured at a distance of 270 m downgradient of the source zone (i.e. just upgradient of the river), providing a qualitative basis for evaluating relative risk reduction associated with each source zone alternative. The plume strength versus time expected for use of a source zone PRB is not shown although this is expected to be similar to the data shown for thermal given that both would result in significant source strength reduction within the first year of implementation.

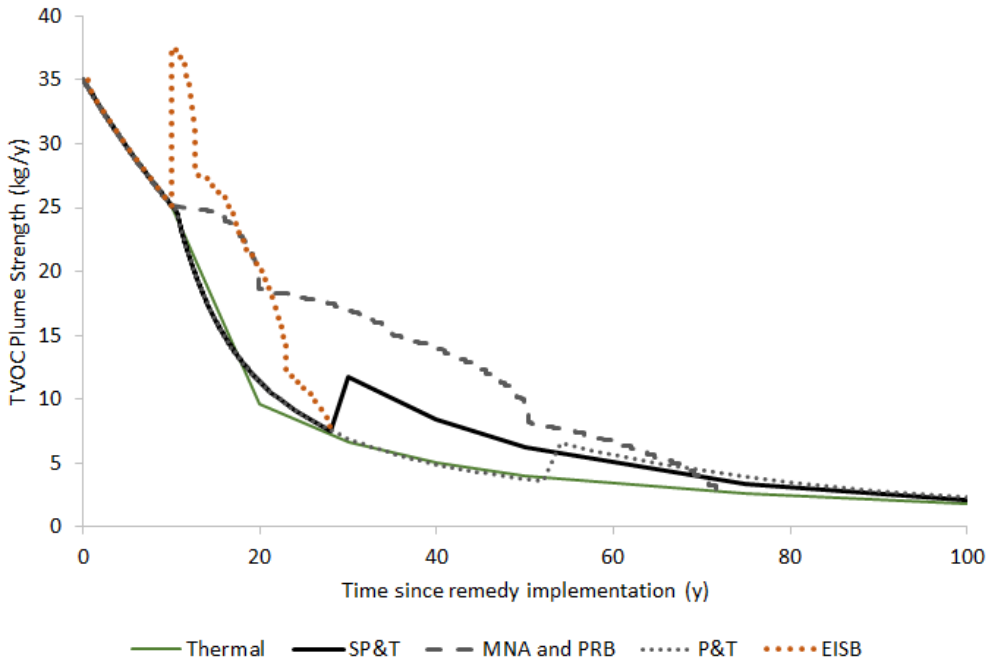

Figure 3.10 – Simulated plume strength versus time at a distance of 270 m downgradient from the source zone for various source zone treatment alternatives combined with the plume P&T alternative.

Figure 3.10 shows that there is a 20 to 30 year gap in the time when plume strength drops below 10 kg/y for MNA versus the other alternatives, and that the estimated plume strength for the different alternatives become closer after this threshold is reached. While MNA takes longer (50 years vs 20 to 30 years) to reduce the plume strength from 35 kg/y down to below 10 kg/y, none of the alternatives eliminate the risk to the river because of back-diffusion from the aquitard. The active source zone alternatives do help to reduce (but not eliminate) the risk to the river in the

event of downtime for the plume P&T system, although in the longer term (more than 50 years) there is little difference in plume strength between MNA and the active source depletion alternatives.

Figure 3.11 compares the net present values for the 14 combined source zone/plume alternatives for the base case. An analysis of cumulative NPV over time indicates that alternatives with timeframes longer than 20 to 30 y have diminishing influence on the total NPV beyond the initial two to three decades. For containment of the plume, the NPV for P&T is, on average, 25 percent lower than the NPV for a PRB; therefore, P&T is carried below as plume containment alternative. There are indirect benefits to a PRB, such as less required maintenance, although for the low pumping rates needed for plume containment in this example (i.e., 45 to 65 m^3/d) it is anticipated that plume P&T will also have relatively low maintenance needs.

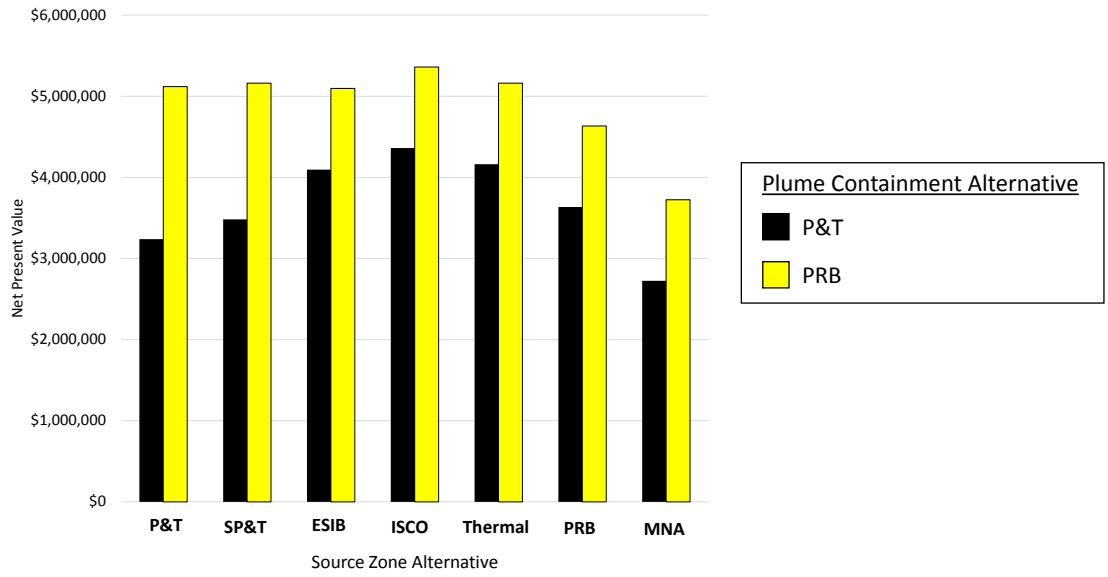

Figure 3.11 – Simulated net present value for source treatment and plume containment alternatives for base case.

The life-cycle cost (NPV) for source zone P&T and SP&T ($3.2MM and $3.5MM, respectively) are lower than the NPV for EISB, ISCO, and thermal ($4.1MM, $4.4MM, and $4.2MM, respectively). The lower cost of P&T and SP&T is due to the low incremental O&M costs associated with the pumping alternatives when plume P&T is used for containment. This demonstrates that savings may be realized when using the same technology for managing both the source zone and plume remediation, and illustrates why strategies for long-term source zone and plume management should be developed concurrently. The additional source strength reduction that may be obtained using the thermal alternative (47x estimated) does not

materialize into a substantial benefit for this site example because of the slow plume response caused by long-term back-diffusion from the thick aquitard.

Source zone SP&T is similar in cost to the P&T remedy and yet has a timeframe to achieve the interim source strength reduction goal that is significantly less than that for P&T (i.e., 27 y versus 45 y, respectively). Of the active source zone technologies considered, SP&T appears to be the best alternative based on combined metrics of price and depletion timeframe. On a purely cost basis, MNA appears to be the best alternative given that there is no reduction in site cleanup timeframe due to back-diffusion with more aggressive source treatment alternatives, and given that there is little difference in plume response between the passive and active source zone alternatives. If an active source zone alternative is required due to regulatory and public stakeholder concerns, SP&T is the best alternative on a combined cost and timeframe basis.

3.4.5.2 Pool Thickness and Through-Discharge Sensitivity Analysis

A sensitivity analysis was conducted to evaluate how different distributions in pool thickness or simulation of through-pool discharge affect the relative NPV of the source zone alternatives, and to determine if a different remedial decision is reached for different conditions such as thinner versus thicker pools. As discussed in Carey et al. (2014a), the NDM simulates through-pool discharge on the basis of a parameter

referred to as the Pool Flux Factor (*PFF*), which ranges from 0 to 1 depending on whether this discharge is zero or full strength. The base case scenario specified pool thickness (*h*) ranged from 2 to 10 cm and did not include simulation of through-pool discharge (*PFF*=0). Three scenarios were used to evaluate thinner pools: (a) *h*=2 to 4 cm, *PFF*=0; (b) *h*=2 to 4 cm, *PFF*=1; and (c) uniform *h*=3 cm, *PFF*=0. One additional simulation was conducted with *h*=2 to 10 cm, *PFF*=1. Two simulations were simulated with thicker pools: (a) *h*=2 to 20 cm, *PFF*=0; and (b) *h*=2 to 20 cm, *PFF*=1.

Table 3.6 presents initial TCE DNAPL mass and source strength simulated using the NDM for each of the above scenarios. Results from the simulations shown in Table 3.6 indicate that there is a large range in initial mass (253 to 1,500 kg) for the various scenarios, but only a small range in initial source strength (19.5 to 29.3 kg/y). This demonstrates that pool conditions in a source zone which combine to provide a general magnitude of source strength (e.g., 20 to 30 kg/y) are non-unique and not easily predicted on the basis of source strength alone. This also demonstrates when source strength is estimated at a site, it should not be used as the sole basis for predicting how much DNAPL mass remains or must be removed to achieve a target goal.

Table 3.6 – Simulated initial DNAPL mass, source strength, and naturally-occurring dissolution rate in first five year period.

		Pre-treatment Conditions			
Pool Thickness, *h* (cm)	Pool Flux Factor *PFF*	TCE Initial Mass, M_o (kg)	TCE Initial Source Strength, Md_o (kg)	Natural Decline Rate in Years 0 to 5 (1/y)	Natural Half-life in Years 0 to 5 (y)
2 to 4	0	253	19.5	0.017	40.8
2 to 4	1	253	22.6	0.027	25.7
3	0	233	19.5	0.012	57.8
2 to 10	0	616	19.5	0.01	69.3
2 to 10	1	616	25.8	0.017	40.8
6	0	476	19.5	0.002	346.6
2 to 20	0	1500	19.5	0.01	69.3
2 to 20	1	1500	29.3	0.012	57.8
11	0	946	19.5	2.00E-15	∞

Simulated initial decline rates and half-lives are also shown in Table 3.6 for comparison to the pre-treatment decline half-life of approximately 30 y. Two additional scenarios are presented in Table 3.6 (highlighted in gray): one with a uniform h=6 cm and another with uniform h=11 cm. These two scenarios had initial source strength decline half-lives that were substantially slower than the observed pre-treatment half-life of 30 y so were not carried forward in the NPV sensitivity analysis. This demonstrates an example of how a simple screening tool like the NDM may be used to constrain the range of source zone characteristics which may be representative

of conditions at a site by comparing simulated and observed source strength and decline rates.

NDM was used to simulate the depletion timeframes for the P&T, SP&T, EISB, and MNA source zone alternatives. Table 3.7 presents the simulated initial mass and depletion timeframe for each of these four source zone alternatives and for each of the pool distribution/through-pool discharge scenarios (including the base case for comparison). Depletion timeframes for the sensitivity analysis scenarios (i.e., time to reach the interim source strength reduction goal or *MdR* of 10x) were simulated to range as follows: EISB, 6 to 53 y; SP&T, 7 to 70 y; P&T, 13 to 119 y; and, MNA, 17 to 158 y. These results clearly indicate that there is a significant increase in depletion timeframe as the pool thickness increases.

Table 3.7 – Simulated source zone treatment initial TCE source strength and time to reach the interim reduction goal (*MdR*).

Range in Pool Thickness (cm)	Pool Flux Factor	Technology	TCE Initial Source Strength, Md_o (kg/y)	Time to Reach Interim Reduction Goal, MdR (y)
2 to 4	0	EISB	19.5	8
		MNA	19.5	22
		P&T	27.2	17
		SP&T	57.5	10
2 to 4	1	EISB	22.6	7
		MNA	22.6	19
		P&T	30.3	15
		SP&T	60.6	9
3	0	EISB	19.5	6
		MNA	19.5	17
		P&T	27.2	13
		SP&T	57.5	7
2 to 10	0	EISB	19.5	20
		MNA	19.5	61
		P&T	27.2	45
		SP&T	57.5	27
2 to 10	1	EISB	25.8	18
		MNA	25.8	43
		P&T	33.5	35
		SP&T	63.8	23
2 to 20	0	EISB	19.5	53
		MNA	19.5	158
		P&T	27.2	119
		SP&T	57.5	70
2 to 20	1	EISB	29.3	44
		MNA	29.3	94
		P&T	37.0	79
		SP&T	67.3	55

The NPV was calculated for all source zone alternatives (assuming plume containment using P&T) and for all pool scenarios based on these depletion timeframes, and using the same guidelines for ISCO and source zone PRB as discussed above. Figure 3.12 compares the NPV for the more aggressive source zone alternatives (SP&T, EISB, ISCO, and thermal). Inspection of this figure indicates that SP&T consistently has the lowest NPV of these four aggressive alternatives for all of the pool distribution and through-discharge conditions that were simulated. This indicates that if an aggressive source depletion strategy is a regulatory requirement and SP&T is selected on a cost basis, then this remedial decision is not sensitive to the range of pool thickness distributions that were considered. When compared to the NPV for source zone P&T (i.e., containment only), the SP&T alternative had an NPV that ranged from 3% to 11% higher than P&T. This indicates that the incremental cost of enhanced dissolution with SP&T is minor when compared to P&T, and the containment of the source zone provided by SP&T is a benefit when compared to the other aggressive alternatives like EISB and ISCO. The NPV for MNA has a small range for all of the pool scenarios ($2.6MM to $2.7MM), which shows that this alternative is also not sensitive to the range of pool conditions that were simulated.

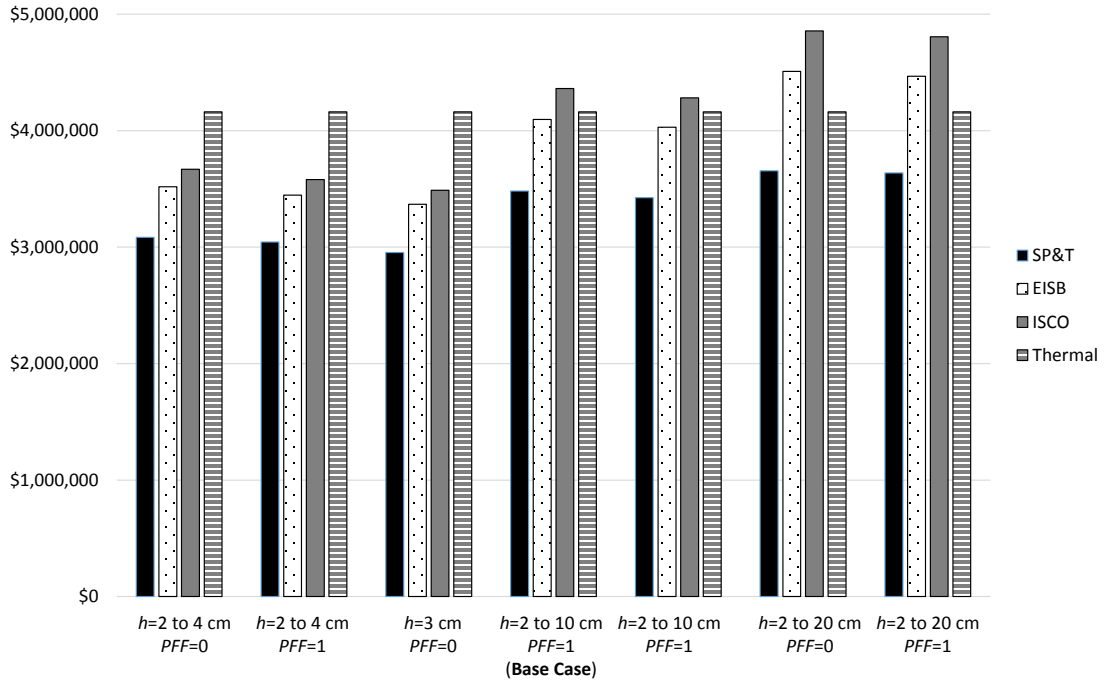

Figure 3.12 – Sensitivity analysis of net present value for SP&T, EISB, ISCO, and thermal source zone treatment alternatives.

This sensitivity analysis demonstrates that given the limited plume strength reduction associated with any of the source zone alternatives due to back-diffusion, MNA for the source zone and plume containment using P&T is a reasonable long-term alternative for this site. If regulatory requirements mandate that an aggressive source depletion alternative be employed, then SP&T is the best alternative for this site example because the incremental cost is low when considered concurrently with the plume P&T containment system. This has important implications for other sites where a P&T containment system is operating; for a low incremental cost, significant

increases in mass removal and source strength reduction may be achieved by strategically placing extraction wells in close proximity to DNAPL and by pumping at higher rates than would be typically used for hydraulic containment. Caution should be taken to not increase velocity too much if DNAPL mobilization is a concern, and relatively low-cost tests may be implemented at a site with an existing P&T system to evaluate the relationship of source strength to pumping rates at source control wells.

3.5 Conclusions

An empirical study of source strength reduction at various DNAPL sites using geometric mean *MdR*s for EISB, ISCO, and thermal treatment and found to be 49x, 9x, and 19x, respectively, based on a log-normal distribution. Lower / upper geometric mean confidence intervals were calculated to be 20x / 556x (EISB), 4x / 110x (ISCO), and 6x / 150x (thermal). Comparison to the source strength reduction factor observed at a well documented large, complex site (4x) suggests that the lower confidence interval for the geometric mean may be most applicable for similar sites or for sites with pool-dominated source zones.

A feasibility screening analysis was conducted for an example site to evaluate the benefits and limitations of partial DNAPL depletion relative to the life-cycle costs and risk to downgradient receptors. The source zone at the site was assumed to be

pool-dominated and is based on characteristics similar to those presented in various other studies. The Dandy-Sale model demonstrated that even in the case of complete source depletion or containment, back-diffusion from the thick aquitard underlying the long plume at the site will create a sustained secondary source for more than 1,000 years.

An analysis of plume response (i.e., influent concentrations for a pump-and-treat system and plume source strength) versus time demonstrates there is no reduction in cost and little difference in risk reduction associated with the various source zone alternatives.

A sensitivity analysis with the NDM demonstrated that pool-dominated source conditions with a large range in initial DNAPL mass (250 to 1500 kg) corresponded to a narrow range of source strength (20 to 30 kg/y). This demonstrates that measured source strength is non-unique with respect to DNAPL mass in the subsurface, and thus source strength should not be used as the sole basis for predicting how much DNAPL mass remains or must be removed to achieve a target goal.

A NPV analysis indicates that MNA consistently has the lowest NPV and is not sensitive to the range of pool conditions that were simulated. Given the limited plume response to aggressive source depletion and the long-term source (greater than 1000 y) due to back-diffusion, MNA for the source zone is a reasonable alternative for the example site. If regulatory requirements mandate that an aggressive source depletion alternative be implemented, then this feasibility analysis indicates that SP&T

is the best alternative on a combined cost and depletion timeframe basis. The additional source strength reduction (47x) that can be achieved with thermal treatment has limited benefit compared to the other alternatives at this site because of back-diffusion. This decision analysis is insensitive to the range of uncertainty in pool thickness and through-pool discharge.

The finding that SP&T is the most cost-effective aggressive source depletion alternative has important implications for other sites where a P&T containment system is operating; for a low incremental cost, significant increases in mass removal and source strength reduction may be achieved by strategically placing extraction wells in close proximity to DNAPL and by pumping at higher rates than would be typically used for hydraulic containment. The feasibility of SP&T may be easily determined through in-situ performance testing.

3.6 References

Air Force Center for Environmental Excellence (AFCEE). (2009). *Sustainable Remediation Tool (SRT) User Guide*, Air Force Center for Environmental Excellence, Brooks City-Base, Texas.

Anderson, M. R., Johnson, R. L., & Pankow, J.F. (1992). Dissolution of Dense Chlorinated Solvents into Groundwater: 3. Modeling Contaminant Plumes from Fingers and Pools of Solvents. *Environmental Science & Technology*, 26(5), 901-908.

Battelle. (2007). Electrical Resistance Heating (ERH): Design and Performance Criteria. Presented at the *RITS 2007 Spring Conference*.

Brusseau, M. L., Hatton, J., & DiGuiseppi, W. (2011). Assessing the Impact of Source-Zone Remediation Efforts at the Contaminant-Plume Scale Though Analysis of Contaminant Mass Discharge. *Journal of Contaminant Hydrology*, 126, 130-139.

Carey, G. R. (2014). NAPL Depletion Model User's Guide (Version 1.0). Porewater Solutions, Ottawa, Ontario, http://www.porewater.com/NDM.htm.

Carey, G. R., McBean, E. A., & Feenstra, S. (2014a). DNAPL Source Depletion: 1. Predicting Rates and Timeframes, Remediation Journal.

Carey, G. R. McBean, E. A., & Feenstra, S. (2014b). NAPL Depletion Model for Evaluating Performance of Naturally-Occurring and Enhanced Dissolution. In preparation.

Chapman, S. W. & Parker, B. L. (2005). Plume Persistence Due to Aquitard Back Diffusion Following Dense Nonaqueous Phase Liquid Source Removal or Isolation. *Water Resources Research*. Vol. 41, W12411, p. 1-16.

EPA. (1993). *Revisions to OMB Circular A-94 on Guidelines and Discount Rates for Benefit-Cost Analysis*. United States Environmental Protection Agency, OSWER Directive No. 9355.3-20, June 25, 1993.

EPA. (2000). *A Guide to Developing and Documenting Cost Estimates During the Feasibility Study*. United States Environmental Protection Agency, Report EPA/540/R-00-002.

EPA. (2001). *Cost Analyses for Selected Groundwater Cleanup Projects: Pump and Treat Systems and Permeable Reactive Barriers*. United States Environmental Protection Agency, Report EPA/542/R-00-013.

EPA. (2005). *Cost Effective Design of Pump and Treat Systems*. United States Environmental Protection Agency, Report EPA/542/R-05-008.

Environmental Security Technology Certification Program (ESTCP). (2008). *ESTCP Cost and Performance Report: Biodegradation of Dense Non-Aqueous Phase Liquids (DNAPL) Through Bioaugmentation of Source Areas – Dover National Test Site, Dover, Delaware*. United States Department of Defense ESTCP, Washington, D.C.

ESTCP. (2011). *User's Manual: Chlorinated Solvent DNAPL Technology Evaluation Screening Tool (DNAPL TEST v1.0)*. United States Department of Defense ESTCP, Washington, D.C.

Farhat, S. K., Newell, C. J., Sale, T. C., Dandy, D. S., Wahlberg, J. J., Seyedabbasi, M. A., McDade, J.M., & Mahler, N.T. (2012). Matrix Diffusion ToolKit User's Manual (Version 1.0). United States Department of Defense ESTCP, September 2012.

Guilbeault, M. A., Parker, B. L., & Cherry, J. A. (2005). Mass and Flux Distributions from DNAPL Zones in Sandy Aquifers. *Ground Water*, 43(1), 70-86.

Heiderscheidt, J. L., Siegrist, R. L., & Illangasekare, T. H. (2008). Intermediate-Scale 2D Experimental Investigation of In Situ Chemical Oxidation Using Potassium Permanganate for Remediation of Complex DNAPL Source Zones. *Journal of Contaminant Hydrology*, 102, 3-16.

Interstate Technology Regulatory Council (ITRC). (2010). *Technology Overview: Use and Measurement of Mass Flux and Mass Discharge*. ITRC, Washington, D.C.

ITRC. (2013). *Use and Measurement of Mass Flux and Mass Discharge*. Web Seminar.

Kavanaugh, M.C., Arnold, W. A., Beck, B. D., Chin, Y., Chowdhury, Z., Ellis, D. E., Illangasekare, T. H., Johnson, P. C., Mehran, M., Mercer, J. W., Pennell, K. D., Rabideau, A. J., Shapiro, A. M., Siegel, L. M., Walsh, W. J., Ehlers, L. J., Johnson, S. E., Schaffer, K., Aquilino, J., Deguzman, E., & Hall, A. (2013). *Alternatives for Managing the Nation's Complex Contaminated Groundwater Sites*. The National Academies Press, Washington, D.C.

Krembs, F. J., Siegrist, R. L., Crimi, M. L., Furrer, R. F., & Petri, B. G. (2010). ISCO for Groundwater Remediation: Analysis of Field Applications and Performance. *Ground Water Monitoring & Remediation*, 30(4), 42-53.

Kueper, B. H. & Davies, K. L. (2009). *Assessment and Delineation of DNAPL Source Zones at Hazardous Waste Sites*. United States Environmental Protection Agency, Publication EPA/600/R-09/119.

Lynch, K. (2009). A Regulator's Perspective on the Use of Mass Flux and Mass Discharge as a Performance Metric in CERCLA Decision Documents. Presented at the *2009 SERDP-ESTCP Partners in Environmental Technology Technical Symposium & Workshop*. Washington, D.C., December 1-3, 2009.

McBean, E. A. & Rovers, F. A. (1998). *Statistical Procedures for Analysis of Environmental Monitoring Data & Risk Assessment*. Prentice Hall, Upper Saddle River, New Jersey.

McDade, J. M., McGuire, T. M., & Newell, C. J. (2005). Analysis of DNAPL Source-Depletion Costs at 36 Field Sites. *Remediation*, Spring 2005, p. 9-18.

McGuire, T. M., McDade, J. M., & Newell, C. J. (2006). Performance of DNAPL Source Depletion Technologies at 59 Chlorinated Solvent-Impacted Sites. *Ground Water Monitoring & Remediation*, 26(1), 73-84.

Parker, B. L., Cherry, J. A., Chapman, S. W., & Guilbeault, M. A. (2003). Review and Analysis of Chlorinated Solvent Dense Nonaqueous Phase Liquid Distribution at Five Sandy Aquifers. *Vadose Zone Journal*, 2, 116-137.

Parker, B. L., Cherry, J. A., & Chapman, S.W. (2004). Field Study of TCE Diffusion Profiles Below DNAPL to Assess Aquitard Integrity. *Journal of Contaminant Hydrology*, 74, 197-230.

Parker, B. L., Chapman, S. W. & Guilbeault, M. A. (2008). Plume Persistance Caused by Back Diffusion from Thin Clay Layers in a Sand Aquifer Following TCE Source-Zone Hydraulic Isolation. *Journal of Contaminant Hydrology*, 102, 86-104.

Sale, T. C., Zimbron, J. A. & Dandy, D. S. (2008). Effects of Reduced Contaminant Loading on Downgradient Groundwater Quality in an Idealized Two-Layer Granular Porous Media. *Journal of Contaminant Hydrology*, 102, 69-81.

Seyedabbasi, M. A., Newell, C. J., Adamson, D. T., & Sale, T. C. (2012). Relative Contribution of DNAPL Dissolution and Matrix Diffusion to the Long-Term

Persistence of Chlorinated Solvent Source Zones. *Journal of Contaminant Hydrology*, 134-135, 69-81.

Stroo, H. F., Leeson, A., Marqusee, J. A., Johnson, P. C., Ward, C. H., Kavanaugh, M. C., Sale, T. C., Newell, C. J., Pennell, K. D. Lebron, C. A., & Unger, M. (2012). Chlorinated Ethene Source Remediation: Lessons Learned. *Environmental Science & Technology*, 46, 6438-6447.

Triplett Kingston J.L. (2008). *A Critical Evaluation of In-Situ Thermal Technologies*. Doctor of Philosophy Dissertation. Arizona State University, 490 p.

Chapter 4

Estimating Tortuosity Based on Hydraulic Conductivity

4.1 Abstract

While the tortuosity coefficient is commonly estimated using an expression based on total porosity, results show that this relationship is not applicable (and thus is often mis-applied) over a broad range of soil textures. The fundamental basis for a correlation between the tortuosity coefficient and hydraulic conductivity is demonstrated, although such a relationship is not typically considered. An empirical regression for estimating the tortuosity coefficient based on hydraulic conductivity for saturated, unconsolidated soil is derived based on results from 18 previously reported diffusion experiments performed with a broad range of soil textures. Analyses of

these experimental results confirm that total porosity is a poor predictor for the tortuosity coefficient over a large range of soil textures. A simple screening model was derived to estimate effective porosity based on hydraulic conductivity. The classic relationship proposed by Millington and Quirk (1961), based on effective porosity and an exponent of 0.33, while reasonable for sands or gravels, is shown to overestimate the apparent tortuosity coefficient by up to 80% for fine-grained silts and clays. The tortuosity coefficient is more reliably estimated based on hydraulic conductivity.

4.2 Introduction

Although molecular diffusion is a relatively slow process in water, there are circumstances in which it may have a significant influence on contaminant transport. For example, back-diffusion from low-permeability silts, clays, or rock matrix may cause a substantial increase in remediation timeframe at contaminated sites (Parker et al., 1994; Chapman and Parker, 2005; Parker et al., 2008; Sale et al., 2008; Seyedabbasi et al., 2012). Diffusion also influences the performance of caps on contaminated sediment, which may be comprised of a wide range of soil textures (USEPA, 1998a; Reible and Lampert, 2014), as well as clay landfill liners (Rowe et al., 1988; Johnson et al., 1989; Rowe and Bady, 1996). Molecular diffusion is also a

contributing factor to the rate of dissolution from DNAPL (Johnson and Pankow, 1992; Grathwohl, 1998). Thus, there is a wide range of applications and soil textures where molecular diffusion may play an important role in solute transport.

Modeling the rate of molecular diffusion in porous media requires estimation of the tortuosity coefficient. The most common model used to estimate tortuosity coefficients for simulating chemical diffusion is a simple power law relationship based on total porosity, or θ_t (e.g. Parker et al., 1994; Grathwohl, 1998). As will be shown below, however, the tortuosity coefficient is, at best, weakly correlated with total porosity over a large range in unconsolidated soil texture, and thus this commonly-used model has limited reliability. Soil permeability and hydraulic conductivity are proportional to the tortuosity coefficient (Carmen, 1937; Bear, 1972). Results of various diffusion experiments as cited in Al-Tarawneh et al. (2009), Boving and Grathwohl (2001), Klinkenberg et al. (1951), Parker et al. (1994), and Sale et al. (2014) confirm qualitatively that there is a general correlation between the tortuosity coefficient and hydraulic conductivity; however, such a relationship has not yet been quantified based on the results of chemical diffusion experiments.

The objective of this paper is to provide a more reliable basis for estimating the tortuosity coefficient for modeling chemical diffusion. A comprehensive literature review provides insights on mechanisms which may influence the tortuosity coefficient, and to clarify the relationship between the tortuosity coefficient and hydraulic conductivity or porosity. Results from previous experiments that measured

effective diffusion coefficients for a wide range of soil textures (clays, silts, sands, and glass beads) are synthesized. Tortuosity coefficients are re-calculated for some studies based on a consistent methodology for estimating the free-water diffusion coefficient (Hayduk and Laudie, 1974). Regression is used to estimate a new model for estimating the tortuosity coefficient as a function of hydraulic conductivity. The synthesized experimental data are also used to evaluate the relative applicability of using effective versus total porosity for estimating the tortuosity coefficient.

4.3 Literature Review

4.3.1 Modeling Chemical Diffusion in Porous Media

The one-dimensional solute transport equation for chemical diffusion in porous media is

$$R\frac{\partial C}{\partial t} = \left(D_e \frac{\partial^2 C}{\partial x^2}\right) \tag{4.1}$$

where C is the solute concentration [M/L^3], x is distance [L], t is time [T], D_e is the effective diffusion coefficient [L^2/T], and R is the retardation coefficient [dimensionless] used to represent chemical sorption. The effective diffusion coefficient is defined using

$$D_e = \tau_{app}\, D_o \tag{4.2}$$

where τ_{app} represents the apparent tortuosity coefficient (Shackelford and Daniel, 1991), and D_o represents the free-water diffusion coefficient [L^2/T].

The apparent tortuosity coefficient is used to represent the total impedance to molecular diffusion in porous media relative to diffusion in free solution. This impedance to diffusion is caused by two types of factors: (1) hydraulic impedance due to crooked (i.e. sinuous) flow paths through connected pore networks; and (2) chemical processes which may further impede the rate of molecular diffusion. The tortuosity coefficient which represents only the effects of hydraulic impedance, will be referred to herein as τ_{path}.

In cases where solute transport is due solely to molecular diffusion, the solute mass flux through a cross-sectional area in a porous medium is calculated using

$$J = -\theta_t D_e \frac{\partial c}{\partial x} \tag{4.3}$$

where J is mass flux [M/L^2-T] and θ_t is total porosity. The actual diffusive flux through a cross-section in porous media may be a little lower than that defined in Eq. 4.3 because the actual pore space available for molecular diffusion may be less than total porosity; however, the relative significance of this difference has been shown by Rowe et al. (1988) and Rowe and Bady (1996) to be relatively minor.

Depending on the form of the solute transport equation, some studies in the literature (e.g. Millington and Quirk, 1961; Reible and Lampert, 2014) define an alternate form of the effective diffusion coefficient and mass flux equations as

$$D_e{}^* = \theta_t \tau_{app} D_o \tag{4.4a}$$

and

$$J = -D_e^* \frac{\partial \mathcal{C}}{\partial x} \tag{4.4b}$$

4.3.2 Hydraulic Definition of the Tortuosity Coefficient (τ_{path})

The hydraulic definition for τ_{path} is typically given as

$$\tau_{path} = \left(\frac{L}{Le}\right)^2 \tag{4.5}$$

where L_e is the actual (i.e. effective) path length of a molecule in a porous medium, and L is the straight-line or net distance between the starting and ending points of the effective flow path (Carmen, 1937; Bear, 1972; Epstein, 1989; Grathwohl, 1998). L_e is greater than L due to the sinuous nature of connected pore channels in porous media, and thus $\tau_{path} < 1$. While the use of the squared term on the right-hand side of Eq. 4.5 has been verified for the purpose of estimating hydraulic conductivity using the Kozeny-Carmen equation and other hydraulic radius models, the same rigor has not been applied to confirm that the definition in Eq. 4.5 should also be used for modeling chemical diffusion.

τ_{path} is inversely proportional to the sinuosity of a flow path, so larger values of τ_{path} indicate that there is less sinuosity in connected pore networks, and thus less impedance of molecular diffusion. The magnitude of τ_{path} is governed by:

- the shape, size distribution, and types of grains (Guo, 2012);
- pore size distribution and pore connectivity (Guo, 2012; Perkins and Johnston, 1963; Petersen, 1958; Vervoort and Cattle, 2003); and
- orientation of sediment beds (Guo, 2012).

For example, Guo (2012) demonstrates there is a lower degree of sinuosity in flow channels parallel to horizontal sediment bedding planes, and a higher sinuosity in flow channels perpendicular to vertical bedding planes. The impedance to diffusion will have a similar trend. In addition to the above influencing factors, the presence of cementing material in bedrock formations will reduce τ_{path} (Klinkenberg, 1951) relative to unconsolidated soil.

The hydraulic definition of the tortuosity coefficient τ_{path} was first introduced in mathematical derivations of intrinsic permeability, or k [L^2]. Based on the Kozeny-Carmen equation for intrinsic permeability defined in Carmen (1937), k may be estimated using

$$k = \theta_e \tau_{path} r_h^2 / c \qquad (4.6)$$

where θ_e represents effective porosity [L^3/L^3], r_h represents the mean hydraulic radius [L], and c is a constant that represents a pore channel shape factor ranging from 1.7 to

2.5, and is typically taken to be approximately 2 for circular pore channels. Hydraulic conductivity (K) of saturated, unconsolidated porous media [L/T] is then defined as

$$K = \rho g k / \mu \quad (4.7)$$

where ρ is groundwater density [M/L^3], g is the gravitational acceleration constant [L/T^2], and μ is dynamic viscosity [ML^{-1}T^{-1}]. Combining Eq. 4.6 and 4.7 indicates that there is a direct relationship between τ_{path} and K.

There are various definitions of effective porosity in the literature; we will use the definition in Bear (1972), as cited in Guo (2012), which defines effective porosity as the total inter-connected pore space available for groundwater flow, and is represented by the drainable porosity which may be estimated based on specific yield (Bear, 1972). Ineffective pore space does not contribute to groundwater flow, and is defined by Bear (1972) to include isolated pores, dead-end pores, and stagnant pockets, and represents the difference between total porosity (θ_t) and θ_e. While Carmen (1937) did not explicitly state that the porosity term in Eq. 4.6 represents effective porosity, Bear (1972) and Guo (2012) indicate that effective porosity should be used in equations for estimating k.

In some cases, a different dimensionless parameter referred to as the tortuosity factor ($\tau_f = L_e/L$) is used in hydraulic evaluations of intrinsic permeability or correlations with total and effective porosity (e.g. Epstein, 1989; Knackstedt and

Zhang, 1994; Koponen et al., 1996; Matyka et al., 2008; and Guo, 2012). The relationship between τ_{path} and τ_f is

$$\tau_{path} = \frac{1}{\tau_f^2} \tag{4.8}$$

based on the assumption that $\tau_{path} = (L/L_e)^2$.

4.3.3 Apparent Tortuosity Coefficient (τ_{app})

The sinuosity of a flow path in porous media is only one contributing mechanism to the actual, or apparent tortuosity coefficient (τ_{app}) which governs the rate of diffusion (Shackelford and Daniel, 1991; Grathwohl, 1998). Other factors which may influence D_e for non-reactive solutes in saturated, unconsolidated soils may include:

- Exclusion in small pore spaces (Shackelford and Daniel, 1991; Grathwohl, 1998);
- Increased viscosity in the adhesive water layer around clay particles which causes a local reduction in the free-water diffusion coefficient (Shackelford and Daniel, 1991; Grathwohl, 1998);
- Intra-particle and/or intra-organic matter diffusion (Grathwohl, 1998; Boving and Grathwohl, 2001);

- Electrical potential gradient between two oppositely charged ions (Shackelford and Daniel, 1991)
- Ionic strength which is particularly high in landfill leachate (Barone et al., 1989);
- Varying pore diameters along a flow path (Petersen, 1958).

The concept of an apparent tortuosity coefficient (τ_{app}) is described in Shackelford and Daniel (1991). The influencing factors listed above may result in a value for τ_{app} (determined from diffusion experiments) that is less than the hydraulic tortuosity coefficient (τ_{path}) based on

$$\tau_{app} = f_i \tau_{path} \tag{4.9}$$

where f_i represents an impedance factor that is slightly modified from the definition presented in Shackelford and Daniel (1991). In most circumstances, $f_i \leq 1$ which represents a range of impedance to diffusion from negligible to some significant value. It is possible for $f_i > 1$ when ions with opposite charges are present and the slower-diffusing ion has an accelerated diffusion rate because of an electrical potential gradient (e.g. Shackelford and Daniel, 1991).

The magnitude of f_i is typically not calculated quantitatively in experimental diffusion studies. Grathwohl (1998) presents an interesting quantitative analysis of the impedance factor based on combined effects of exclusion from small pores and increased viscosity in the adhesive water layer. Grathwohl (1998) determined that

these two factors (typically defined as *constrictivity*) contribute to additional impedance for most organic contaminants (molecular diameter < 1 nm) in pore spaces with diameter < 10 nm. Therefore, restricted diffusion based on constrictivity may be expected to increase the impedance of diffusion in fine-grained silts and clays.

4.4 Estimating Tortuosity and Effective Diffusion Coefficients

4.4.1 Diffusion Experiments

The most accurate method for estimating τ_{app} is to measure D_e for a conservative tracer in a laboratory or field-scale column experiment, estimate D_o, and then calculate the tortuosity coefficient using $\tau_{app} = D_e/D_o$. Shackelford (1991) presents a review of various methods available for measuring D_e. Experimental conditions which may result in significant uncertainty in τ_{app} include:

- Simultaneous occurrence of advection and diffusion;
- Relatively short column (e.g. 1 centimeter or less) which may result in significant boundary influence on the diffusion coefficient;
- Insufficient experiment duration;
- Reactive transport of the tracer, such as degradation, sorption, or ionic interference; and/or

- Mass loss during sampling or analysis of volatile organic compounds (VOCs).

Shackelford and Daniel (1991) and Hong et al. (2009) indicate that values of D_e derived based on declining source reservoir concentrations are not as reliable as are D_e values based on calibration of a model to the measured profile of soil or porewater concentrations in the column.

4.4.2 Screening-Level Methods

Tortuosity Coefficient versus K

As described above, the hydraulic tortuosity coefficient is based on the sinuosity of effective flow paths through porous media. Combining Eqs. 6 and 7 and re-arranging to solve for τ_{path} yields

$$\tau_{path} = \frac{36K\mu c}{\rho g d_e^2}\left[\frac{(1-\theta_e)^2}{\theta_e^3}\right] \tag{4.10}$$

based on the definition of hydraulic radius in Carmen (1937), where d_e is the effective grain size. Similarly, the Millington and Quirk (1961) equation for saturated hydraulic conductivity may be re-arranged to give

$$\tau_{path} = \frac{4K\mu c}{\rho g \theta_e r_e^2} \tag{4.11}$$

based on the assumption of spherical soil particles, where r_e is the effective pore channel radius.

Given that the effective pore channel radius is proportional to the effective particle size (Klinkenberg and Grathwohl, 2002), the hydraulic tortuosity coefficient is a function of the following three porous media properties: K, θ_e, and d_e. These three parameters are not independent, however. As shown below, there is a direct relationship between θ_e and K over a large range of soil texture; also, Shepherd (1989) summarizes numerous studies which demonstrate a direct relationship between K and d_e. Therefore, it is reasonable to expect that a general relationship for the hydraulic tortuosity coefficient may be written as

$$\tau_{path} = aK^b \tag{4.12}$$

where a and b are empirically-derived constants. A similar relationship may also be written for τ_{app}, where a and b may differ from those determined for τ_{path} if the impedance factor deviates from one.

To the best of our knowledge, this simple form has not yet been evaluated quantitatively for a wide range of textures including both fine-grained and coarse-grained soils, based on the results of diffusion experiments. Al-Tarawneh et al. (2009) did propose that the hydraulic equation for hydraulic conductivity (e.g. Eq. 4.10) be re-arranged to solve for τ_{path} and/or τ_{app}. Their study included a proposed methodology for estimating the hydraulic radius for non-uniform soils with a range of particle sizes, which is an improvement over Eqs. 4.10 and 4.11 based on the assumption that particle sizes and pore radii are uniform. Al-Tarawneh et al. (2009)

provided an equation for estimating K (and then τ_{path}) which is incorrect, however. (See Eq. 4.4 in Al-Tarawneh et al., where the equation to estimate K based on a volumetric flow rate through a column includes effective porosity in the denominator.) Therefore, the validity of their quantitative findings are uncertain, although the principles that they describe are valid, and represent the first study we are aware of which attempts to estimate τ_{path} based on measured K values.

For modeling molecular diffusion, Bear (1972) recommends using a tortuosity coefficient of 0.67. de Marsily (1986) recommends using a tortuosity coefficient of 0.1 for clay and 0.7 for sand. Chapman and Parker (2005) used a range of 0.2 to 0.4 for clay. Freeze and Cherry (1979) cite a range from 0.01 to 0.5 as being commonly observed during laboratory experiments. The variability in recommended tortuosity coefficients suggests that further validation is needed to facilitate estimation of τ_{app} for a wide range of soil textures.

Tortuosity Coefficient versus Porosity

Given the challenges of measuring site-specific D_e, a number of empirical regression models have been developed to estimate τ_{path} based on total or effective porosity using one of the following equations:

$$\tau_{path} = \theta_e^p \tag{4.13a}$$

$$\tau_{path} = \theta_t^p \tag{4.13b}$$

The most commonly used derivation is that of Millington and Quirk (1961), which defines τ_{path} based on effective porosity and p=0.33 in Eq. 4.13a. The Millington and Quirk equation is based on a mathematical derivation of intrinsic permeability, and has not been extensively validated based on diffusion experiments. For example, USEPA (1998a) and Reible and Lampert (2014) provide guidance which recommends the use of p=0.33 when modeling diffusion in sediment caps, with the assumption that $\tau_{app} = \tau_{path}$. USEPA (1998a) is not explicit with regard to the use of effective versus total porosity, however, and it is common practice to use total porosity given that site-specific effective porosity is challenging to measure directly and is commonly estimated.

A more recent mathematical review of the hydraulic tortuosity coefficient by Guo (2012) indicates that Eq. 4.13a may be used to define τ_{path} with p=0.8 to 1.0, based on the Kozeny-Carmen equation for intrinsic permeability (Carmen, 1937) and the definition of τ_{path} in Bear (1972). This is based on the Guo (2012) derivation of the tortuosity factor, $\tau_f = L_e/L = (\theta e)^m$, where m ranges from -0.5 to -0.4. Guo (2012) does not indicate why this analysis differs from that of Millington and Quirk (1961) which indicated that p=0.33 for Eq. 4.13a based on a probabilistic derivation of k.

It is instructive to evaluate the general relationship between porosity and K for a wide range of soil textures. Table 4.1 presents ranges of K, θ_t, and θ_e for various textures that include clays, silts, sands, and gravels based on USEPA (1998b) and

Spitz and Moreno (1996). Assuming that the middle of the ranges for θ_t and θ_e represent the approximate average values for the specified texture category in Table 4.1, and using the middle of the K range for each texture, Figures 1a and 1b show the general relationship for θ_t versus K and θ_e versus K, respectively. As shown in Figures 1a and 1b, there appears to be a general inverse relationship between θ_t and K, and a direct relationship between θ_e and K.

Table 4.1. Ranges of effective porosity, total porosity, and hydraulic conductivity for various soil textures.

Soil Texture Description	Hydraulic Conductivity (m/s)	Effective Porosity [a] (m^3/m^3)	Total Porosity [a] (m^3/m^3)
clay	$1x10^{-11}$ to $5x10^{-9}$ [a]	0.01 to 0.2	0.34 to 0.6
silt	$1x10^{-7}$ to $1x10^{-5}$ [b]	0.01 to 0.3	0.34 to 0.61
fine to medium sand	$1x10^{-5}$ to $1x10^{-4}$ [b]	0.1 to 0.3	0.26 to 0.53
medium to coarse sand	$1x10^{-4}$ to $1x10^{-3}$ [b]	0.2 to 0.35	0.31 to 0.46
fine to medium gravel	$1x10^{-3}$ to $1x10^{-2}$ [b]	0.2 to 0.35	0.25 to 0.38
medium to coarse gravel	$1x10^{-2}$ to $1x10^{-1}$ [b]	0.1 to 0.25	0.24 to 0.36

Notes:
[a] Modified from USEPA (1998b)
[b] Modified from Spitz and Moreno (1996)

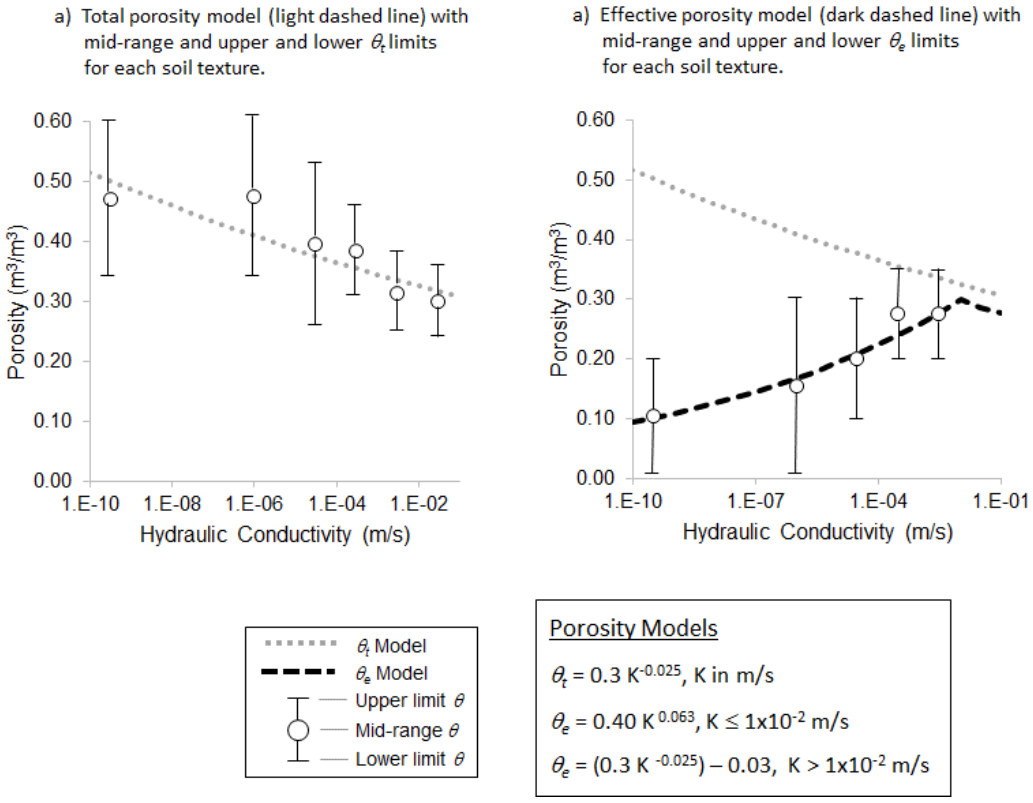

Figure 4.1. Total and Effective porosity models versus hydraulic conductivity.

The whiskers shown in Figure 4.1a indicate that there is relatively high variability in total porosity for any soil texture category, which is consistent with the experience of the authors of this study. The regression equation estimated for θ_t versus K is shown on Figure 4.1a for illustrative purposes, and is given as

$$\theta_t = 0.3K^{-0.025} \tag{4.14}$$

with *K* in units of m/s. Site-specific total porosity may be readily measured based on collection of soil samples, which is recommended over the use of the simplified regression equation in Eq. 4.14. It should also be noted that porous media exhibiting a broad range of grain sizes in unconsolidated soil do not fit with the regression equation shown in Figure 4.1a. For example, clay till may have a permeability similar to that of clay, but is expected to have a lower total porosity than a homogeneous clay.

Figure 4.1b illustrates that there may also be significant variability in effective porosity for a given class of soil texture; however, the direct relationship between intrinsic permeability and effective porosity has a more theoretical basis given the classic relationship shown in Eq. 4.6.

Based on the use of middle range values for K and porosity, the following screening-level equations were derived:

$$\theta_e = 0.4K^{0.063}, \quad K \leq 0.01\ m/s \tag{4.15a}$$

$$\theta_e = (0.3K^{-0.025}) - 0.03, \quad K > 0.01\ m/s \tag{4.15b}$$

where *K* has units of m/s. Eq. 4.15b is based on the simplifying assumption that $\theta_e = \theta_t - 0.03$. In other words, it was assumed that the difference between total and effective porosity at K=0.01 m/s, as estimated from Eqs. 4.14 and 4.15a, remained constant for K>0.01 m/s. While there is uncertainty associated with these regression equations, they are consistent with the general ranges observed by others (e.g. USEPA, 1998b) and provide convenient screening-level equations which may be used when

site-specific measurements are not available (as is often the case for effective porosity).

Given that there appears to be a direct relationship between θ_e and K, and between θ_e and τ_{path}, it is reasonable to expect that there is also a general relationship between T_{path} and θ_e as has been shown theoretically by Guo (2012) and Millington and Quirk (1961), albeit with a wide range of exponents (p=0.33 to 1.0).

In contrast, mathematical analyses by Knackstedt and Zhang (1994) and Koponen et al. (1996) for high-porosity media (θ_t = 0.45 to 0.95) suggest that τ_{path} may be estimated based on total porosity. This work was updated by Mateyka et al. (2008) using a more rigorous mathematical representation, which indicates that estimating τ_{path} using Eq. 4.13b (based on θ_t) results in a poor correlation, and that a better correlation for the hydraulic tortuosity coefficient is given by $\tau_{path} = 1/[1 - p \ln \theta_t]^2$.

Matyka et al. (2008) also cite other mathematical studies which found that this same relationship provided a reasonably good fit (e.g. Weissberg, 1963; and Comiti and Renaud, 1989). Matyka et al. (2008) cite several other forms of regression equations which may be used to estimate τ_{path}, and indicate that there is no general relationship between τ_{path} and total porosity; however, Matyka et al. (2008) state that: "…one may hope to establish such relations at least for some classes of porous media." This is consistent with the relatively good correlation between the τ_{app} and θ_t shown by Boving and Grathwohl (2001) for a combined set of limestone and bedrock

samples. Boving and Grathwohl (2001) also show that for this same dataset, there was a good correlation between total porosity and hydraulic conductivity, which may explain why this specific set of bedrock samples demonstrated a correlation between τ_{app} and θ_t.

In summary, the above studies (which are based on simplified mathematical representations of porous media) indicate that there should be a direct relationship between the hydraulic tortuosity coefficient (τ_{path}) and θ_e (Millington and Quirk, 1961; Guo, 2012), and that there is no universal equation which holds for τ_{path} versus θ_t. Unfortunately, however, diffusion experiments reported in the literature typically only report total porosity. This is due, in part, to the challenges associated with determining effective porosity. This is probably also due to the lack of recognition (or at least acknowledgement in the literature) that the tortuosity coefficient is theoretically proportional to θ_e, and that there is a weak correlation, at best, with θ_t. For these reasons, various diffusion studies have evaluated the simplified relationship between τ_{app} and θ_t based on Eq. 4.13b. Parker et al. (1994) observed a large degree of variability in τ_{app} versus θ_t, with p in Eq. 4.13b having a large range (from 0.4 to 2.0) for a narrow range in texture (fine-grained soils including silts, clays, and tills). More complex relationships for τ_{app} are presented in Boudreau (1996), Boudreau and Meysman (2006), and Iversen and Jorgensen (1993), and these studies demonstrate

that there is a large deviation between observed and predicted τ_{app} values based on total porosity for unconsolidated soils.

4.5 Empirical Regression of Apparent Tortuosity Coefficient

4.5.1 Methodology

The main objectives of this study were to: 1. Derive an empirical-based regression equation for estimating τ_{app} based on hydraulic conductivity for a wide range of saturated soil textures (i.e. clays, silts, and sands); and 2. Evaluate the correlation of τ_{app} with total or effective porosity. To accomplish these objectives, a number of diffusion studies were reviewed including: Al-Tarawneh et al. (2009); Barone et al. (1989); Barone et al. (1992); Barraclough and Tinker (1981, 1982); Boudreau (1996); Boudreau and Meysman, 2006; Boving and Grathwohl, 2001; Chapman and Parker (2005); Chapman et al. (2012); Cotten et al. (1998); Crooks and Quigley (1984); Desaulniers et al. (1981); Gillham et al. (1984); Hong et al. (2009); Iversen and Jorgensen, 1993; Klinkenberg (1951); Johnson et al. (1989); Latrilla and Zoia (2011); McCarty and Johnson (1995); Morin et al. (2010); Murphy et al. (2006); Myrand et al. (1992); Overman (1975); Parker et al. (1994, 2004); Prudic (1986);

Rowe et al. (1988); Rowe and Bady (1996); Shackelford et al. (1989); Rasa et al. (2011); Reiter (1999); Wang et al. (1991); and Yanful and Quigley (1990).

Studies were excluded from the empirical regression in those cases in which there was sufficiently high uncertainty in D_e measurements resulting from factors such as:

- Simultaneous model calibration of the average linear groundwater velocity and D_e in a mixed advection-diffusion system;
- Large uncertainty in reported soil hydraulic conductivity;
- Calibration of a model to declining reservoir concentrations which is not as reliable for estimating D_e as measured concentration profiles along the column;
- Limited documentation of experimental procedures prohibited the authors of this study from conducting a quality check on the results;
- Substantial heterogeneity in the experimental column;
- Leachate source concentrations with sufficiently high ionic strength to influence the effective diffusion coefficient.
- Extreme long-term diffusion profiles that developed over thousands of years with uncertainty in groundwater velocity conditions over this period;
- Organic compounds used as tracers with uncertainty in the retardation coefficient; and
- Very thin test columns (e.g. as low as 0.7 cm).

In addition, experimental diffusion data derived based on fine-grained marine sediments or bedrock samples were not included in the regression analysis which was focused on saturated, unconsolidated subsurface soils.

In several cases (e.g. Rowe, 1996; Al-Tarawneh et al., 2009), hydraulic conductivity (K) of tested columns was not documented but there were sufficient data available to facilitate estimation of the hydraulic conductivity (e.g. the approximate d_{10} grain size which was used to estimate K of silt or sand based on the Chapuis (2004) method). While the Chapuis method is known to be an approximation to within a factor of 2 to 3 for hydraulic conductivity in soil with grain size between 0.003 and 3 mm, this error is acceptable for the regression conducted in this study with K values ranging over nine orders-of-magnitude.

Most of the studies used in this empirical analysis included documentation of a calculated τ_{app}; however, a range of methods were used in these studies to estimate the free-water diffusion coefficient (D_o). To avoid a situation where differences in τ_{app} determined in different studies may arise due to the use of different methods for estimating D_o, this parameter (D_o) was calculated consistently for each of the selected studies based on the method described by Hayduk and Laudie (1974). The apparent tortuosity coefficient (τ_{app}) was then re-calculated for this empirical analysis based on the documented D_e from each study and standardized D_o using $\tau_{app}=D_e/D_o$. The exception to this standardization of D_o was the Klinkenberg (1951) study which did

not present sufficient data to re-calculate τ_{app}. If multiple tests were performed in a single study on the same soil texture, then the average D_e was used instead of the individual test results from that study. Once the study results were compiled, correlations of τ_{app} versus K and total porosity were evaluated.

4.5.2 Results and Discussion

A total of eight studies with 18 calculated apparent tortuosity coefficient values (τ_{app}) were selected for the regression analysis. Table 4.2 describes each laboratory experiment including soil texture, test methodology, measured values of total porosity, and measured or estimated values of hydraulic conductivity. As shown in Table 4.2, values of hydraulic conductivity in the selected experiments ranged from $6x10^{-11}$ m/s to 0.15 m/s. Table 4.3 presents estimated values for D_o, measured D_e, and calculated τ_{app}. Table 4.3 also presents the original estimates of D_o and τ_{app} reported in the referenced study. As shown in Table 4.3, estimates of the apparent tortuosity coefficients ranged from 0.28 to 0.67 for the various studies.

Figure 4.2 presents a scatter plot comparing the re-calculated τ_{app} conducted as part of this present study, relative to the original tortuosity coefficients reported in the referenced studies. Figure 4.2 indicates that the re-calculated coefficients are typically 15% to 20% lower than the original reported values. Inspection of Table 4.3 indicates

that the lower re-calculated values of τ_{app} are consistent with standardized D_o values based on Hayduk and Laudie (1974), that are higher than the D_o values reported in the original studies. Given the relatively small range in observed τ_{app} over a large range in soil texture in Table 4.3, these results indicate that using a consistent method for estimating D_o and τ_{app} has merit.

Table 4.2. Description of diffusion experiments.

Reference	ID	Soil Texture Description	Test Column Length (cm)	Test Duration (days)	Number of Tests	Sample Type	K (m/s)	Total Porosity
Al-Tarawneh et al., 2009	1a	Sand: 0.3 to 0.425 mm	Unknown	Unknown	1	Packed columns in laboratory	9.7e-04 [1]	0.40
	1b	Sand: 0.425 to 4.75 mm			1		6.2e-04 [1]	0.29
	1c	Sand: 1.18 to 4.75 mm			4		4.8e-04 [1]	0.33
	1d	Sand: 2.36 to 4.75 mm			1		1.2e-04 [1]	0.32
Barone et al., 1989	2	Clay till	4.5	15	4	Undisturbed core from field site; Laboratory test	2.8E-10	0.39
Johnson et al., 1989	3	Clay till	83	1825	1	Undisturbed core from field sit; In-situ test	6.0E-11	0.37
Klinkenberg (1951)	4a	Sand: 0.125 to 0.210 mm	Unknown				2.4E-04	0.40
	4b	Sand: <0.297 mm					2.7E-04	0.40
	4c	Glass powder: 0.12 to 0.84 mm					4.1E-04	0.47
	4d	Glass spheres: 8 mm					1.5E-01	0.44
	4e	Glass beads: 1 to 8 mm					1.7E-03	0.26
	4f	Glass beads (1 to 8 mm) and fine sand					2.7E-05	0.10
Latrille and Zoia, 2011	5	Sand with average grain diameter of 0.2 mm	80	2.5	1	Packed column in laboratory	3.0E-04	0.33
McCarthy and Johnson, 1995	6	Ottawa sand (no. 8 sieve)	2.8	6	1	Packed column in laboratory	1.0E-02	0.34
Rowe et al., 1988	7	Clay till	10	84 to 141	5	Undisturbed core from field site; Laboratory test	2.8E-10	0.39
Rowe, 1996	8a	Uniform fine Ottawa sand	13.1	3 to 21	3	Packed columns in laboratory	6.E-05 [1]	0.37
	8b	Silt	12.8	11 to 23	2		7.E-07 [1]	0.40
	8c	Halton till	6.42	5 to 12	2		3.3E-10	0.31

Notes:

[1] Hydraulic conductivity estimated based on Chapuis (2004) method.

Table 4.3. Estimated effective diffusion and apparent tortuosity coefficients.

Reference	ID	Constituent	Experiment Temperature (°C)	D_e (cm^2/s)	D_o used in Referenced Study (cm^2/s)	τ_{app} Reported in Referenced Study	Estimated D_o for Present Study[1] (cm^2/s)	Estimated τ_{app} for Present Study[2]
Al-Tarawneh et al., 2009	1a	Bromide	30	7.8E-06	2.1E-05	0.37	2.5E-05	0.31
	1b	Bromide	30	9.7E-06	2.1E-05	0.46	2.5E-05	0.39
	1c	Bromide	30	1.3E-05	2.1E-05	0.61	2.5E-05	0.53
	1d	Bromide	30	1.7E-05	2.1E-05	0.78	2.5E-05	0.67
Barone et al., 1989	2	Chloride	10	5.9E-06	n/a	n/a	1.5E-05	0.39
Johnson et al., 1989	3	Chloride	10	5.0E-06	1.5E-05	0.20 to 0.33[3]	1.5E-05	0.33
Klinkenberg, 1951	4a	Unknown				0.63	n/a	n/a
	4b					0.61	n/a	n/a
	4c					0.58	n/a	n/a
	4d					0.70	n/a	n/a
	4e					0.64	n/a	n/a
	4f					0.51	n/a	n/a
Latrille and Zoia, 2011	4	Bromide	20	2.1E-05	2.1E-05	0.56	n/a	0.56
McCarthy and Johnson, 1995	5	TCE	n/a	n/a	9.0E-06	n/a	9.6E-06	0.55
Rowe et al., 1988	6	Chloride	22	6.0E-06	1.9E-05	0.320	2.2E-05	0.28
Rowe, 1996	7a	Chloride	23	9.8E-06	1.9E-06	0.53	2.2E-05	0.45
	7b	Chloride	2	9.0E-06	1.9E-06	0.49	2.2E-05	0.41
	7c	Chloride	23	5.7E-06	1.9E-06	0.31	2.2E-05	0.26

Notes:

[1] D_o estimated for this present study using method of Hayduk and Laudie (1974).

[2] Tortuosity estimated based on ratio of reported D_e to estimated D_o.

[3] The reported upper range of tortuosity may be incorrect; it should be 0.40 based on reported D_e range.

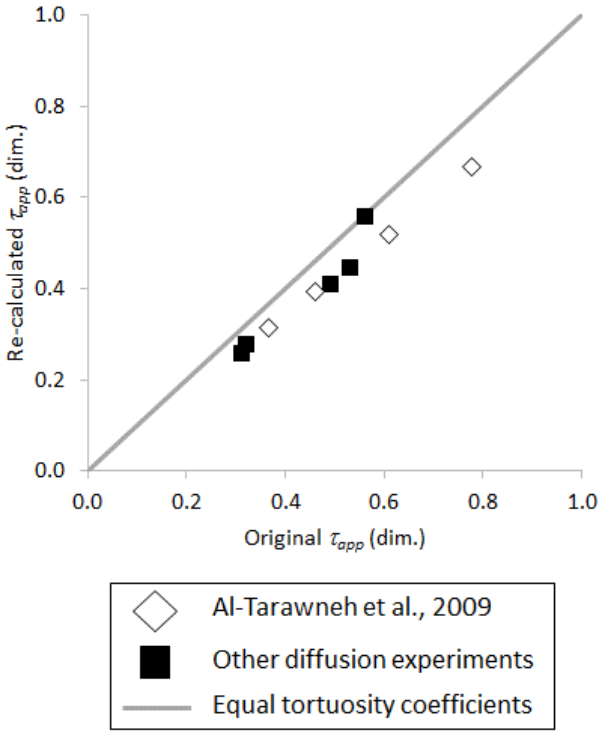

Figure 4.2. Comparison of re-calculated tortuosity coefficients versus original values reported in referenced studies. The solid line represents equal tortuosity coefficients.

4.5.3 τ_{app} versus Hydraulic Conductivity

Figure 4.3 plots τ_{app} versus K for each of the unconsolidated soil laboratory experiments listed in Tables 1 and 2. Different symbols are used in Figure 4.3 to show results from Klinkenberg (1951) and Al-Tarawneh (1951) because the effective diffusion coefficients for these two studies have higher uncertainty than the other unconsolidated soil experiments; this is because there were not sufficient data to verify

the quality of results from these two studies. These results were included in Figure 4.3, however, given the sparse diffusion experimental data available for higher permeability media.

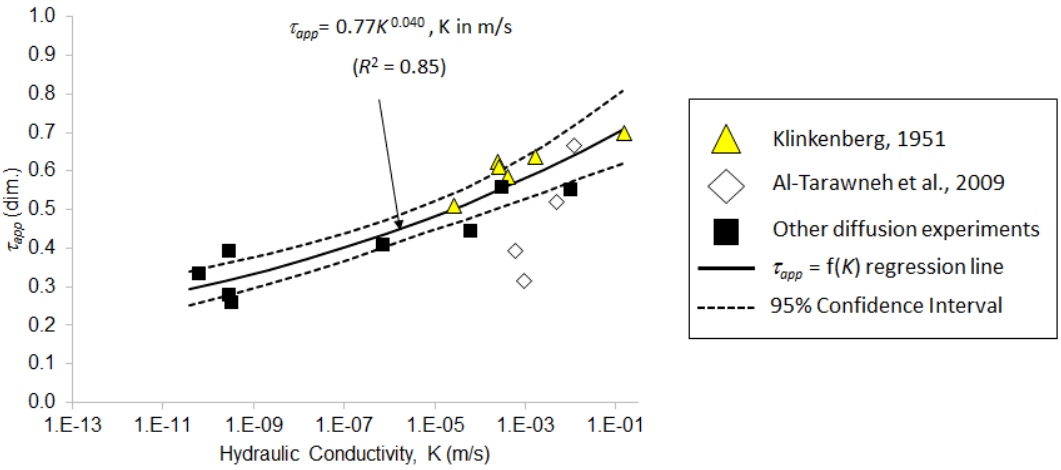

Note: Regression equation calculated based on Klinkenberg (1951) and other diffusion experiments shown above. Data from Al-Tarawneh et al. (2009) were not used for the regression calculations.

Figure 4.3. Correlation of tortuosity coefficient (τ_{app}) with hydraulic conductivity.

Inspection of Figure 4.3 indicates that the Klinkenberg (1951) results have a similar trend for τ_{app} versus K when compared to other diffusion experiments, whereas the Al-Tarawneh et al. (2009) data demonstrate a significantly different trend for τ_{app} versus K. Two of the re-calculated tortuosity coefficients from the Al-Tarawneh et al. (2009) dataset appear low for medium to coarse sands (0.31 and 0.39). The higher value is associated with a non-uniform sand (see ID No. 1b in Table 4.1). However, the lower τ_{app} of 0.31 is associated with a medium sand having a relatively uniform

grain size distribution (see ID No. 1a in Table 4.1). Also, Klinkenberg reports a higher τ_{app} of 0.51 for a soil with a broader range in grain sizes. These findings indicate that the reason for the two low values of τ_{app} based on the Al-Tarawneh et al. (2009) study are likely not related to grain size or uniformity, and are uncertain at this time.

The regression line shown in Figure 4.3 was derived using Klinkenberg et al. (1951) and the other experimental data, but not the Al-Tarawneh et al. (2009) dataset, and is given as

$$\tau_{app} = 0.77K^{0.040} \tag{4.16a}$$

with K in units of m/s and a correlation coefficient (R^2) of 0.85. For comparison, the regression equation based on inclusion of the above data plus the Al-Tarawneh et al. (2009) results is

$$\tau_{app} = 0.69K^{0.036} \tag{4.16b}$$

with K in units of m/s and R^2 of 0.63. Comparison of Eq. 4.16a and b demonstrates that inclusion of the Al-Tarawneh et al. (2009) data does not have a significant influence on the final regression equation. Given the uncertainty in the cause of the apparently two low τ_{app} values in the Al-Tarawneh et al. (2009) dataset and the lack of available data to verify the results, it is recommended that Eq. 4.16a be used as a screening-level model for estimating τ_{app} for a wide range of saturated, unconsolidated soil textures.

This is the first published regression between τ_{app} and K based on diffusion experimental data over a large range in textures including both fine-grained and coarse-grained soils. The results indicate that there is a strong correlation between τ_{app} and K over a broad K range. This demonstrates that there is a reduction in diffusion impedance in porous media as soil permeability increases, which is consistent with findings of others (e.g. Sale et al., 2014). Given that site-specific K is typically measured at contaminated sites, this metric is considered to be a more readily applied predictor of τ_{app} than effective porosity, which is typically only estimated.

There were five τ_{app} estimates for low-permeability soil included on Figure 4.3 ranging from 0.26 to 0.41 with an average of 0.33. This observed range is consistent with the estimated approximate range of 0.2 to 0.4 used by Chapman and Parker (2005). These empirical results provide a relatively narrow range which may be used to estimate τ_{app} when modeling forward or backward diffusion in clay or silt aquitards.

4.5.4 τ_{app} versus Total Porosity

Figure 4.4a presents a scatter plot of θ_t versus K for various diffusion experiments listed in Table 4.1. The square symbols represent experimental results, except for Klinkenberg (1951) results which are shown with triangular symbols. The dashed line shown in Figure 4.4a is based on the independent screening-level

regression equation developed for estimating θ_t as a function of K (see Eq. 4.16a); this line is not a regression of the data shown in Figure 4.4a

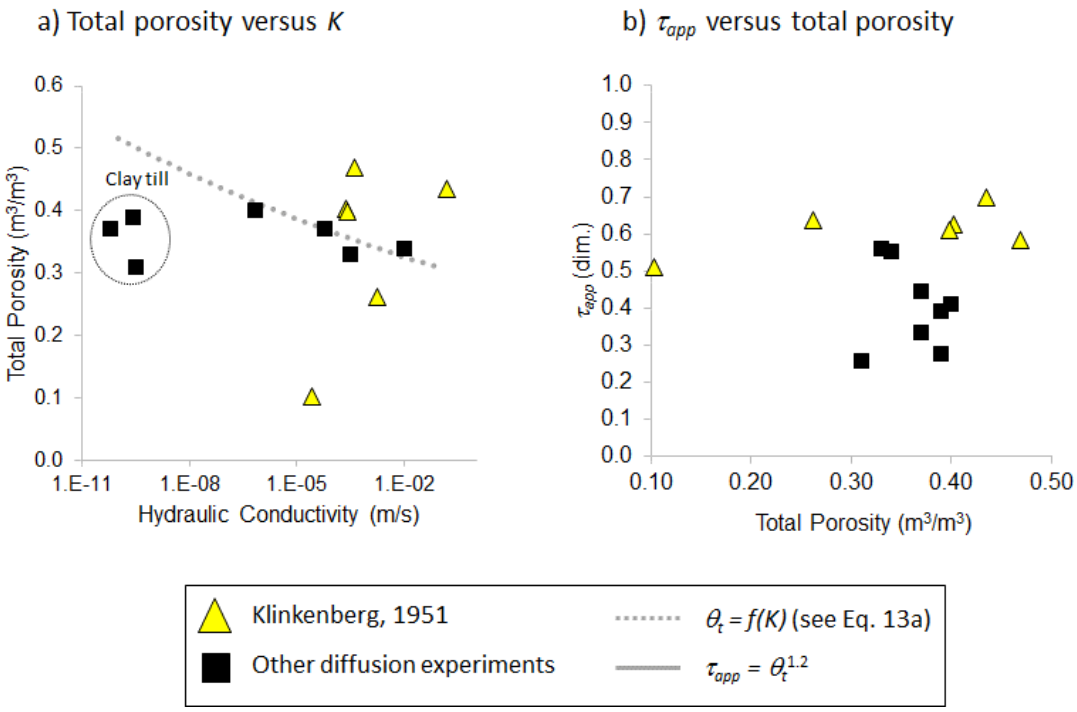

Figure 4.4. Scatter plots of total porosity versus hydraulic conductivity, and tortuosity coefficient (τ_{app}) versus hydraulic total porosity.

The square symbols representing silt and sand samples (i.e. K>1E-6 m/s) plot reasonably well on the dashed line. The square symbols that are plotted relatively far below this dashed regression line represent clay till samples, which typically have a lower total porosity than homogeneous clay. As discussed above, clay till will not fit well with Eq. 4.14 (see above). The Klinkenberg (1951) data are shown to have a

wide range of θ_t over a relatively narrow range in K. As discussed above, the experimental methods used to estimate D_e, including the methodologies for packing the columns and measuring porosity, are not presented in Klinkenberg (1951), so the representativeness of these porosity measurements is uncertain. For example, a single experiment was indicated to have a column with a porosity of only 0.1 which is very low (glass beads mixed with fine sand).

Figure 4.4b presents a scatter plot of τ_{app} versus θ_t. This figure indicates that for the Klinkenberg (1951) dataset, there is a relatively small change in τ_{app} (0.51 to 0.70) for a large range in θ_t (0.10 to 0.47), although there is uncertainty regarding the representativeness of porosity measurements reported in this study. The other unconsolidated data shown in Figure 4.4b (square symbols) do not exhibit a specific trend with respect for τ_{app} versus θ_t. A regression was not conducted for the unconsolidated data because of the apparent lack of correlation between τ_{app} and θ_t. This poor correlation is consistent with the discussion above, regarding the lack of a theoretical basis for a correlation between τ_{app} and θ_t.

4.5.5 τ_{app} versus Effective Porosity

As discussed above, theoretical mathematical studies suggest that there should be a correlation between τ_{app} based on θ_e, such that Eq. 4.13a may be used with possible values of p=0.33 (Millington and Quirk, 1961), or p=0.8 to 1.0 (Guo, 2012). These estimated relationships are based on the assumption that $\tau_{app} = \tau_{path} = (L/L_e)^2$. To the extent that processes other than flow path sinuosity impede chemical diffusion in porous media, τ_{app} will be lower than τ_{path}. The purpose of the analysis presented in this section was to provide insights on the extent to which these additional impedance processes may be occurring in more permeable soil textures, and to evaluate the relative merits of the various relationships proposed for estimating τ_{app} based on θ_e.

All studies used in the empirical regression (see Table 4.2) included measurements of total porosity, but there were none that estimated effective porosity. Table 4.1 presents estimated ranges for θ_e for various soil texture categories, including clay, silt, fine to medium sand, medium to coarse sand, fine to medium gravel, and medium to coarse gravel. To facilitate an approximate estimation of effective porosity for each diffusion experiment in Table 4.2, each diffusion experiment was assigned a soil texture category based on comparison of the textures listed in Table 4.2 with the categories listed in Table 4.1. Three methods were then utilized to estimate effective porosity for each experiment based on the specified soil texture category: 1)

based on the mid-range value of θ_e; 2) minimum range value of θ_e; and 3) maximum range value of θ_e.

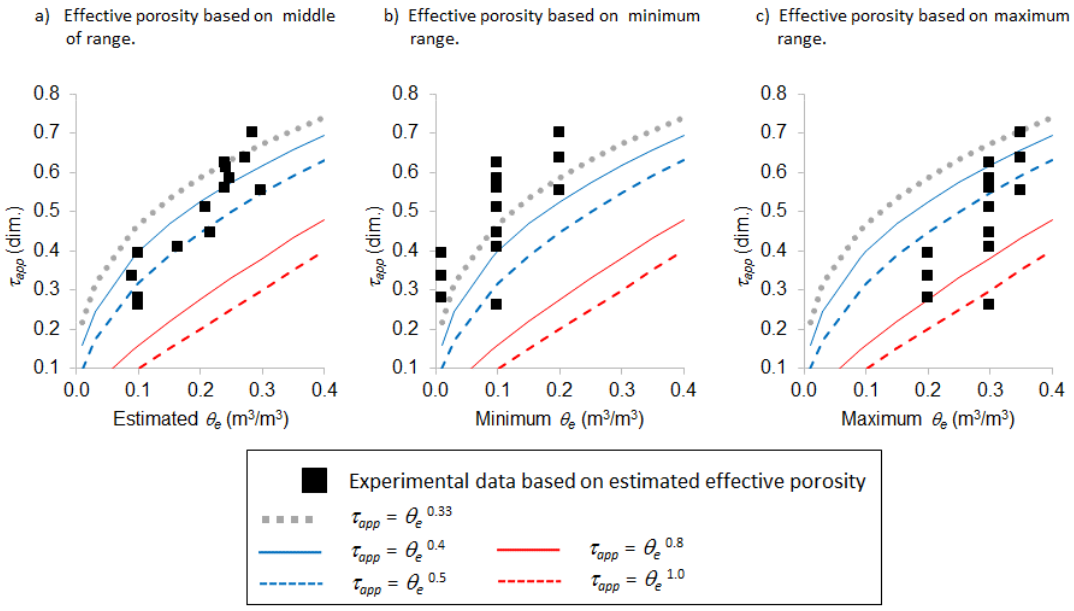

Figure 4.5. Scatter plot of calculated apparent tortuosity coefficient (τ_{app}) versus effective porosity (θ_e), with comparison to various regression equations.

Figures 4.5a through c present scatter plots of τ_{app} versus θ_e for the experiments listed in Table 4.1, except for the Al-Tarawneh et al. (2009) data, based on the three methods for estimating θ_e (see above). Various independent predicted lines are plotted in Figures 4.5a through 5c based on Eq. 4.13a, corresponding to p=0.33 (Millington and Quirk, 1961), p=0.8 and 1.0 (Guo, 2012), and p=0.4 and 0.5. The latter two p values are consistent with Guo (2012) and the assumption that

$\tau_{app}=L/L_e$ (i.e. the term on the right-hand side is not squared, which is different than the common assumption in Eq. 4.5 that has not been rigorously verified).

Figures 4.5a through c all illustrate a direct relationship between τ_{app} and $\theta_e K$ which is consistent with the theoretical discussion above. This trend is independent of the method used to estimate θ_e, indicating that this finding is conclusive even given the uncertainty in effective porosity estimates for each experimental study. It is also clear that τ_{app} is well above the estimated regression by Guo (2012) with p=0.8 to 1.0 for all three θ_e estimation methods shown in Figures 4.5a through 5c.

Figures 4.5a through c also illustrate that regardless of whether the minimum, mid-range, or maximum θ_e is assumed, τ_{app} is generally equal to, or lower than, τ_{path} if τ_{path} may be defined based on the Millington and Quirk (1961) p=0.33. Figure 4.5a, which is based on the use of mid-range θ_e as an average for each soil texture category, indicates that τ_{app} is similar to the values predicted using p=0.33 for relatively permeable soil having $\theta_e \geq 0.24$, and that the Millington and Quirk relationship ovestimates τ_{app} by up to 80% for finer-grained soils with effective porosity between 0.10 and 0.24.

Figure 4.5a indicates that the experimentally-derived τ_{app} data, based on the mid-range effective porosity values, are consistent with predictions based on Eq. 4.13a and p=0.4 to 0.5. These p values represent the range for the inverse of τ_f (i.e. L/L_e) determined mathematically by Guo (2012). One possible explanation for this general

correlation is that $\tau_{app} = (L/L_e)$ instead of $(L/L_e)^2$. Unfortunately there are insufficient data to conclusively determine which of these two τ_{app} models (i.e. Millington and Quirk, 1961 or modified Guo, 2012) is most likely to be representative.

4.6 Conclusions and Recommendations

A review and re-evaluation of published literature suggests that there should be a good correlation between τ_{app} and K, although such a relationship has not previously been quantified. This review also demonstrates that there is no theoretical basis for estimating τ_{app} based on θ_t, and that there are several alternative relationships for τ_{app} versus θ_e (i.e. Millington and Quirk, 1961; and Guo, 2012) which have not yet been validated for a wide range of soil textures

A simple screening-level model was derived to estimate effective porosity as a function of K. An attempt to validate the relationship for τ_{app} versus θ_e based on Millington and Quirk (1961) and results from previously published diffusion experiments is inconclusive, although it is conclusively shown that there is a direct relationship between τ_{app} versus θ_e, and that the Guo (2012) relationship based on Eq. 4.13a and p=0.8 to 1.0 is not valid for simulating chemical diffusion. An alternative explanation is hypothesized, such that the Guo (2012) derivation of the tortuosity

factor is correct, and that $\tau_{app} = L/L_e$ and not $(L/L_e)^2$. Additional experimental study is required to clarify which of these explanations is most likely.

An empirical relationship for τ_{app} versus K (see Eq. 4.16a) was derived for saturated, unconsolidated soil and is shown to be applicable to soil textures with a range of nine orders-of-magnitude in K. This is the first known empirical regression of τ_{app} versus hydraulic conductivity for a wide range in textures including fine-grained and coarse-grained soils. This regression equation is more readily applied at field sites than a relationship based on effective porosity, because hydraulic conductivity is often measured whereas effective porosity is not.

4.7 References

Al-Tarawneh, K.K., O. Buzzi, K. Krabbenhoft, A.V. Lyamin, and S.W. Sloan, 2009. An indirect approach for correlation of permeability and diffusion coefficients. Defect and Diffusion Forums, 283-286: 504-514.

Barone, F.S., E.K. Yanful, R.M. Quigley, and R.K. Rowe, 1989. Effect of multiple contaminant migration on diffusion and adsorption of some domestic waste contaminants in a natural clayey soil. Canadian Geotechnical Journal, 26(2): 189-198.

Barone, F.S., R.K. Rowe, and R.M. Quigley, 1992. A laboratory estimation of diffusion and adsorption coefficients for several volatile organics in a natural clayey soil. Journal of Contaminant Hydrology, 10(3): 225-250.

Barraclough, P.B., and P.B. Tinker, 1981. The determination of ionic diffusion coefficients in field soils. I. Diffusion coefficients in sieved soils in relation to water content and bulk density. Journal of Soil Science, 32: 225-236.

Barraclough, P.B., and P.B. Tinker, 1982. The determination of ionic diffusion coefficients in field soils. II. Diffusion of bromide ions in undisturbed soil cores. Journal of Soil Science, 33: 13-24.

Bear, J., 1972. Dynamics of Fluids in Porous Media. Dover Publications, Inc. New York, NY.

Boudreau, B.P., 1996. The diffusive tortuosity of fine-grained unlithified sediments. Geochimica et Cosmochimica Acta, 60(16): 3139-3142.

Carmen, P.C., 1937. Fluid flow through granular beds. Transactions, Institution of Chemical Engineers, London, 15: 150-166.

Chapman, S.W. and B.L. Parker, 2005. Plume persistence due to aquitard back diffusion following dense nonaqueous phase liquid source removal or isolation. Water Resources Research, 41(12), W12411.

Chapman, S.W., B.L. Parker, T.C. Sale, and L.A. Doner, 2012. Testing high resolution numerical models for analysis of contaminant storage and release from low permeability zones. Journal of Contaminant Hydrology, 136-137: 106-116.

Chapuis, R.P., 2004. Predicting the saturated hydraulic conductivity of sand and gravel using effective diameter and void ratio. Canadian Geotechnical Journal, 41: 787-795.

Chou, H., L. Wu, L. Zeng, and A. Chang, 2012. Evaluation of solute diffusion tortuosity factor models for variously saturated soils. Water Resources Research, 48, W10539.

Cotten, T.E., M.M. Davis, and C.D. Shackelford, 1998. Effects of test duration and specimen length on diffusion testing of unconfined specimens. Geotechnical Testing Journal, 21(2): 79-94.

Crooks, V.E., and R.M. Quigley, 1984. Saline leachate migration through clay: a comparative laboratory and field investigation. Canadian Geotechnical Journal, 21: 349-362.

de Marsily, G., 1986. Quantitative Hydrogeology: Groundwater Hydrology for Engineers. Academic Press, Inc. Orlando, FL.

Desaulniers, D.E., J.A. Cherry, and P. Frtiz, 1981. Origin, age, and movement of pore water in argillaceous quarternary deposits at four sites in Southwestern Ontario. Journal of Hydrology, 50: 231-257.

Dullien, F.A.L., 1992. Porous Media: Fluid Transport and Pore Structure, 2nd edition. Academic Press, Inc. San Diego, CA.

Freeze, R.A. and J.A. Cherry, 1979. Groundwater. Prentice-Hall, Inc. Englewood Cliffs, NJ.

Gillham, R.W., M.J.L. Robin, D.J. Dytynyshyn, and H.M. Johnston, 1984. Diffusion of nonreactive and reactive solutes through fine-grained barrier materials. Canadian Geotechnical Journal, 21: 541-550.

Grathwohl, P., 1998. Diffusion in Natural Porous Media: Contaminant Transport, Sorption/Desorption and Dissolution Kinetics. Kluwer Academic Publishers. Norwell, MA.

Hayduk, W. and H. Laudie, 1974. Prediction of diffusion coefficients for nonelectrolytes in dilute aqueous solutions. American Institute of Chemical Engineers (AIChE) Journal, 20 (3): 611-615.

Hong, C.S., M.M. Davis, and C.D. Shackelford, 2009. Non-reactive solute diffusion in unconfined and confined specimens of a compacted soil. Waste Management, 29: 404-417.

Horton, R., M.L. Thompson, and J.F. McBride, 1987. Method of estimating the travel time of noninteracting solutes through compacted soil material. Soil Science Society of America Journal, 51: 48-53.

Huysmans, M. and A. Dassargues, 2005. Review of the use of Péclet numbers to determine the relative importance of advection and diffusion in low permeability environments. Hydrogeology Journal, 13: 895-904.

IDENR, 1984. Effective Porosity of Geologic Materials - First Annual Report. Illinois Department of Energy and Natural Resources SWS Contract Report 351. Champaign, IL.

Johnson, R.L. and J.F. Pankow, 1992. Dissolution of dense chlorinated solvents into groundwater. 2. Source functions for pools of solvent. Environmental Science & Technology, 26: 896-901.

Johnson, R.L., J.A. Cherry, and J.F. Pankow, 1989. Diffusive contaminant transport in natural clay: A field example and implications for clay-lined waste disposal sites. Environmental Science & Technology, 23(3): 340-349.

Klinkenberg, L.J., 1951. Analogy between diffusion and electrical conductivity in porous rocks. Geological Society of America Bulletin, 62(6): 559-564.

Kosugi, K., 1999. General model for unsaturated hydraulic conductivity for soils with lognormal pore-size distribution. Soil Science Society of America Journal, 63: 270-277.

Latrille, C. and A. Zoia, 2011. Estimating apparent diffusion coefficient and tortuosity in packed sand columns by tracer experiments. Journal of Porous Media, 14(6): 507-520.

McCarthy, K.A., and R.L. Johnson, 1995. Measurement of trichloroethylene diffusion as a function of moisture content in sections of gravity-drained soil columns. Journal of Environmental Quality, 24(1): 49-55.

McWhorter, D.B., 1984. Specific Yield by Geophysical Logging Potential for the Denver Basin. Research Project Technical Completion Report, Colorado Water Resources Research Institute, July 1984.

Millington, R.J. and J.P. Quirk, 1961. Permeability of porous solids. Transactions of the Faraday Society, 57: 1200-1207.

Morin, R.H., D.R. LeBlanc, and B.M. Troutman, 2010. The influence of topology on hydraulic conductivity in a sand-and-gravel aquifer. USGS Staff – Published Research, Paper 351.

Mualem, Y., 1976. A new model for predicting the hydraulic conductivity of unsaturated porous media. Water Resources Research, 12(3): 513-522.

Murphy, P., A. Marquette, D. Reible, and G. V. Lowry, 2006. Predicting the performance of activated carbon-, coke-, and soil-amended thin layer sediment caps. Journal of Environmental Engineering, 132(7): 787-794.

Myrand, D., R.W Gillham, E.A Sudicky, S.F O'Hannesin, and R.L Johnson, 1992. Diffusion of volatile organic compounds in natural clay deposits: Laboratory tests. Journal of Contaminant Hydrology, 10(2): 159-177.

Overman, A.R., 1975. Ion transport through sand by convective diffusion. Plant and Soil, 43: 663-670.

Parker, B.L., J.A. Cherry, and S.W. Chapman, 2004. Field study of TCE diffusion profiles below DNAPL to assess aquitard integrity. Journal of Contaminant Hydrology, 74: 197-230.

Parker, B.L., R.W. Gillham, and J.A. Cherry, 1994. Diffusive disappearance of immiscible-phase organic liquids in fractured geologic media. Ground Water, 32(5): 805-820.

Parker, B.L., S.W. Chapman, and, M.A. Guilbeault, 2008. Plume persistence caused by back diffusion from thin clay layers in a sand aquifer following TCE source-zone hydraulic isolation. Journal of Contaminant Hydrology, 102: 86-104.

Perkins, T.K. and O.C. Johnston, 1958. A Review of Diffusion and Dispersion in Porous Media. Society of Petroleum Engineers Journal, 3(1): 70-84.

Petersen, E.E., 1958. Diffusion in a pore of varying cross section. American Institute of Chemical Engineers Journal, 4(3): 343-345.

Prudic, D.E., 1986. Ground water hydrology and subsurface migration of radionuclides at a commercial radioactive-waste burial site, West Valley, Cattaraugus County, New York. USGS Professional Paper 1325. Washington, D.C.

Rasa, E., S.W. Chapman, B.A. Bekins, G.E. Fogg, K.M. Scow, and D.M. Mackay, 2011. Role of back diffusion and biodegradation reactions in sustaining an MTBE/TBA plume in alluvial media. Journal of Contaminant Hydrology, 126: 235-247.

Reible, D.D. and D.J. Lampert, 2014. Capping for Remediation of Contaminated Sediments. In D.D. Reible, Processes, Assessment and Remediation of Contaminated Sediments (325-363). SERDP and ESTCP Remediation Technology Monograph Series. Springer Science+Business Media. New York, NY.

Reiter, B.R., 1999. Assessment of Laboratory methods for quantifying aqueous bacterial diffusion. Master of Science Thesis, University of Saskatchewan. Saskatoon, SK.

Rowe, R.K. and K Badv, 1996. Chloride migration through clayey silt underlain by fine sand or silt. Journal of Geotechnical Engineering, 122(1): 60-68.

Rowe, R.K., C.J. Caers, and F. Barone, 1988. Laboratory determination of diffusion and distribution coefficients of contaminants using undisturbed clayey soil. Canadian Geotechnical Journal, 25(1): 108-118.

Sale, T.C., J.A. Zimbron, and D.S. Dandy, 2009. Effects of reduced contaminant loading on downgradient water quality in an idealized two-layer granular porous media. Journal of Contaminant Hydrology, 102: 72-85.

Seyedabbasi, M.R., C.J. Newell, D.T. Adamson, and T.C. Sale, 2012. Relative contribution of DNAPL dissolution and matrix diffusion to the long-term persistence of chlorinated solvent source zones. Journal of Contaminant Hydrology, 134-135: 69-81.

Shackelford, C.D. and D.E. Daniel, 1991. Diffusion in saturated soil, I. Background. Journal of Geotechnical Engineering, 117(3): 467-483.

Shackelford, C.D., D.E. Daniel, and H.M. Liljestrand, 1989. Diffusion of inorganic chemical species in compacted clay soil. Journal of Contaminant Hydrology, 4: 241-273;

Shackelford, C.D., 1991. Laboratory diffusion testing for waste disposal – A review. Journal of Contaminant Hydrology, 7: 177-217.

Spitz, K. and J. Moreno, 1996. A Practical Guide to Groundwater and Solute Transport Modeling. John Wiley and Sons, New York, NY.

USEPA, 1998a. Assessment and Remediation of Contaminated Sediments (ARCS) Program: Guidance for In-Situ Subaqueous Capping of Contaminated Sediments. U.S. Environmental Protection Agency, Report EPA/905-B96-004. Chicago, IL.

USEPA, 1998b. Technical Protocol for Evaluating Natural Attenuation of Chlorinated Solvents in Ground Water. U.S. Environmental Protection Agency, Report EPA/600/R-98/128. Washington, D.C.

Van Genuchten, 1981. Analytical solutions for chemical transport with simultaneous adsorption, zero-order production and first-order decay. Journal of Hydrology, 49: 213-233.

Vervoort, R.W., and S.R. Cattle, 2003. Linking hydraulic conductivity and tortuosity parameters to pore space geometry and pore-size distribution. Journal of Hydrology, 272(1-4): 36-49.

Wang, X.Q., L.J. Thibodeaux, K.T. Valsaraj, D.D. Reible, 1991. Efficiency of capping contaminated bed sediments in situ. 1. Laboratory-scale experiments on diffusion-adsorption in the capping layer. Environmental Science & Technology, 25(9): 1578-1584.

Yanful, E.K. and R.M. Quigley, 1990. Tritium, oxygen-18, and deuterium diffusion at the Confederation Road landfill site, Sarnia, Ontario, Canada. Canadian Geotechnical Journal, 27(3): 271-275.

Chapter 5

Estimating Transverse Vertical Dispersivity

5.1 Abstract

The depletion timeframe for a non-aqueous phase liquid (NAPL) pool is strongly dependent on transverse vertical dispersivity, yet there is little guidance available for estimating this parameter over the wide range of soil textures in which NAPL resides at contaminated sites. Previous studies on estimating transverse vertical dispersivity, based largely on results from a single two-dimensional tank apparatus, indicate that this parameter is directly proportional to the average grain diameter. Through the compilation of a number of alternative case studies from the literature including multiple NAPL dissolution experiments, the trend of transverse vertical

dispersivity is opposite to what has previously been modeled; transverse vertical dispersivity is inversely proportional to the effective grain diameter when groundwater velocity (v) is below a critical threshold (v_c). A novel empirical relationship is developed for estimating transverse dispersivity based on hydraulic conductivity when $v<v_c$. The critical velocity for NAPL pool dissolution appears to range from 3 to 5 m/d based on a limited number of studies with NAPL pool lengths of 1 m or more. The method derived by Klenk and Grathwohl (2002) is validated for estimating a correction factor for dispersivity when $v>v_c$. Another empirical method is derived for estimating dispersivity based on the effective grain diameter (d_{10} in this study), groundwater velocity, and the free-water diffusion coefficient. Results of a sensitivity analysis compare the influence of these new dispersivity estimation models when estimating mass discharge from DNAPL pools of varying length in aquifers with a wide range of hydraulic conductivity and groundwater velocity.

5.2 Introduction

Sites with NAPL contamination may require expensive, long-term remediation, particularly when NAPL pools are present in the subsurface (Parker et al., 2003; Kavanaugh et al., 2012). The rate of dissolution from the surface of horizontal NAPL pools is proportional to transverse vertical dispersivity (Hunt et al., 1988; Johnson and

Pankow, 1992), and this dispersivity may be dependent on groundwater velocity at some sites (Klenk and Grathwohl, 2002; Olsson and Grathwohl, 2007; Chiogna et al.., 2010). Klenk and Grathwohl (2002) cite laboratory studies indicating that there is a wide range in this dispersivity, or α_{TV} [L] from 0.05 to 1 mm. Schafer and Therrien (1995) calibrated a field-scale model simulating dissolution from a large NAPL pool using α_{TV} = 10 mm. The wide range of α_{TV} in these studies indicates that there is relatively high uncertainty in this parameter, which contributes to substantial uncertainty in estimates of NAPL pool depletion timeframe.

NAPL pools are formed at contaminated sites in a wide range of soil textures including silt, sand, or gravel; however, most of the work on estimating dispersivity in laboratory experiments has been conducted using medium to coarse sand or relatively large diameter spherical glass beads. There is a need to better understand how to estimate dispersivity for a wide range of soil textures and groundwater velocity at contaminated sites because these experimentally-derived dispersivity values are not broadly applicable to field-scale contaminated sites. It is typically assumed that transverse vertical dispersivity is directly proportional to the mean grain size, d_{50} [L] (de Josselin de Jong, 1958; Perkins and Johnston, 1963; Klenk and Grathwohl, 2002; Ollson and Grathwohl, 2007; Chiogna et al., 2010). As shown below, the proportionality to mean grain size is not representative of α_{TV} trends observed during experiments in sand with a broad range in grain and pore size.

A companion paper demonstrated that soil tortuosity correlates with hydraulic conductivity (Carey et al., 2014b), and in some cases α_{TV} has been shown to be related to tortuosity (e.g. Klenk and Grathwohl, 2002). The objective of this study was to evaluate if α_{TV} may be correlated to hydraulic conductivity, given that K is commonly measured or estimated at contaminated sites. A detailed literature review was conducted to tabulate results of laboratory experiments where vertical dispersion was estimated as part of the original study. In a number of cases, α_{TV} was re-analyzed in this present study using a consistent methodology for estimating the tortuosity coefficient and free-water diffusion coefficient (Carey et al., 2014b). Empirical relationships are derived based on the compiled dispersivity estimates from other studies, and compared to earlier empirical models. Results of various NAPL pool dissolution studies are used to indicate a new lower limit for critical velocity (v_c) when NAPL pools are relatively long (e.g. greater than 1 m), and the sensitivity of pool depletion timeframe to critical velocity is discussed. A sensitivity analysis is conducted using the NAPL Depletion Model (Carey et al., 2014a, c) to compare the influence of these new empirical models for transverse vertical dispersivity on estimating mass discharge for DNAPL pools with varying lengths, and scenarios having a wide range of hydraulic conductivity and velocity.

5.3 Background

Hydrodynamic dispersion represents the overall spreading of a contaminant plume along the direction of bulk groundwater flow and is comprised of two components: molecular diffusion and mechanical dispersion. Transverse vertical dispersion represents vertical spreading of a solute about the centerline of a plume, and is the driving process for mass dissolution from the surface of a NAPL pool. Transverse vertical dispersion is generally caused by deviations from the bulk groundwater flow direction due to tortuous flow paths, vertical heterogeneity, and diffusion between active flow channels.

Transverse vertical dispersion, or D_z [L^2/T] may be calculated using

$$D_z = \alpha_{TV} v + \tau D_o \qquad (5.1)$$

where τ is the tortuosity coefficient [dimensionless], and D_o is the free-water diffusion coefficient [L^2/T]. The first term on the right side of Eq. 5.1 represents mechanical dispersion, and the second term represents the effective diffusion coefficient. Mechanical dispersion processes contributing to transverse vertical dispersivity include the effect of tortuous, or sinuous flow paths as well as molecular diffusion between streamlines. The latter component of mechanical dispersion is a physical mixing process.

Transverse dispersivity tends to increase as the scale of contaminant migration increases, due to a corresponding increase in the vertical heterogeneity. Transverse

dispersivity measured based on a large-scale field test (e.g. hundreds of meters) represents macro-scale field conditions; the transverse dispersivity which drives NAPL pool dissolution typically occurs over a scale of only meters, and thus will be smaller than macro-scale dispersivity. As an illustrative example, Figure 5.1 shows the thickness of aquifer above a trichloroethene (TCE) pool in which 90% of the mass discharge occurs, as a function of pool length and groundwater velocity ranging from 0.1 to 1 m/d. For a long pool length of 10 m and a slow groundwater velocity of 0.1 m/d, the thickness of aquifer with 90% of the mass from pool dissolution is only approximately 0.13 m. These calculations were conducted based on the concentration versus depth analytical solution presented in Johnson and Pankow (1992). This simple example illustrates that vertical dispersion above a pool occurs over a thin zone with a scale of centimeters, and thus is governed by pore-scale dispersivity.

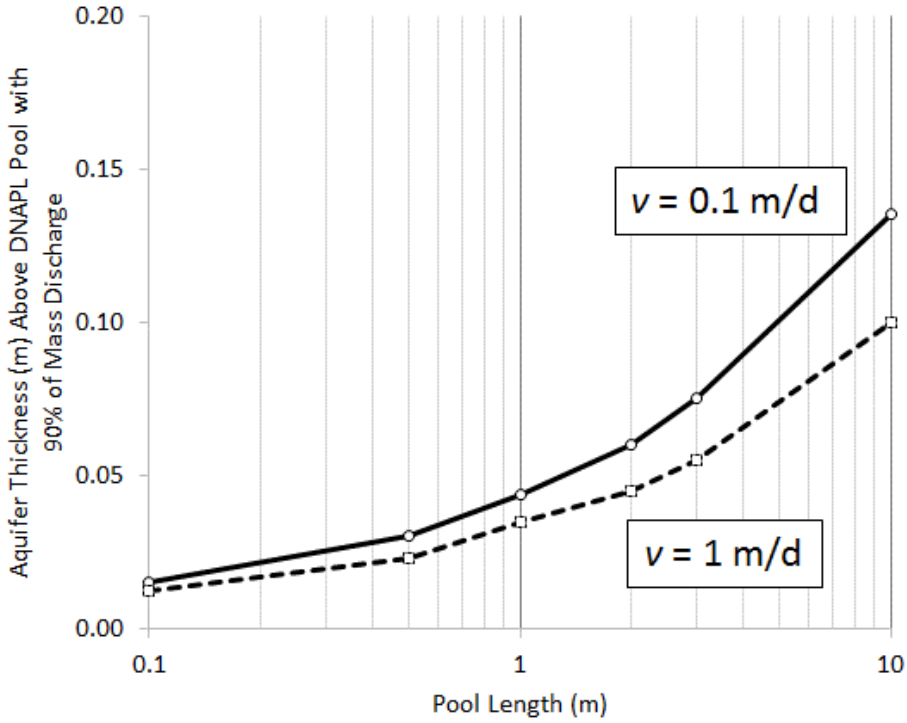

Figure 5.1 – Thickness of aquifer above a DNAPL pool with 90% of the mass discharge from the pool, as a function of pool length.

5.3.1 Factors Influencing Pore-Scale Transverse Dispersion

Naturally-occurring in situ conditions which may influence α_{TV} in the field include:

- When velocity is sufficiently high, there is insufficient time for diffusion to equalize concentrations within water flowing through a pore space, resulting in a reduction in the apparent dispersivity as discussed in Perkins and Johnston (1963) and Klenk and Grathwohl (2002). See below for a more detailed discussion regarding the influence of velocity on α_{TV};
- Well-graded soil with a broad distribution (i.e. large variance) in particle and pore size distribution will have higher dispersion relative to poorly-graded (i.e. well sorted) soil (Perkins and Johnston, 1963; Nimmo, 2004);
- The dispersivity of a porous medium will increase as the tortuosity of the porous medium increases, which corresponds to a decrease in the tortuosity coefficient (τ). For example, Klenk and Grathwohl (2002) demonstrated that the transverse dispersivity in the capillary fringe is relatively high due to increased tortuosity resulting from the presence of entrapped air.

Soil with smaller grain sizes and lower hydraulic conductivity will tend to have a broader pore size distribution (Perkins and Johnston, 1963; Carey et al., 2014c) and larger tortuosity i.e. lower tortuosity coefficient (Carey et al., 2014b) than coarser-grained soil. For these reasons it is expected that α_{TV} will be inversely proportional to

grain size and hydraulic conductivity. As shown in Table 5.1, however, previous models used to estimate α_{TV} incorporate the opposite relationship, such that α_{TV} is directly proportional to grain size (de Josselin de Jong, 1958; Carvalho and Delgado, 1999; Klenk and Grathwohl, 2002; Olsson and Grathwohl, 2007; Chiogna et al., 2010). This relationship is discussed further below based on a review of estimated dispersivity measurements for experiments utilizing a wide range of soil texture.

Table 5.1 – Various relationships for estimating dispersivity.

Reference	**α_{TV} Model**
De Josselin de Jong, 1958	$\alpha_{TV} = 0.19 d_{50}$
Carvalho and Delgado, 1999	$\alpha_{TV} = 0.08 d_{50}$, Pe<80
Carvalho and Delgado, 2000	$\alpha_{TV} = 0.5 {d_{50}}^{0.57} v^{-0.43} Do^{0.43}, 80 < Pe < 1400$
Klenk and Grathwohl, 2002	$\alpha_{TV} = 0.19 d_{50}, v \leq vc$ $\alpha_{TV} = 1.69 {d_{50}}^{0.5} v^{-0.5} Do^{0.5}, v > vc$
Olsson and Grathwohl, 2007	$\alpha_{TV} = 0.28 {d_{50}}^{0.72} v^{-0.28} Do^{0.28}$
Chiogna et al., 2010	$\alpha_{TV} = d_{50} / \sqrt{(Pe + 123)}$

Note:
In the above equations, α_{TV} and d_{50} have units of m, v has units of m/d, D_o has units of m^2/d, and Pe is dimensionless.

Pore-scale transverse dispersivity is typically estimated in the laboratory based on the use of tracer tests or NAPL dissolution experiments. There are some experimental conditions which may result in measured dispersion which is not representative of in situ pore-scale dispersion in the field, such as:

- Cells packed with spherical particles (e.g. glass beads) tend to have lower dispersivity than cells packed with non-spherical particles such as sand (Perkins and Johnston, 1963);
- Experimental cells having a large ratio of particle diameter to column width ($R_{p\text{-}c}$) will have packing irregularities which may propagate throughout the cell (Perkins and Johnston, 1963). For example, $R_{p\text{-}c}$ values greater than 0.1 may create a boundary effect which results in higher dispersivity values relative to a similarly-sized medium which does not have this boundary effect;
- Dissolution of multi-component NAPL may result in non-equilibrium conditions with an apparent reduction in α_{TV} due to intra-NAPL diffusion limitations.

5.3.2 Influence of Velocity on α_{TV}

Studies such as Seagren et al. (1999a) and Klenk and Grathwohl (2002) indicate that there is an apparent drop in α_{TV} when groundwater velocity exceeds a critical threshold (v_c), and in the case of NAPL dissolution, a corresponding decrease in dissolution mass flux (Seagren et al., 1999a). There are two potential explanations for this apparent decrease in α_{TV}: (1) an increase in groundwater velocity results in incomplete diffusive mixing between active flow channels (Klenk and Grathwohl,

2002; Olsson and Grathwohl, 2007; Chiogna et al., 2010); and/or (2) mass transfer limitations at or below the NAPL-water interface in the case of NAPL dissolution (Seagren et al., 1999a,b). As shown below, based on a review of previous studies, the former (i.e. No. 1 above) appears to generally be the cause of this apparent reduction in α_{TV} when $v > v_c$, although the latter mechanism (i.e. No. 2 above) may also be a contributing factor in NAPL dissolution studies with relatively short NAPL pool lengths or very high velocity (Seagren et al., 1999b).

For simplicity, we will refer herein to the case where $v \leq v_c$ as a *local equilibrium* (LE) condition, and the case where $v > v_c$ as a *non-equilibrium* (NE) condition. Applicable dispersivity values in these cases will be referred to as α_{TV_LE} and α_{TV_NE}, respectively. Various studies have shown that α_{TV_LE} is similar for a range in groundwater velocity (e.g. Johnson and Pankow, 1992; Eberhardt and Grathwohl, 2002; Seagren et al., 1999a), which supports the theory that transverse dispersivity is independent of groundwater velocity provided that $v < v_c$ (Klenk and Grathwohl, 2002).

Figure 5.2 was derived based on a hypothetical example of a fine to medium sand medium with a hydraulic conductivity of approximately 2×10^{-4} m/s, d_{50} of 0.3 mm, free-water diffusion coefficient of 6×10^{-5} m^2/d, tortuosity of 0.36 (based on Carey et al., 2014b), α_{TV_LE} of 0.36 mm, and use of the Klenk and Grathwohl methodology for estimating the influence of velocity on dispersivity (see below) based on the assumption that v_c is 3 m/d. This figure presents a conceptual illustration of the type

of relationship observed by Seagren et al. (1999a) and Klenk and Grathwohl (2002) for D_z/D_o versus the Peclet number (Pe) which is defined as

$$Pe = \frac{vd_{50}}{D_o} \tag{5.2}$$

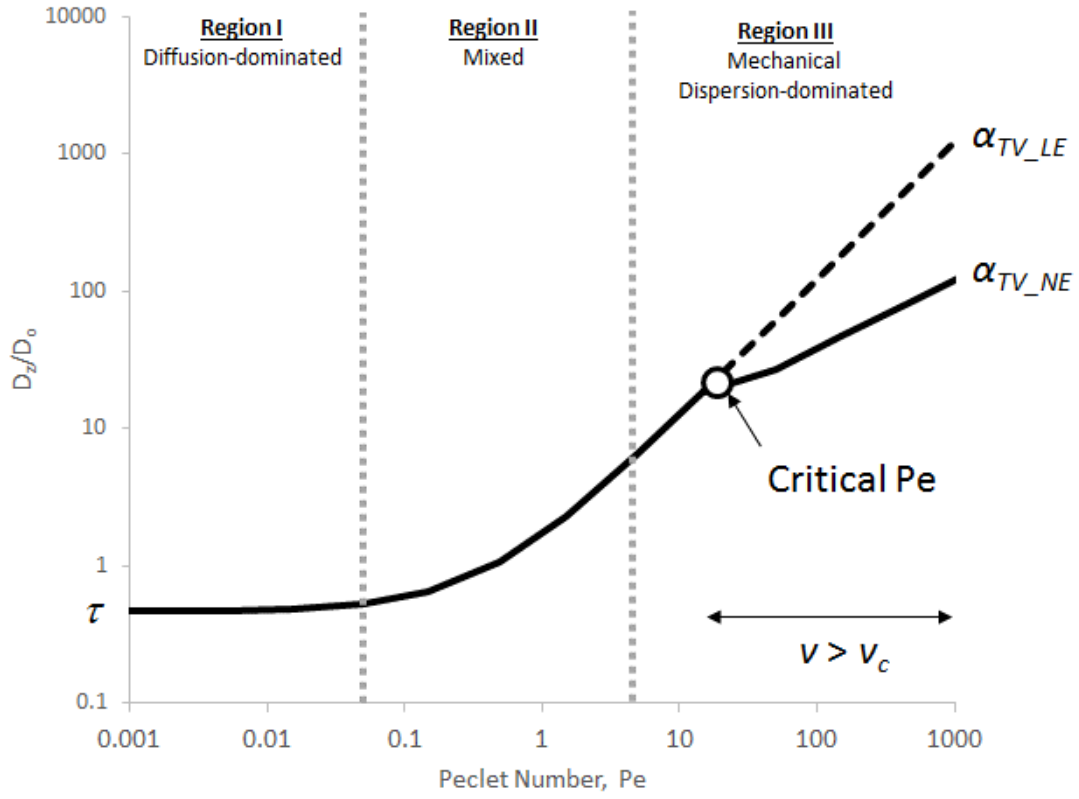

Figure 5.2 – Conceptual representation of D_z/D_o versus *Pe* curve.

Figure 5.2 indicates that there are three distinct regions on a typical D_z/D_o versus Pe curve. Region I represents diffusion-dominated conditions where mechanical dispersion is negligible. Region II represents conditions where both

diffusion and mechanical dispersion contribute significantly to the hydrodynamic dispersion, and in Region III the effects of diffusion are negligible relative to mechanical dispersion. Figure 5.2 also shows that there is a critical Pe (i.e. $v = v_c$) where a reduction occurs in the apparent dispersivity (i.e. α_{TV_NE}) and the transverse dispersion becomes lower than what would be measured if α_{TV_LE} still applied (as represented by the dashed line shown on Figure 5.2).

It is important to be able to estimate the apparent reduction in α_{TV} that occurs at high groundwater velocity under some in situ remediation scenarios; otherwise, for NAPL pool dissolution, the mass flux will be overestimated and remediation timeframe will be underestimated. Seagren et al. (1999a,b) proposed a complex model for estimating mass flux from a NAPL pool under non-equilibrium conditions; however, it is difficult to transform this flux model into a model which may be used to estimate α_{TV_NE}. Klenk and Grathwohl (2002) provide a simple equation for estimating dispersivity under non-equilibrium conditions:

$$\alpha_{TV\_NE} = \alpha_{TV\_LE}\left(0.8\sqrt{v_c/v}\right) \tag{5.3}$$

Eq. 3 will henceforth be referred to as the *NE Model*. Klenk and Grathwohl (2002) also derived an equation for the critical velocity based on the assumption that close to complete mixing occurs when the effective diffusion distance is equal to the pore radius between active flow channels, and is given as

$$v_c = \frac{2D_o d_{50}}{a^2} \quad (5.4)$$

where a represents the radius of a pore between two active flow channels in which diffusion is occurring, to equilibrate concentrations between the two channels.

The concept of a local equilibrium condition, where α_{TV_LE} is insensitive to groundwater velocity, contradicts more recent studies which derived empirical models for dispersivity that are always dependent on velocity (see equations by Olsson and Grathwohl (2007) and Chiogna et al. (2010) in Table 5.1). The applicability of both types of models are discussed further below, with a focus on estimating transverse dispersivity for estimating mass flux associated with NAPL pool dissolution.

5.4 Dispersivity Trends – Local Equilibrium ($v \leq v_c$)

A detailed literature review was conducted to compile results of laboratory experiments where transverse vertical dispersion was measured based on NAPL pool dissolution or tracer tests under local equilibrium conditions (i.e. where dispersivity was insensitive to velocity). Table 5.2 presents a list of 12 case studies with available study data including grain size, hydraulic conductivity, groundwater velocity, and a description of the method used in the original study to estimate transverse dispersion. In some cases, hydraulic conductivity was not measured or reported in the original study. For these studies, the Chapuis (2004) method was used to estimate hydraulic

conductivity (K) based on the d_{10} grain size and porosity. As shown in Table 5.2, hydraulic conductivity for the cited laboratory experiments ranges between 8.0×10^{-5} to 1.9×10^{-2} m/s.

Table 5.2 – Dispersivity laboratory experiment descriptions.

Study	Test Type	Peclet Number, Pe	Constituent	Porous Medium	Grain Size (mm)	d_{50} (mm)	d_{10} (mm)	Method used to estimate Dz and/or α_{TV}	K (m/s)	Velocity, v (m/d)	Porosity (m^3/m^3)
Anderson et al., 1992	Tracer Test	0.8	PCE	Sand	0.1 to 0.84	0.5	0.1	Calibrated Dz using steady-state 2-D analytical solution for concentration profile measured downgadient of residual NAPL zone	3.0E-04	0.1	0.36
Chrysikopoulos et al, 1994	NAPL Dissolution	0.9	1,1,2-TCA	Sand	0.60 to 0.84	0.69	0.6	Conducted physical NAPL pool dissolution experiment, calibrated dispersion for sampling ports within 3 cm of the pool surface using a steady-state analytical model. Original study calibrated dispersion assuming a mass transfer resistance at the NAPL-water interface; for the present study, the Hunt et al. (1988) solution was used based on the assumption of zero resistance to mass transfer. K estimated based on Voudrias and Yeh, 1994	5.1E-03	0.08	Uncertain
Chrysikopoulos et al, 2000	Tracer Test	2.5	Bromide	Sand	0.25 to 0.45	0.35	0.25	Used three-dimensional analytical solution to calibrate D_x and D_y=D_z.	8.6E-04	1.2	0.42
Cirpka et al., 2006	Tracer Test	38.5	Hydrogen	Sand	1 to 2.5	1.75	1	Developed analytical solution to calculate transverse dispersion coefficient based on length of reactive plume, where a basic solution was injected into acidic water medium. Original study estimated D_e=1x10^{-9} m^2/s.	5.0E-03	1.9	n/a
Eberhardt and Grathwohl, 2002	NAPL Dissolution	102.0	Coal tar	Sand	0.8 to 2.5	1.3	0.8	Two independent methods provided consistent dispersivity estimations: a) steady-state analytical solution used to match concentrations at various sampling ports with varying height above pool; and b) steady-state analytical solution for mass discharge downgradient of pool. Estimated dispersivity was similar for various NAPL constituents. Used toluene Do to estimate peclet number for this study.	5.5E-03	5.1	Uncertain
Johnson & Pankow, 1992	NAPL Dissolution	21.3	TCE	Sand	Uncertain	0.6	0.3	Calibrated dispersivity through simulation of pool dissolution mass discharge and comparison to mass discharge measured by Schwille	3.5E-03	2.7	0.35
Oostrom et al., 1992	Tracer Test	17.0	Sodium Iodide	Sand	0.25 to 1	0.5	0.25	Calibrated 2-D steady-state analytical solution to observed vertical profile in dense plume at two distances downgradient of source.	4.2E-04	3.2	0.37
Pearce et al, 1994	NAPL Dissolution	0.8	1,1,2-TCA	Sand	0.30 to 0.84	0.69	0.425	Calibrated vertical dispersion using a steady-state analytical model based on concentration measurements.	2.2E-03	0.08	0.46
Seagren et al., 1999 - Reactor 1	NAPL Dissolution	92.8	Toluene	Glass beads	1.8 to 2.2 mm	2	1.8	Original study measured steady-state mass discharge. Present study calculated D_z and α_{TV} based on mass discharge.	1.5E-02	3.2	0.39
Seagren et al., 1999 - Reactor 2	NAPL Dissolution	8.1	Toluene	Glass beads	1.8 to 2.2 mm	2	1.8	Original study measured steady-state mass discharge. Present study calculated D_z and α_{TV} based on mass discharge.	1.9E-02	0.3	0.42
Szocsody et al, 1994	Tracer Test	2.6	Salt and/or organic tracer(s)	Sand	0.074 to 0.21	0.15	0.074	Continuous injection of tracer and estimation of dispersivity based on steady-state mass flux downgradient of source.	8.0E-05	3.0	0.40
Voudrias and Yeh, 1994	NAPL Dissolution	2.8	Toluene	Sand	0.30 to 0.84	0.69	0.425	Calibrated vertical dispersion using a steady-state analytical model based on concentration measurements.	4.5E-03	0.28	0.47

Seven of these tests were based on mass flux or concentration measurements associated with NAPL dissolution (Chrysikopoulos et al., 1994 and 2000; Eberhardt and Grathwohl, 2002; Johnson and Pankow, 1992; Pearce et al., 1994; Seagren et al. 1999a Reactors 1 and 2; and Voudrias and Yeh, 1994). The other five experiments were based on tracer tests (Anderson et al., 1992; Cirkpa et al., 2006; Oostrom et al., 1992; and Szecsody et al., 1994). Ten of these experiments were conducted using sand and two experiments were conducted using glass beads (Seagren et al., 1999a Reactors 1 and 2). A wide range of constituents were used in these 12 experiments including bromide, hydrogen, multicomponent coal tar, sodium iodide, tetrachloroethene (PCE), neat and multicomponent toluene mixtures, 1,1,2-trichloroethane (1,1,2-TCA), trichloroethene (TCE), and salt and organic tracers.

For most of these experiments, the vertical dispersion and corresponding calculation of dispersivity were provided with the original study. To ensure that differences in dispersivity values between studies do not reflect a difference in methods for estimating τ and D_o, values of dispersivity were re-calculated based on a consistent methodology for estimating the effective diffusion coefficient ($D_e = \tau D_o$). The Hayduk and Laudie (1974) method was generally used in this study to estimate D_o, and the empirical model derived by Carey et al. (2014b) was used to estimate τ (τ=0.6$K^{0.03}$) The values of α_{TV_LE} were then re-calculated for the studies listed in Table 5.2 where sufficient data were available. For studies where estimates of dispersivity

were determined over a range of velocities, those dispersivities that were apparently insensitive to velocity were used to calculate an average α_{TV_LE} for this study.

Chrysikopoulos et al. (1994) conducted a NAPL pool dissolution experiment and calibrated vertical dispersion based on the assumption of rate-limited mass transfer. The length of the pool was 0.28 m and the groundwater velocity for the experiment was 0.08 m/d. Based on a comparison to other local equilibrium studies presented in Table 5.2, it is reasonable to assume that the local equilibrium assumption applies to the experiment conducted by Chrysikopoulos et al. (1994). A new value of D_z was calibrated as part of this present study (see Figure 5.3) based on the analytical solution presented in Carey et al. (2014d). Chrysikopoulos et al. (1994) had originally calculated α_{TV_LE} to be 0.73 mm based on the assumption of non-equilibrium mass transfer at the NAPL-water interface and a tortuosity coefficient of 0.7. Based on the assumption of local equilibrium and a tortuosity coefficient of 0.51 estimated as part of this present study, α_{TV_LE} was calculated to be 0.41 mm which is 44% lower than the original estimate by Chrysikopoulos et al. (1994). This demonstrates why it is important to assess the assumptions and input parameters in the original studies, to confirm that α_{TV_LE} estimates reflect a consistent approach across all studies.

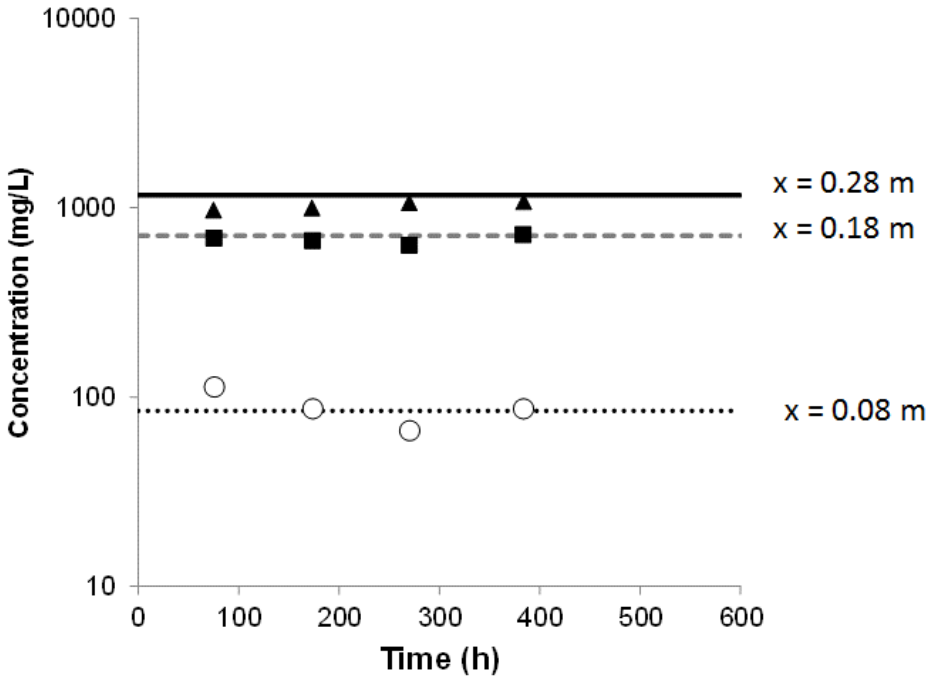

Figure 5.3 – Calibrated Steady-State Concentrations for Monitoring Data in Chrysikopoulos et al. (1994). Symbols represent observed data, and lines represent simulated steady-state concentrations based on a calibrated vertical dispersion coefficient of 7.1×10^{-5} m^2/d.

Seagren et al. (1999a) present steady-state mass flux results for four sets of experiments conducted with neat toluene or a multicomponent NAPL mixture consisting of toluene and dodecane, with groundwater velocity ranging from 0.1 m/d to 30 m/d and NAPL pool lengths slightly less than 5 cm. Two reactors packed with glass beads were used by Seagren et al. (Reactors 1 and 2). Prior to the NAPL dissolution experiments, Seagren et al. (1999a) conducted tracer studies using

fluorescein to estimate the transverse vertical dispersivity for two reactor columns (Reactors 1 and 2). The tracer tests were conducted using a range of velocity (11 to 23 m/day) for which transverse dispersion would be dominated by mechanical dispersion (i.e. Region III in Figure 5.2). Based on the results of these tracer tests, Seagren et al. (1999a) estimated α_{TV_LE} to be 0.042 and 0.031 mm for these two reactors, respectively.

As part of the present study, α_{TV_LE} was independently estimated based on mass flux measurements presented in Seagren et al. (1999a) for the NAPL dissolution experiments. Based on the results of these toluene experiments, α_{TV_LE} was estimated to be 0.13 and 0.22 mm for Reactors 1 and 2, respectively. The reason for the underestimation of dispersivity based on the fluorescein tracer tests (by 56% to 87% for Reactors 1 and 2, respectively) is due to the use of a high velocity which probably resulted in non-equilibrium conditions (i.e. incomplete diffusive mixing within pores).

Johnson and Pankow (1992) calculated an average transverse vertical dispersivity of 0.23 mm based on a DNAPL pool dissolution experiment by Schwille (1988) and an assumed effective diffusion coefficient of 2.7×10^{-10} m^2/s. Using the parameters estimated in this study for Do and the tortuosity coefficient (Table 3), the effective diffusion coefficient was re-calculated to be 5.4×10^{-10} m^2/s. Figure 5.4 compares the original and re-calculated transverse vertical dispersivity values for each of the velocity scenarios run by Schwille (1988). The average transverse vertical

dispersivity was re-calculated to be 0.14 mm in this present study, which is 39% lower than the original value presented in Johnson and Pankow (1992).

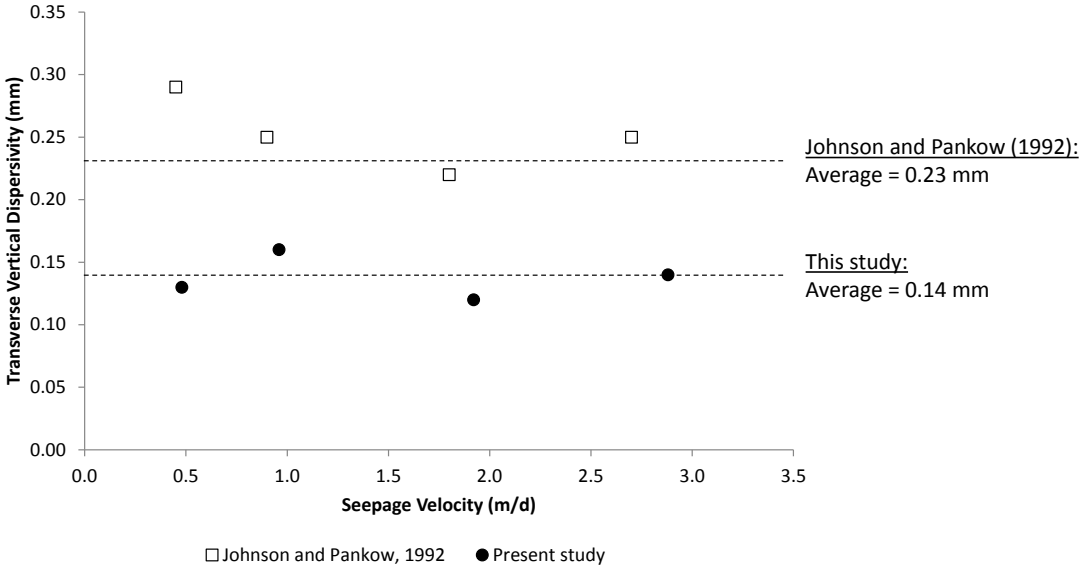

Figure 5.4 – Re-calculation of calibrated transverse dispersivity based on Schwille (1988) experiment, and revised D_o.

Table 5.3 presents original estimates of dispersivity, as well as the re-calculated values from this study. Most of the differences between original and current dispersivity estimates are due to a difference in the effective diffusion coefficient (D_e), particularly with respect to the estimated tortuosity coefficient (τ). For example, six of the original dispersion experiments cited in Table 5.3 assumed τ=0.7. Based on the Carey et al. (2014b) empirical model for estimating the tortuosity coefficient based on K, the values of τ in this study had a narrow range from 0.53 to

0.66. Given these studies are based on local equilibrium conditions where velocity and mechanical dispersion are relatively small, the differences in the tortuosity coefficient result in a significant difference in the estimated α_{TV_LE}. Figure 5.5 compares the original and present dispersivity estimates graphically, illustrating that the use of a consistent methodology for estimating D_e for a broad range of studies has a significant influence on dispersivity estimates.

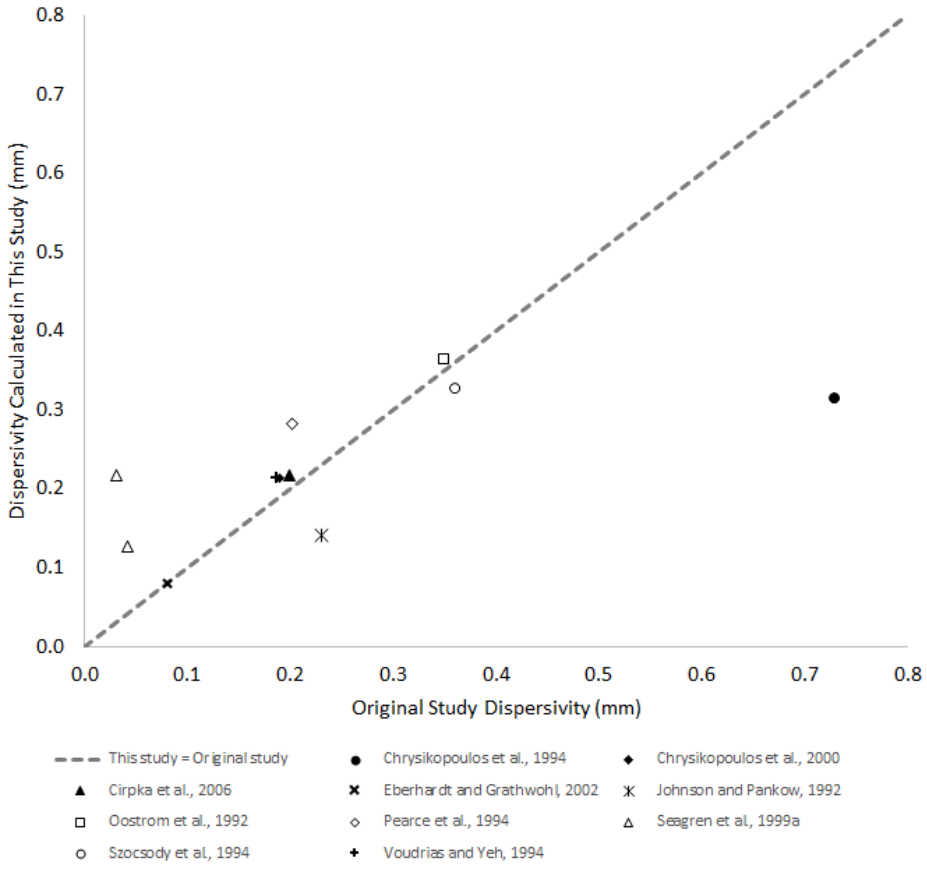

Figure 5.5 – Dispersivity values estimated in this study versus original studies.

Table 5.3 – Estimated α_{TV} based on local equilibrium conditions for laboratory studies.

	Original Study				This Study				
Study	Calibrated D_y or D_z (m^2/d)	Original study Tortuosity (dim.)	Original study Do (m^2/s)	$Alpha_{TV}$ Based on Original Study (mm)	Calibrated D_z (m^2/d)	Estimated Tortuosity (dim.)	Estimated Do (m^2/s)	Average α_{TV} at $v \le v_C$ (mm)	Temperature (°C)
Anderson et al., 1992	6.83E-05	n/a	n/a	n/a	6.83E-05	0.56	7.6E-10	0.32	20
Chrysikopoulos et al, 1994	1.10E-04	0.7	8.1E-10	0.73	7.01E-05	0.62	8.1E-10	0.31	20
Chrysikopoulos et al, 2000	3.46E-04	0.70	2.0E-09	0.19	3.46E-04	0.58	1.9E-09	0.21	20
Cirpka et al., 2006	4.66E-04	n/a	1.0E-09	0.20	4.66E-04	0.62	1.0E-09	0.22	20
Eberhardt and Grathwohl, 2002	n/a	n/a	n/a	0.08	n/a	0.63	n/a	0.08	20
Johnson & Pankow, 1992	Various	n/a	n/a	0.23	Various	0.61	8.8E-10	0.14	21
Oostrom et al., 1992	1.20E-03	n/a	1.1E-09	0.35	1.20E-03	0.56	1.1E-09	0.36	
Pearce et al, 1994	6.59E-05	0.7	8.1E-10	0.20	6.59E-05	0.60	8.1E-10	0.28	20
Seagren et al., 1999 - Reactor 1	n/a	0.67	n/a	0.042	4.51E-04	0.65	8.0E-10	0.13	20
Seagren et al., 1999 - Reactor 2	n/a	0.67	n/a	0.031	1.06E-04	0.66	8.0E-10	0.22	20
Szocsody et al, 1994	1.08E-03	n/a	n/a	0.36	1.08E-03	0.53	2.0E-09	0.33	20 (est.)
Voudrias and Yeh, 1994	1.03E-04	0.7	8.4E-10	0.19	1.03E-04	0.62	8.0E-10	0.21	20

Figure 5.6 plots α_{TV_LE} (this study) versus K with solid symbols representing the 12 studies listed in Tables 1 and 2. Figure 6 demonstrates that transverse dispersivity for these studies generally declines with increasing hydraulic conductivity, which is consistent with the conceptual model described in Blackwell (1962) and Perkins and Johnston (1963). A regression was performed for α_{TV_LE} versus K based on the dispersivity data obtained from laboratory experiments performed with sand-packed cells. The resulting correlation was determined to be

$$\alpha_{TV\_LE} = 0.08K^{-0.16}, v \leq v_c \quad (5.5)$$

where α_{TV_LE} has units of mm and K has units of m/s. Eq. (5) will henceforth be referred to as the *LE(K) Model*. The prediction interval for this model is also shown on Figure 5.6.

Figure 5.6 also includes results from several studies which had lower estimates of transverse vertical dispersivity (Olsson and Grathwohl, 2007; Chiogna et al., 2010; Rolle et al., 2012 and 2013) . There were some experimental runs in these four studies where the tank thickness (8 to 11 mm) was too narrow relative to coarse glass beads used in the study, with a width to maximum grain size diameter less than 15; these specific results are not shown on Figure 5.6 due to possible boundary effects which result in artificially increased dispersivity (Perkins and Johnston, 1963).

These four studies used the same two-dimensional tank apparatus, and as shown on Figure 5.6 have different results when compared to the other studies.

Specifically, these four studies have lower values of α_{TV_LE} in general, and exhibit an increasing α_{TV_LE} with increasing hydraulic conductivity which is opposite to the trend observed with the other 12 studies. The reasons for these marked differences are not certain, although they may be related to relatively homogeneous conditions in these four studies relative to the other 12 studies. Given that the other 12 studies used different experimental equipment and are based on both tracer studies and NAPL dissolution studies, these 12 studies are more representative for the purpose of simulating NAPL depletion.

Several field-scale test results (Fiori and Dagan, 1999; Jensen et al., 1993; and van der Kamp, 1994) are also shown on Figure 5.6 for illustrative purposes to represent the upper limit of dispersivity expected at the pore scale. These field studies were specifically selected because they were conducted in relatively homogeneous aquifers, and in the case of Fiori and Dagan (1999) and Jensen (1993), stratigraphic influences were considered during the derivation of dispersivity.

Figure 5.6 shows that, as expected, dispersivity based on field-scale tests are generally higher than dispersivity values estimated based on laboratory experiments, likely due to increased heterogeneity in the field tests that were conducted at scales of hundreds to thousands of meters. In addition, there may be a broader pore size distribution in the field-scale tests which also results in an increase in transverse dispersivity.

Figure 5.6 shows a regression line for dispersivity predicted based on the Chiogna et al. (2010) model listed in Table 1. As shown on Figure 5.6, the Chiogna et al. (2010) model is not representative of dispersivity trends for the 12 studies listed in Tables 2 and 3.

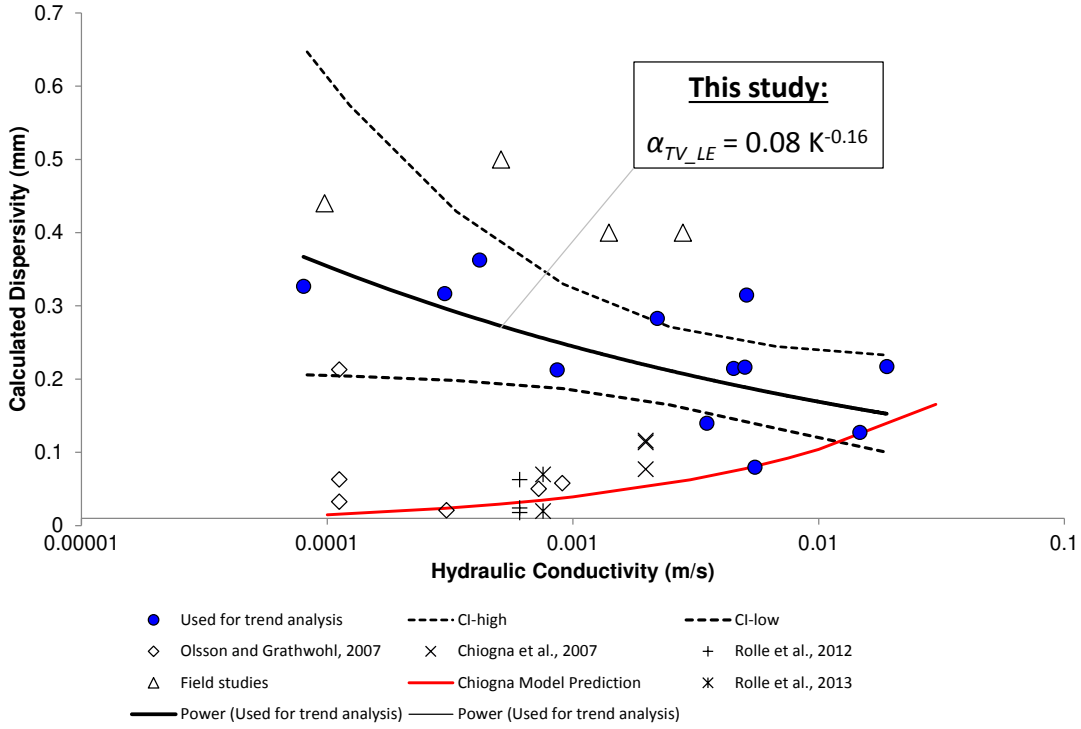

Figure 5.6 – Transverse vertical dispersivity versus hydraulic conductivity for local equilibrium conditions.

A multi-parameter model was also evaluated with respect to its ability to estimate dispersivity for both local equilibrium ($v \leq v_c$) and non-equilibrim ($v > v_c$) conditions. (See below for a discussion of the influence of velocity on dispersivity

under non-equilibrium conditions.) This second model is similar to that developed by Olsson and Grathwohl (2007) shown in Table 5.1, with the exception that the term $d_{50}^{0.72}$ has been replaced with $0.001 d_{10}^{-0.28}$ where d_{50} and d_{10} have units of m in these regression equations In other words, we were able to obtain a better fit to the dispersivity data under both local and non-equilibrium conditions by changing the relationship in the model from being directly proportional to grain size to inversely proportional, and by multiplying by a factor of 0.001. This regression equation was arrived at accidentally, so the reason for this factor of 0.001 is uncertain. In this manner, dispersivity is estimated to be smaller for coarser-grained soil, which is consistent with the experimental data shown in Figure 5.6. This second model will henceforth be referred to as the *Empirical Model*, and is given as:

$$\alpha_{TV\_LE} = 0.28 \frac{(d_{10})^{-0.28}}{1000} v^{-0.28} D_o^{0.28} \tag{5.6}$$

where α_{TV_LE} and d_{10} have units of m, v has units of m/d, and D_o has units of m^2/d. While the Empirical Model uses d_{10} to be consistent with the relationship to K, there is little difference in the model regardless of whether d_{10} or d_{50} are used, possibly because the laboratory experiments used relatively uniformly-sized sands.

Based on general concepts discussed above, the transverse vertical dispersivity is not supposed to be sensitive to velocity or chemical-specific diffusion coefficients under local equilibrium conditions. That is, at relatively low velocity there should be sufficient residence time in pore spaces for complete diffusive mixing to occur

between active flow channels. The Empirical Model provides a reasonable fit to the limited experimental data under local equilibrium conditions, however. A sensitivity analysis is presented below to further compare the use of the LE(K) and Empirical Models for a range of soil texture and velocity. The Empirical Model should be used with caution, however, in that it will predict continued increases in dispersivity as velocity is decreased with no upper-bound limit to dispersivity, which is not realistic based on the concept of diffusive mixing as a governing factor in transverse dispersivity. In addition, the Empirical Model will predict chemical-specific dispersivity values which is also not supported by the above conceptual model. The Empirical Model is presented herein to provide a comparison with similar models cited in Table 5.1.

5.5 Velocity Influence on Dispersivity at Non-Equilibrium ($v > v_c$) Condition

Klenk and Grathwohl (2002) derived the NE Model (see Eq. 3) based on the theory that incomplete diffusive mixing at the pore scale will result in a reduction to transverse dispersivity, when velocity exceeds a critical threshold (i.e. $v>v_c$). This theory matches well with the experimental evidence cited above. For example, Seagren et al. (1999a) noted that there was an apparent reduction in mass flux from NAPL dissolution, below what was expected under local equilibrium conditions, as

velocity increased. Seagren et al. (1999a) noted, based on plots of mass flux versus velocity, that the critical velocity was approximately 18 m/d.

In contrast, Figure 5.7 presents plots of dispersivity (calculated as part of the present study) versus velocity for four sets of experiments. The apparent values of v_c are shown on Figure 5.7 as ranging from 0.3 to 6.0 m/d, where v_c is defined as the maximum velocity at which dispersivity appears to be insensitive to velocity. Peclet numbers associated with these velocity thresholds ranged from 8 to 175. The difference in v_c identified based on Figure 5.7 relative to the original study demonstrates the importance of plotting dispersivity versus velocity when quantifying v_c. Changes in dispersivity are more apparent on this type of graph than plots of mass flux versus velocity for NAPL dissolution. Figure 5.7 illustrates that the NE Model reasonably matches the apparent deline in dispersivity with increasing v when $v>v_c$, which further validates the theoretical derivation by Klenk and Grathwohl (2002). Figure 5.7 indicates that the Empirical Model also provides a reasonable match to the observed dispersivity values under both local equilibrium and non-equilibrium conditions, although the rate of dispersivity decline is milder than the NE Model predicts. Figure 5.7b indicates that if the Empirical Model is used to estimate dispersivity for velocity values less than 0.3 m/d, then it will no longer provide a reasonable match to the data under local equilibrium conditions. This gives an example of how the Empirical Model may give inaccurate results for scenarios where groundwater velocity is relatively low (i.e. $v<<v_c$).

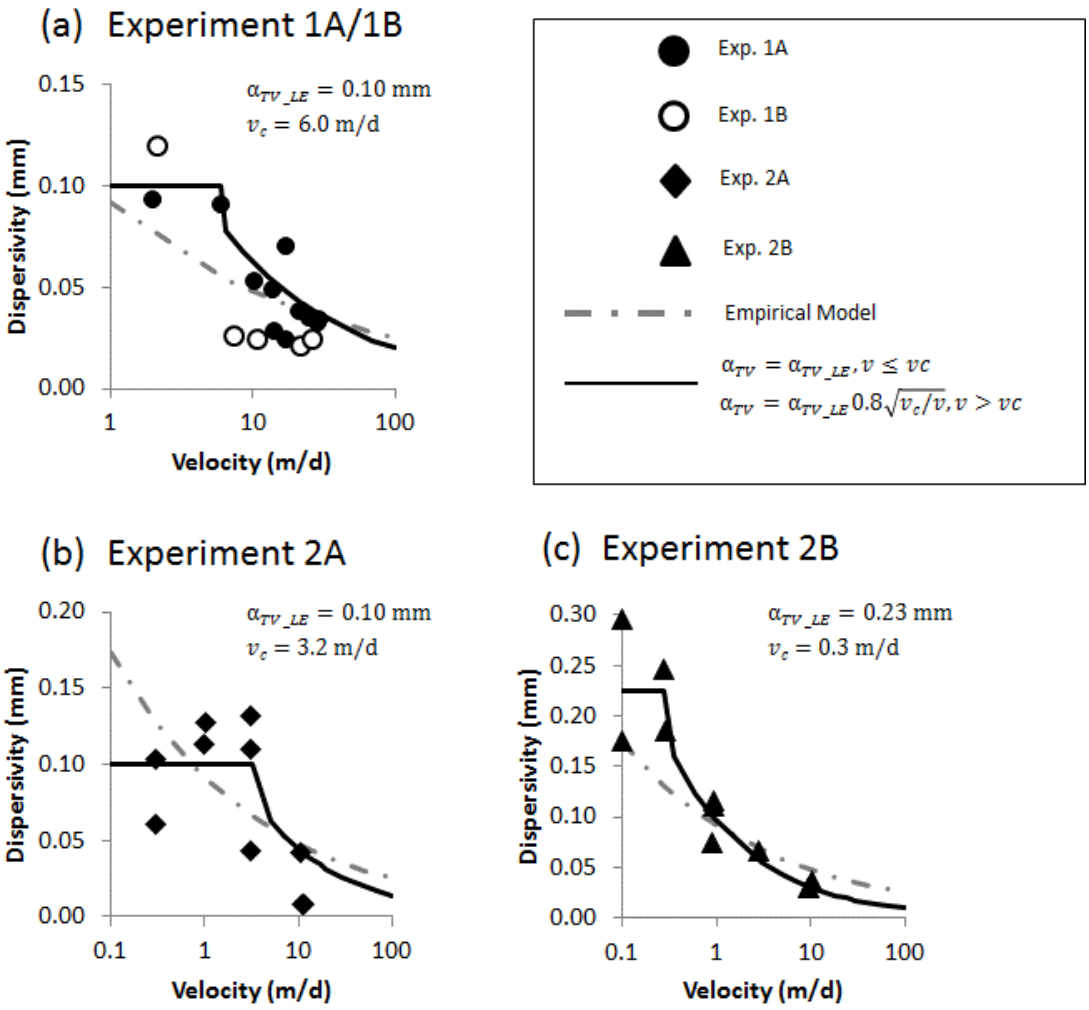

Figure 5.7 – Transverse vertical dispersivity calculated in this study based on Seagren et al. (1999) experimental results, with comparison to various non-equilibrium models.

Review of other NAPL dissolution studies where a critical velocity may be identified include Pearce et al. (1994) with v_c = 0.08 m/d and Pe=0.8; and Voudrias

and Yeh (1994) with v_c = 0.28 m/d and Pe=3. Two NAPL dissolution studies were conducted at multiple velocities with no apparent reduction in dispersivity, meaning that the highest velocity in each of these two experiments represents the lower limit for v_c: Eberhardt and Grathwohl (2002) used a maximum velocity of 5.1 m/d (Pe=102), and Johnson and Pankow (1992) cite a maximum velocity from a Schwille (1988) experiment of 2.7 m/d (Pe=21). For comparison, Klenk and Grathwohl (2002) observed a v_c of 4 m/d for transverse dispersion in a capillary fringe, and cited Pe ranges of 70 to 128 as being critical thresholds based on other experiments reported in the literature.

Based on the studies cited above, a wide range of critical thresholds for transition from local to non-equilibrium conditions have been observed with v_c ranging from 0.08 to 6 m/d, and critical Pe ranging from 0.8 to 175. These thresholds are obviously highly system-specific and are thus difficult to predict. Figure 5.8a shows a plot of v_c estimated for the above NAPL studies based on Eq. (4), versus the observed v_c (or lower limit v_c where no apparent reduction in dispersivity had been observed). While there are some points where the calculated v_c is close to the observed (i.e. small deviation from the dashed line of best fit), there are other points with marked differences between the estimated and observed v_c. Figure 5.8b plots the observed v_c (or lower limit) versus the pool length (L_p) from each experiment. Based on the limited experimental data, this figure indicates that for longer pools (i.e. L_p > 1 m) a conservative estimate of v_c may be on the order of 3 to 5 m/d for relatively coarse-

grained aquifers, which is consistent with the Klenk and Grathwohl (2002) v_c of 4 m/d with dispersion in the capillary fringe. Pool length is not an indicator for v_c if the degree of pore-scale diffusive mixing is the governing factor, although pool length is an influencing variable when NAPL-related mass transfer limitations occur (Seagren et al., 1999b). Since there are only a few data available to develop an empirical formula for v_c, the observations cited above should be used with caution.

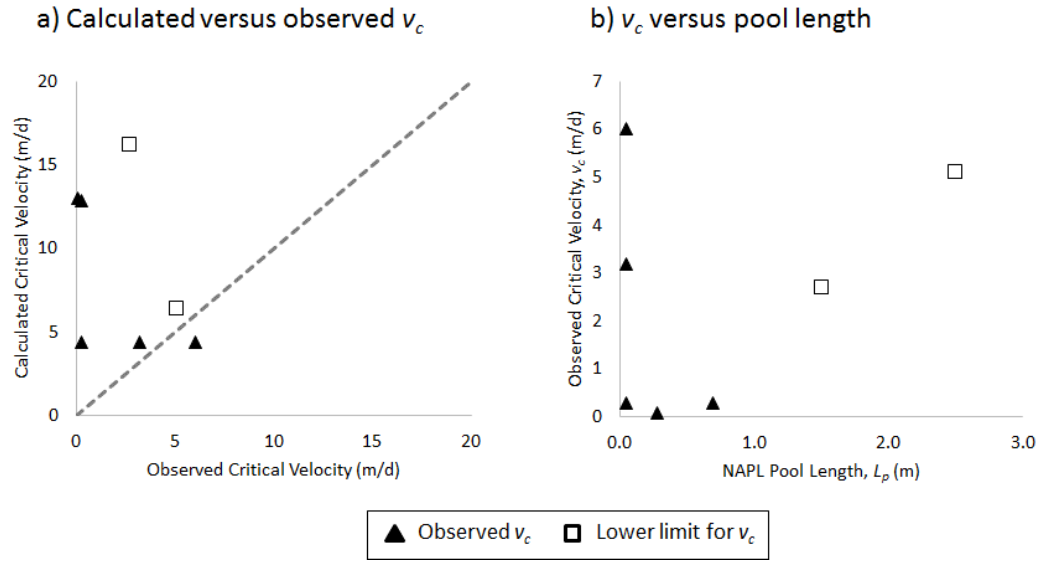

Figure 5.8 – Critical velocity trends for NAPL dissolution studies.

The LE and NE dispersivity estimates for studies cited in Table 5.2 were used to compare the efficacy of the LE(K)/NE Model and the Empirical Model for estimating dispersivity in experiments with a wide range in soil texture and groundwater velocity. Figure 5.9 shows scatter plots of estimated versus observed dispersivity (where observed is based on the calculations in this present study) for the

LE(K)/NE and Empirical Models, and the models of Olsson and Grathwohl (2007) and Chiogna et al. (2010) cited in Table 5.1. A v_c of 3 m/d was assumed for the LE(K)/NE Model application to all experiments. The residual sum of squares is also shown in Figure 5.9 for each of these models. The Empirical Model appears to have the best fit to observed data, with the LE(K)/NE Model having the next best fit.

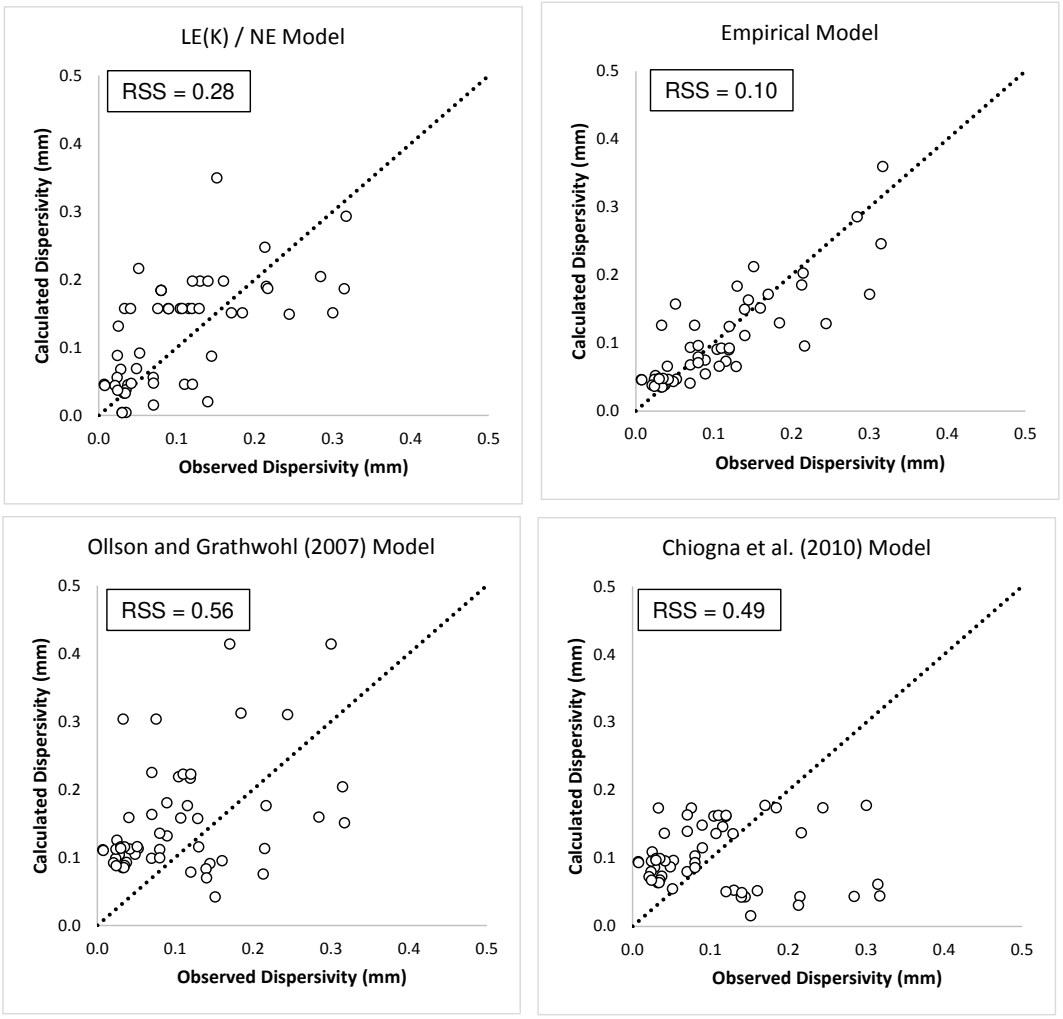

Figure 5.9 – Comparison of α_{TV} models for laboratory experiment data.

5.6 Sensitivity of NAPL Dissolution to LE(K), NE and Empirical Models

A sensitivity analysis was conducted to evaluate how estimates of mass discharge from a TCE DNAPL pool are influenced by the use of the LE(K), NE, and Empirical Models for a wide range of soil textures and groundwater velocity. The NAPL Depletion Model (Carey et al., 2014c,d) was used to estimate mass discharge for a TCE pool with dimensions of 3 m length, 1 m width, and 0.05 m thickness. Three hydraulic conductivity scenarios were utilized: $1x10^{-5}$, $1x10^{-4}$, and $1x10^{-3}$ m/s. The baseline horizontal hydraulic gradient for these *K* scenarios were 0.03, 0.01, and 0.003 m/m, respectively. Additional simulations were conducted with multipliers of 2, 5, and 10 for hydraulic gradient to account for increased flow which may occur with in situ remediation alternatives such as SP&T (Carey et al., 2014a) or enhanced in situ bioremediation (EISB) when a recirculation system is employed. Effective and total porosity, groundwater velocity, and corresponding α_{TV} values are presented in Table 5.4. α_{TV} was calculated using the LE(K) and Empirical Models for all scenarios, and the NE Model was used to estimate α_{TV} for all scenarios where the groundwater velocity was higher than the assumed v_c of 3 m/d.

Table 5.4 – Model scenario α_{TV} estimated based on LE(K), NE, and Empirical Models.

K (m/s)	d10 (mm)	Hydraulic Gradient (m/m)	Effective Porosity (m^3/m^3)	Total Porosity (m^3/m^3)	Groundwater Velocity, v (m/d)	v > 3 m/d?	α_{TV} (mm)		
							LE(K) Model	NE Model	Empirical Model
1.E-05	0.0125	0.03	0.2	0.42	0.13	no	0.36	--	0.75
1.E-05	0.0125	0.06	0.2	0.42	0.26	no	0.36	--	0.61
1.E-05	0.0125	0.15	0.2	0.42	0.65	no	0.36	--	0.48
1.E-05	0.0125	0.3	0.2	0.42	1.30	no	0.36	--	0.39
1.E-04	0.054	0.01	0.25	0.38	0.35	no	0.28	--	0.38
1.E-04	0.054	0.02	0.25	0.38	0.69	no	0.28	--	0.31
1.E-04	0.054	0.05	0.25	0.38	1.73	no	0.28	--	0.24
1.E-04	0.054	0.1	0.25	0.38	3.46	yes	0.28	0.25	0.20
1.E-03	0.24	0.003	0.3	0.33	0.86	no	0.22	--	0.19
1.E-03	0.24	0.006	0.3	0.33	1.73	no	0.22	--	0.16
1.E-03	0.24	0.015	0.3	0.33	4.32	yes	0.22	0.17	0.12
1.E-03	0.24	0.03	0.3	0.33	8.64	yes	0.22	0.10	0.10

Comparison of the dispersivity values estimated using the different models (see Table 5.4) indicates that at velocities more than 10 times below v_c (i.e. v<0.3 m/d in this case), the Empirical Model predicted substantially higher α_{TV_LE} relative to the LE(K) Model. As noted above, this is caused by the lack of an upper-bound for dispersivity in the Empirical Model, indicating that this model should be employed with caution, and typically only in cases where the groundwater velocity is higher than v_c/10. Table 5.4 also indicates that when v>v_c, the NE Model and Empirical Model predict relatively similar dispersivity values. It is also noteworthy that only three of the twelve scenarios involved v>v_c, which suggests that typical field conditions may have sufficiently low velocity that non-equilibrium conditions are negligible. This is based on the assumption that v_c =3 m/d, although more research is needed to provide insights and ranges for v_c with finer-grained soil.

Figure 5.10 compares the simulated DNAPL pool mass discharge for each of the scenarios shown in Table 5.4. Figure 5.10 illustrates that for the three scenarios where velocity was greater than v_c (see Table 5.4), the simulated pool discharge for the NE Model are similar to the Empirical Model predictions. Figure 5.10 also shows the relative difference between simulated mass discharges based on the LE(K) and Empirical Models. A negative difference means that the LE(K) model predicted a lower mass discharge than the Empirical Model. Inspection of the relative differences indicates that they are relatively (within 20%) for all eight scenarios with K values of $1x10^{-5}$ and $1x10^{-4}$ m/s. The only two scenarios with more than a 20% difference have a K of $1x10^{-3}$ m/s where $v>v_c$. In these cases, using a constant α_{TV} would result in overestimation of mass discharge from the TCE pool and underestimation of the remediation timeframe.

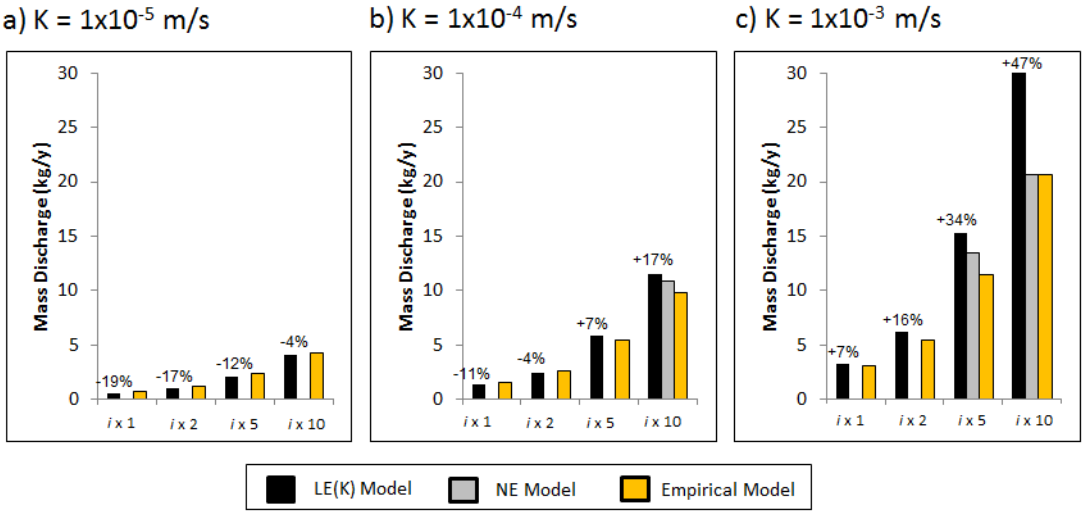

Notes:
- *i* represents the horizontal hydraulic gradient, and *i* x 1 represents the natural (i.e. pre-remedy) gradient.
- Percentages shown above the LE(K) Model result represent the difference in mass discharge relative to simulations based on the Empirical Model.

Figure 5.10 - Comparison of pool initial mass discharge based on LE(K), NE, and Empirical Models.

5.7 Conclusions and Recommendations

A review of various experimental datasets in the literature indicates that transverse vertical dispersivity is inversely proportional to grain size and hydraulic conductivity, which contradicts findings from a number of earlier studies (e.g. de Josselin de Jong, 1958; Perkins and Johnston, 1963; Klenk and Grathwohl, 2002; Olsson and Grathwohl, 2007; Chiogna et al., 2010). The inverse relationship observed

between dispersivity and hydraulic conductivity means that transverse vertical dispersivity is lower for coarser-grained soil, relative to the dispersivity that would be observed in a finer-grained soil. This relationship is likely due to the corresponding reduction in vertical heterogeneity, and variance in pore size distribution, as grain size increases.

For the first time, a model has been developed to estimate α_{TV} under local equilibrium conditions as a function of only hydraulic conductivity. Laboratory experiments performed with packs of glass beads are shown to generally have a lower dispersivity than sand packs with similarly-sized grains.

Another Empirical Model was developed to estimate α_{TV} under both equilibrium and non-equilibrium conditions, and is shown to be a reasonable fit to the limited experimental data presented here. It is recommended that the empirical model be only employed in cases where $v > v_c/10$.

A sensitivity analysis demonstrates that there is only a large difference in simulated pool discharge between the use of the LE(K) Model and the Empirical Model when velocity is higher than a critical threshold (v_c).

5.8 References

Anderson, M.R., R.L. Johnson, and J.F. Pankow, 1992. Dissolution of dense chlorinated solvents into ground water: 1. Dissolution from a well-defined residual source. Ground Water, 30(2): 250-256.

Blackwell, 1962. Laboratory studies of microscopic dispersion phenomena. Society of Petroleum Engineers, March 1962,

Carey, G. R., McBean, E. A., & Feenstra, S. 2014a, DNAPL Source Depletion: 2. Attainable goals and cost-benefit analysis, Remediation Journal.

Carey, G. R., McBean, E. A., & Feenstra, S. 2014b. Estimation of tortuosity based on hydraulic conductivity, submitted to Ground Water.

Carey, G.R., McBean, E.A. & Feenstra, S., 2014c. Screening-Level NAPL Depletion Model: Natural Attenuation, in preparation.

Carey, G. R., McBean, E. A., & Feenstra, S. 2014d, DNAPL Source Depletion: 1. Predicting Rates and Timeframes, Remediation Journal.

Carey, G. R., McBean, E. A., & Feenstra, S. 2014e. Screening-Level NAPL Depletion Model: Enhanced Dissolution, in preparation.

Chapuis, R.P., 2004. Predicting the saturated hydraulic conductivity of sand and gravel using effective diameter and void ratio. Canadian Geotechnical Journal, 41: 787-795.

Chiogna, G., C. Eberhardt, P. Grathwohl, O.A. Cirpka, and M. Rolle, 2010. Evidence of compound-dependent hydrodynamic and mechanical transverse dispersion by multitracer laboratory experiments. Environmental Science and Technology, 44: 688-693.

Chrysikopoulos, C.V., E.A. Voudrias, and M.M. Fyrillas, 1994. Modeling of contaminant transport tesulting from dissolution of nonaqueous phase liquid pools in saturated porous media. Transport in Porous Media, 16: 125-145.

Chrysikopoulos, C.V., K.Y. Lee, and T.C. Harmon, 2000. Dissolution of a well-defined trichloroethylene pool in saturated porous media: Experimental design and aquifer characterization. Water Resources Research, 36(7): 1687-1696.

Cirpka, O.A., A. Olsson, Q. Ju, M.A. Rahman, and P. Grathwohl, 2006. Determination of transverse dispersion coefficients from reactive plume lengths. Ground Water, 44(2): 212-221.

de Josselin de Jong, G., 1958. Longitudinal and transverse diffusion in granular deposits. Transactions, American Geophysical Union, 39(1): 67-74.

Eberhardt, C. and P. Grathwohl, 2002. Time scales of organic contaminant dissolution from complex source zones: coal tar pools vs. blobs. Journal of Contaminant Hydrology, 59: 45-66.

Fiori, A. and G. Dagan, 1999. Concentration fluctuations in transport by groundwater: Comparison between theory and field experiments. Water Resources Research, 35(1): 105-112.

Hayduk, W., and H. Laudie, 1974. Prediction of diffusion coefficients for nonelectrolytes in dilute aqueous solutions, .merican Institute of Chemical Engineers (AIChE) Journal, 20 (3): 611-615.

Hunt, J.R., N. Sitar, and K.S. Udell, 1988. Nonaqueous phase liquid transport and cleanup: 1. Analysis of mechanisms. Water Resources Research, 24(8): 1247-1258.

Jensen, K.H., K. Bitsch, and P.L. Bjerg, 1993. Large-scale dispersion experiments in a sandy aquifer in Denmark: Observed tracer movements and numerical analyses. Water Resources Research, 29(3): 673-696.

Johnson, R.L. and J.F. Pankow, 1992. Dissolution of dense chlorinated solvents into groundwater. 2. Source functions for pools of solvent. Environmental Science & Technology, 26: 896-901.

Kavanaugh, M.C., Arnold, W. A., Beck, B. D., Chin, Y., Chowdhury, Z., Ellis, D. E., Illangasekare, T. H., Johnson, P. C., Mehran, M., Mercer, J. W., Pennell, K. D., Rabideau, A. J., Shapiro, A. M., Siegel, L. M., Walsh, W. J., Ehlers, L. J., Johnson, S. E., Schaffer, K., Aquilino, J., Deguzman, E., & Hall, A. (2013). *Alternatives for Managing the Nation's Complex Contaminated Groundwater Sites*. The National Academies Press, Washington, D.C.

Klenk, I.D. and P. Grathwohl, 2002. Transverse vertical dispersion in groundwater and the capillary fringe. Journal of Contaminant Hydrology, 58: 111-128.

Nimmo, J.R., 2004. Porosity and pore size distribution. Encyclopedia of Soils in the Environment, 3: 295-303.

Olsson, A. and P. Grathwohl, 2007. Transverse dispersion of non-reactive tracers in porous media: A new nonlinear relationship to predict dispersion coefficients. Journal of Contaminant Hydrology, 92(3-4): 149-161.

Oostrom, M., J.H. Dane, O. Guven, and J.S. Hayworth, 1992. Experimental investigation of dense solute plumes in an unconfined aquifer model. Water Resources Research, 28(9): 2315-2326.

Parker, B.L., J.A. Cherry, S.W. Chapman, and M.A. Guilbeault, 2003. Review and analysis of chlorinated solvent dense nonaqueous phase liquid distributions in five sandy aquifers. Vadose Zone Journal, 2: 116-137.

Pearce, A., E. Voudrias, and M. Whelan, 1994. Dissolution of TCE and TCA pools in saturated subsurface systems. Journal of Environmental Engineering, 120(5): 1191-1206.

Perkins, T.K. and O.C. Johnston, 1963. A review of diffusion and dispersion in porous media. Society of Petroleum Engineers Journal, 70-84.

Rolle, M., D.L. Hochstetler, G. Chiogna, P.K. Kitanidis, and P. Grathwohl, 2012. Experimental investigation and pore-scale modeling interpretation of compound-specific transverse dispersion in porous media. Transport in Porous Media, 93: 347-362.

Rolle, M., G. Chiogna, D.L. Hochstetler, and P.K. Kitanidis, 2013. On the importance of diffusion and compound-specific mixing for groundwater transport: An investigation from pore to field scale, Journal of Contaminant Hydrology, 153: 51-68.

Schafer, W. and R. Therrien, 1995. Simulating transport and removal of xylene during remediation of a sandy aquifer. Journal of Contaminant Hydrology, 19: 205-236.

Schwille, F., 1988. Dense Chlorinated Solvents in Porous and Fractured Media – Model Experiments. Translated by J.F. Pankow. Lewis Publishers, Boca Raton,FL.

Seagren, E.A., B.E. Rittmann, and A. J. Valocchi, 1999a. An experimental investigation of NAPL pool dissolution enhancement by flushing. Journal of Contaminant Hydrology, 37: 111-137.

Seagren, E.A., B.E. Rittmann, and A. J. Valocchi, 1999b. A critical evaluation of the local-equilibrium assumption in modeling NAPL-pool dissolution. Journal of Contaminant Hydrology, 39: 109-135.

Transport and biodegradation of quinoline in horizontally stratified porous media. Journal of Contaminant Hydrology, 15: 277-304.

van der Kamp, G., L.D. Luba, J.A. Cherry, and H. Maathuis, 1994. Field study of a long and very narrow contaminant plume. Ground Water, 32(6): 1008-1016.

Voudrias, E.A. and M-F.Yeh, 1994. Dissolution of a toluene pool under constant and variable hydraulic gradients with implications for aquifer remediation. Ground Water, 32(2): 305-311.

Chapter 6

Empirical Regression of the Through-Discharge Decline Rate for Residual DNAPL Layers

6.1 Abstract

The development of preferential flow channels within layers of residual dense non-aqueous phase liquid (DNAPL) cause a reduction in mass discharge over time. Estimating the rate of mass discharge decline in individual DNAPL layers at field-scale is both challenging and important since this influences the depletion timeframe. However, models derived based on laboratory experiments are shown to have limited applicability for field-scale dissolution. A process-oriented, screening NAPL

Depletion Model (NDM) is used to calibrate the through-discharge decline rates for three constituents in a multicomponent DNAPL for the Emplaced Source experiment conducted at a field site in Borden, Ontario. Results from this calibration were used to demonstrate that constituent-specific decline rates are proportional to the product of initial effective solubility and groundwater velocity (i.e. flushing rate), and inversely proportional to initial constituent mass in DNAPL. Through-discharge decline rates were calculated from previously published laboratory experiments, to support the derivation of an empirical regression (R^2=0.94). This regression is shown to be applicable at both the laboratory- and field-scale, for homogeneous and heterogeneous DNAPL layers, and for residual and mixed source zones. The validity of this regression is demonstrated by successfully simulating conditions observed during two independent sets of experiments, using a simple process-oriented screening model (NDM).

6.2 Introduction

The predominant source architecture at aged chlorinated solvent sites involves horizontal DNAPL layers consisting of residual and/or free phase DNAPL (i.e. pools), since vertical fingers of residual DNAPL are typically depleted relatively quickly following a release (Parker et al., 2003). The total mass discharge (Md_{tot}) from an

individual layer of DNAPL is equal to the sum of contributions from: (1) surface discharge (Md_{surf}) at the top and/or bottom of the horizontal layer (Johnson and Pankow, 1992); and (2) discharge from groundwater flow through the DNAPL layer (i.e. through-discharge, or Md_{thru}).

Mechanisms causing the naturally-occurring decline in mass discharge observed at aged DNAPL sites (Suarez et al., 2004; Newell et al., 2006) may include declining lengths of DNAPL layers. Declining lengths cause a corresponding decline in NAPL-water interfacial area and surface discharge (Carey et al., 2014a, b). Overall declines in mass discharge may also be caused by complete depletion of distinct DNAPL layers sub-zones (e.g. layers). In addition, the formation of preferential groundwater flow channels within individual DNAPL layers (herein referred to as intra-source bypassing), resulting in enhanced downgradient dilution of average concentrations and a corresponding reduction in through-discharge (Rivett and Feenstra, 2005). Newell et al. (2006) indicates that the rate of decline observed in mass discharge from DNAPL source zones at sites included in their study exhibited linear and/or exponential trends; however, Newell et al. recommend using exponential decline models which are more likely to represent the tailing observed in mass discharge in later stages of DNAPL dissolution.

This latter mechanism, referring to a decline in mass discharge through a DNAPL layer (i.e. *through-discharge*) is the least understood and most difficult of the three mechanisms to quantify at the field-scale. The occurrence of through-discharge

decline due to intra-source bypassing has been observed in a number of laboratory studies with residual DNAPL (e.g. Imhoff et al., 1996; Powers et al., 1998; Nambi and Powers, 2000; Brusseau et al. (2002); Marble et al., 2008; Russo et al., 2009; Farthing et al., 2012). At present, however, there is no broadly applicable methodology available for estimating the through-discharge decline rate for layers of residual DNAPL at the field-scale *a priori* i.e., without fitting a model to high resolution monitoring data from a controlled dissolution experiment. Farthing et al. (2012) indicate that various upscaled (i.e. domain-averaged) models which were developed for this purpose have significant limitations in their range of applicability and/or data requirements.

In two-dimensional flow systems with an initially thin DNAPL layer, an additional mechanism which may cause a decline in through-discharge is thinning of the DNAPL layer over time due to dissolution at the top and/or bottom surface. The influence of this thinning mechanism on the rate of through-discharge decline is not well understood because most studies of intra-source bypassing have been based on one-dimensional columns (e.g. Imhoff et al., 1996; Powers et al., 1998; Russo et al., 2009); or two-dimensional DNAPL layers where surface discharge is too small to significantly reduce the thickness of the source zone (e.g. Rivett and Feenstra, 2005).

The purpose of this study was to enhance the understanding of factors which influence the rate of through-discharge decline due to intra-source bypassing at the field-scale, and to evaluate a potential new regression model for estimating the rate of

through-discharge decline *a priori*, at both field- and laboratory-scales. NDM, a process-oriented, screening-level model, was used to simulate the declining rate of mass discharge through what were apparently (at least initially) uniform layers of residual DNAPL. The influence of declining effective solubility (during multicomponent dissolution) on the rate of mass discharge decline is quantified through simulation of the Emplaced Source experiment conducted at a field site in Borden, Ontario. A new correlation between the rate of declining mass discharge and several key characteristics is quantified using data from previously published dissolution experiments, and is shown to be applicable at both the laboratory- and field-scale. The validity of this empirically-derived relationship is demonstrated by successfully modeling the depletion of a thin DNAPL layer in a two-dimensional (2-D), heterogeneous laboratory experiment previously published by Brusseau et al. (2002), using the NDM screening model without calibration of parameters. The contribution of DNAPL layer thinning, to the decline in through-discharge due to dissolution at the top and bottom surfaces of the DNAPL layer, is also evaluated.

6.3 Background

6.3.1 DNAPL Dissolution

A number of studies have been conducted to evaluate why flux-weighted average concentrations observed downgradient of a residual DNAPL zone are less

than the constituent solubility, or less than effective solubility (C_{eff}) in the case of multicomponent DNAPL. These trends have been observed at the laboratory-scale (Miller et al., 1990; Powers et al., 1992, 1994, 1998; Imhoff et al., 1994; Imhoff et al., 1996; Nambi and Powers, 2000; Brusseau et al., 2002; Russo et a., 2009; Farthing et al., 2012) and field-scale (Rivett and Feenstra, 2005), for residual DNAPL source zones that were initially believed to be relatively uniform. Some of these studies document initial average concentrations at, or near, the solubility limit followed by temporal declines in the downgradient average concentration.

Initial studies by Miller et al. (1990), Powers et al. (1992, 1994), and Imhoff et al. (1994) attributed these lower-than-expected average concentrations to the development of non-equilibrium dissolution resulting from mass transfer resistance at the NAPL-water interface. Subsequent studies have demonstrated that the observed declines in average concentration and through-discharge were caused mainly by the formation of preferential groundwater flow channels through/within the DNAPL zone, resulting in physical dilution of average downgradient concentrations (Imhoff et al., 1996; Powers et al., 1998; Nambi and Powers, 2000; Brusseau et al., 2002; Rivett and Feenstra, 2005; Russo et al., 2009; Farthing et al., 2012).

Farthing et al. 2012 distinguish between two mechanisms which cause intra-source bypassing: (1) larger-scale variations in soil texture which result in the formation of relatively large preferential flow channels within a source zone; and (2) smaller-scale preferential dissolution (i.e. dissolution fingering) due to small-scale

variations in DNAPL saturation and relative permeability to groundwater flow. Through-discharge eventually begins to decline over time due to breakthrough of these preferential flow channels with cleaner groundwater at the downgradient boundary of the DNAPL zone. This is analogous to a reduction in the number of active flow channels over time that intercept DNAPL within the source zone, which is represented by the streamtube concept described in Jawitz et al. (2005), Fure et al. (2006), and Basu et al. (2008). This intra-source bypassing process results in increasing dilution of the flux-weighted average concentration at the downgradient boundary of the DNAPL layer. This bypassing process has been visually illustrated in Powers et al. (1998); Schnaar et al. (2006); and Farthing et al. (2012).

Some studies document an initial period where the average concentration at the downgradient boundary of a DNAPL layer or columnar source is initially at or near the constituent solubility; after this initial period, declines in the average concentration and corresponding through-discharge are observed (e.g. Imhoff et al., 1994; Russo et al., 2008; Farthing et al., 2012). Farthing et al. (2012) conducted experiments which suggest that the length of this initial period of high concentrations close to solubility levels is proportional to the homogeneity of the source; as the degree of heterogeneity in soil texture and DNAPL distribution increases, the duration of this initial period of constant, high concentrations becomes shorter.

Frind et al. (1999) and Rivett and Feenstra (2005) determined that mass transfer was generally at local equilibrium conditions for an emplaced source

experiment at a field site where the source length was 0.5 m. Rivett and Feenstra (2005) indicate that dissolution within DNAPL layers having lengths greater than 10 cm may be expected to occur under local equilibrium conditions. This finding is consistent with laboratory experiments by Imhoff et al. (1994) which demonstrate that local equilibrium was achieved in a one-dimensional column over a length of only 1 to 2 cm. Klenk and Grathwohl (2002) and Carey et al. (2014c) demonstrate that DNAPL layer dissolution reaches an apparent non-equilibrium condition when the average linear groundwater velocity (v) exceeds a critical threshold (v_c) estimated to be 3 to 5 m/d at a field scale. When $v > v_c$, there is an apparent reduction in the transverse dispersivity coefficient that governs the rate of surface dissolution.

6.3.2 Modeling Through-Discharge in a DNAPL Layer (Sub-Zone)

Mass discharge due to reduced groundwater flow through an individual DNAPL layer (i.e. sub-zone) is given by

$$Md_{thru} = \left(q k_{rw} C_{eff\_o} WH\right) f_{thru} \tag{6.1}$$

where q is the average specific discharge upgradient of the sub-zone, k_{rw} is the relative water permeability within the DNAPL sub-zone [dimensionless], C_{eff_o} is the initial effective solubility, W and H represent the width and height of the sub-zone, and f_{thru} represents a dilution factor at time t which is attributed to physical mechanisms such

as intra-source bypassing within the DNAPL sub-zone. This dilution factor (f_{thru}) is analogous to the declining proportion of active flow channels which intercept DNAPL, and will range from 0 to 100%. Although f_{thru} is referred to as a dilution factor, the value of this parameter is inversely proportional to dilution of flux-weighted concentrations at the downgradient boundary of the source zone (C_{avg}); i.e. f_{thru} will decrease as dilution increases. Similar to its use for estimating through-discharge for an individual sub-zone or DNAPL layer, Eq. 6.1 may be also be used in an up-scaled model to simulate through-discharge for an entire source zone.

Parker and Park (2004) provide an analytical model which may be used for estimating f_{thru}:

$$f_{thru} = 1 - \exp\left(\frac{-K_{eff}L}{q}\right) \tag{6.2}$$

where K_{eff} is a transient, lumped parameter governing the decline in through-discharge that is analogous to a rate-limited mass transfer coefficient [T^{-1}] at time t, and L is the length of the DNAPL sub-zone, or layer. Christ et al. (2006) indicate that K_{eff} is typically calculated using

$$K_{eff} = K_o'(M/Mo)^{\beta ia} \tag{6.3}$$

where K_o' is the initial mass transfer coefficient, M is the DNAPL mass remaining in the sub-zone at time t, M_o is the initial DNAPL mass in the sub-zone, and βia is a fitting parameter for the term representing the decline in NAPL-water interfacial area.

Powers et al. (1994) provide the following regression equations for estimating βia and $K_o^{'}$ based on a series of 1-D column experiments:

$$\beta_{ia} = 0.518 + 0.114\delta + 0.10U_i \quad (6.4a)$$

$$K_o' = \alpha Re'^{\beta 1}\delta^{\beta 2}U_i^{\beta 3}D_o/d_{50}^2 \quad (6.4b)$$

where δ=d_{50}/d_M, d_{50} is the mean grain diameter and d_M is a reference grain diameter typically defined as 0.5 mm, U_i is the uniformity coefficient (Ui=d_{60}/d_{10}), D_o is the free-water diffusion coefficient [L2/T], *Re'* is a modified Reynold's number defined as *Re'*=$v\rho_w d_{50}/\mu_w$ where v is the average linear groundwater velocity, ρ_w is the density of water, and μ_w is the dynamic viscosity of water. α, $\beta 1$, $\beta 2$, and $\beta 3$ are regression fitting parameters that were determined by Powers et al. (1992) to be 4.13, 0.598, 0.673, and 0.369, respectively.

The Powers et al. (1994) regression equations shown in Eqs. 6.4a and 6.4b were derived based on 1-D residual DNAPL dissolution experiments which were constructed in a manner that likely resulted in non-equilibrium dissolution. For example, the experiments relied upon by Powers et al. (1994) were based on column lengths of only 3 to 4 cm, and average linear groundwater velocities on the order of 15 to 60 m/d based, resulting in an average retention time of approximately 2 minutes for the column experiments. This may explain why the regression equations derived by Powers et al. (1994) in Eqs. 6.4a and 6.4b are focused largely on grain size and

diffusion coefficient parameters which are important for quantification of non-equilibrium dissolution. Thus, Eq. 6.4b for $K_o^{'}$ is not likely to be applicable to field-scale dissolution under local equilibrium conditions, as demonstrated by Parker and Park (2004) and Farthing et al. (2012). Christ et al. (2006) provide a simple equation for estimating $K_o^{'}$ based on the observed initial average concentration and effective solubility, however. Eq. 6.4a for βia has not been proven to be applicable at the field-scale, and thus this parameter is challenging to determine for a single DNAPL layer at field-scale.

Imhoff et al. (1996) derive a model for estimating the average length of dissolution fingers along the upgradient interface of a source zone for a relatively homogeneous residual DNAPL. From this derivation, it is apparent that the length of dissolution fingers is proportional to the ratio of $C_{eff}\ v\ /\ S_{no}$, where C_{eff} is the effective solubility of a constituent, v is the average linear groundwater velocity, and S_{no} is the initial DNAPL saturation in the source zone. The implication of this relationship is that an increase in contaminant flushing rate (which is proportional to $C_{eff}\ v$), or a decrease in the initial DNAPL saturation or mass, corresponds to larger dissolution fingers and higher downgradient dilution (i.e. lower f_{thru}) at time t.

Imhoff et al. (2003) utilize this model to predict a new mass transfer rate coefficient which simulates the faster decline in f_{thru} that occurs as a result of dissolution fingering. Two of the parameters used in this model were fitted to numerical simulations conducted as part of the Imhoff et al. (2003) study, for a

relatively homogeneous source zone. Farthing et al. (2012) conducted two 2-D experiments of DNAPL dissolution with different degrees of heterogeneity, and fitted new parameters for the Imhoff et al. (2003) model for each of the two physical experiments conducted by Farthing et al.: one experiment having a lower heterogeneity in soil texture, and the other with a higher heterogeneity.

Farthing et al. (2012) found that the Imhoff et al. (2003) K_{eff} model, which incorporates the influence of increasing length of dissolution fingers (henceforth referred to as the LDF Model), matched reasonably well for the first experiment where dissolution fingering was a dominant mechanism affecting downgradient average concentrations. The LDF Model matched poorly to results from the second experiment, however. Reasons for this poor match given by Farthing et al. (2012) were the relatively high heterogeneity in soil texture and the larger-scale preferential flow channels that developed (which differs from the assumptions used for derivation of the LDF Model), and also because a relatively high proportion of DNAPL (67%) was present as free phase pools.

A more straightforward option for simulating f_{thru} based on constant, exponential decline, or linear decline trends involves the use of one of the respective equations below:

<u>*Constant model*</u>: $$f_{thru} = f_{thru\_o} \quad (6.5a)$$

<u>*Exponential decline model*</u>: $$f_{thru} = f_{thru\_o} e^{\lambda_{thru} t} \quad (6.5b)$$

Linear decline model: $$f_{thru} = f_{thru\_o} - f_{thru\_o} mt \quad (6.5c)$$

where f_{thru_o} is the initial dilution factor, λ_{thru} represents a first-order (exponential) decline rate, and m represents the slope of a linear decline. f_{thru_o} in this context is analogous to the initial mass transfer rate coefficient (K_o') used in Eq. 6.3 but with different dimensions. As an example, if the initial flux-weighted average concentration (C_{avg_o}) at the downgradient boundary of a source zone is 10% of the initial effective solubility (C_{eff_o}), f_{thru_o} will be specified as 0.10. (Note that this apparent dilution factor is independent of additional dilution which may be realized when collecting groundwater samples from a depth interval or capture zone width that is greater than the extent of the source zone.)

The alternative models for f_{thru} (Eqs. 6.5a to 6.5c) represent how this factor changes over time for through-discharge in a DNAPL layer. The challenge remains, however, in that the decline rate λ_{thru} (for exponential decline) is not readily estimated based on site-specific data without some type of simple equation which is applicable at the field-scale. A potential regression equation which may be used for field-scale models is evaluated below.

6.4 Evaluation of Multicomponent DNAPL Influence on Md_{thru} Decline Rate (λ_{thru})

Rivett and Feenstra (2005) document findings from the Emplaced Source experiment which involved high resolution monitoring of multicomponent DNAPL dissolution in a block-shaped source zone that was emplaced into the aquifer at the Borden, Ontario field site. Although the residual DNAPL source zone was characterized as being relatively uniform, significant dilution was qualitatively documented downgradient of the emplaced source, and was attributed to a variety of factors including: intra-source bypassing which caused preferential flow channel development within the source, as observed during later stages of the experiment (after 1,000 days); dilution in downgradient monitoring wells with clean groundwater which did not flow through the source zone; and a decline in effective solubility for constituents with faster dissolution rates (Rivett and Feenstra, 2005).

Details of the Emplaced Source field experiment are presented in Rivett and Feenstra (2005). The emplaced source zone had a length (parallel to groundwater flow) of 0.5 m, width of 1.5 m, and a thickness of 1.0 m. The total initial mass of DNAPL emplaced in the source was 23 kg, with initial mole fractions for the three DNAPL constituents (trichloromethane (TCM), TCE, PCE) of 0.078, 0.435, and 0.487, respectively. The initial DNAPL saturation was estimated by Rivett and

Feenstra (2005) to be 5%, and they observed that this initial saturation was relatively uniform throughout the emplaced source zone.

Rivett and Feenstra (2005) present mass discharge and maximum constituent concentration trends measured at a transect 1 m downgradient from the source zone. Average constituent concentrations and corresponding decline rates in average concentrations were not published; however, it was apparent from transect isoconcentration contour plots that significant dilution was occurring relative to the initial effective solubility concentrations for each constituent (Rivett and Feenstra, 2005).

As discussed above, f_{thru} represents the influence of physical dilution mechanisms such as intra-source bypassing on flux-weighted average concentrations and mass discharge at the downgradient boundary of a DNAPL sub-zone. Dissolution of a multicomponent DNAPL introduces another potential factor which may cause additional apparent dilution in downgradient average concentrations i.e. declining effective solubility for preferentially dissolved constituents.

The objectives of this present study were to: (a) quantify the initial dilution factor (f_{thru_o}) and verify that this was generally consistent for each of the three constituents in the multicomponent DNAPL (which is expected, if only physical dilution mechanisms are governing f_{thru_o}; (b) estimate relative decline rates for through-discharge (λ_{thru}) and combined apparent dilution ($\lambda_{combined}$), where λ_{thru} represents the decline in through-discharge caused by an increase in physical dilution

(i.e. intra-source bypassing), and $\lambda_{combined}$ represents the combined effects of intra-source bypassing and declining effective solubility; (b) determine when intra-source bypassing may have started to cause an observable reduction in through-discharge (Md_{thru}) during the experiment; (c) evaluate temporal trends in $\lambda_{combined}$ to confirm that this rate followed an exponential decline trend and whether this rate was generally consistent over time; (d) validate the re-equilibration process conceptualized by Rivett and Feenstra (2005) for flow through the multicomponent source due to spatial and temporal variations in effective solubility; (e) compare f_{thru} versus time trends based on decline rates calibrated in this study, and based on various previous regression equations for $K_o^{'}$ and βia to assess the applicability of these regressions at the field-scale; and (f) identify source zone and DNAPL characteristics which may have influenced λ_{thru}, to facilitate the development of a new regression model for λ_{thru} (see below) based on this and previously published laboratory experiment data.

6.4.1 Estimation of Observed Average Concentration Decline Rates

For multicomponent dissolution, we refer herein to $f_{combined}$, which represents the combined dilution effect of all physical and chemical mechanisms during multicomponent DNAPL dissolution that result in apparent dilution of the downgradient average concentration. $f_{combined}$ represents the ratio of the flux-weighted average concentration (C_{avg}) and the initial effective solubility of a constituent (C_{eff_o})

at time t. The initial value for $f_{combined}$ at the start of dissolution will be equal to f_{thru_o} which is attributed to physical dilution mechanisms (i.e. prior to a decline in effective solubility in the source zone). Note that in the case of a single component DNAPL, $f_{combined} = f_{thru}$ at all times because solubility is constant.

The difference between constituent-specific decline rates (λ_{thru} and $\lambda_{combined}$) represents the relative influence of declining effective solubility on the apparent dilution of average downgradient concentrations, which were calculated based on mass discharge estimates at a monitoring transect situated 1 m downgradient from the source zone. Analysis of the initial values of Md_{surf} and Md_{thru} (not shown) indicates that surface dissolution was relatively small and therefore, was not considered further in this analysis.

Figure 6.1 illustrates temporal trends in $f_{combined}$ (= C_{avg} / C_{eff_o}) for each of the three DNAPL constituents, where $f_{combined}$ was calculated as part of this present study over the initial 430 days based on data presented in Rivett and Feenstra (2005). After this time period there is higher uncertainty in the average concentration calculation so we have limited our analysis to the initial 430-day monitoring period. Average exponential decline rates for each constituent are also shown in Figure 6.1 based on observations after day 90 of the experiment. Prior to day 90, $f_{combined}$ and mass discharge were observed to be increasing for each of these constituents. The travel time between the source zone and the downgradient monitoring transect was estimated to be approximately 7 days, so it is not certain why there were continuing increases in

mass discharge over the initial 90 day period of the experiment. This trend may be related to shifts observed in the groundwater flow direction during the experiment (Rivett and Feenstra, 2005) which may have resulted in underestimation of the initial mass discharge measurements.

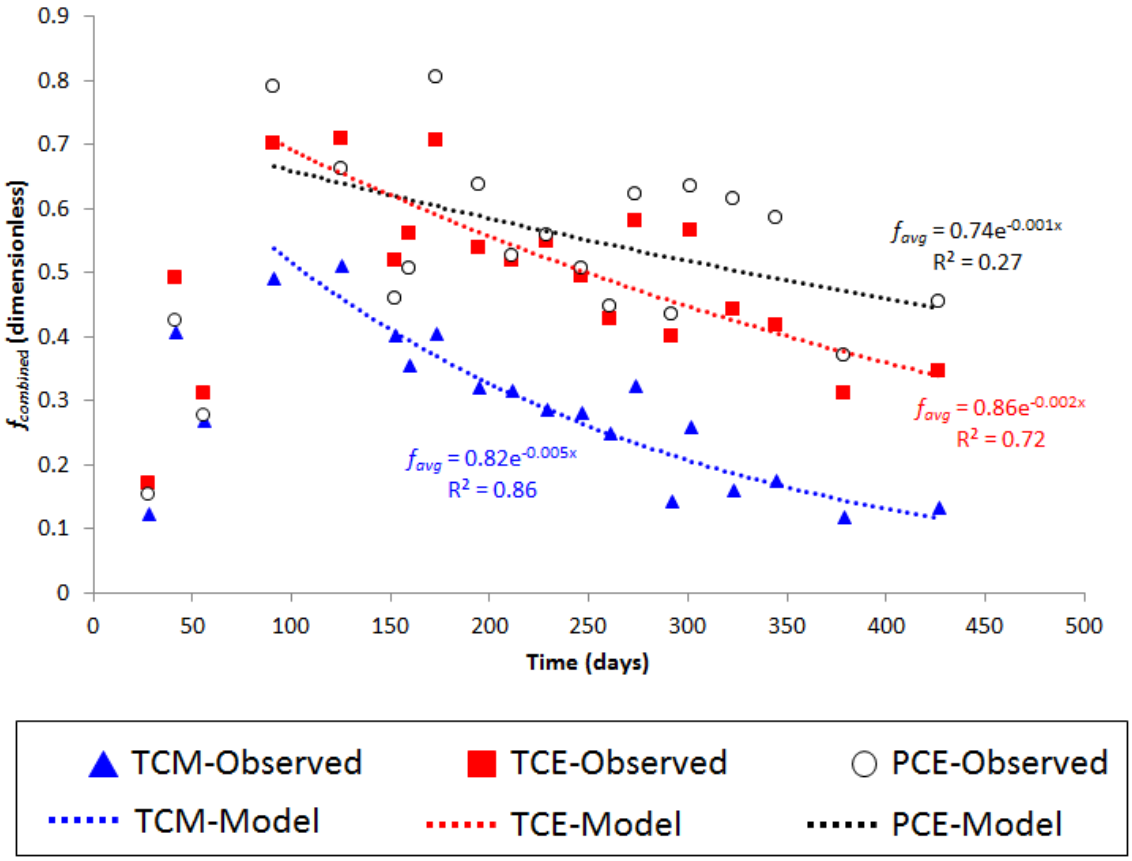

Figure 6.1 – Calculation of the apparent f_{avg} versus time with exponential regression models for TCM, TCE, and PCE in the Emplaced Source experiment at Borden, Ontario.

Figure 6.1 indicates that the rate of decline in $f_{combined}$ generally exhibited exponential trends for all three constituents, with average decline half-lives of 0.4, 1, and 2 years for TCM, TCE, and PCE, respectively. There is considerably more scatter (and uncertainty) in the PCE decline half-life, however. It is interesting to note that the decline rates are generally constant in time for the first 430 days of the experiment.

Figure 6.1 also indicates that all three constituents have a similar initial value (f_{thru_o}) of approximately 0.8, which means that the average concentration is 80% of the initial effective solubility for each constituent. This similarity in f_{thru_o} is expected, given that this initial parameter represents physical (i.e. chemical-independent) dilution mechanisms. This calculated initial dilution is qualitatively consistent with the observed transect isoconcentration contours for each constituent at a multilevel sampler fence situated 1 m downgradient from the source zone. These contours indicate that only a portion of groundwater downgradient of the source zone is at concentrations approaching the initial effective solubility. This initial dilution is likely due to small-scale heterogeneity in hydraulic conductivity, or relative permeability caused by small-scale variations in DNAPL saturation (Rivett and Feenstra, 2005).

6.4.2 Model Simulations

NDM, a process-oriented screening model, was used to simulate multicomponent dissolution by representing changes in effective solubility over time

for each constituent. NDM is capable of simulating surface and/or through discharge for one or more DNAPL sub-zones, where each sub-zone may be defined to be an individual DNAPL region (e.g. layer). NDM provides the option to represent the declining length of the DNAPL sub-zone as dissolution occurs, predominantly at the leading (i.e. upgradient) end; in this case, NDM is based on the use of a 1-D grid to represent the DNAPL sub-zone, oriented in the direction of groundwater flow. NDM functionality is described in Carey et al. (2014a, b). Figure 6.2 shows a conceptual illustration of the discharge components that may be simulated using NDM, and Table 6.1 presents empirical regression equations derived elsewhere for NDM input parameters (Carey et al., 2014b, c, d).

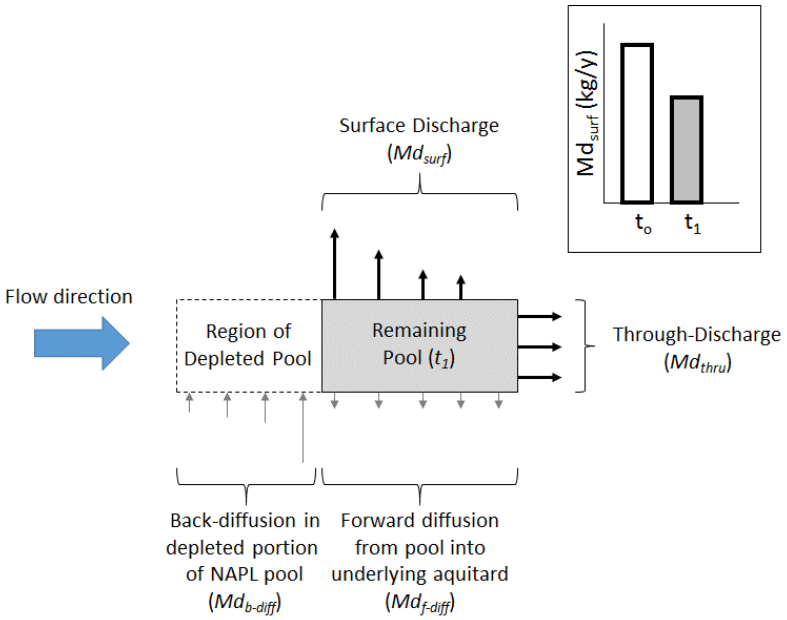

Figure 6.2 – Conceptual representation of mass discharge components for one-dimensional NAPL sub-zone dissolution, and back-diffusion once NAPL depletion occurs.

Table 6.1 – Relationship of various NDM input parameters with hydraulic conductivity.

Reference	Empirical Relationship (K in m/s)	
Carey et al. (2014d)	$\tau = 0.6\ K^{0.030}$	(i)
	$\theta_t = 0.3\ K^{-0.026}$	(ii)
	$\theta_e = 0.41\ K^{0.064}$, $K \leq 1x10^{-2}$ m/s	(iii)
	$\theta_e = (0.29\ K^{-0.026}) - 0.03$, $K > 1x10^{-2}$ m/s	(iv)
Carey et al. (2014c)	$\alpha_{TV} = 0.091\ K^{-0.16}$, $v \leq v_c$	(v)
	$\alpha_{TV} = 0.073\ K^{-0.16}\ (v_c/v)^{0.5}$, $v > v_c$	(vi)
Carey et al. (2014b)	$A_{aw} = 0.112\ (100\ K)^{0.211}$	(vii)
	$n = 13.14\ (100\ K)^{0.246}$	(viii)
	$S_{wr} = 0.015\ (100\ K)^{-0.218}$	(ix)

Multicomponent DNAPL dissolution across the length of the source zone (parallel to groundwater flow) was conceptualized by Rivett and Feenstra (2005) as follows: groundwater flowed through the upgradient region of the source zone causing a decrease in effective solubility for TCM; the groundwater then flowed into the downgradient region of the source zone and re-equilibrated with DNAPL that had a higher TCM effective solubility, resulting in groundwater effluent from this downgradient portion of the source zone being at, or near, the initial effective solubility for TCM. This was demonstrated by Rivett and Feenstra (2005) based on the maximum concentration of TCM at the downgradient monitoring transect, which stayed at, or near, the initial effective solubility for the first 300 days in the experiment. The maximum concentration at a point along the downgradient source boundary, however, is not an indicator of the dilution occurring in other regions of the source zone as a result of intra-source bypassing.

NDM represents this re-equilibration process associated with multicomponent DNAPL dissolution using a 1-D grid for the source zone oriented in the direction of groundwater flow. NDM was also constructed to simulate the re-dissolution of TCE and PCE into DNAPL in the downgradient region of the source zone when the upgradient region had a higher effective solubility for these constituents than the downgradient region. The 0.5-m long source zone was discretized into 20 grid cells with uniform spacing of 0.025 m. The initial effective solubility was uniformly

specified for all grid cells, and then transient changes to effective solubility were simulated for each source zone grid cell. A time step of 0.1 day was used to simulate dissolution over the initial 500 days of the experiment, and a simple mass balance is incorporated in NDM to calculate DNAPL mass remaining and effluent mass discharge at each time step. Three scenarios were simulated with the 1-D model: (a) constant f_{thru}=80%; (b) declining f_{thru} half-life of 1 y for all three constituents; and declining f_{thru} half-life of 1.3 y for PCE, 1 y for TCE, and 0.5 y for TCM. This latter case appears to result in the best match between simulated and observed $f_{combined}$ data. f_{thru_o} was specified to be 80% for all three scenarios.

Figure 6.3a compares the simulated and observed $f_{combine}$ for the scenario based on a constant f_{thru} (i.e. there is no increase in physical dilution mechanisms such as intra-source bypassing). In this case, the upgradient region of the source zone exhibits declining TCM effective solubility immediately, although the most downgradient grid cell does not start to experience a decline in TCM effective solubility until approximately 200 days into the experiment. (Based on the re-equilibration concept, the simulated downgradient mass discharge and average concentration are based on the effective solubility at the downgradient end of the source zone.) Figure 6.3a indicates that for this scenario, NDM predicts an increase in the TCE and PCE average concentrations over time with a corresponding increase in effective solubility at the downgradient edge of the source zone, and a sharp reduction in TCM average concentration between 200 and 300 days. Neither of these simulated trends are

consistent with observed trends i.e. almost immediate declines in average concentrations (and $f_{combine}$) for PCE and TCE, and a decline in average TCM concentrations downgradient of the source zone that was observed to be more gradual than the steep decline simulated with this first scenario.

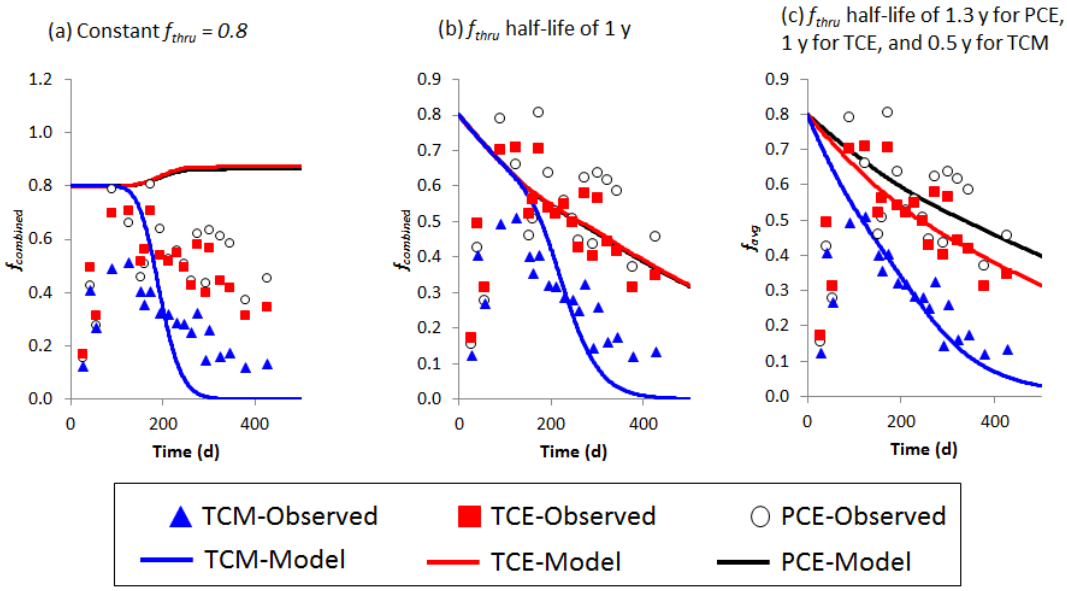

Figure 6.3 – Simulated versus observed $f_{combined}$ with the source length discretized into 20 grid cells and three scenarios for the dilution factor.

Figure 6.3b shows that the use of a 1 year half-life for PCE and TCE f_{thru} results in a reasonable match between simulated and observed PCE and TCE average concentration decline trends which are represented by $f_{combine}$, although the PCE $f_{combine}$ may be slightly underestimated with this case. The use of this half-life, and the resulting increase in dilution of downgradient average concentrations which occurs, is

conceptualized as being caused by intra-source bypassing. That is, the increasing dilution over time in average PCE and TCE downgradient concentrations, may be due to a decline in effective solubility for PCE and TCE in some of the active flow channels within the source zone where these constituents are continuing to dissolve. This is consistent with the observations of Rivett and Feenstra (2005), in that there were vertical horizons in the source zone which exhibited almost no dissolution of TCE and PCE after 1,000 days due to preferential flow channels that developed as a result of small-scale variations in hydraulic conductivity and DNAPL saturation (Rivett and Feenstra, 2005).

Figure 6.3b shows that using a half-life of 1 year in the TCM f_{thru} model results in overestimation of the downgradient average concentration (and $f_{combine}$) in early time and underestimation of average concentrations at later time (i.e. the TCM dissolution front is too sharp relative to observed data which indicates a higher degree of tailing in the average TCM concentration). Figure 6.3c shows that using a half-life of 0.5 years in the TCM f_{thru} model, which infers an increasing rate of dilution in average TCM concentration relative to TCE and PCE, results in a better match to the observed tailing of TCM average concentrations. This increased rate of physical dilution for TCM represents an increased rate of intra-source bypassing (i.e. preferential flow channel development) as TCM depletion occurred.

This suggests that there may be a higher degree of tailing in average concentrations as DNAPL constituents get closer to depletion, or as the DNAPL

saturation in situ decreases. It is noteworthy, however, that the TCM f_{thru} decline rate is relatively consistent in time over the initial 430 days of the experiment based on the match between observed and modeled conditions. Rivett and Feenstra (2005) do note that a long tailing of low TCM concentrations was observed downgradient of the source zone, which is reflected in the quicker f_{thru} decline half-life used for TCM (and corresponding slower rate of mass depletion) relative to TCE and PCE. This NDM scenario indicates that using a decline half-life of 0.5 years for f_{thru}, to represent the effects of physical dilution (i.e intra-source bypassing), results in only a slightly faster overall mass discharge (i.e. $f_{combine}$) decline half-life of 0.4 years. This small difference in decline rates for f_{thru} and $f_{combine}$ means that the declining TCM effective solubility has a relatively small influence on the observed TCM dilution occurring downgradient of the source zone.

Evaluating Applicability of Powers et al. (1994) and Imhoff/Farthing Regressions

There have been relatively few studies which have evaluated the applicability of the Powers et al. (1994) regression models for βia and $K_o^{'}$ (see Eqs. 6.4a and 6.4b, respectively) for field-scale dissolution of residual DNAPL sub-zones. Frind et al. (1999) conducted an analysis of a rate-limited mass transfer coefficient for the Emplaced Source experiment, but assumed that the source was uniform and that the observed downgradient dilution was due to groundwater by-passing around the source

zone which contradicts later findings of significant dissolution fingering that occurred within the source by Rivett and Feenstra (2005).

In this study, we applied both the Powers et al. (1994) and the LDF models to evaluate their applicability for predicting the decline in f_{thru} that was determined through calibration for the Emplaced Source experiment using the NDM model. We first evaluated the applicability of the K_o' regression in Powers et al. (1994). Using Eq. 6.4b, K_o' is calculated to be 24.6 d^{-1}. For comparison, we used the Christ et al. (2006) relationship to estimate

$$K_o' = \frac{q}{L}\left[ln\left(1 - \frac{C_{avg\_o}}{C_{eff\_o}}\right)\right] \quad (6.6)$$

using the observed ratio of C_{avg_o}/C_{eff_o} = 80% as discussed above. Based on Eq. 6.6, Ko' is 0.03 d^{-1} in order to match this observed concentration ratio of 80%, which is three orders of magnitude lower than the value calculated based on the Powers et al. (1994) regression in Eq. 6.4b. The result of using the value for K_o' based on the regression in Eq. 6.4b is that a constant value of 1.0 would be simulated for f_{thru} (work not shown), resulting in overestimation of mass discharge and underestimation of the depletion timeframe. This demonstrates that the K_o' regression, which is based on 1-D laboratory column experiments where non-equilibrium mass transfer may have influenced the initial dilution of average concentrations, is not applicable for this three-dimensional field-scale experiment.

To evaluate the regression equation for βia in Eq. 6.4a, the f_{thru} model in Eqs. 6.2 and 6.3 (i.e. Powers Beta Model) was simulated with a calculated βia of 1.15. For this model, the calculated K_o' of 0.03 d^{-1} was used so that the initial condition in the Powers Beta Model matched the observed condition (i.e. C_{avg_o}/C_{eff_o}=80%). In addition, the LDF Model was used to simulate f_{thru} based on the regression presented in Farthing et al. (2012) for the experiment conducted using a higher heterogeneity in soil texture, where preferential channeling (and not dissolution fingering) was the governing mechanism for downgradient dilution. This Farthing et al. (2012) set of fitted parameters was determined to provide the best match of the three available sets, to the Emplaced Source experiment data (work not shown).

Figures 6.4a, 6.4b, and 6.4c compare the f_{thru} models that were fit with NDM relative to the Power Beta Model and the LDF Model for TCM, TCE, and PCE, respectively. With two exceptions, these two regression models provided poor predictions of the f_{thru} model that was calibrated to observed conditions: The Powers Beta Model provided a reasonable match to the TCM f_{thru} model, and the LDF Model provided a reasonable match to the PCE f_{thru} model after a time of approximately 100 days. The disadvantage with use of the LDF Model for this example is that the initial condition is required to start at f_{thru}=1 which resulted in overestimation of f_{thru} for the early portion of the experiment. Also, the LDF model overestimated the length of dissolution fingers and underestimated the mass transfer coefficient (i.e. K_{eff}) for constituents having a relatively high effective solubility (588 to 653 mg/L) and low

initial DNAPL saturation (0.2% to 3%). The Powers Beta Model underestimates the rate of decline in through-discharge due to intra-source bypassing, and will therefore overestimate mass discharge and underestimate the depletion timeframe for PCE and TCE. The magnitude of the differences for PCE and TCE indicate that the Powers et al. model is not applicable, at least for this experiment, for DNAPL constituents with relatively slow mass depletion rates. For constituents that are depleting relatively quickly (e.g. TCM in this case), the Powers et al. model provided a reasonably good match to observed conditions. In general, however, Figure 6.6 illustrates that neither of these models is applicable for predicting f_{thru} trends for all three constituents in this application.

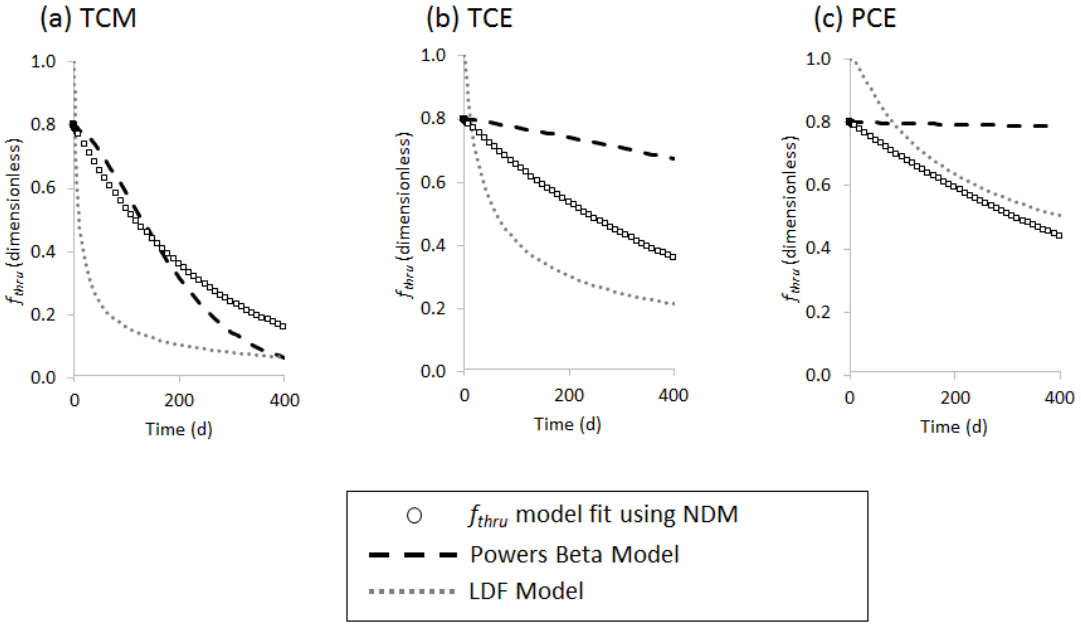

Figure 6.4 – Comparison of f_{thru} versus time for mass transfer coefficient correlation models (Powers et al., 1994 and the Imhoff/Farthing model), relative to the f_{thru} model that was fit using NDM.

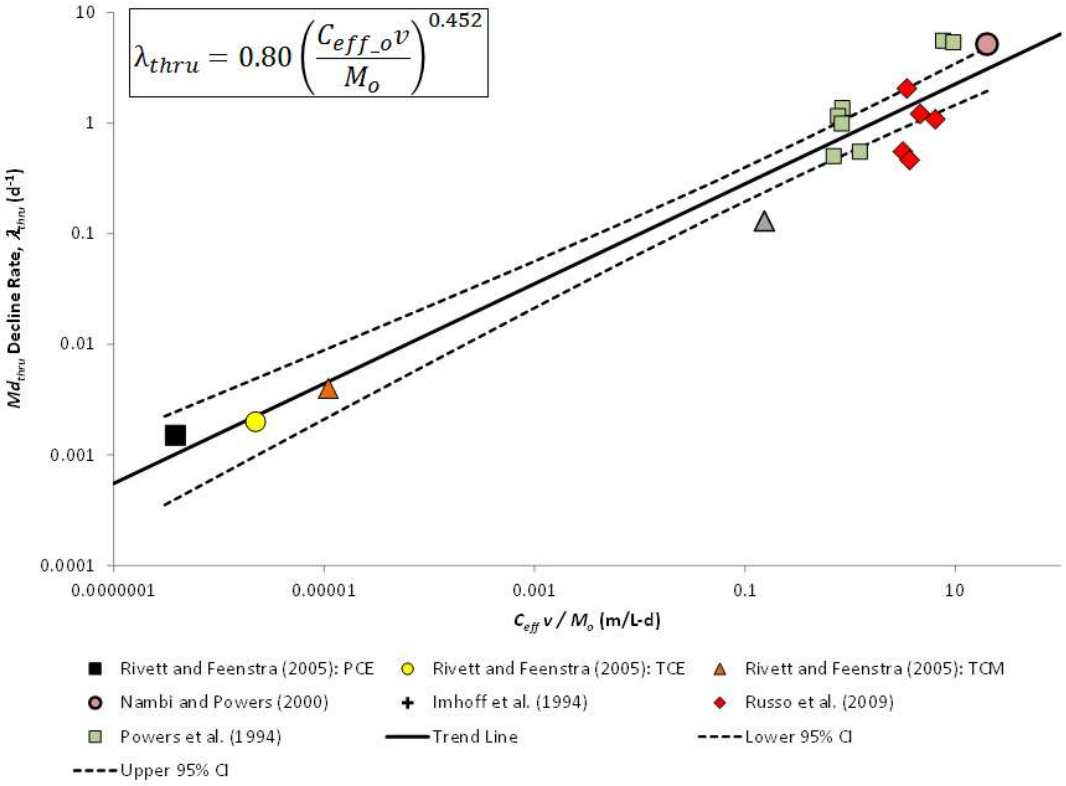

Figure 6.6 – Correlation of Md_{thru} decline rate (λ_{thru}) versus C_{eff} v / (S_n L).

6.5 Derivation of Regression Between λ_{thru} and Key Characteristics

6.5.1 Empirical Derivation

Results of the above analysis indicate that the mass discharge decline rate (λ_{thru}) is proportional to the rate of mass flushing (which is proportional to the product of C_{eff} and v), and inversely proportional to the initial mass (M_o) in a layer of residual DNAPL. In other words, these relationships result in an increased rate of intra-source bypassing caused by the formation of preferential flow channels, which results in a corresponding decrease in through-discharge. These relationships between λ_{thru} and the rate of mass flushing and initial DNAPL mass are similar to the Imhoff et al. (1996) model which indicates that the length of dissolution fingers (and corresponding through-discharge) is proportional to the ratio of $C_{eff}\, v/S_{ni}$ (see above).

The decline half-lives determined for the Rivett and Feenstra (2005) experiment above were on the order of years, whereas decline rates determined for laboratory studies of residual DNAPL dissolution are typically on the order of days. Our goal was to evaluate whether there is an empirical regression relationship using the above three experimental characteristics (i.e. $C_{eff,}$ v, and M_o) that explains the difference in observed decline rates between laboratory studies and the Emplaced Source experiment conducted in the field.

Based on the relative decline rates determined for TCM, TCE, and PCE in the Emplaced Source experiment, it is hypothesized that the rate of decline in through-discharge (i.e. λ_{thru}) is proportional to (C_{eff} v) / (M_o). To test this hypothesis, the regression equation was evaluated based on previously published experiments with residual DNAPL dissolution, whereby the through-discharge decline rate (λ_{thru}) due to intra-source bypassing could be quantified.

A review of the literature indicated that 14 column dissolution experiments conducted by Powers et al. (1994), Imhoff et al. (1994), Nambi and Powers (2000), and Russo et al. (2009) appeared to be appropriate for testing this hypothesis. While the initial C/Co observed in the Powers et al. (1994) experiments may have been affected by non-equilibrium dissolution, the rate of decline in C/C_o observed in these experiments may be caused by physical dilution due to intra-source bypassing.

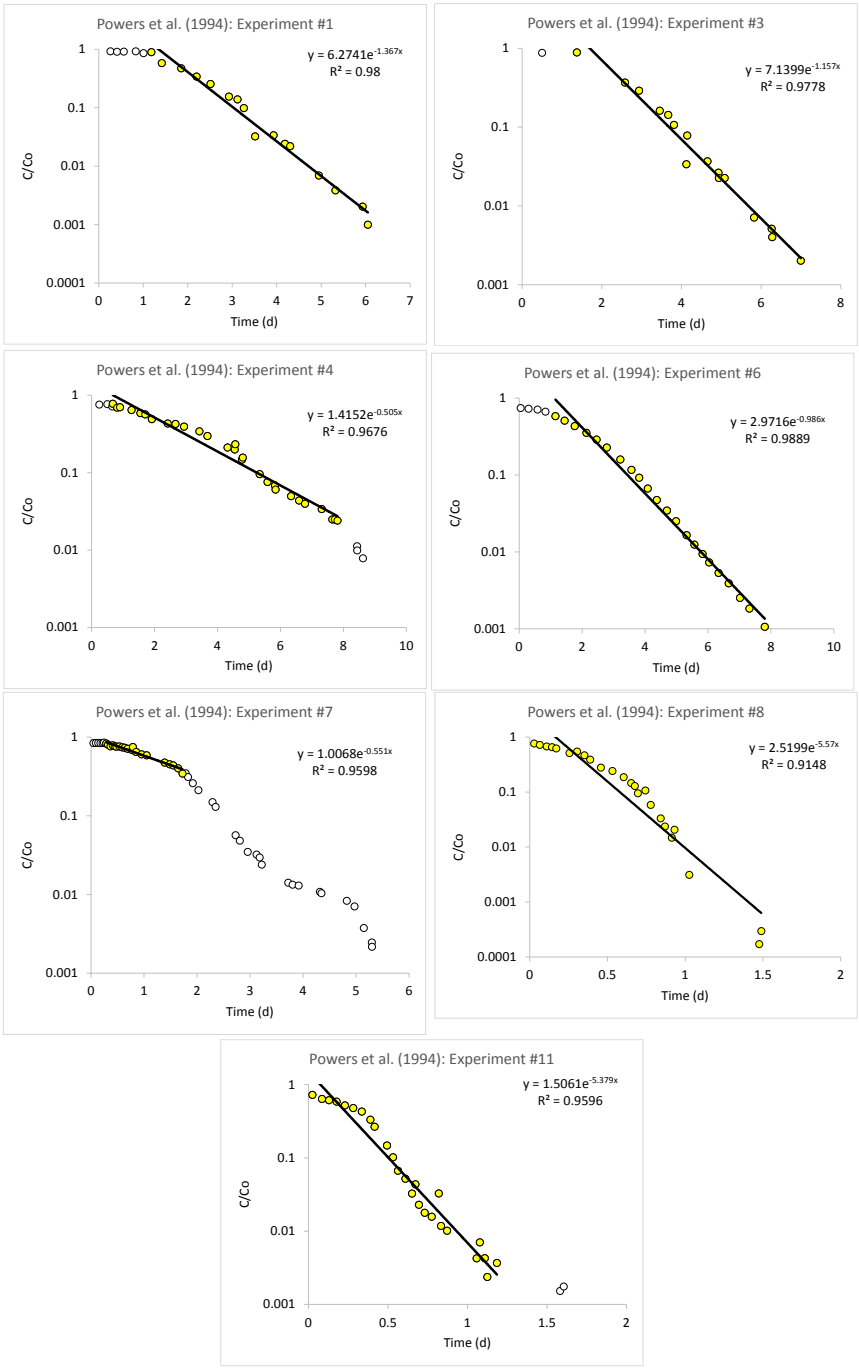

Figure 6.5a – Regression trend lines for first-order decline rates (λ_{thru}) for Powers et al. (1994) laboratory experiments.

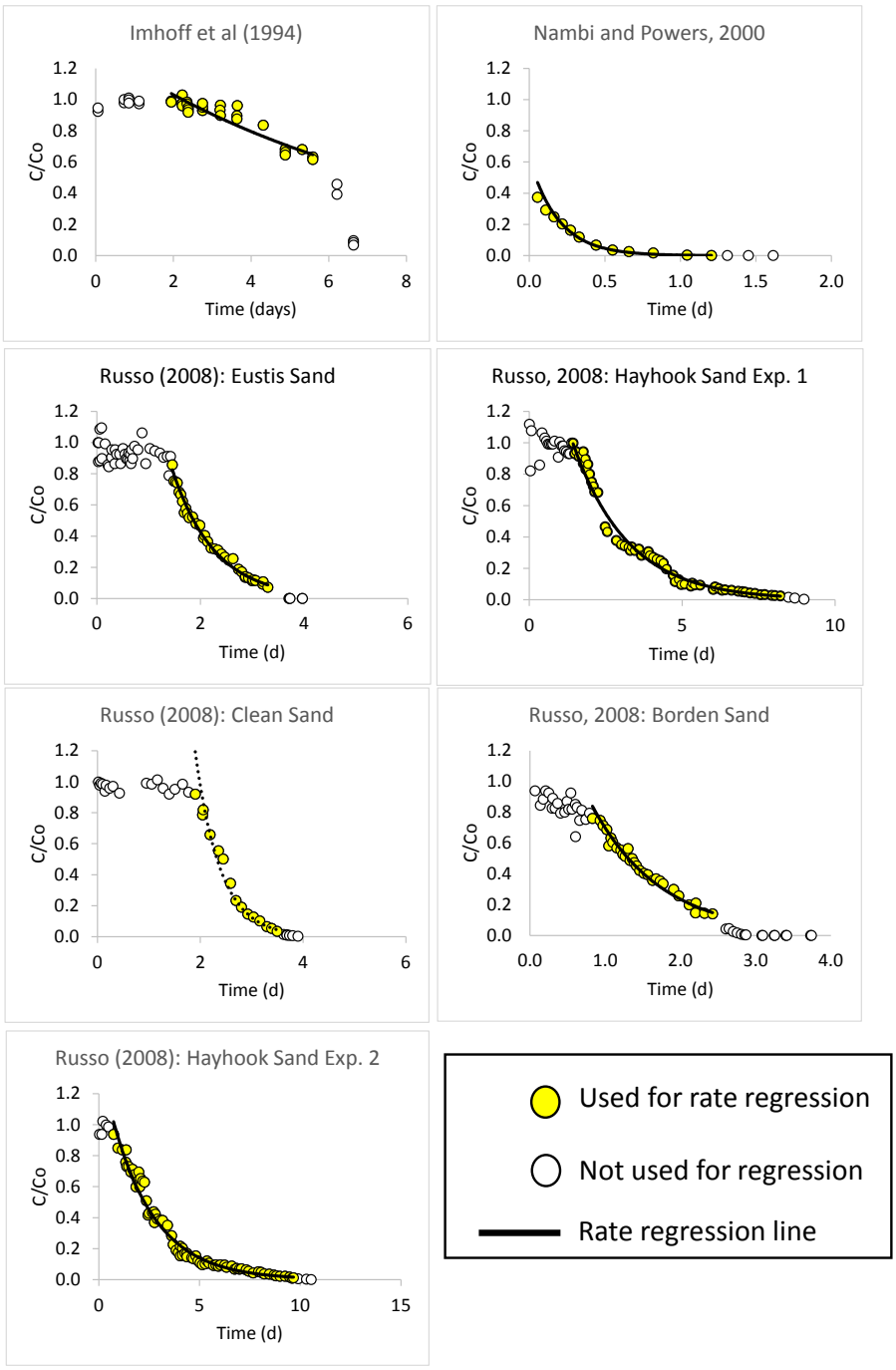

Figure 6.5b – Regression trend lines for first-order decline rates (λ_{thru}) for various laboratory experiments.

Figures 6.5a and 6.5b show C/C_o versus time plots based on data presented in these three studies, where C is the concentration measured at the downgradient boundary of the DNAPL source zone at time t, and C_o is the initial concentration for the respective single component DNAPL that was studied (TCE, PCE, styrene, or o-toluidine). Inspection of Figures 6.5a and 6.5b indicates that most of the experiments are characterized with an initial average C/Co at or near 1.0 for a short lag period, followed by an exponential decline in C/C_o. In some cases, the rate of decline increased sharply near the end of the experiment when the DNAPL was becoming depleted throughout the column.

Exponential decline rates were calculated based on statistical regression for each of the 14 experiments shown in Figures 6.5a and 6.5b, and the corresponding half-lives for the decline in through-discharge caused by intra-source bypassing ranged from 0.1 to 5 days. This demonstrates that even at the lab scale, there is a range of almost two orders of magnitude in decline rates, and the slowest laboratory half-life is almost two orders-of-magnitude lower than the half-lives calibrated for TCE and PCE in the Emplaced Source experiment.

Table 6.2 – Dissolution experiment parameters used for regression of decline rate (λ_{thru}).

Original Study	Constituent	Effective Solubility, C_{eff} (mg/L)	Velocity Through Source Zone, v (m/d)	Initial DNAPL Saturation, S_{no}	Source Zone Length, L (m)	Initial DNAPL Mass (g)	Md_{thru} Decline Rate, λ_{thru}^{-1} (d^{-1})	Md_{thru} Decline Rate, HL_{thru} (d)	$(C_{eff}\ v)\ /\ (M_o)$ (m/L-d)
Imhoff et al. (1994)	TCE	1400	3.45	0.16	0.07	31.48	0.13	5.33	1.53E-01
Nambi and Powers (2000)	o-Toluidine	16500	7.55	0.3	0.05	6.224	5.189	0.13	2.00E+01
Powers et al. (1994) Exp. #1	Styrene	230	15.12	0.049	0.0389	4.11	1.367	0.51	8.46E-01
Powers et al. (1994) Exp. #3	Styrene	230	14.08	0.045	0.0394	4.21	1.157	0.60	7.69E-01
Powers et al. (1994) Exp. #4	Styrene	230	15.2	0.053	0.0397	5.00	0.505	1.37	6.99E-01
Powers et al. (1994) Exp. #6	Styrene	230	15.48	0.055	0.0326	4.26	0.986	0.70	8.36E-01
Powers et al. (1994) Exp. #7	Styrene	230	32.68	0.065	0.0393	6.07	0.551	1.26	1.24E+00
Powers et al. (1994) Exp. #8	TCE	1270	30.4	0.065	0.0326	5.03	5.57	0.12	7.67E+00
Powers et al. (1994) Exp. #11	TCE	1270	29.72	0.05	0.0332	3.94	5.379	0.13	9.57E+00
Rivett and Feenstra (2005)	TCM	653	0.045	0.003	0.5	2680	0.004	173.29	1.10E-05
Rivett and Feenstra (2005)	TCE	588	0.045	0.020	0.5	11830	0.002	346.57	2.24E-06
Rivett and Feenstra (2005)	PCE	113	0.045	0.026	0.5	13200	0.0015	462.10	3.85E-07
Russo et al. (2009): well sorted sand	TCE	1400	7.91	0.182	0.07	3.20	2.059	0.34	3.46E+00
Russo et al. (2009): Borden sand	TCE	1400	8.93	0.114	0.07	1.94	1.086	0.64	6.43E+00
Russo et al. (2009): Eustis sand	TCE	1400	8.77	0.147	0.07	2.65	1.215	0.57	4.63E+00
Russo et al. (2009): Hayhook sand Exp. 1	TCE	1400	10.57	0.245	0.07	4.67	0.555	1.25	3.17E+00
Russo et al. (2009): Hayhook sand Exp. 2	TCE	1400	10.57	0.211	0.07	4.02	0.464	1.49	3.68E+00

Table 6.2 presents a summary of the characteristics for each of these laboratory experiments as well as for the Emplaced Source experiment, and Figure 6.6 plots λ_{thru} versus $(C_{eff}\, v) / (M_o)$. Figure 6.6 shows that there is a good correlation over the wide range of conditions involved with these laboratory and field experiments. Use of regression indicates that based on this correlation (R^2=0.94), the rate of decline in through-discharge in a residual DNAPL due to intra-source bypassing (λ_{thru}) may be estimated using

$$\lambda_{thru} = 0.80 \left(\frac{C_{eff} v}{M_o}\right)^{0.452} \tag{6.7}$$

This regression equation is specifically derived for estimating the average Md_{thru} decline rate (λ_{thru}) for dissolution of DNAPL layers or columnar source zones. This decline rate regression equation is not demonstrated to be applicable for use in upscaled DNAPL depletion models, however. The regression between λ_{thru} and $C_{eff}\, v/S_{no}$ was also considered but it was not as good of a fit to the observed data as the relationship shown in Eq. 6.7.

The regression equation (Eq. 6.7) suggests that the influence of intra-source bypassing is more closely related to the initial DNAPL mass than the decline in interfacial area that Powers et al. (1994) and many others have used for evaluating the rate of through-discharge decline in residual DNAPL. The use of the fractional mass remaining term in up-scaled models (e.g. Parker and Park, 2004) is quite appropriate,

however, as this represents a lumped parameter for many factors governing the rate of decline in source mass discharge.

6.5.2 Testing the Regression with the Farthing et al. (2012) Experiments

Farthing et al. (2012) present the results of TCE dissolution experiments conducted in intermediate-scale laboratory cells (0.6 m long, 0.3 m high, and 0.01 m wide). Two experiments were conducted using different degrees of heterogeneity in soil texture; the first experiment involved horizontal and vertical correlation lengths of 0.16 and 0.06 m, respectively (*lower heterogeneity* experiment), and the other experiment had correlation lengths of 0.04 and 0.01 m, respectively (*higher heterogeneity* experiment).

TCE was released into the two experimental cells so that DNAPL was generally present throughout each cell, creating two very different NAPL architectures: less than 5% of the DNAPL present in the lower heterogeneity experiment was determined to be free phase (i.e. small pools), whereas 66% of the DNAPL present in the higher heterogeneity experiment was present as free phase (pools). The former experiment is considered to be generally representative of a residual DNAPL sub-zone, and the latter experiment is representative of a mixed sub-zone containing both residual and free phase DNAPL. Assuming an effective porosity of approximately 0.25, the average linear groundwater velocity for the two

experiments was 19 and 36 m/d, respectively. Farthing et al. (2012) conducted numerical simulations using velocities that were 10 and 100 times lower than those applied during the experiments, to demonstrate that the observed dissolution behavior was not influenced by the high groundwater velocities used in the physical experiments.

Farthing et al. document the occurrence of mainly smaller-scale dissolution fingering in the lower heterogeneity experiment. The higher heterogeneity experiment was characterized by larger-scale channeling caused by more heterogeneous soil texture and DNAPL distribution within the source zone. These two Farthing et al. (2012) experiments are very different than the laboratory experiments cited in Table 6.2 for the regression of λ_{thru} versus $C_{eff}\ v/M_o$, given that the other experiments were based on one-dimensional columns with more homogeneous soil texture and DNAPL distributions.

The Farthing et al. (2012) experiments incorporated heterogeneity by using five different soil textures during packing of the cells, with minimum horizontal and vertical spacing of 0.015 and 0.01 m, respectively. Details of the experimental set-up are presented in Farthing et al. (2012). A light transmission method was used for high resolution characterization of the distribution in DNAPL saturations for each experiment. Farthing et al. (2012) used a sophisticated numerical model based on the Powers et al. (1994) regression equations for estimating the mass transfer coefficient.

The numerical model had horizontal and vertical grid spacing of 0.0025 and 0.0017 m, respectively, for a total of more than 40,000 grid cells.

Although the Farthing et al. (2012) experiments are two-dimensional, the main contribution to overall mass discharge in the experiment effluent is through-discharge because the source zone extended from the top to the bottom of each experiment cell. Using the regression in Eq. 6.7, the f_{thru} decline half-lives were estimated to be 6.0 and 4.8 days for the lower and higher heterogeneity experiments, respectively. The f_{thru} exponential decline model (Eq. 6.5b) was then used to predict the decline in C/Co for both experiments, starting at when breakthrough was observed. Figures 6.7a and 6.7b show the f_{thru} decline model results that were estimated simply by using the half-lives estimated a priori using the regression equation (Eq. 6.7), without any fitting or calibration to observed data. These figures also illustrate the C/Co trends simulated by Farthing et al. (2012) using the sophisticated numerical model. These figures demonstrate that that the regression in Eq. 6.7 results in reasonably good estimates of λ_{thru} for both experiments. The later tailing in the later portions of each experiment are particularly well represented by the simple f_{thru} model based on the *a priori* decline rate estimates. These results offer further validation that the simple regression in Eq. 6.7 is generally applicable for a wide range of groundwater velocity, soil texture and DNAPL architecture heterogeneity, effective solubility, and initial DNAPL mass.

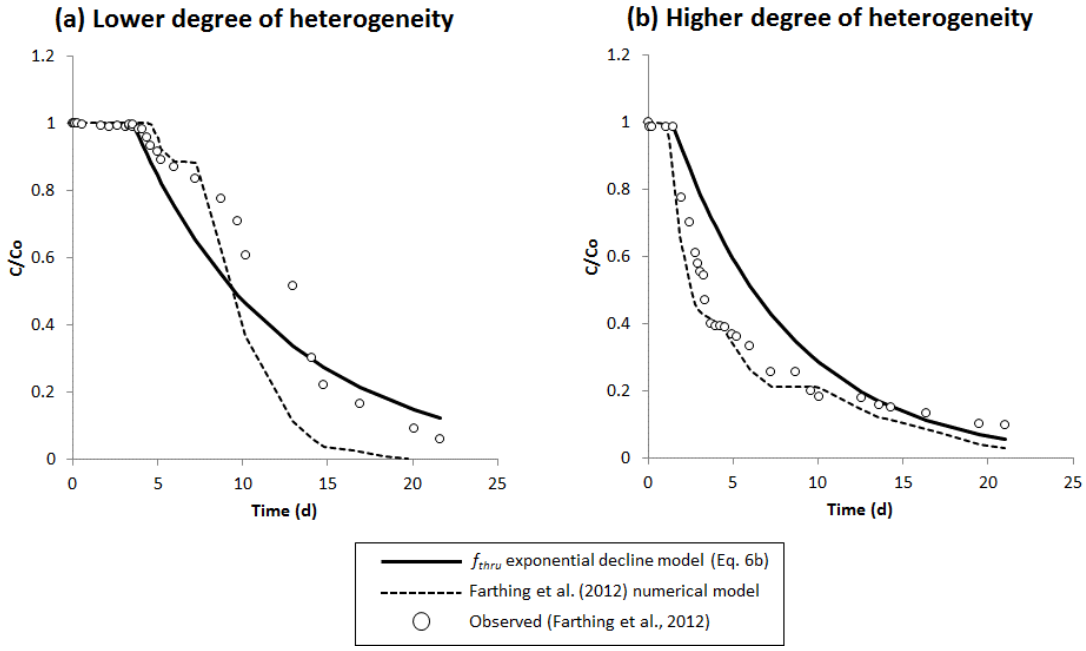

Figure 6.7 – Comparison of Farthing et al. (2012) numerical model and NDM upscaled model simulations for 2-D physical experiments of DNAPL dissolution with varying degrees of heterogeneity.

6.5.3 Testing the Regression with the Brusseau et al. (2002) 1,2-DCA Experiment

To further test the validity of Eq. 6.7 for estimating λ_{thru} and to evaluate the potential influence of source zone thinning on the through-discharge decline, a 2-D flow cell experiment with 1,2-dichloroethane (1,2-DCA) presented in Brusseau et al. (2002) was modeled with NDM using a one-dimensional grid. For this simulation, the NDM inputs were derived based on experiment-specific measurements and the

regression equations presented in Table 6.1. λ_{thru} was estimated using Eq. 6.7, and the model simulation of 1,2-DCA mass discharge versus time was compared to observed conditions (i.e. without calibration or fitting of any model input parameters).

The residual DNAPL dissolution experiment was conducted by Brusseau et al. (2002) in a 2-D flow cell using an emplaced source of 1,2-DCA with an average residual saturation of 6.3%. The source zone had a length (parallel to groundwater flow) of 0.66 m, thickness of 0.10 m, and a width of 0.0586 m. Initial DNAPL mass in the source zone was approximately 104 g. The emplaced source zone was comprised of the same soil material as the remainder of the experimental cell.

Due to the relatively low DNAPL saturation, relative permeability was estimated to be approximately 0.8, which is sufficiently high that through-discharge was one component of the total source strength (i.e. mass discharge). In addition, surface dissolution was occurring on both the top and bottom surface of the source zone. A downgradient extraction well was used to measure diluted 1,2-DCA concentrations which were initially well below the solubility of 1,2-DCA due to the thick extraction well sampling interval relative to the thin vertical extent of the source zone. 1,2-DCA concentrations continued to decline exponentially until the source was depleted in approximately 3.3 days.

Brusseau et al. (2002) used a three-dimensional (3-D) groundwater flow and transport model to simulate the combined effects of surface discharge, through-discharge, and by-passing of groundwater flow above and below the emplaced source

zone. The 3-D model used 18,000 grid cells, and rate-limited mass transfer was simulated based on the regression equations developed by Powers et al. (1994) for estimating K_{eff} and βia (see Eqs. 6.3 and 6.4a). The numerical model used by Brusseau et al. included transient updating of relative permeability in the source zone as DNAPL depletion occurred. The initial mass transfer coefficient K_o' was estimated by Brusseau et al. (2002) based on the results of column studies conducted using the same sand that was used in the 2-D flow cell experiment. Based on their model results, Brusseau et al. (2002) concluded that dissolution in the source zone was occurring under local equilibrium conditions, and that the overall decline in concentrations was due primarily to intra-source bypassing caused by small-scale heterogeneity in saturated hydraulic conductivity, as well as DNAPL saturation and the corresponding relative permeability.

Based on an average flow rate through the experiment cell of 41 mL/min and an effective porosity of 0.27 that was estimated in this present study, the average linear groundwater velocity (v) is 4.6 m/d. (Note that most DNAPL dissolution experimental studies use total porosity to estimate velocity, whereas we use effective porosity to estimate v in Table 6.2 and for use with Eq. 6.7, using the regression in Eq. iii of Table 6.1.) 1,2-DCA has a solubility of approximately 8,500 mg/L. Based on these experiment parameters and using Eq. 6.7, the through-discharge decline rate due to intra-source bypassing for this experiment was estimated to be 0.45 d^{-1} (i.e. half-life of 1.5 days).

NDM was used to simulate the depletion of the 1,2-DCA DNAPL zone based on study-specific or empirically-derived parameters. The goals of this present analysis were to: (a) test the validity of Eq. 6.7 for estimating λ_{thru}; (b) evaluate the relative contribution of surface and through-discharge over time; (c) determine whether the initial f_{thru_o} was diluted or equal to 1.0, which would indicate whether intra-source bypassing occurred at the start of the experiment; and (d) evaluate the relative contribution of source zone thinning and intra-source bypassing to the declining through-discharge.

The simulated dissolution processes using NDM were similar to those simulated for a DNAPL pool: surface dissolution (Md_{surf}) which occurred at both the top and bottom of the source zone in this experiment because the source zone was underlain by sand; and through-discharge (i.e. Md_{thru}) based on reduced groundwater flow through the DNAPL source zone. The one-dimensional grid used for the 0.66-m long source zone was discretized into 33 cells with uniform spacing of 0.02 m. Two cases were simulated: (1) a constant value of 1 for f_{thru}; and (2) exponential decline in the dilution factor (f_{thru}) with a half-life of 1.5 days. The average linear groundwater velocity was 4.6 m/d which is above the minimum critical velocity (v_c) threshold of 3 m/d recommended by Carey et al. (2014c). The non-equilibrium transverse dispersivity governing surface discharge was estimated to be 0.17 based on Eq. (vi) in Table 6.1 and v_c=3 m/d. The 1,2-DCA free-water diffusion coefficient was estimated

to be 9.1x10-10 m^2/s based on Hayduk and Laudie (1974), and tortuosity was estimated to be 0.49 based on Eq. (i) in Table 6.1.

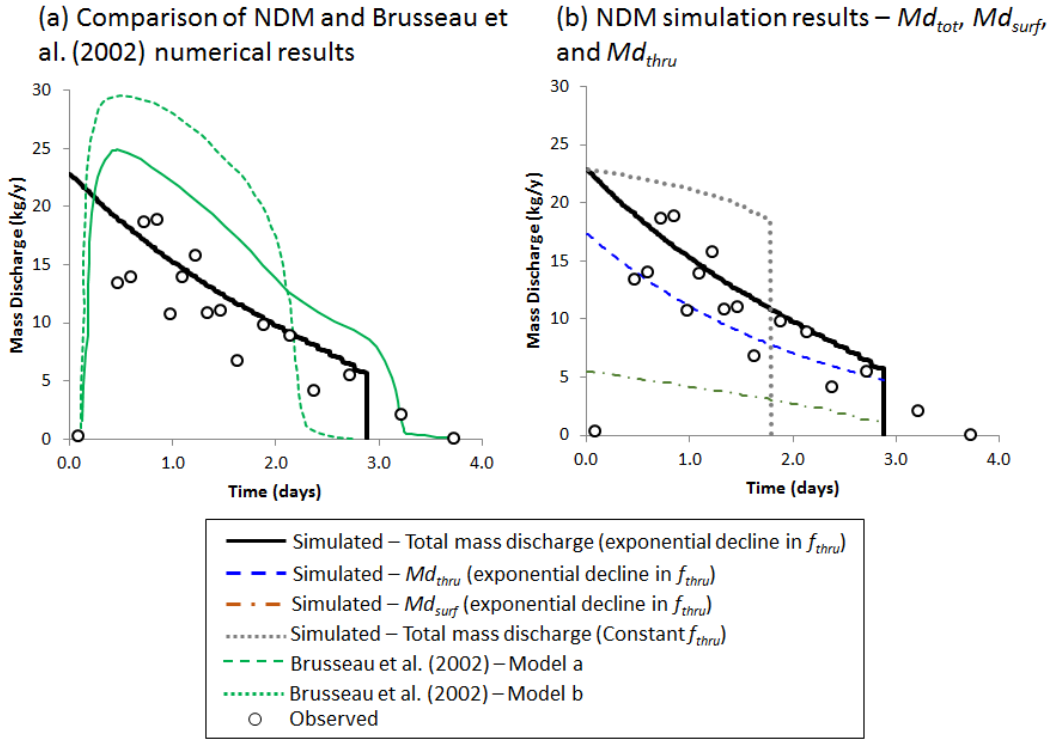

Figure 6.8 – Simulated and observed trends for 1,2-DCA laboratory experiment based on data presented by Brusseau et al. (2002).

Figure 6.8a compares the observed source strength to the mass discharge simulated using NDM without calibrating any of the input parameters. This figure illustrates that the NDM results provide a good match to the observed source strength decline, and to the time of DNAPL depletion (modeled depletion time of 2.9 days compared to the observed time of 3.3 days). For comparison, the results of two 3-D

model simulations presented by Brusseau et al. (2002) are also shown in Figure 6.8a. Brusseau et al. (2002) used the Powers et al. (1994) regression to estimate K_{eff} without fitting, except for the initial mass transfer coefficient which was based on column studies conducted by Brusseau et al. Figure 6.8a shows that the NDM simulation, which had only 33 grid cells compared to the 18,000 grid cells used in the Brusseau et al. (2002) sophisticated numerical model, provides a better fit to the observed data than the earlier model. This indicates that the correlation presented in Eq. 6.7 is valid for use with this experiment, and that the process-oriented NDM screening model provides a reasonable representation of the combined effects of surface discharge, through-discharge, and reduced groundwater flow through the DNAPL zone.

Figure 6.8b compares the NDM simulated mass discharge for the two cases that we simulated (i.e. constant f_{thru}=1, and an exponential decline in f_{thru}). Figure 6.8b illustrates that even with f_{thru} =1 and a corresponding constant Md_{thru} over time, the source strength was simulated to decline over time due to the simulated shrinking length of the DNAPL zone which resulted in a declining Md_{surf}. Both cases simulated with NDM had an initial Md_{surf} equal to approximately 25% of the total mass discharge, indicating that surface dissolution was a significant process contributing to DNAPL depletion during this experiment.

Figure 6.8b shows that use of a constant Md_{thru}, which implies that intra-source bypassing was negligible, resulted in underestimation of the 1,2-DCA depletion time. Figure 6.8b illustrates that the modeled case with an exponential decline in Md_{thru} and

a half-life of 1.5 days, provided a better match to the observed source strength decline rate and DNAPL depletion timeframe. Using f_{thru_o}=1 provided a reasonable match to observed data, indicating that intra-source bypassing was negligible at the start of the experiment, in contrast to the Emplaced Source experiment where the initial dilution factor was 80% (possibly due to the thicker source zone height of 1 m for the latter experiment compared to a thickness of 0.1 m for the former experiment).

The decline in Md_{thru} is analogous to an exponential decline over time in the number of active flow channels through the source zone which intercept DNAPL. The simulated exponential decline in Md_{thru} and Md_{surf} are also shown in Figure 6.8b for the case where f_{thru} declines exponentially, which illustrates that the contribution of surface dissolution to the overall source strength increased over time as preferential flow channels continued to develop inside the source zone.

Because surface dissolution was occurring relatively quickly at both the top and bottom surface of the 1,2-DCA source zone, it was hypothesized that a decline in thickness of the source zone may have resulted in a corresponding reduction in the cross-sectional area of this zone over time which would have also contributed to the apparent reduction in f_{thru}. A mass balance analysis was conducted to evaluate the declining thickness of the last (i.e. downgradient-most) segment in the DNAPL source zone over time based on NDM simulation output. (Initially surface discharge from the downgradient end of the source zone is low relative to the upgradient end, so thinning

of the cross-sectional area would be, at a minimum, at the downgradient end of the source zone.)

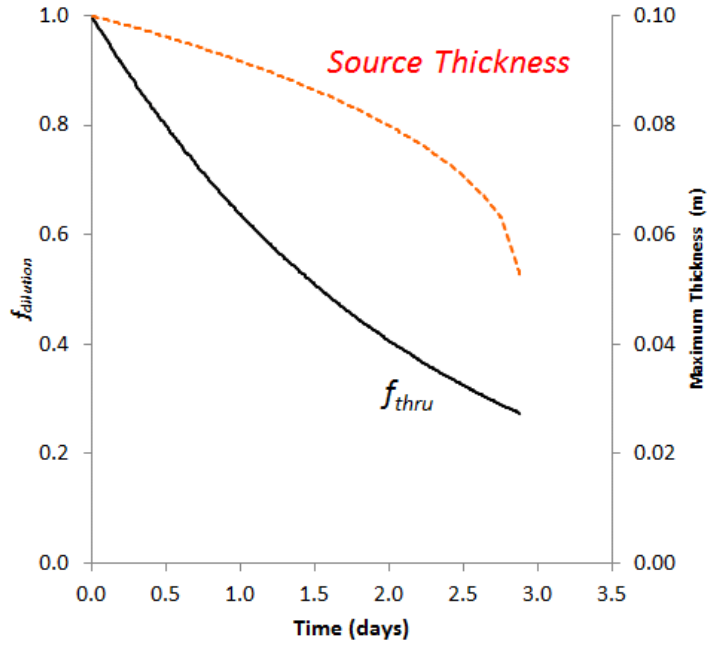

Figure 6.9 – Simulated decline in f_{avg} (exponential model) compared to the calculated reduction in DNAPL zone thickness over time.

Figure 6.9 compares the temporal reduction in thickness of this downgradient source zone segment (with length of 0.02 m) relative to the calibrated reduction in f_{thru}. This figure indicates that the declining f_{thru} is caused by more than a reduction in source zone thickness, which confirms that increasing preferential flow channelling due to intra-source bypassing was the main reason for the decline in Md_{thru} through most of the experiment, similar to that observed by Imhoff et al. (1996) and Rivett and

Feenstra (2005). Figure 6.9 shows that only 25% of the original source zone cross-sectional area had active flow channels intercepting DNAPL at the end of the experiment, which demonstrates the importance that this intra-source bypassing process can have on mass discharge trends. Figure 6.9 also indicates that source thinning was still a significant process (i.e. reduction in thickness of up to 50% by the end of the experiment), and thus may warrant consideration in other DNAPL depletion scenarios (e.g. thin, short pools with significant surface discharge).

6.6 Conclusions and Recommendations

High resolution monitoring data from the Emplaced Source experiment in Borden, Ontario (Rivett and Feenstra, 2005) were re-evaluated to quantify the observed rate of decline in average constituent concentrations downgradient of the source zone. The NAPL Depletion Model, a process-oriented screening model, was used to simulate dissolultion of the multicomponent DNAPL with results indicating that the rapidly declining effective solubility of TCM had little influence on the overall rate of downgradient dilution that was observed. This dilution was attributed primarily to the development of preferential flow channels through the source as a result of intra-source bypassing. Evaluation of the Powers et al. (1994) regression equation for $K_o^{'}$ and βia, and the LDF model,indicate that these models are not generally applicable to field-scale residual DNAPL layer dissolution. The re-

equilibration process conceptualized by Rivett and Feenstra (2005) for multicomponent DNAPL dissolution was validated based on model simulations.

The rate of decline in through-discharge observed during the Emplaced Source experiment was observed to be proportional to the product of initial effective solubility and groundwater velocity (i.e. rate of flushing), and inversely proportional to the initial mass of each constituent, similar to the proportional relationship proposed by Imhoff et al. (1996) for determining the length of dissolution fingers. A good correlation (R^2=0.94) was observed, indicating that this regression equation is applicable for the studies examined, at both the laboratory- and field-scale, for homogeneous and heterogeneous DNAPL layers, and for residual and mixed source zones. The validity of this correlation is demonstrated by successfully simulating conditions observed during two independent sets of experiments (Brusseau et al., 2002; Farthing et al., 2012), using a simple process-oriented screening model (NDM), without having to calibrate any input parameters.

For simulation of the Brusseau et al. (2002) experiment with a 10-cm thick residual DNAPL layer, thinning of the DNAPL zone is demonstrated to have a significant influence on the reduction in cross-sectional area available for through-discharge, although intra-source bypassing is shown to still be the main process governing the decline in through-discharge for most of the experiment. This result validates the general applicability of the correlation in Eq. 6.7 for approximate

estimation of λ_{thru} for field-scale simulations where high resolution monitoring data are not available for calibrating this input parameter.

6.7 References

Broholm, K., S. Feenstra, and J.A. Cherry, 1999. Solvent release into a sandy aquifer. 1. Overview of source distribution and dissolution behaviour. Environmental Science & Technology, 33: 681-690.

Brusseau, M.L., Z. Zhang, N.T. Nelson, R.B. Cain, G.R. Tick, and M. Oostrom, 2002. Dissolution of nonuniformly distributed immiscible liquid: Intermediate-scale experiments and mathematical modeling. Environmental Science & Technology, 36: 1033-1041.

Carey, G.R., E.A. McBean, and S. Feenstra, 2014a. DNAPL source depletion: Predicting rates and timeframes. Remediation Journal, Summer 2014, p. 21-47.

Carey, G.R., E.A. McBean, and S. Feenstra, 2014b. Screening Model for DNAPL Source Zone Depletion: Natural Attenuation, in preparation.

Carey, G.R., E.A. McBean, and S. Feenstra, 2014c. Estimating Properties Based on Hydraulic Conductivity: Transverse Vertical Dispersivity. In preparation for submittal to the Journal of Contaminant Hydrology.

Carey, G.R., E.A. McBean, and S. Feenstra, 2014d. Estimating Properties Based on Hydraulic Conductivity: Tortuosity Coefficient and Effective Porosity. Submitted to the Journal of Contaminant Hydrology.

Christ, J.A., C.A. Ramsburg, K.D. Pennell, and L.M. Abriola, 2006. Estimating mass discharge from dense nonaqueous phase liquid source zones using upscaled mass transfer coefficients: An evaluation using multiphase numerical simulations. Water Resources Research, 42: W11420.

Christ, J.A., C.A. Ramsburg, K.D. Pennell, and L.M. Abriola, 2010. Predicting DNAPL mass discharge from pool-dominated source zones. Journal of Contaminant Hydrology, 114: 18-34.

Falta, R.W., P.S. Rao, and N. Basu, 2005. Assessing the impacts of partial mass depletion in DNAPL source zones 1. Analytical modeling of source strength functions and plume response. Journal of Contaminant Hydrology, 78: 259-280.

Frind, E.O., J.W. Molson, M. Schirmer, and N. Guiger, 1999. Dissolution and mass transfer of multiple organics under field conditions: The Borden emplaced source. Water Resources Research, 35(3): 683-694.

Hayduk, W., and H. Laudie, 1974. Prediction of diffusion coefficients for nonelectrolytes in dilute aqueous solutions. American Institute of Chemical Engineers (AIChE) Journal, 20 (3): 611-615.

Imhoff, P.T., P.R. Jaffe, and G.F. Pinder, 1994. An experimental study of complete dissolution of a nonaqueous phase liquid in saturated porous media. Water Resources Research, 30(2): 307-320.

Imhoff, P.T., G.P. Thyrum, and C.T. Miller, 1996. Dissolution fingering during the solubilization of nonaqueous phase liquids in saturated porous media 2. Experimental observations. Water Resources Research, 32(7): 1929-1942.

Imhoff, P.T., M.W. Farthing, and C.T. Miller, 2003. Modeling NAPL dissolution fingering with upscaled mass transfer rate coefficients. Advances in Water Resources, 26: 1097-1111.

Johnson, R.L. and J.F. Pankow, 1992. Dissolution of dense chlorinated solvents into groundwater. 2. Source functions for pools of solvent. Environmental Science & Technology, 26: 896-901.

Klenk, I.D. and P. Grathwohl, 2002. Transverse vertical dispersion in groundwater and the capillary fringe. Journal of Contaminant Hydrology, 58: 111-128.

Marble, J.C., E.L. DiFilippo, Z. Zhang, G.R. Tick, and M.L. Brusseau, 2008. Application of a lumped-process mathematical model to dissolution of nonuniformly distributed immiscible liquid in heterogeneous porous media. Journal of Contaminant Hydrology, 100: 1-10.

Miller, C.T., M.M. Poirier-McNeill, and A.S. Mayer, 1990. Dissolution of trapped nonaqueous phase liquids: Mass transfer characteristics. Water Resources Research, 26(11): 2783-2796.

Mobile M.A., M.A. Widdowson, and D.L. Gallagher, 2012. Multicomponent NAPL source dissolution: Evaluation of mass-transfer coefficients. Environmental Science & Technology, 46: 10047-10054.

Moreno-Barbero, E. and T.H. Illangasekare, 2006. Influence of dense nonaqueous phase liquid pool morphology on the performance of partitioning tracer tests: Evaluation of the equilibrium assumption. Water Resources Research, 42: W04408.

Nambi, I.M. and S.E. Powers, 2000. NAPL dissolution in heterogeneous systems: An experimental investigation in a simple heterogeneous system. Journal of Contaminant Hydrology, 44: 161-184.

Newell, C.J., I. Cowie, T.M. McGuire, and W.W. McNab, 2006. Multiyear temporal changes in chlorinated solvent concentrations at 23 monitored natural attenuation sites. Journal of Environmental Engineering, 132(6), 653-663.

Parker, J.C. and E. Park, 2004. Modeling field-scale dense nonaqueous phase liquid dissolution kinetics in heterogeneous aquifers. Water Resources Research, 40: W05109.

Parker, B.L., J.A. Cherry, S.W. Chapman, and M.A. Guilbeault, 2003. Review and analysis of chlorinated solvent dense nonaqueous phase liquid distributions in five sandy aquifers. Vadose Zone Journal, 2: 116-137.

Powers, S.E., L.M. Abriola, and W.J. Weber Jr., 1992. An experimental investigation of nonaqueous phase liquid dissolution in saturated subsurface systems: Steady state mass transfer rates. Water Resources Research, 28(10): 2691-2705.

Powers, S.E., L.M. Abriola, and W.J. Weber Jr., 1994. An experimental investigation of nonaqueous phase liquid dissolution in saturated subsurface systems: Transient mass transfer rates. Water Resources Research, 30(2): 321-332.

Powers, S.E., I.M. Nambi, and G.W. Curry Jr., 1998. Non-aqueous phase liquid dissolution in heterogeneous systems: Mechanisms and a local equilibrium modeling approach. Water Resources Research, 34(12): 3293-3302.

Rivett, M.O. and S. Feenstra, 2005. Dissolution of an emplaced source of DNAPL in a natural aquifer setting. Environmental Science & Technology, 39: 447-455.

Russo, A.E., M.K. Mahal, and M.L. Brusseau, 2009. Nonideal behaviour during complete dissolution of organic immiscible liquid 1. Natural porous media. Journal of Hazardous Material, 172: 208-213.

Seyedabbasi, M.R., C.J. Newell, D.T. Adamson, and T.C. Sale, 2012. Relative contribution of DNAPL dissolution and matrix diffusion to the long-term

persistence of chlorinated solvent source zones. Journal of Contaminant Hydrology, 134-135: 69-81.

Suarez, M. P., H.S. Rifai, T.J. Rittaler, and S. Hausman, S, 2004. Natural attenuation of chlorinated solvent plumes at Texas dry cleaners. Remediation, 14(3), 7-33.

Chapter 7

Conclusions and Recommendations

Chlorinated solvent DNAPLs in the subsurface represents a long-term source of contamination at many sites. Due to technological limitations, and site factors such as heterogeneity and back-diffusion, restoration of groundwater to strict cleanup criteria is not attainable within a reasonable timeframe at many DNAPL sites. In recognition of this, it is imperative that a new paradigm for management of DNAPL sites be considered for adoption, which includes a cost-benefit analysis for aggressive in-situ remediation, relative to more passive source treatment alternatives such as MNA. Two questions which must be answered in this type of cost-benefit analysis are:

(1) How much reduction in source strength is realistically attainable for a given in-situ remediation technology at sites with varying degrees of heterogeneity? and

(2) What is the relative timeframe to achieve this target source strength reduction for various natural and enhanced alternatives such as EISB, ISCO, SP&T, or MNA?

This thesis examined the applicability of various statistical and modeling tools, and model input parameter regression equations, for estimating attainable goals and timeframes for natural or enhanced depletion of DNAPL source zones. The intention of this thesis was also to add to existing knowledge regarding the relative contribution of various processes influencing DNAPL depletion rates, particularly sites with layers of DNAPL which dominate source zone architecture at aged contaminated sites. This section summarizes the findings of the research and provides a list of recommendations for future work.

7.1 Statistical and Process-Based Modeling of DNAPL Pool Depletion Rates

Naturally occurring pool depletion half-lives are proportional to the square root of the length of the pool and are linearly proportional to the thickness of the pool. Constant-length pool discharge models (CLM) are shown to not be applicable for

evaluating DNAPL pool decline rates. Through-pool discharge was shown to be a potentially significant process that reduces the DNAPL pool depletion timeframe, particularly for thin pools or from the upper regions of thicker pools. The pool mass discharge decline half-life is shown to be generally proportional to solubility for single component DNAPLs.

The median naturally-occurring TCE DNAPL depletion half-life of 6.1 years reported in Newell et al. (2006) is shown to be consistent with pool-dominated source zones. A naturally-occurring source strength decline half-life of 7.5 years was estimated for a large, complex site in Tuscon, Arizona based on data reported in Brusseau et al. (2011). The median TCE decline half-life of 1.6 years determined by Suarez et al. (2004) appears to be too rapid to be representative of most pool-dominated source zones.

An exponential decline model is shown to be a reasonable if not the best representation relative to a linear regression. Less than 40 percent of the ISCO and EISB wells exhibited general declining concentration trends that were deemed suitable for the regression analysis. The mean normalized decline rates calculated for ISCO and EISB sites show a concentration decline half-life for ISCO sites of 0.39 year, with a 95 percent confidence interval of 0.15 to 1.20 years. The mean concentration decline half-life for EISB sites is 0.29 years, with a confidence interval of 0.14 to 0.60 years.

The EISB empirical study sites have a decline rate that is significantly faster than expected for a pool-dominated source zone. EISB is simulated using NDM to

have a corresponding decline half-life of 2.5 years for a pool-dominated source zone with 12 TCE pools with lengths and widths of several meters and thicknesses ranging from 2 to 4 cm. Data from a case study presented by Brusseau et al. (2011) are used to calculate an ISCO-enhanced decline half-life of 2.5 years for a large, complex site in Tucson, Arizona. Limitations in the general representativeness of the empirical study dataset are that most of the decline data are based on dry cleaning sites with source zone geology characterized as fine-grained (clay, silt, and/or silt/clayey sand).

7.2 Defining Attainable, Technology-Specific Goals for Mass Discharge Reduction

For this study, only trends observed at wells at EISB or ISCO sites with concentrations exceeding 1% of solubility (i.e. potentially downgradient of DNAPL zones) were utilized. Geometric mean *MdR*s for EISB, ISCO, and thermal treatment and found to be 49x, 9x, and 19x, respectively, based on a log-normal distribution. Lower / upper geometric mean confidence intervals were calculated to be 20x / 556x (EISB), 4x / 110x (ISCO), and 6x / 150x (thermal). Comparison to the *MdR* observed at a well documented, large, complex site (4x) suggests that the lower confidence interval for the geometric mean may be most applicable for similar sites or for sites with pool-dominated source zones.

The Dandy-Sale model demonstrated that even in the case of complete source depletion or containment, back-diffusion from the thick aquitard underlying the long plume at the site will create a sustained secondary source for more than 1,000 years. An analysis of plume response (i.e., influent concentrations for a pump-and-treat system and plume source strength) versus time demonstrates there is no reduction in plume management cost, and little difference in risk reduction associated with the various source zone alternatives.

A sensitivity analysis with the NDM demonstrated that pool-dominated source conditions with a large range in initial DNAPL mass (250 to 1500 kg) corresponded to a narrow range of source strength (20 to 30 kg/y). This demonstrates that measured source strength is non-unique with respect to DNAPL mass in the subsurface, and thus source strength should not be used as the sole basis for predicting how much DNAPL mass remains or must be removed to achieve a target goal.

A net present value (NPV) analysis indicates that MNA consistently has the lowest NPV and is not sensitive to the range of pool conditions that were simulated. Given the limited plume response to aggressive source depletion and the long-term source (greater than 1000 y) due to back-diffusion, MNA for the source zone is a reasonable alternative for the example site. If regulatory requirements mandate that an aggressive source depletion alternative be implemented, then this feasibility analysis indicates that SP&T is the best alternative on a combined cost and depletion timeframe basis. The additional source strength reduction (47x) that can be achieved with

thermal treatment has limited benefit in comparison with other alternatives at this site because of back-diffusion. This decision analysis is insensitive to the range of uncertainty in pool thickness and through-pool discharge.

7.3 Estimating Process-Based Model Input Parameters

Chapters 3 and 4 focused on derivation of empirical regression equations which may be used to estimate the tortuosity coefficient and transverse vertical dispersivity (see Sections 7.3.1 and 7.3.2, respectively). Chapter 5 presents an alternative model for estimating transient through-discharge for layers of residual DNAPL, relative to previous regression equations by Powers et al. (1994) and Imhoff et al. (1996 and 2003). Chapter 5 also presents the derivation of a simple regression equation for estimating the rate of through-discharge decline for a wide range of source zone characteristics (see Section 7.3.3, below).

7.3.1 Tortuosity Coefficient

A simple empirical formula is developed to facilitate estimation of total and effective porosity based on hydraulic conductivity. It is shown that the widely-used empirical relationship proposed by Millington and Quirk (1961) is for estimating τ_{path} based on effective porosity, not total porosity. The value of m=0.33 proposed by

Millington and Quirk is shown to overestimate τ_{app}, and an empirical regression of m=0.46 is derived herein based on a meta case study review. A number of case studies documenting the estimation of D_e and corresponding estimate of τ_{app} were reviewed. Based on these case study results and in some cases, a re-analysis of the tortuosity coefficient, an empirical relationship for τ_{app} versus hydraulic conductivity was derived. The average τ_{app} for clayey deposits based on laboratory and in situ column studies was calculated to be 0.33. This is the first known empirical regression of τ_{app} versus effective porosity or hydraulic conductivity based on a meta study review for widely ranging soil textures.

7.3.2 Transverse Vertical Dispersivity

A review of various experimental datasets in the literature indicates that transverse vertical dispersivity is inversely proportional to grain size and hydraulic conductivity, which contradicts findings from a number of earlier studies (e.g. de Josselin de Jong, 1958; Perkins and Johnston, 1963; Klenk and Grathwohl, 2002; Olsson and Grathwohl, 2007; Chiogna et al., 2010). The inverse relationship observed between dispersivity and hydraulic conductivity means that transverse vertical dispersivity is lower for coarser-grained soil, relative to the dispersivity that would be observed in a finer-grained soil. This relationship is likely due to the corresponding

reduction in vertical heterogeneity, and variance in pore size distribution, as grain size increases.

For the first time, a model has been developed to estimate α_{TV} under local equilibrium conditions as a function of only hydraulic conductivity. The non-equilibrium dispersivity model (NE Model) developed by Klenk and Grathwohl (2002) is validated by comparison to various studies where $v > v_c$.

7.3.3 Through-Discharge Decline Rate for Layers of Residual DNAPL

The rapidly declining effective solubility of TCM had little influence on the overall rate of downgradient dilution that was observed during the Emplaced Source experiment in Borden, Ontario (Rivett and Feenstra, 2005). This dilution was attributed primarily to the development of preferential flow channels through the source as a result of intra-source bypassing. Evaluation of the Powers et al. (1994) regression equation for K_o' and βia, and the LDF model, indicate that these models are not generally applicable to field-scale residual DNAPL layer dissolution. The re-equilibration process conceptualized by Rivett and Feenstra (2005) for multicomponent DNAPL dissolution was validated based on model simulations.

The rate of decline in through-discharge observed during the Emplaced Source experiment was observed to be proportional to the product of initial effective solubility and groundwater velocity (i.e. rate of flushing), and inversely proportional to the

initial mass of each constituent, similar to the proportional relationship proposed by Imhoff et al. (1996) for determining the length of dissolution fingers. A good correlation (R^2=0.94) was observed, indicating that this regression equation is applicable for the studies examined, at both the laboratory- and field-scale, for homogeneous and heterogeneous DNAPL layers, and for residual and mixed source zones. The validity of this correlation is demonstrated by successfully simulating conditions observed during two independent sets of experiments (Brusseau et al., 2002; Farthing et al., 2012), using a simple process-oriented screening model (NDM), without having to calibrate any input parameters.

For simulation of the Brusseau et al. (2002) experiment with a 10-cm thick residual DNAPL layer, thinning of the DNAPL zone is demonstrated to have a significant influence on the reduction in cross-sectional area available for through-discharge, although intra-source bypassing is shown to still be the main process governing the decline in through-discharge for most of the experiment. This result validates the general applicability of the correlation in Eq. 7 for approximate estimation of λ_{thru} for field-scale simulations where high resolution monitoring data are not available for calibrating this input parameter.

7.4 Future Work for Evaluating Depletion of DNAPL Source Zones

There are currently two additional papers in preparation, regarding the application of a process-based screening model (NDM) for simulating DNAPL depletion for natural attenuation and enhanced dissolution alternatives, respectively. These papers will provide examples of scenarios where application of a process-based model is applicable, and provides valuable insights which may help to improve remedial efficiency at some sites.

Other suggestions for future work include:

1. Conduct field-scale pilot tests to demonstrate the efficacy of strategic pump-and-treat (SP&T). There are potentially enormous cost savings to be realized by adopting SP&T for enhanced treatment of DNAPL source zones where infrastructure for a pump-and-treat system already exists (as is the case for many contaminated sites).
2. Further validate the use of NDM for field-scale source depletion, by conducted detailed delineation of sub-zone DNAPL architecture using high resolution techniques, and then testing NDM for simulation of historical trends in, and current source strength (i.e. mass discharge).
3. Conduct a probabilistic assessment of depletion timeframes for scenarios with stochastic representation for the number of DNAPL sub-zones, as well

as dimensions (length, width, height) and initial DNAPL saturation, to evaluate the range of uncertainty in source strength trends over time relative to the uncertainty in sub-zone characteristics.

4. Evaluate how future trends for mixed DNAPL sub-zones or overall source zones (i.e. combined layers of free phase and residual DNAPL) may be estimated.
5. Revise NDM to simulate the vertical evolution of the transition zone in pools, and/or vertical changes in residual DNAPL layers which cause thinning as a result of surface discharge, and evaluate when it may be important to consider these transient vertical effects.
6. Simulate various ISCO experiments to develop a range for the enhanced dissolution factor for ISCO which is used an input parameter for NDM. (The enhanced dissolution factor for EISB is already well documented e.g. ITRC, 2008; Stroo et al., 2012.)

7.5 Concluding Remarks

Starting in the early 2000s, we have gone through a "Decade of Reflection", where intense research has been undertaken and regulatory guidance documents have been developed, regarding the management of DNAPL sites. The U.S. Department of Defense, through the SERDP and ESTCP programs, played a major role in this intensive undertaking.

This Decade of Reflection started off with an EPA workshop (Kavanaugh et al., 2003) asking many important and challenging questions regarding the efficacy of partial DNAPL depletion. A game-changer that occurred early in this period was the publication of work led by Beth Parker and John Cherry at a Connecticut field site, which quantitatively demonstrated the influence that back-diffusion may have on remediation timeframes (Parker et al., 2004; Chapman and Parker, 2005). I see now that Beth and John, and a select few others, have been referring to this back-diffusion process since the late 1980s and 1990s, but these recent papers really provided the proof that was needed to open the industry's eyes to the magnitude of this problem. This Decade of Reflection was closed with the NRC report (Kavanaugh et al., 2012) which recommended a new management framework for complex sites – an important step towards improving how we manage these long-term problems.

I believe that, as our industry moves towards higher resolution characterization of these source zones and the ability to better predict past, current, and future trends,

there will eventually be a 'Sea Change' with respect to how regulators perceive, and allow us to manage, these sites. But before we get to that point, we need to demonstrate that as an industry, we have an adequate understanding of these complex source zones. And we need to continue to educate, and improve our own understanding of how things unfold at the complex – but still understandable and predictable at some level - field-scale.

In the future, I hope and expect to see more research done at the field-scale to continue to facilitate this evolution. I also hope to see more work conducted using process-based screening models which will continue to enhance our knowledge and understanding, and less work using lumped mass transfer coefficients which have little physical meaning, and poor applicability to a broad range of contaminated sites, when used in upscaled models.

A. NAPL Depletion Model (NDM) Development

A.1 Conceptual Model

The NAPL Depletion Model (NDM) is a semi-analytical screening model which may be used to estimate NAPL depletion under conditions of naturally-occurring or enhanced dissolution. NDM is a process-oriented model, which means that it explicitly represents various porous media and NAPL characteristics which influence the rate of dissolution for one or more NAPL sub-zones within an overall source zone. A sub-zone refers to a NAPL body (e.g. layer) which is relatively continuous, and may not be further discretized into smaller sub-zones on the basis of geometry, porous media characteristics, and/or NAPL characteristics (e.g. chemical composition, NAPL saturation, or density). A NAPL source zone in NDM is comprised of one or more individual sub-zones.

NDM is an alternative to the use of simpler up-scaled models, which typically represent domain-averaged dissolution rates or decline rates for a uniform source zone. NDM may be used for LNAPL or DNAPL, and was developed with the flexibility to simulate NAPL pools, residual sub-zones, and/or mixed zones of NAPL. NDM simulates three types of dissolution or discharge processes: (a) surface dissolution at the top or bottom of a sub-zone; (b) reduced groundwater flow through a sub-zone based on a user-specified or model-calculated relative water permeability; and (c) flux into or out of lower-permeability zones adjacent to one or more NAPL sub-zones.

The key output variables for NDM are the mass discharge and NAPL mass remaining for each individual sub-zone, and the total metrics for the combined source zone. NDM does not simulate changes in aqueous concentrations outside of the NAPL sub-zones, although it is possible to use simple multipliers to simulate or calibrate the ratios of daughter product formation for mass discharge calculations.

Uses of NDM may include:

- Interpretation of NAPL architecture based on calibration of a model to historical discharge trends;
- Estimation of future mass discharge decline rates and depletion timeframes for an existing alternative;
- Evaluation of the relative performance of various potential alternatives as part of feasibility study;

- Quantifying the relative sensitivity of predicted trends (e.g. depletion timeframe) to various site characteristics, in order to identify those characteristics which require further investigation.

NDM is a Fortran-based program which offers a number of options for representing NAPL pools, residual NAPL sub-zones, and/or mixed NAPL zones. A simple mass balance approach is used within NDM to simulate the mass discharge, and mass remaining, in each NAPL sub-zone of a simulation at the end of each time step. The analytical governing equations for NDM are described in more detail below. General functionality in NDM includes:

- Use of a one-dimensional grid to represent each NAPL sub-zone, with user-defined length, width, thickness, and average NAPL saturation (or depth-specific NAPL saturation calculations performed by the model for NAPL pools with a capillary pressure of zero at the top surface).
- NDM simulates dissolution from the upgradient end of each sub-zone, and upgradient grid cells that become depleted in mass during a simulation are defined to be inactive for the remainder of the simulation. In this manner, the pool-scale declining NAPL-water interfacial area may be represented, as well as the corresponding influence on mass discharge associated with surface dissolution.
- Option to apply through-discharge to the upgradient-most, active cell in a NAPL sub-zone, or uniformly to all cells within a NAPL sub-zone.
- A user-defined multiplier which allows for simulation of surface discharge for none, one, or both the top and bottom surfaces of a NAPL sub-zone, or for simulating an accelerated specific discharge adjacent to the NAPL-water interface.
- Option to make the start of surface and/or through discharge for a NAPL sub-zone to be dependent on the depletion of another zone (e.g. an upgradient sub-zone, or an overlying or underlying layer of NAPL).
- Option for constant, exponential or linear decline models to represent the transient influence of intra-source bypassing and other rate-limited kinetics on the through-discharge with a NAPL sub-zone;
- Quasi-2D representation of discharge through the transition zone in the upper portion of NAPL pools where the relative water permeability is sufficiently large to allow for significant mass discharge, and the NAPL saturation is optionally calculated at specific depths within the pool;
- Enhanced dissolution corresponding to temporal changes in hydraulic gradient (e.g. at the start of pumping near a source zone), or an enhanced dissolution factor associated

with in-situ remedies such as enhanced in-situ bioremediation (EISB) or in-situ chemical oxidation (ISCO).

- Automated non-linear calibration of the β term in $Md/Md_o = (M/M_o)$ for each sub-zone;
- An adaptive time-stepping scheme to account for changing system dynamics when a sub-zone grid cell becomes inactive; and
- Option for through-discharge simulations for multicomponent NAPL (see Section A.6).
- Batch mode so that hundreds of simulations may be executed automatically. (A separate processor may be used to generate text input files and post-process output files for use with monte carlo or latin hypercube realizations.)

A.2 Sub-zone Mass Balance

As long as mass remains in NAPL sub-zone *i*, the total mass discharge related to NAPL dissolution to the aqueous phase is based on

$$Md_{i,diss}^{t} = Md_{i,thru}^{t} + Md_{i,surf}^{t} + Md_{i,diff}^{t} \quad \text{(A-1)}$$

where $Md_{i,diss}^{t}$ = total mass discharge from dissolution of NAPL to the aqueous phase in sub-zone *i* at time step *t* [ML^{-1}];

$Md_{i,thru}^{t}$= mass discharge from dissolution of NAPL into groundwater flowing through sub-zone *i* at time step *t* [ML^{-1}];

$Md_{i,surf}^{t}$= mass discharge from dissolution of NAPL into groundwater flowing across the top and/or bottom of sub-zone *i* at time step *t* [ML^{-1}]; and

$Md_{i,diff}^{t}$= mass discharge from dissolution of NAPL and subsequent diffusion into a low-permeability unit above and/or below sub-zone *i* at time step *t* [ML^{-1}].

The mass remaining in each grid cell *j* of NAPL sub-zone *i* at the end of the time step t is calculated using

$$M_{ij}^{t} = M_{ij}^{t-1} - \left(Md_{ij,thru}^{t} + Md_{ij,surf}^{t} + Md_{ij,diff}^{t}\right)\Delta t \quad \text{(A-2)}$$

Where M_{ij}^{t-1}refers to the mass remaining in NAPL sub-zone i cell *j* at the end of the previous time step [M], and Δt represents the length of the time step [T]. The total NAPL mass

remaining in sub-zone *i* at the end of the time step is calculated by summing the NAPL mass remaining in each cell of the sub-zone grid. The total mass added to storage in low-permeability unit(s) adjacent to each NAPL source zone is also accounted for in the mass balance.

The equations and potential uses of each of the individual mass discharge terms in Eq. A-1 are discussed further below.

Finally, the source strength contributing to the downgradient plume from NAPL dissolution is calculated as

$$Md_{i,source}^{t} = \left(Md_{i,thru}^{t} + Md_{i,surf}^{t}\right) f_{RXN1}^{t} \quad \text{(A-3)}$$

Where f_{RXN1}^{t}represents a multiplier for the reduction in source strength due to chemical transformations occurring in the source zone when NAPL is present. This term is useful for simple, quasi-representation of transformation reactions that may occur upon implementation of an active remedial technology such as EISB or ISCO.

When mass has been completely depleted in NAPL sub-zone *i*, mass discharge contributing to ongoing source strength via back-diffusion from adjacent diffusive source zones (if simulated) is then simulated for the time step using

$$Md_{i,source}^{t} = \left(Md_{b-diff}^{t}\right) f_{RXN2} \quad \text{(A-4)}$$

where f_{RXN2}represents a multiplier for the reduction in source strength due to chemical transformations occurring in the source zone once NAPL has been depleted. This term may be used to represent sustained transformation reactions which may occur after the cessation of EISB.

A.3 Sub-Zone Through-Discharge

Residual/Mixed Source Zones

For residual and mixed NAPL source zones, mass discharge due to dissolution of NAPL into groundwater flowing through sub-zone *i* is given by

$$Md_{i,thru}^{t} = \left(krw_i q_x^t C_{eff}^t w_i h_i\right) f_i^t f_{ed1}^t \quad \text{(A-5)}$$

where krw_i is the relative water permeability, q_x^t is the average specific discharge at time step *t*, C_{eff}^t is the effective solubility (which is the same as solubility for a single component NAPL),

w_i and h_i represent the width and height of source zone i, f_i^t is a multiplier representing the proportion of the source zone cross-section which has streamtubes containing NAPL at time step t, and f_{ed1}^t is a multiplier for mass discharge through the zone representing potential enhanced dissolution at time step t as a result of active remediation. The current version of NDM does not consider transient krw_i during source depletion; further study is warranted to determine when transient representation of this parameter may be helpful.

As discussed above, NDM represents three types of decline models for the f_i^t term to provide a surrogate representation for the rate of decline in NAPL-water interfacial area (IA) in the source zone:

- Exponential decline, $f_i^t = f_{io}e^{-\lambda_i^t t}$where f_{io} represents the initial proportion of the source zone cross-section which has streamtubes containing NAPL, and λ_i^trepresents the first-order rate of decline of the proportion of streamtubes containing NAPL at time step t;
- Linear decline, $f_i^t = f_{io} - f_{io}m_i^t t$where m_i^trepresents the linear decline slope at time step t; and
- Constant$f_i^t = f_{io}$.

As an example, if a transect across the downgradient boundary of a source zone has 10% of the cross-sectional area with NAPL upgradient of the transect, f_{io} will be specified as 0.10. At field sites, it is expected that exponential decline models will typically be used to represent aged sources and/or sources with a heterogeneous NAPL distribution, and the constant f_i^t model will be used to represent high-saturation portions of pools with relatively homogeneous distributions of NAPL.

For sites where an exponential decline model is applicable, the first-order rate (λ) may be estimated based on historical monitoring data. Of note is the relationship summarized by Newell and Adamson (2005) such that $\lambda = Md_o/M_o$, where Md_o represents the source strength at the time of characterization and M_o represents an estimate of initial source mass contributing to the this source strength. If the first-order rate can be estimated from site monitoring data, then an estimate of M_o and the corresponding average NAPL saturation (Sn_o) in a source zone can also be readily estimated. For residual and mixed source zones, the average NAPL saturation source zone (Sn_o) is an input parameter for NDM to facilitate estimation of the initial NAPL mass in a source zone.

To represent the influence of changes in the specific discharge rate which may occur during active remediation, the time-dependent exponential and linear decline rates are calculated respectively based on:

$$\lambda_i^t = \lambda_{io} q_x^t / q_{xo} \quad \text{(A-6)}$$

$$m_i^t = m_{io} q_x^t / q_{xo} \quad \text{(A-7)}$$

Pool Source Zones

Given the higher NAPL saturation in pools and the corresponding reduction in water permeability, as well as the occurrence of some pools that form in topographic depressions on the surface of a low-permeability layer, a relatively small flux of groundwater will occur through the body of the pool.

To facilitate a comparison of the mass discharge which may occur through pool sub-zones relative to the discharge arising from surface dissolution, NDM incorporates the flexibility of simulating the rate of reduced water flow at various depths within a NAPL pool. NDM also incorporates the option of specifying an average Sn_{io} and krw_i for use in estimating the initial mass discharge through the NAPL source zone based on Equation A-5, or to specify a mass discharge of zero based on the assumption that the relative permeability in the pool layer is negligible relative to the mass discharge from the surface of the pool.

McWhorter and Kueper (1996) document the following equation for estimating the elevation in a pool corresponding to an effective saturation:

$$z = T - \frac{P_o}{\Delta\rho g}\left[\left(\frac{Sw-Swr}{Sm-Swr}\right)^{-1/m} - 1\right]^{1-m} \quad \text{(A-8)}$$

where z refers to an elevation in a pool layer with height T, P_o is the reference capillary pressure defined as $\rho_w g/\alpha$, where α [L^{-1}] and m [dim.] are capillary pressure-saturation curve coefficients defined by Van Genuchten (1980), ρ_w is the density of water[ML^{-3}], g is the gravitational acceleration constant [LT^{-2}], $\Delta\rho$ is the difference between NAPL and water density [ML^{-3}], Sw is the water saturation, Swr is the irreducible water saturation, and Sm is the maximum water saturation.

Re-arranging the above equation and solving for Sn=1-Sw at elevation z gives

$$Sn(z) = 1 - Swr - (Sm - Swr)\left[1 + \left(\frac{\alpha\Delta\rho(T-z)}{\rho_w}\right)^{\frac{1}{1-m}}\right]^{-m} \quad \text{(A-9)}$$

Van Genuchten (1980) defines the relative water permeability for a two-phase system as

$$krw = {Se_{krw}}^{1/2}\left[1 - \left(1 - {Se_{krw}}^{1/m}\right)^{m}\right]^{2} \quad \text{(A-10)}$$

where Se_{krw}, the effective saturation used to estimate relative water permeability, is given by

$$Se_{krw} = \frac{Sw - Swr}{1 - Swr} \quad \text{(A-11)}$$

To estimate the total mass discharge through a pool layer with variable *Sn(z)*, the pool layer is vertically discretized into *m* layers with uniform thickness Δz. The NAPL saturation in each layer (Sn_{im}) is calculated by substituting the pool height (h_i) for T in Equation A-8. The effective saturation Se_{krw} is calculated by substituting Sw_{im}=1-Sn_{im} for *Sw* in Equation A-11, and the relative water permeability in layer *m* of the pool source zone *i* (krw_{im}) is then calculated using Equation A-10. The mass discharge arising from NAPL dissolution into groundwater flowing through source zone *i* at time step *t* is then calculated by summing the depth-specific discharges using

$$Md^{t}_{i,thru} = \left(\sum_{m=1}^{nlay} krw_{im} q^{t}_{x} C^{t}_{eff} w_i \Delta z\right) f^{t}_{i} f^{t}_{ed1} \quad \text{(A-12)}$$

Equation A-12 includes a time-dependent enhanced dissolution multiplier, which may be used to represent enhanced dissolution periods within an overall model simulation (e.g. EISB or Strategic Pump-and-Treat). Note that NDM does not represent potential mobilization of NAPL that may occur with some in-situ remediatino technologies. Care must be exercised during in-situ remediation to ensure that expansion of the source zone does not occur.

A.4 Sub-Zone Surface Discharge

NAPL pools are typically characterized by a relatively limited NAPL-water interfacial area at the surface of pools where dissolution into flowing groundwater occurs. Solute transport at this surface interface is driven by transverse vertical dispersion. The solute transport equation is

$$\theta\frac{\partial C}{\partial t} = \theta D_z \frac{\partial^2 C}{\partial z^2} - q_x \frac{\partial C}{\partial x} \quad \text{(A-13)}$$

where C is the solute concentration [ML^{-3}], D_z is the hydrodynamic dispersion coefficient [L^2T^{-1}], and q_x is specific discharge [$L^3L^{-2}T^{-1}$]. In this form of the advection-dispersion equation, the hydrodynamic dispersion coefficient is calculated using

$$D_z = \alpha_{TV} v_x + D_e, \text{ and } D_e = \tau D_o \quad \text{(A-14)}$$

where α_{TV} is the transverse vertical dispersivity [L], v_x (=q_x/θ) is the average linear groundwater velocity [LT^{-1}], D_e is the effective diffusion coefficient [$L2T^{-1}$], τ is the tortuosity coefficient, and D_o is the free-water molecular diffusion coefficient [L^2T^{-1}].

In some cases, the above equation A-13 is written as

$$\frac{\partial C}{\partial t} = D_z \frac{\partial^2 C}{\partial z^2} - v_x \frac{\partial C}{\partial x} \quad \text{(A-15)}$$

where the hydrodynamic dispersion coefficient and effective molecular diffusion coefficient are estimated based on Equation A-14. In contrast, Hunt et al. (1988) expressed the advection dispersion equation based on an alternative form of the governing equation

$$\theta \frac{\partial C}{\partial t} = D_z^* \frac{\partial^2 C}{\partial z^2} - q_x \frac{\partial C}{\partial x} \quad \text{(A-16)}$$

where the adjusted hydrodynamic dispersion coefficient is calculated using

$$D_z^* = \alpha_{TV} q_x + D_e^*, \text{ and } D_e^* = \theta \tau D_o \quad \text{(A-17)}$$

In other words, when specific discharge is used in the advection term of the governing equation and for calculating mechanical dispersion, it is important to include a porosity term in the term representing the effective molecular diffusion coefficient.

Analytical Solution for Mass Discharge from a Pool Surface

Based on the analytical solution cited by Johnson and Pankow (1992) for the steady-state form of Equation A-15, mass discharge from dissolution along the surface of a pool with length L and width w is

$$Md = LwC_{eff}\theta\sqrt{\frac{4D_z v_x}{\pi L}} \quad \text{(A-18)}$$

Hunt et al. (1988) present the analytical solution based on Equation E-16 as

$$Md = LwC_{eff}\sqrt{\frac{4D_z^* q_x}{\pi L}} \quad \text{(A-19)}$$

Note that both Equations E-18 and E-19 yield the identical solution provided that θ is used to estimate v_x. Equation E-19 can be further re-arranged to yield

$$Md = \left(2LwC_{eff}\sqrt{\frac{q_x}{\pi L}}\right)\sqrt{\alpha_{TV} q_x + \theta\tau D_o} \quad \text{(A-20)}$$

It is not clear whether θ should represent total or effective porosity, since both advection and diffusion contribute to solute transport to some degree during surface dissolution from a pool. From Equation A-19 it is clear that under high specific discharge conditions, mechanical dispersion will dominate over the effective molecular diffusion term and porosity will have a negligible influence on the mass discharge calculation. In low specific discharge environments, molecular diffusion is likely to dominate the hydrodynamic dispersion term and it is appropriate then to assign θ as total porosity. When considering the middle case where mechanical dispersion and effective molecular terms are equal in a fine sand, the total porosity may be twice as high as effective porosity (e.g. 0.40 vs. 0.20, respectively). In this case, mass discharge calculated using total porosity is approximately 20% higher than the discharge that would be calculated using effective porosity. There is a smaller range for total vs. effective porosity for a coarse sand (e.g. 0.35 to 0.275), resulting in a smaller difference for mass discharge calculated based on total versus effective porosity.

Given that these differences are relatively minor when compared to uncertainty in specific discharge or pool dimensions, and that total porosity is more directly measured at the site and more applicable under conditions of low specific discharge, it is recommended that the total porosity be used when estimating mass discharge on the basis of Equation A-19.

It is also recommended that the solution in Equation in A-19 be used for estimating mass discharge instead of Equation A-18, since v_x is typically calculating using effective porosity which is not the appropriate porosity to use in Equation A-18 for sites where transport is diffusion-dominated.

Based on the analytical solution presented in Equation A-19, NDM estimates the mass discharge from the surface of source zone *i* discretized in *j*=1 to grid cells using the equations

$$Md_{i,surf}^t = \left[\sum_{j=1}^{ncol}\left(Md_{i,surf,j}^t - Md_{i,surf,j-1}^t\right)\right] \quad \text{(A-21)}$$

$$Md_{i,surf,j}^{t} = \left[x_{ij} w_i C_{eff}^{t} \sqrt{\frac{4D_z^{*t} q_x^t}{\pi x_{ij}}}\right] f_{ed2}^{t} f_{surf} \qquad \text{(A-22)}$$

where x_{ij} is the length from the upgradient edge of the pool to the downgradient end of column j, $f_{ed2}^{t} \geq 1$ is a multiplier that is used during the portion of the simulation where a dissolution enhancement technology has been implemented, and f_{surf} is a multipler that is equal to 0, 1, or 2 to represent the number of source zone surfaces where dissolution is occurring into overlying and/or underlying groundwater. f_{surf} may also be assigned a real number to represent a multiplier for accelerated specific discharge adjacent to the boundary surface of the NAPL sub-zone. For a pool source zone, typically f_{surf}=1. For a residual NAPL layer that has transmissive layers both above and below it, f_{surf}=2.

A.5 Diffusive Mass Discharge Into and Out of Low-Permeability Units

NDM has the flexibility to represent diffusion from a source zone into a low-permeability unit, and then the reverse back-diffusion once the NAPL source zone has been depleted. Seyedabbasi et al. (2012) present the analytical equations used to estimate mass discharge associated with both forward diffusion into the low-permeability unit (which is based on work presented in Parker et al., 1994), as well as for back-diffusion into the more transmissive unit.

Mass discharge from a single component NAPL source zone *i* to a low-permeability unit is estimated based on

$$Md_{i,diff}^{t} = \varphi L_i w_i C_s \sqrt{\frac{R\pi D_o}{\pi t}} \quad ; \; t < t_{depletion} \qquad \text{(A-23)}$$

where φ is total porosity in the low-permeability unit [L^3L^{-3}], C_s is solubility [ML^{-3}], R is the retardation coefficient in the low-permeability unit, τ' is the tortuosity coefficient for the low-permeability unit, and $t_{depletion}$ is the simulation time at which all NAPL in the source zone has been depleted. This equation is based on the assumption that the low-permeability unit is a semi-infinite domain; therefore, this equation is only valid when the low-permeability unit is sufficiently thick that significant mass does not diffuse through the exit boundary of the low-permeability unit. This equation also assumes a constant solubility in time in the source zone and therefore is not applicable for multicomponent NAPLs when effective solubility changes significantly over time.

Based on the analytical solution for back-diffusion from the low-permeability unit into the depleted source zone presented in Seyedabbasi et al. (2012), NDM uses the following equation to simulate mass discharge arising from back-diffusion

$$Md_{i,b-diff}^{t} = \varphi L_i w_i C_s \left(\sqrt{\frac{R\pi D_o}{\pi t}} - \sqrt{\frac{R\pi D_o}{\pi (t-t')}} \right) \quad ; \; t > t_{depletion} \tag{A-24}$$

The reader is referred to Seyedabbasi et al. (2012) for an evaluation of the relative longevity of plumes sustained by back-diffusion relative to the initial NAPL dissolution period.

A.6 Multicomponent NAPL Dissolution

A version of NDM has been prepared to simulate multicomponent NAPL dissolution (NDM-MC). The present version of NDM-MC is limited in that surface discharge is not simulated; only through-discharge may be simulated for a multicomponent NAPL, and the maximum number of species in this current version is limited to three.

The model equations are similar to those described above for NDM, with the main difference being that the effective solubility for each species is calculated in each sub-zone grid cell at the end of each time step, based on an automated re-calculation of the species molar fraction in each cell. If an upgradient cell has a smaller effective solubility for a species than a downgradient cell, then mass will be dissolved from the downgradient cell to ensure that local equilibrium is achieved at the NAPL-water interface. Similarly, if an upgradient cell has a larger effective solubility than a downgradient cell, then mass will be re-dissolved into the NAPL in the downgradient cell to maintain equilibrium. The influence of intra-source by-passing may be simulated using one of the transient dilution factor equations (see Section A.3).